BioMed Research International

Emerging Insights on Surgical Techniques and Biomaterials for Total Hip and Knee Arthroplasty

Guest Editors: Kengo Yamamoto, Michiaki Takagi, and Hiroshi Ito

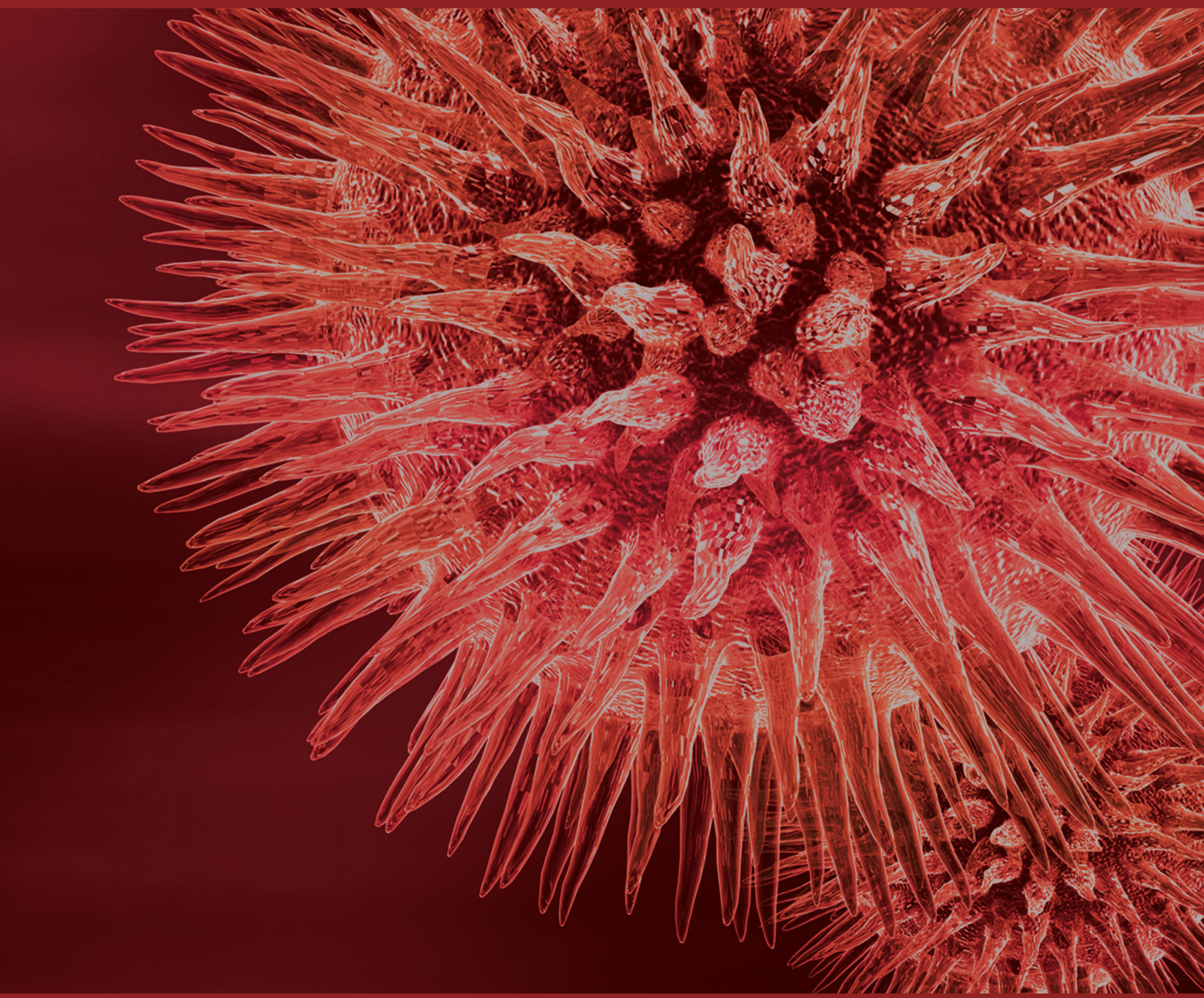

Emerging Insights on Surgical Techniques and Biomaterials for Total Hip and Knee Arthroplasty

BioMed Research International

Emerging Insights on Surgical Techniques and Biomaterials for Total Hip and Knee Arthroplasty

Guest Editors: Kengo Yamamoto, Michiaki Takagi, and Hiroshi Ito

Copyright © 2016 Hindawi Publishing Corporation. All rights reserved.

This is a special issue published in "BioMed Research International." All articles are open access articles distributed under the Creative Commons Attribution License, which permits unrestricted use, distribution, and reproduction in any medium, provided the original work is properly cited.

Contents

Hindawi Publishing Corporation
BioMed Research International
Volume 2016, Article ID 1496529, 2 pages
http://dx.doi.org/10.1155/2016/1496529

Editorial

Emerging Insights on Surgical Techniques and Biomaterials for Total Hip and Knee Arthroplasty

Kengo Yamamoto,[1] Michiaki Takagi,[2] and Hiroshi Ito[3]

[1]*Department of Orthopedic Surgery, Tokyo Medical University, 6-7-1 Nishishinjuku, Shinjuku-ku, Tokyo 160-0023, Japan*
[2]*Department of Orthopaedic Surgery, Yamagata University Faculty of Medicine, 2-2-2 Iida-Nishi, Yamagata 990-9585, Japan*
[3]*Department of Orthopaedic Surgery, Asahikawa Medical University, Midorigaoka Higashi 2-1-1-1, Asahikawa 078-8510, Japan*

Correspondence should be addressed to Kengo Yamamoto; kengo-y@tkg.att.ne.jp

Received 4 January 2016; Accepted 4 January 2016

Copyright © 2016 Kengo Yamamoto et al. This is an open access article distributed under the Creative Commons Attribution License, which permits unrestricted use, distribution, and reproduction in any medium, provided the original work is properly cited.

There has been a great interest by global orthopedic community in the development of new surgical techniques and biomaterials to improve clinical outcomes after total joint hip and knee arthroplasty (THA and TKA). There are currently enormous variations of the surgical treatment options by considering technical factors (surgical approaches, cement/cementless fixation, cup/stem positioning, and a computer-assisted navigation system) as well as prosthetic factors (material structures, properties, and design concepts). In the last decade, the prevalence of osteolysis decreased significantly in THA particularly after the refinement of hip implants including the development of highly cross-linked ultra-high molecular weight polyethylene (HXLPE) and porous coating for cementless fixation. Nevertheless, the postoperative complications such as aseptic loosening, dislocation, and infection still represent the most critical problems limiting the long-term success of the joint replacement surgery. The aim of this special issue is to provide novel concepts beneath the modern joint replacement surgery and to ultimately build successful future operative strategies based on the cutting-edge biomaterials science and clinical experience.

Regarding THA and TKA, this issue presents 13 articles consisting of 9 basic researches, 3 clinical studies, and 1 review paper. The review of R. P. van Hove et al. summarizes the available clinical literatures regarding the surface coating technology of titanium-nitride (TiN) ceramic in orthopaedic implants. K. Watanabe et al. experimentally demonstrated the efficacy of surface modification technology, poly(2-methacryloyloxyethyl phosphorylcholine [MPC])- (PMPC-) grafting, in further reducing HXLPE wear. On the other hand, in molecular scale, Y. Takahashi et al. offered new microstructural insights into the further improvement of wear resistance in HXLPE hip and knee prostheses by means of a novel spectroscopic approach using confocal polarized Raman microprobe spectroscopy. S. Gabarre et al. proposed polycarbonate-urethane as a favorable alternative to traditional bearing surfaces in THA because of its biomechanical characteristics similar to those of joint cartilage. The retrieval study performed by E. K. Fredette et al. contributed to improving our understanding of metal transfer on CoCr and ceramic femoral head surfaces, which may lead to more accurate HXLPE wear studies through more realistic recreation of metal transfer in *in vitro* wear simulation testing.

Excellent short to midterm clinical outcomes were presented by A. Hozumi et al. in anatomically difficult Asian patients with developmental dysplasia of hips, postosteotomy hip, and posterior pelvic tilt using the S-ROM-A prosthesis. The study of P. Sa-ngasoongsong et al. showed that, in order to minimize blood loss without significant increase in systemic absorption, low-dose intra-articular tranexamic acid (IA-TXA) application in TKA with prolonged clamping drain method was a safe and effective blood conservative technique. In preventing and treating postoperative infection, T. Kabata et al. showed the great success of short-term clinical trial using iodine-supported THA implants, which they have

originally developed in the recent years. For the detection and diagnosis of occult infection, J. T. Kempthorne et al. recommended conventional routine intraoperative sampling techniques rather than ultrasound sonication of the removed prosthesis potentially leading to the increased risk of contamination.

From the viewpoints of preventive medicine against hip fracture and knee osteoarthritis (OA), the risk assessments were conducted in the two studies. According to finite element models constructed from quantitative computed tomography (QCT), it was found by H. Kheirollahi and Y. Luo that femoral neck and the intertrochanteric region had a greater risk of fracture than other parts of the femur, and women were more prone to hip fracture than men. On the other hand, N. Lanocha-Arendarczyk et al. evaluated the concentrations of 10 chemical elements (F^-, K, Zn, Fe, Sr, Pb, Mn, Se, Cd, and THg) in tibial bone with OA and found statistically significant effects of environmental exposure factors including smoking, seafood diet, and geographical distribution on the levels of the elements.

In the technical aspects of THA including operational planning, T. A. Weber et al. reported improved hip joint reaction forces and patient's gait parameters by their originally developed method of a novel computer-assisted operation for minimal-invasive THA following the concept of "femur first/combined anteversion," which incorporates various aspects of performing a functional optimization of the stem and cup position (CAS FF), as compared to the conventional THA procedures. On the other hand, for TKA, the optimum design of femoral cutting guide was suggested by O.-R. Kwon et al. as patient-specific instruments (PSI), which can potentially shorten operative time and improve implant alignment.

We hope that the knowledge reported in this issue will be a hint to promote new study for the readers working in the same field and will lead to future development of new surgical techniques and implant devices that can respond to the increasing expectations of patients.

Acknowledgments

The Guest Editors greatly thank all the authors for contributing their excellent works to this special issue as well as all the reviewers for their many invaluable suggestions on the manuscript. Special thanks are due to Dr. Yasuhito Takahashi (Tokyo Medical University) for his management supports in editing this issue.

Kengo Yamamoto
Michiaki Takagi
Hiroshi Ito

Hindawi Publishing Corporation
BioMed Research International
Volume 2015, Article ID 978686, 8 pages
http://dx.doi.org/10.1155/2015/978686

Research Article

The Effect of Femoral Cutting Guide Design Improvements for Patient-Specific Instruments

Oh-Ryong Kwon,[1] Kyoung-Tak Kang,[2] Juhyun Son,[2] Yun-Jin Choi,[1] Dong-Suk Suh,[1] and Yong-Gon Koh[1]

[1]*Joint Reconstruction Center, Department of Orthopaedic Surgery, Yonsei Sarang Hospital, 10 Hyoryeong-ro, Seocho-gu, Seoul 06698, Republic of Korea*
[2]*Department of Mechanical Engineering, Yonsei University, 50 Yonsei-ro, Seodaemun-gu, Seoul 03722, Republic of Korea*

Correspondence should be addressed to Yong-Gon Koh; yonggonkoh@gmail.com

Received 20 April 2015; Accepted 18 November 2015

Academic Editor: Carla R. Arciola

Copyright © 2015 Oh-Ryong Kwon et al. This is an open access article distributed under the Creative Commons Attribution License, which permits unrestricted use, distribution, and reproduction in any medium, provided the original work is properly cited.

Although the application of patient-specific instruments (PSI) for total knee arthroplasty (TKA) increases the cost of the surgical procedure, PSI may reduce operative time and improve implant alignment, which could reduce the number of revision surgeries. We report our experience with TKA using PSI techniques in 120 patients from March to December 2014. PSI for TKA were created from data provided by computed tomography (CT) scans or magnetic resonance imaging (MRI); which imaging technology is more reliable for the PSI technique remains unclear. In the first 20 patients, the accuracy of bone resection and PSI stability were compared between CT and MRI scans with presurgical results as a reference; MRI produced better results. In the second and third groups, each with 50 patients, the results of bone resection and stability were compared in MRI scans with respect to the quality of scanning due to motion artifacts and experienced know-how in PSI design, respectively. The optimized femoral cutting guide design for PSI showed the closest outcomes in bone resection and PSI stability with presurgical data. It is expected that this design could be a reasonable guideline in PSI.

1. Introduction

Total knee arthroplasty (TKA) has high success rates with the majority of patients experiencing rapid improvement in pain, function, and quality of life [1]. Accurate bone resection and well-calibrated alignment are key factors in the success of TKA. As a favorable alternative to the standard procedure and navigation, PSI have been introduced recently as a means of improving bone resection accuracy through custom cutting blocks constructed using preoperative 3-dimensional (3D) imaging [2, 3]. Computer models of the distal femur and proximal tibia are defined from computer tomography (CT) or magnetic resonance imaging (MRI). Based on these models, presurgical TKA planning is performed and is available to the surgeon via web-based interfaces. These guides are used to manufacture cutting blocks that are precisely molded to the patients' anatomy and designed to reproduce the functionality of off-the-shelf conventional instruments. Both surgeons and manufacturers alike have suggested that the operative time can be reduced with the elimination of conventional instruments, which may translate into decreased costs and increased volume capacity for the surgeon. Furthermore, improvements in the accuracy of alignment and reductions in operative time have been suggested with PSI use [4].

These theoretical advantages have been postulated but have not been confirmed in the literature to date [5]. It is also unclear whether PSI improve TKA operation prognosis compared to the primary technique using conventional instruments [6]. Furthermore, concerning the PSI surgical technique, there are still varying opinions among orthopaedic surgeons regarding the relative advantages and disadvantages of CT versus MRI [7–9]. White et al. reported that MRI leads to higher costs, whereas CT is likely to provide the optimal surgical outcome at lower cost when it is used to manufacture patient-specific templates [7]. Asada et al. stated that both CT and MRI reduce operative time with the same accuracy

in three planes, but MRI is not as cost effective [8]. Silva et al. implied that MRI may be more accurate than CT using the Signature system (Biomet, Inc., Warsaw, IN, USA) when planning surgical guides for TKA [9]. In order to provide PSI with the highest accuracy, 3D reconstructed images must be composed well in CT and MRI images and PSI should be fitted securely to the patient's anatomy. If the guide is not fitted securely, PSI stability is reduced and bone cutting is not completed as planned in the presurgical program, leading to malalignment. However, there have been no studies related to design improvements in PSI femoral cutting guides with respect to the quality of imaging or difference of individual anatomy.

Therefore, the purpose of this study is (1) to evaluate the effect of PSI design in CT and MRI with respect to secure fit and bone cutting, (2) to compare bone cutting in different PSI designs with respect to motion artifacts in MRI, (3) to compare bone cutting with respect to optimized PSI designs, and (4) to develop a preoperative plan and resultant custom guides that could accurately replicate surgeon preference with infrequent intraoperative changes.

2. Materials and Methods

2.1. Patient Enrollment. This retrospective cohort study was approved by the institutional review board of our hospital. All patients provided informed consent before surgery. Between March and December 2014, we included 120 patients with end-stage knee osteoarthritis scheduled for TKA in the study. Patients with rheumatoid arthritis, previous osteotomy, fractures, retained hardware in the limb, or claustrophobia were excluded. The inclusion criteria were diagnosis of primary knee osteoarthritis and the ability to undergo MRI at our facility. Mean patient age was 70.9 years (range, 64–85 years) and mean body mass index (BMI) was 27.4 kg/m^2 (range, 20–42 kg/m^2).

2.2. Image Protocol. For the 20 patients in the first group, both CT and MRI (1 mm and 2 mm slice thickness) images were taken for accuracy comparisons. CT images of the knee joint were taken with a slice interval of 1 mm using a 64-channel CT scanner (Somatom Sensation 64; Siemens Healthcare, Erlnagen, Germany), whereas 5 mm slice thickness was applied to hip and ankle joints. The tube parameters were 120 kVp and 135 mA. The acquisition matrix was 512 × 512. The field of view was 200 mm.

MRI images were acquired using a 1.5T MRI scanner (Achieva 1.5T; Philips Healthcare, Netherlands). MRI scans of the tibiofemoral knee joint were obtained at 1 or 2 mm slice thickness in the sagittal plane, whereas 5 mm slice thickness was applied to hip and ankle joints in the axial plane. For the nonfat saturation condition, MRI consisted of an axial proton-density (PD) sequence. A high-resolution setting was used for the spectral presaturation inversion recovery sequence (TE: 25.0 ms, TR: 3,590.8 ms, acquisition matrix: 512 × 512 pixels, NEX: 2.0, and field of view: 140 × 140 mm). All procedures were identical to those in Signature from Biomet.

2.3. Presurgical TKA Techniques and PSI Design Methods. The first author (Oh-Ryong Kwon) had participated in 30 TKA operative cases with Signature at the time of the study. Signature charges $900 to fit each patient's unique anatomy and to guide surgical bone resection in order to manufacture femoral and tibial PSI guides [10]. The time elapsed from the submission of the MRI to the receipt of guides was 4 to 6 weeks. However, it is illegal to impose charges related to surgical instruments in the Republic of Korea; thus our hospital has developed our own presurgical planning and design platform in order to provide PSI services to patients for free.

3D data can be acquired through either MRI or CT. The 3D reconstruction processes were performed with Mimics software (version 17.0; Materialise, Leuven, Belgium). Using Mimics, the resulting 3D images were converted to STL files and implemented in the digital CAD software, 3-Matic, also produced by Materialise. 3-Matic allows the user to combine geometry from mixed sources into a single project. PSI guides were designed with 3-Matic commercial software (version 9.0; Materialise, Leuven, Belgium).

Patients from the first group were divided into two different groups with respect to slice thickness, 1 mm from CT, 1 mm from MRI, and 2 mm from MRI scans (Materialise). CT has limitations in delineating articular cartilage (3D model inaccuracies) [11, 12]. Cartilage was not able to be reconstructed using CT and 2 mm thickness was considered followed by contact with bone using spikes, in order to overcome the limitations of the apparatus (Figure 1). We believe that the more segmented the scans obtained, the more accurate the 3D model that could be developed from the images. PSI guides for MRI scans with 1 mm and 2 mm slice thickness in group 1 were designed with full contact. Following the analysis of the first group, we created the second group. For group 2, MRI with 2 mm slice thickness was used. Group 2 was categorized based on the quality of images (Figure 2). There are two designs with and without motion artifacts. A PSI design with only bone contact regions was constructed for scans with motion artifacts, whereas the tolerances were considered for others. For those without motion artifacts, a full contact design was developed according to the bony geometry (Figure 1). Throughout the learning curve, group 3 represented those with optimized designs. Group 3 was also divided into subgroups with respect to the patients' motion. However, group 3 is not only different in terms of motion artifacts; but they also had the advantage of preventing movement while drilling by using a perfect fit between bone and cutting guides (Figure 1). For the PSI design, each company has unique design techniques to make the bone fit guides (Figure 3). Our PSI design was optimized to be perfectly fitted to the bone at the anterior flange.

Each step was evaluated for each group and intraoperative changes were recorded, including resection level, component size, and coronal/sagittal alignment. The resected bone was then measured with a 3D laser scanner (Comet VZ; Steinbichler Optotechnik GmbH, Neubeuern, Germany) with 50 μm accuracy. The distal femur resections were measured medially and laterally, thus obtaining distal femur medial and lateral resection measurements. Posterior femoral condyle

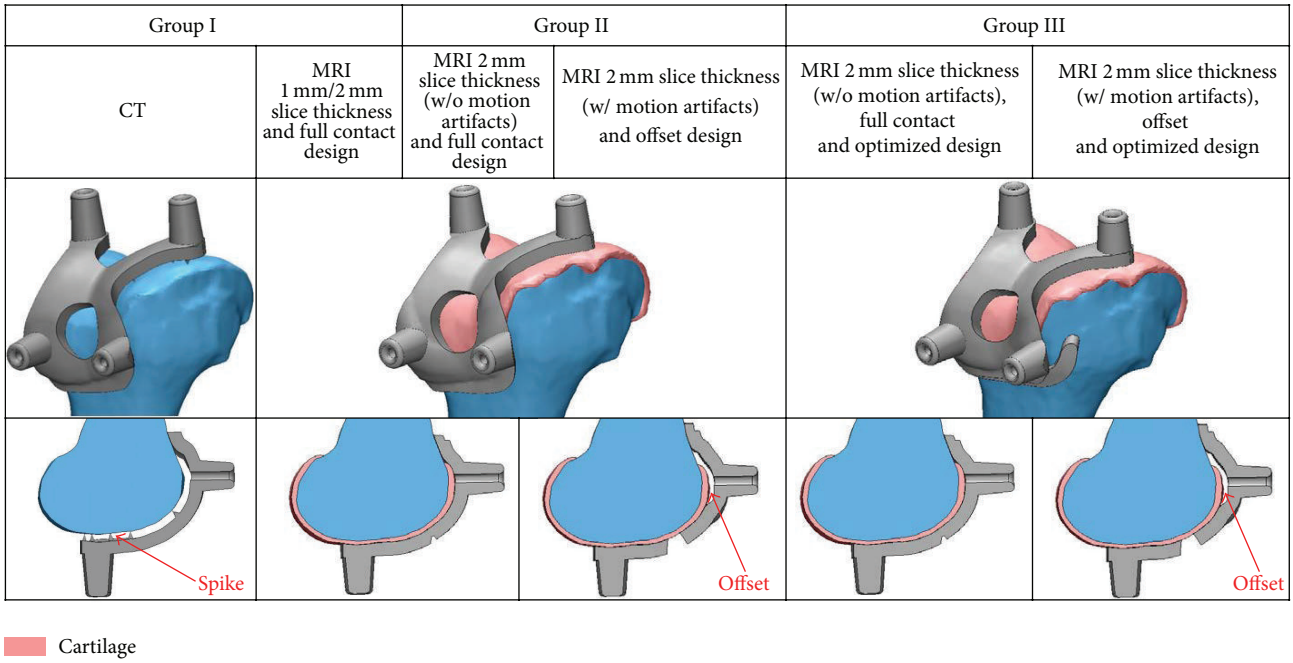

Figure 1: PSI guides of each group used in this study.

cuts were made and resections in the medial and lateral posterior femoral condyles were measured. Bone cutting data was comparatively analyzed with preplanning results. The thickness of the saw blade was added to the resection thickness to calculate the total resection for each cut.

All operations followed by TKA surgical preplanning were conducted by an experienced surgeon (Oh-Ryong Kwon). A computer-generated preoperative plan was created according to the surgeon's preferences, as follows: default alignment for femoral component rotation was parallel to the surgical epicondylar axis, femoral component coronal alignment 90 degrees to the mechanical axis, and femoral component sagittal alignment 3 degrees of flexion with 9.5 mm distal medial resection. We retained the default plan when it appeared appropriate and recorded all changes when made. The time from submission of the 3D image to receipt of the guides was 4 days. All patients in both cohorts received a posterior-stabilized, fixed-bearing implant. The operation was performed through an anteromedial parapatellar approach, without everting the patella. Cement fixation was used in all patients. The implant used was the Genesis II Total Knee System (Smith & Nephew, Inc., Memphis, TN, USA).

The results presented are the intraoperative changes for measurements of femoral component size and alignment in groups 1, 2, and 3. The differences between preplanning results and actual bone cutting were measured in groups 2 and 3.

3. Results

One hundred and twenty patients underwent an operation with custom-fit technology. Table 1 summarizes the demographic profiles. There were no hematomas, infections, manipulations, or reoperations.

Table 1: Summary of demographics used in this study.

Demographic	
Number of TKAs	120
Average age years (±SD)	70.9 (±9.2)
Male : female	23 : 97
Left : right	53 : 67
BMI average (kg/m^2)	27.4

BMI: body mass index.

Intraoperative changes to the implant sizing and alignment proposed by PSI were observed (groups 1–3). A total of 94 intraoperative changes were made in 120 TKAs (0.8 changes per knee) with the use of PSI (groups 1–3, Table 2). PSI predicted the implanted component size in 90% ($n = 12$) of femurs. PSI predicted the varus and valgus alignment and internal and external rotations in 96% ($n = 5$) and 89% ($n = 13$), respectively, of femurs.

Throughout the path from group 1 to group 3, the frequency of intraoperative changes of the implant size and alignment decreased. In group 3, the percentage of changes was 3% ($n = 3$). In group 1, for the 13 patients within the subgroup with 1 mm slice thickness MRI, the time spent in the MRI machine was long and impatience led to motion artifacts. Therefore, bone models and PSI guides could not be developed and manufactured due to the inaccuracy of the scans. In group 1, the PSI cutting guides that were manufactured using 1 mm slice thickness MRI scans were used for only one of 20 patients. Similarly, in group 1, the PSI cutting guides based on CT scans and 2 mm slice

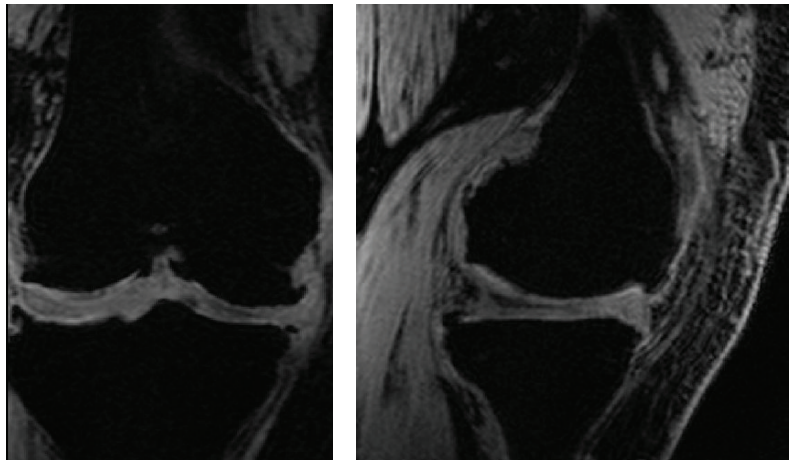

(a)

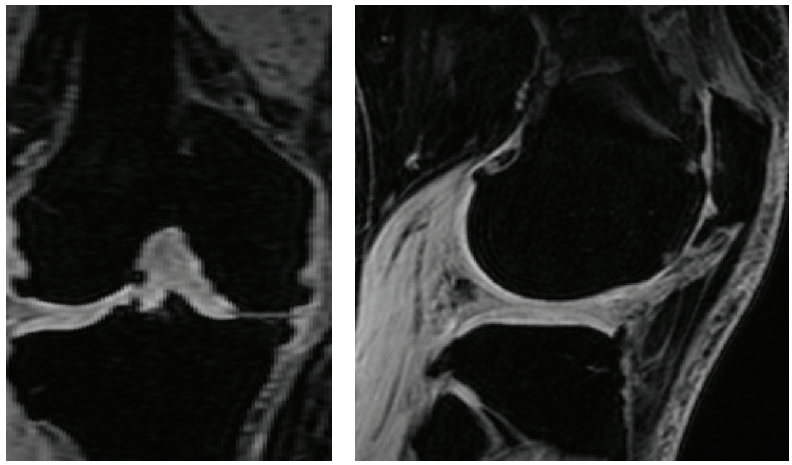

(b)

Figure 2: MRI images categorized based on the quality of images: (a) with motion artifacts; (b) without motion artifacts.

Figure 3: Signature system (Biomet, Inc., Warsaw, IN, USA) PSI guide for femur.

Table 2: Intraoperative changes made to the femoral components in 120 PSI.

Femur	Change made	Group I ($n = 20$)		Group II ($n = 50$)		Group III ($n = 50$)	
		Number	Percentage	Number	Percentage	Number	Percentage
Size	Up/down	7	35%	5	10%	0	0%
Resection	Proximal	18	90%	16	32%	1	2%
	Distal	11	55%	9	18%	1	2%
	Varus	3	15%	1	2%	0	0%
	Valgus	1	5%	0	0%	0	0%
4 : 1 block	External rotation	3	15%	2	4%	0	0%
	Internal rotation	3	15%	4	16%	1	2%
	Anterior	2	10%	3	12%	0	0%
	Posterior	1	5%	2	8%	0	0%

Table 3: Differences between planned bone resections and bone resections recorded from the PSI intraoperatively (mm).

		Group II			Group III		
		MRI 2 mm slice thickness (w/motion artifacts) & offset design ($n = 21$)	MRI 2 mm slice thickness (w/o motion artifacts) & full contact design ($n = 29$)	Ave.	MRI 2 mm slice thickness (w/motion artifacts), offset & optimized design ($n = 18$)	MRI 2 mm slice thickness (w/o motion artifacts), full contact & optimized design ($n = 32$)	Ave.
Distal	M (±SD)	0.56 (±0.12)	0.28 (±0.04)	0.44 (±0.17)	0.26 (±0.04)	0.16 (±0.04)	0.21 (±0.06)
	L (±SD)	0.46 (±0.09)	0.18 (±0.03)	0.32 (±0.15)	0.14 (±0.03)	0.12 (±0.02)	0.13 (±0.03)
Posterior	M (±SD)	0.34 (±0.07)	0.23 (±0.03)	0.27 (±0.08)	0.20 (±0.03)	0.18 (±0.02)	0.19 (±0.02)
	L (±SD)	0.19 (±0.03)	0.17 (±0.01)	0.18 (±0.02)	0.14 (±0.02)	0.12 (±0.01)	0.13 (±0.01)

thickness MRI scans were used for four and fifteen patients, respectively.

The mean (±standard deviation) discrepancies between the predicted and actual resection thicknesses ("cutting error") are shown in Table 3 (groups 2, 3). Those of groups 2 and 3 were 0.44 mm and 0.21 mm on the medial sides and 0.32 mm and 0.13 mm on the lateral sides, respectively. There was no significant difference between the two groups, but the femoral distal resection error diminished going from group 2 to group 3. The range of differences between the planned and the measured resections was larger for the medial posterior condyle resection, while the lateral posterior condyle resections were well matched with the planned results (groups 2, 3). The discrepancies between the planned and the measured bone resections were close to 0% in group 3. The difference between the planned and the actual bone resections was the lowest in the optimized design from group 3 without motion artifacts, and the values from group 3 with motion artifacts and group 2 without motion artifacts were similar. In other words, the superiority of an optimum PSI design has been proven.

4. Discussion

The most important finding of this study was the optimal medical imaging method and critical thickness for MRI slices for the design of PSI and the development of the optimal design for a PSI guide well-fitted to the patient's anatomy without any micromotion in contact with the bony surface.

The outcome of TKA greatly depends on the surgical technique used [13, 14]. Technical errors such as malalignment may lead to early failure [15]. Variations in surgical performance and outliers in TKA still occur and they may affect outcome. Improvement in the outcomes of TKA, particularly for difficult cases in young, active patients, patients with bone abnormalities, and patients who have revision surgery, remains a major concern [14]. Outcome improvement has to be viewed for cost-effectiveness and minimizing complications. Computer-assisted surgery aims to improve the alignment of the TKA components. However, all computer-navigated and robotic systems require an additional stage of registration, which can be time-consuming and costly; this is of particular concern in low-volume hospitals [6, 16, 17]. Despite the increased intraoperative complexity, initial reports on computer-assisted surgeries have been encouraging, but registry data show that conventional instrumented surgery remains the standard treatment [18]. PSI, built according to 3D medical images, have been designed to address the disadvantages of conventional techniques. PSI should be considered as an alternative to conventional instrumentation, but controversy remains regarding this issue [2, 4–6, 19]. The points of dispute are whether PSI improve tibiofemoral alignment [5, 6] and reduce blood loss due to shortened operation times compared to conventional

methods [20]. There are also conflicting opinions on whether CT and MRI scans are more reliable for PSI [7–9].

We hypothesized, based on the experience using Signature PSI systems, that inaccuracy in 3D models and PSI guides not perfectly fitted to bone are the main two reasons for the resulting dissimilarities between preplanned outputs and measured bone resections in the operating room.

It is prohibited for the hospital to charge patients for PSI in Republic of Korea. Preplanning and design processes were conducted using previously validated commercial software from Materialise [14, 21], and a cost-effective 3D printer allowed us to perform this research [6]. In the design of the PSI, 3D reconstruction of the bone is a key step; thus this interobserver study was completed by two observers (Kyoung-Tak Kang, Juhyun Son) using a rule-based protocol suggested by Koo et al. for cartilage reconstruction using MRI scans [22].

In this study, the difference between CT and MRI scans was analyzed first. There is a lack of soft tissue modeling in the models based on CT scans; thus the contact surface was considered to be bone [23]. Even for a surgeon who has already experienced 30 cases of PSI-TKA, a surgical guide with only several points of contact on the bony surface without considering the cartilage thickness was not ideal. Similar uncertainties from CT scans have been reported in previous studies as well [24, 25].

The required scan time for MRI with 1 mm slice thickness is about 70% more than that of MRI with 2 mm slice thickness. There are many motion artifacts disturbing the design of PSI guides in the 1 mm slice MRI scan, especially in elderly patients [8]. For this reason, MRI-based PSI guide designs were modified with respect to the quality of the MRI scans. The first criterion is the existence of motion artifacts. Asada et al. reported that 35% of patients from their study were dropped due to motion artifacts in the MRI-based PSI guide [8]. In our study, the importance of the elimination of motion artifacts during MRI scanning was also emphasized. In other words, small increments in slice thickness are not always accepted as good data. The reasons that implant size and alignment may vary intraoperatively were that PSI guide was designed and manufactured without considering quality of medical image and having unstable contact.

For CT based PSI guides, it did not provide a good stability due to the absence of soft tissue such as articular cartilage and contact using spike for the gap between guide and bone. MRI based PSI guides designed without regard to patient's motion artifact could lead to its instability in contact with bony surface. For MRI image with motion artifact, it was found from group 1 that it might lead to the more inaccurate result if full contact PSI design is applied. If there is uncertainty in cartilage regions due to motion artifact in MRI, it was found that tolerance in design may produce better stability in contact of PSI guide with bone. Therefore, 2 mm slice thickness conditions were used in the group 2 and group 3 designs.

For motion artifacts in group 2, the areas with cartilage were considered contact surfaces, and, if not, tolerance was applied in the design. If there were no motion artifacts, the PSI design was shape-matched following the articular surface. We developed the optimal design for PSI through the learning curve related to cases with motion artifacts. PSI design with only anterior and distal contact regions in group 2 constrained flexion and extension. The current Signature PSI guides which were similarly designed from other companies could not tightly hold internal-external rotation. Therefore, we considered the optimal design to overcome this problem by holding flexion-extension and internal-external rotation fixed. Throughout such modifications, not only translation but also rotational stability was improved during guide drilling. Throughout the process from group 1 to group 3, the intraoperative changes in alignment and implant sizing diminished.

Bone resection was measured with a 3D scanner, instead of a 2D micrometer, to obtain more precise qualitative measurements. The resection cutting results reflect how well PSI-TKA surgery was completed after preoperative planning. To our knowledge, this is the first research paper to evaluate the design of PSI guides with respect to their contact stability and relation to 3D medical images. The overall discrepancy was small for the resection thicknesses compared to the preplanned results (groups 2-3). Thus, we are satisfied with the PSI that were planned. However, it is worth noting that greater variation was noted in the distal femoral resections, which were found to be decreased in the optimal design. The significant finding in this study was that group 3 with motion artifacts and full contact design and group 2 without motion artifacts had similar discrepancies between the predicted and actual resection. In other words, design improvement may compensate for the negative effect of motion artifacts on MRI quality.

A complete patient-specific system can potentially shorten operative time, setup time, operating room space, and hospital space. Setup time is shortened by eliminating the need to bring and open multiple instrumentation sets in the operating room. Procedural time can also be reduced in the complete patient-specific system that includes all instrumentation and a patient-specific implant by eliminating several time-consuming steps. When the instrumentation and implants are completely patient-specific, the implant sizing, rotation, and positional decisions are predetermined. These implant attributes either can be based on a standard set of design rules or could be customized according to surgeon preference.

There were limitations to our study. First, this current study did not assess final implant positioning, which will be investigated in future research. Second, a single experienced surgeon made all the preplanning and intraoperative decisions concerning changes to alignment and implant sizing. This is not representative of the decisions of a low-volume or inexperienced knee surgeon using this technology. A future study with multiple surgeons would provide a more comprehensive representation of this technology based on surgeon experience. One surgeon working on the planning by himself could reduce confusion, compared to working with multiple surgeons [10]. Finally, this study focused on intraoperative validation of patient-specific instruments and comparison of immediate postoperative radiographic outcomes with conventional TKA, without encompassing

other important parameters, such as functional improvement, patient satisfaction, longevity, or cost-effectiveness.

5. Conclusion

In conclusion, the optimum PSI design for stability improvement was suggested. In terms of 3D image scanning time required, this would be beneficial to the hospital and also to the patients. The approach outlined introduces a generic product in addition to the commercial PSI systems offered by other manufacturers. In the future, various PSI design methods should be evaluated for variable conditions ranging from different MRI systems to patient anatomy.

Conflict of Interests

The authors declare that there is no conflict of interests regarding the publication of this paper.

Authors' Contribution

Oh-Ryong Kwon and Kyoung-Tak Kang contributed equally to this work.

References

[1] T. K. Fehring, S. M. Odum, J. L. Troyer, R. Iorio, S. M. Kurtz, and E. C. Lau, "Joint replacement access in 2016: a supply side crisis," *Journal of Arthroplasty*, vol. 25, no. 8, pp. 1175–1181, 2010.

[2] A. V. Lombardi Jr., K. R. Berend, and J. B. Adams, "Patient-specific approach in total knee arthroplasty," *Orthopedics*, vol. 31, no. 9, pp. 927–931, 2008.

[3] V. Y. Ng, J. H. DeClaire, K. R. Berend, B. C. Gulick, and A. V. Lombardi Jr., "Improved accuracy of alignment with patient-specific positioning guides compared with manual instrumentation in TKA," *Clinical Orthopaedics and Related Research*, vol. 470, no. 1, pp. 99–107, 2012.

[4] S. M. Howell, E. E. Hodapp, K. Kuznik, and M. L. Hull, "In vivo adduction and reverse axial rotation (external) of the tibial component can be minimized," *Orthopedics*, vol. 32, no. 5, p. 319, 2009.

[5] R. M. Nunley, B. S. Ellison, E. L. Ruh et al., "Are patient-specific cutting blocks cost-effective for total knee arthroplasty?" *Clinical Orthopaedics and Related Research*, vol. 470, no. 3, pp. 889–894, 2012.

[6] S. P. Krishnan, A. Dawood, R. Richards, J. Henckel, and A. J. Hart, "A review of rapid prototyped surgical guides for patient-specific total knee replacement," *Journal of Bone and Joint Surgery B*, vol. 94, no. 11, pp. 1457–1461, 2012.

[7] D. White, K. L. Chelule, and B. B. Seedhom, "Accuracy of MRI vs CT imaging with particular reference to patient specific templates for total knee replacement surgery," *International Journal of Medical Robotics and Computer Assisted Surgery*, vol. 4, no. 3, pp. 224–231, 2008.

[8] S. Asada, S. Mori, T. Matsushita, K. Nakagawa, I. Tsukamoto, and M. Akagi, "Comparison of MRI- and CT-based patient-specific guides for total knee arthroplasty," *Knee*, vol. 21, no. 6, pp. 1238–1243, 2014.

[9] A. Silva, R. Sampaio, and E. Pinto, "Patient-specific instrumentation improves tibial component rotation in TKA," *Knee Surgery, Sports Traumatology, Arthroscopy*, vol. 22, no. 3, pp. 636–642, 2014.

[10] B. M. Stronach, C. E. Pelt, J. Erickson, and C. L. Peters, "Patient-specific total knee arthroplasty required frequent surgeon-directed changes," *Clinical Orthopaedics and Related Research*, vol. 471, no. 1, pp. 169–174, 2013.

[11] J. Winder and R. Bibb, "Medical rapid prototyping technologies: state of the art and current limitations for application in oral and maxillofacial surgery," *Journal of Oral and Maxillofacial Surgery*, vol. 63, no. 7, pp. 1006–1015, 2005.

[12] J. M. Joffe, S. R. Nicoll, R. Richards, A. D. Linney, and M. Harris, "Validation of computer-assisted manufacture of titanium plates for cranioplasty," *International Journal of Oral and Maxillofacial Surgery*, vol. 28, no. 4, pp. 309–313, 1999.

[13] T. K. Fehring, S. Odum, W. L. Griffin, J. B. Mason, and M. Nadaud, "Early failures in total knee arthroplasty," *Clinical Orthopaedics and Related Research*, no. 392, pp. 315–318, 2001.

[14] M. A. Hafez, K. L. Chelule, B. B. Seedhom, and K. P. Sherman, "Computer-assisted total knee arthroplasty using patient-specific templating," *Clinical Orthopaedics and Related Research*, vol. 444, pp. 184–192, 2006.

[15] F. W. Werner, D. C. Ayers, L. P. Maletsky, and P. J. Rullkoetter, "The effect of valgus/varus malalignment on load distribution in total knee replacements," *Journal of Biomechanics*, vol. 38, no. 2, pp. 349–355, 2005.

[16] K. Bauwens, G. Matthes, M. Wich et al., "Navigated total knee replacement: a meta-analysis," *The Journal of Bone & Joint Surgery—American Volume*, vol. 89, no. 2, pp. 261–269, 2007.

[17] J. D. Slover, A. N. A. Tosteson, K. J. Bozic, H. E. Rubash, and H. Malchau, "Impact of hospital volume on the economic value of computer navigation for total knee replacement," *The Journal of Bone and Joint Surgery—American Volume*, vol. 90, no. 7, pp. 1492–1500, 2008.

[18] S. K. Chauhan, R. G. Scott, W. Breidahl, and R. J. Beaver, "Computer-assisted knee arthroplasty versus a conventional jig-based technique. A randomised, prospective trial," *The Journal of Bone & Joint Surgery—British Volume*, vol. 86, no. 3, pp. 372–377, 2004.

[19] J. Victor, J. Dujardin, H. Vandenneucker, N. Arnout, and J. Bellemans, "Patient-specific guides do not improve accuracy in total knee arthroplasty: a prospective randomized controlled trial," *Clinical Orthopaedics and Related Research*, vol. 472, no. 1, pp. 263–271, 2014.

[20] W. G. Hamilton, N. L. Parks, and A. Saxena, "Patient-specific instrumentation does not shorten surgical time: a prospective, randomized trial," *Journal of Arthroplasty*, vol. 28, no. 8, pp. 96–100, 2013.

[21] G. A. Brown, K. Firoozbakhsh, T. A. DeCoster, J. R. Reyna Jr., and M. Moneim, "Rapid prototyping: the future of trauma surgery?" *The Journal of Bone & Joint Surgery—American Volume*, vol. 85, no. 4, pp. 49–55, 2003.

[22] S. Koo, G. E. Gold, and T. P. Andriacchi, "Considerations in measuring cartilage thickness using MRI: factors influencing reproducibility and accuracy," *Osteoarthritis and Cartilage*, vol. 13, no. 9, pp. 782–789, 2005.

[23] C. O. Tibesku, B. Innocenti, P. Wong, A. Salehi, and L. Labey, "Can CT-based patient-matched instrumentation achieve consistent rotational alignment in knee arthroplasty?" *Archives of Orthopaedic and Trauma Surgery*, vol. 132, no. 2, pp. 171–177, 2012.

[24] A. Ensini, A. Timoncini, F. Cenni et al., "Intra- and post-operative accuracy assessments of two different patient-specific instrumentation systems for total knee replacement," *Knee Surgery, Sports Traumatology, Arthroscopy*, vol. 22, no. 3, pp. 621–629, 2014.

[25] S. M. Howell, K. Kuznik, M. L. Hull, and R. A. Siston, "Results of an initial experience with custom-fit positioning total knee arthroplasty in a series of 48 patients," *Orthopedics*, vol. 31, no. 9, pp. 857–864, 2008.

Hindawi Publishing Corporation
BioMed Research International
Volume 2015, Article ID 625317, 16 pages
http://dx.doi.org/10.1155/2015/625317

Research Article

Does Computer-Assisted Femur First THR Improve Musculoskeletal Loading Conditions?

Tim A. Weber,[1,2] Sebastian Dendorfer,[1] Joachim Grifka,[2] Gijsbertus J. Verkerke,[3,4] and Tobias Renkawitz[2]

[1] *Faculty of Mechanical Engineering, Laboratory for Biomechanics, Ostbayerische Technische Hochschule Regensburg, 93053 Regensburg, Germany*
[2] *Department of Orthopaedic Surgery, Regensburg University Medical Center (UKR), 93077 Bad Abbach, Germany*
[3] *Department of Rehabilitation Medicine, University Medical Center Groningen (UMCG), University of Groningen, Antonius Deusinglaan 1, 9713 AV Groningen, Netherlands*
[4] *Department of Biomechanical Engineering, University of Twente, Drienerlolaan 5, 7522 NB Enschede, Netherlands*

Correspondence should be addressed to Tim A. Weber; tim.weber@oth-regensburg.de

Received 14 August 2014; Revised 15 November 2014; Accepted 26 November 2014

Academic Editor: Michiaki Takagi

Copyright © 2015 Tim A. Weber et al. This is an open access article distributed under the Creative Commons Attribution License, which permits unrestricted use, distribution, and reproduction in any medium, provided the original work is properly cited.

We have developed a novel, computer-assisted operation method for minimal-invasive total hip replacement (THR) following the concept of "femur first/combined anteversion," which incorporates various aspects of performing a functional optimization of the prosthetic stem and cup position (CAS FF). The purpose of this study is to assess whether the hip joint reaction forces and patient's gait parameters are being improved by CAS FF in relation to conventional THR (CON). We enrolled 60 patients (28 CAS FF/32 CON) and invited them for gait analysis at three time points (preoperatively, postop six months, and postop 12 months). Data retrieved from gait analysis was processed using patient-specific musculoskeletal models. The target parameters were hip reaction force magnitude (hrf), symmetries, and orientation with respect to the cup. Hrf in the CAS FF group were closer to a young healthy normal. Phase-shift symmetry showed an increase in the CAS FF group. Hrf orientation in the CAS FF group was closer to optimum, though no edge or rim-loading occurred in the CON group as well. The CAS FF group showed an improved hrf orientation in an early stage and a trend to an improved long-term outcome.

1. Introduction

Total hip replacement (THR) is one of the most successful operations of the 20th century [1]. Instability and early aseptic loosening are the two most common early complications following THR [2–5]. Biomathematical calculations have shown that prosthetic instability can be reduced by regarding stem and cup as coupled partners in a biomechanical system [6]. In this context, several authors have proposed starting with the preparation of the femur and then transferring the orientation of the stem relative to the cup intraoperatively ("femur first," "combined anteversion") in order to minimize the risk of impingement and dislocation [7–10]. We have developed a novel, computer-assisted operation method for THR following the concept of "femur first/combined anteversion" (CAS FF), which incorporates various aspects of performing a functional optimization of the prosthetic stem and cup position [11–13]. Goal of this study was to compare the hip reaction forces (hrf) and their orientation, which are known to influence implant survivorship [14–16], between CAS FF and conventional THR (CON). One method to analyze hrf is to employ instrumented implants (II) [17, 18]. This method is regarded as the gold standard, since it is the only way to measure such forces in vivo; however it bears the disadvantage of being highly invasive. This limits this method to only small sample sizes, making statistical analysis and predictions challenging. Novel computational methods like musculoskeletal modeling (MM) have the potential to accurately predict hrf while being noninvasive [19]. Validation of such models has been achieved by comparing computed

entities to measured ones [20]. After validation has been achieved the models can be employed to investigate larger collectives [16]. Often such studies focus on activities of daily living (ADL) such as walking [21]. By combining experimental data as retrieved from motion capture gait analysis, medical imaging, and MM it is possible to build anatomical correct models that represent the patient accurately [22], allowing the computation of muscle forces and hip reaction forces in a patient-specific manner [19]. Such data can help to further improve implant design and can be used for measuring the outcome after THR [21]. Analyzing strongly varying signals such as joint reaction forces is a challenging task. The question that often remains is if "characteristics" (such as local minima, local maxima or signal slopes) show a distinct pattern or if they appear randomly [23]. Dynamic time warping (dtw) has been established by Bender and Bergmann in order to compute typical signals (TS) which are aiming to provide the best representation of time series [23]. Parameters gathered during the dtw computations are also a measure of signal similarity. They represent different aspects of such the phase shift and the magnitudes, respectively. Healthy and able-bodied persons walk in a symmetrical way [24]. Following the concept of dynamic similarity, the time series of joint reaction force in healthy persons are also symmetrical [25]. Therefore an important outcome after THR is not only magnitude and orientation of hrf, but also symmetry of hrf as a measure to what extent gait pattern is pathological.

The purpose of the current study is to assess whether the artificial joint's hip reaction forces and patient's gait parameters can be improved by CAS FF THR by means of a combined workflow of experimental and computational methods relative to conventional THR. The specific target parameters were: (i) Are the hip reaction forces closer to a healthy, young normal in the CAS FF group? (ii) Are the hip reaction forces distributed more symmetrically in the CAS FF group? (iii) Is critical edge or rim-loading of the acetabular cup less likely to occur in the CAS FF group?

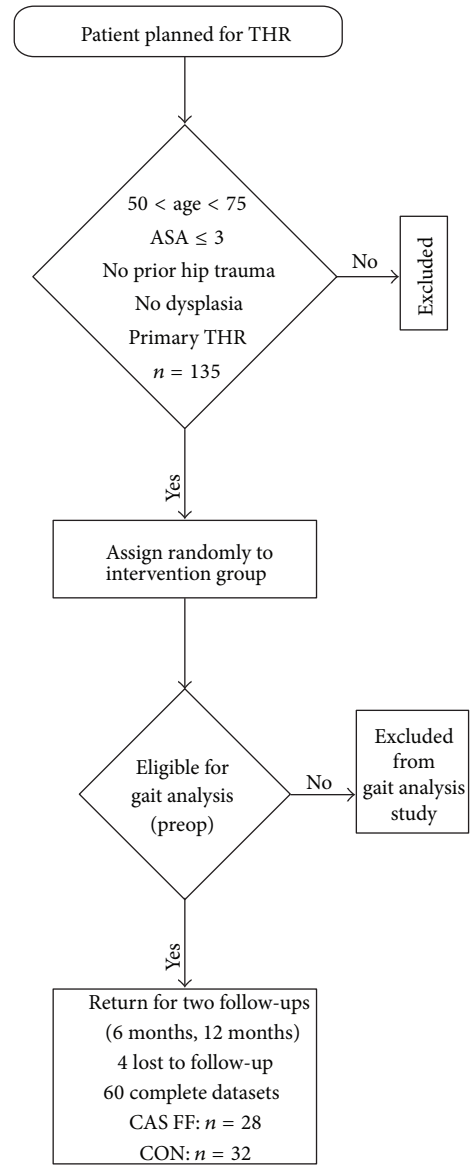

Figure 1: Flow chart of patient acquisition with inclusion criteria according to Renkawitz et al. [11].

2. Patients and Methods

2.1. Patients. The study design, procedures, and informed consent were approved by our local medical ethics committee (number 10-121-0263). This single-center, patient- and observer-blinded randomized controlled trial was registered at the German Clinical Trials Register under the Main ID: (DRKS00000739).

Recruitment of participants, inclusion and exclusion criteria, and surgical procedures for this randomized controlled trial have been published prior to the start of the study [11]. Eligible participants between the ages of 50 and 75 with an American Society of Anesthesiologists (ASA [26]) score ≤3 were recruited from patients admitted for primary uncemented unilateral (minimal or no osteoarthritis in the opposite hip) THA due to primary or secondary osteoarthritis. Exclusion criteria were age <50 and >75 years, ASA score >3, coxarthrosis secondary to hip dysplasia, posttraumatic hip deformities, and prior hip surgery. Informed consent was acquired by one of four clinical investigators. THA in all patients was performed in the lateral decubitus position using a minimally invasive single-incision anterolateral approach. 160 THAs were performed by four orthopaedic surgeons from the Regensburg University Medical Center. Each surgeon had experience with more than 200 fluoroscopy and 200 navigation-controlled THAs. Press-fit acetabular components, uncemented hydroxyapatite-coated stems (Pinnacle cup, Corail stem, DePuy, Warsaw, IN), standard (nondysplastic and nonoffset) polyethylene liners and metal heads with a diameter of 32 mm were used in all patients.

Patients were randomly allocated to receive either Femur First CAS THR or conventional THR; see Figure 1. Patient characteristics according to allocation are presented in

Table 1: Patient characteristics by intervention group.

Group	Sample size (male/female)	Age in years: mean (SD)	Age range: min/max	BMI ([kg/m^2]): mean (SD)	BMI range: min/max	ASA mode (frequency)	Blood loss [g/dL]: mean (SD)	OP-time [minutes]: mean (SD)
CAS FF	28 (10/18)	60 (7)	50/74	26.73 (4.26)	19.45/35.22	2 (21)	−3.0 (1.0)	71 (15)
CON	32 (19/13)	62 (8)	50/74	27.58 (3.08)	21.64/33.68	2 (12)	−3.3 (1.2)	63 (13)

Table 1. The random allocation sequence was computer-generated in a permuted block randomization designed by the associate statistician using certificated randomization software (Rancode 3.6 Professional, IDV, Gauting, Germany).

2.2. Methods

2.2.1. Computer-Assisted Minimally Invasive Femur First THR (CAS FF). In the CAS Femur First group, an imageless navigation system (BrainLAB Navigation System Prototype Hip 6.0 "Femur First", Feldkirchen, Germany) with newly developed prototype software was used [13].

2.2.2. Conventional Minimally Invasive THR (CON). Acetabular components were placed "freehand" without the use of any alignment guides. The target acetabular component position for all patients was within the "safe zone" as defined by Lewinnek et al. 18 (40°± 10° inclination and 15 ± 10°, anteversion) [27].

2.2.3. Gait Analysis (GA). Sixty patients performed a 3D motion-capture (mocap) gait analysis of the lower extremity (SimiMotion, Unterschleißheim, Germany) at three time points (preoperative ($t0$), 6 months postoperative ($t1$), and 12 months postoperative ($t2$)). Only patients that were able to conduct a valid gait experiment (strike one force plate with one foot) were included in the GA-study. A bony and anatomical landmark based marker-set consisting of 27 retroreflective markers was previously tested to record the patient-specific gait pattern by means of six digital video cameras with a video sample rate of 70 Hz [28]. The patients walked at self-selected speed on a 10 m walkway, while the ground reaction forces were recorded simultaneously using two force plates (Kistler, Winterthur, Schweiz; sample rate: 1000 Hz). In order to calculate joint position based on marker data, a static trial was conducted before the gait experiment started. Prior to recording, the patients were asked to walk on the walkway three to five times in order to acquaint themselves with the laboratory situation. One patient missed $t1$-gait analysis but returned for the $t2$-analysis.

2.2.4. Musculoskeletal Modeling (MM). The measured ground reaction forces and trajectories of the mocap markers retrieved during gait analysis were used as the input for the musculoskeletal model to compute the vectorial joint reaction forces during walking (Figure 2). Musculoskeletal analysis was conducted using a commercial software package (AnyBody Technology A/S, Aalborg, Denmark). A generic and previously validated model [29, 30] (AnyGait, AMMR1.6) was first scaled based on anthropometric measurements as an initial guess [31]. This was followed by a nonlinear scaling algorithm based on the maker data gathered during the static trial, further adapting the model to the patient specific anatomy [22]. The hip reaction forces were computed for one complete gait cycle with 150 computation steps for every model (Figure 2). The muscles were parameterized using the mechanical Hill-Type Muscle model, the tendons have been calibrated accordingly [32]. The time-dependent muscle activity is determined by a cubic optimization scheme and according to (1). Consider

$$G = \sum_i \left(\frac{\mathrm{mf}_i}{N_i} \right)^3, \tag{1}$$

where G is the objective function to estimate muscle activation, mf is the muscle force vector (mf_i is the ith element) and N is the normalizing factor (muscle strength) [33]. G is to be minimized while the boundary conditions have to be satisfied (equilibrium fulfilled, muscles can only pull). The 179 MM in total were batch-processed with the aid of parallel computing, allowing eleven models to be computed at the same time using Matlab (Matlab Release 2013a, The MathWorks, Inc., Natick, Massachusetts, United States.).

2.2.5. Method Verification. The measurement chain was evaluated with respect to different sources of variance (Table 2). Three healthy volunteer male subjects were invited (S1: 19 years, 79.4 kg, 1.73 m; S2: 25 years, 70.4 kg, 1.69 m; S3: 31 years, 73.4 kg, 1.82 m) to perform mocap gait analysis. The scope of the verification study was to evaluate the measurement chain and not to conduct a population study; hence such a narrow patient collective was acquired. Data was processed with the same workflow as for the patient study. To evaluate the measurement chain the standard error of mean (SEM) of the respective target parameter (Table 2) was computed according to (2) with n samples and a sample standard deviation σ [34]. Consider

$$\mathrm{SEM}\left(\overline{X}\right) = \frac{\sigma}{\sqrt{n}}. \tag{2}$$

2.2.6. Model Validation. The hrf retrieved from our patient cohort were compared to the publicly available hip 98 dataset (http://www.orthoload.com/) [17]. Hrf retrieved from healthy individuals were checked against literature data, which were obtained by using similar workflows [35].

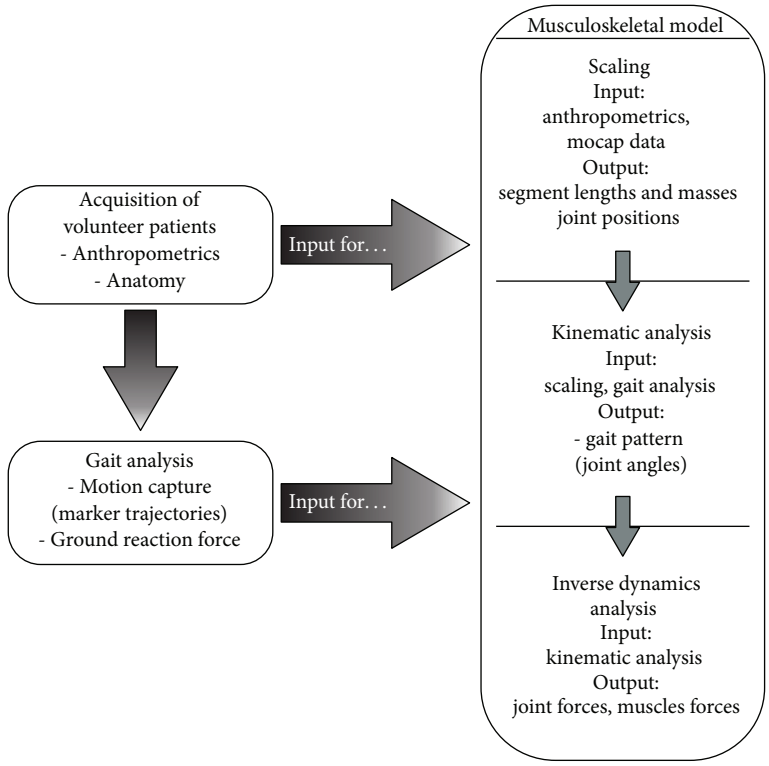

Figure 2: Study workflow combining experimental data with numerical simulations during gait.

Table 2: Different sources of variance of the measurement chain and the studies in order to determine the standard error of mean.

Research question	Source of variance	Study	Target parameter
Is the result obtained dependent on the mocap analyst?	Mocap analyst	One healthy subject (S1), 1 gait analysis, evaluated 10 times by 3 different examiners: A (experienced), B (experienced), and C (not experienced)	Standard error of mean (SEM) of hrf-HRF_{SEM}
How big is the influence of marker-placement on the results obtained?	Mocap—marker placement	One healthy subject (S1), 10 gait analyses, application of marker set in alternating manner by 2 analysts: A (experienced) and B (experienced)	HRF_{SEM}
Is the method robust enough to produce repeatable results?	Measurement chain	Three healthy subjects (S1, S2, and S3), 10 gait analyses, evaluated by 1 experienced analyst (A)	HRF_{SEM}

2.2.7. Dynamic Time Warping. While arithmetic means can only be formed at corresponding time-points $f(t_i)$, dynamic time warping is based on comparing every time-point $f_1(t_{1,\dots,k})$ to every time-point $f_2(t_{1,\dots,k})$. This is done by computing the dtw matrix according to Bender and Bergmann and according to (3). Consider

$$d\left(f_1\left(i_1\right), f_2\left(i_2\right)\right) = \left(\alpha^2\right)\left(\frac{f_1\left(i_1\right)}{\left\|f_1\right\|} - \frac{f_2\left(i_2\right)}{\left\|f_2\right\|}\right)^2 + (1-\alpha)^2\left(\frac{f_1'\left(i_1\right)}{\left\|f_1'\right\|} - \frac{f_2'\left(i_2\right)}{\left\|f_2'\right\|}\right)^2. \quad (3)$$

The two signals are then connected by minimizing the cumulated costs (4) along the "dtw path" ((5), Figure 3) [23]. Consider

$$\mathrm{CC} = \sum_{i_k=1}^{N_k} d\left(f_1\left(w\left(i_k\right)\right), f_2\left(w\left(i_k\right)\right)\right), \quad (4)$$

$$w\left(i_k\right) = \left[\left(i_1\left(i_k\right)\right), \left(i_2\left(i_k\right)\right), i_k = 1, 2, \dots, N_k\right]. \quad (5)$$

By minimizing the cumulated cost dtw takes the most "similar" values into account and permits the computation of a "typical signal" (TS) rather than comparing fixed time points $f_{1,2}(t_{1,\dots,k})$. While the difference between the mean signal and the TS is negligible when comparing "similar

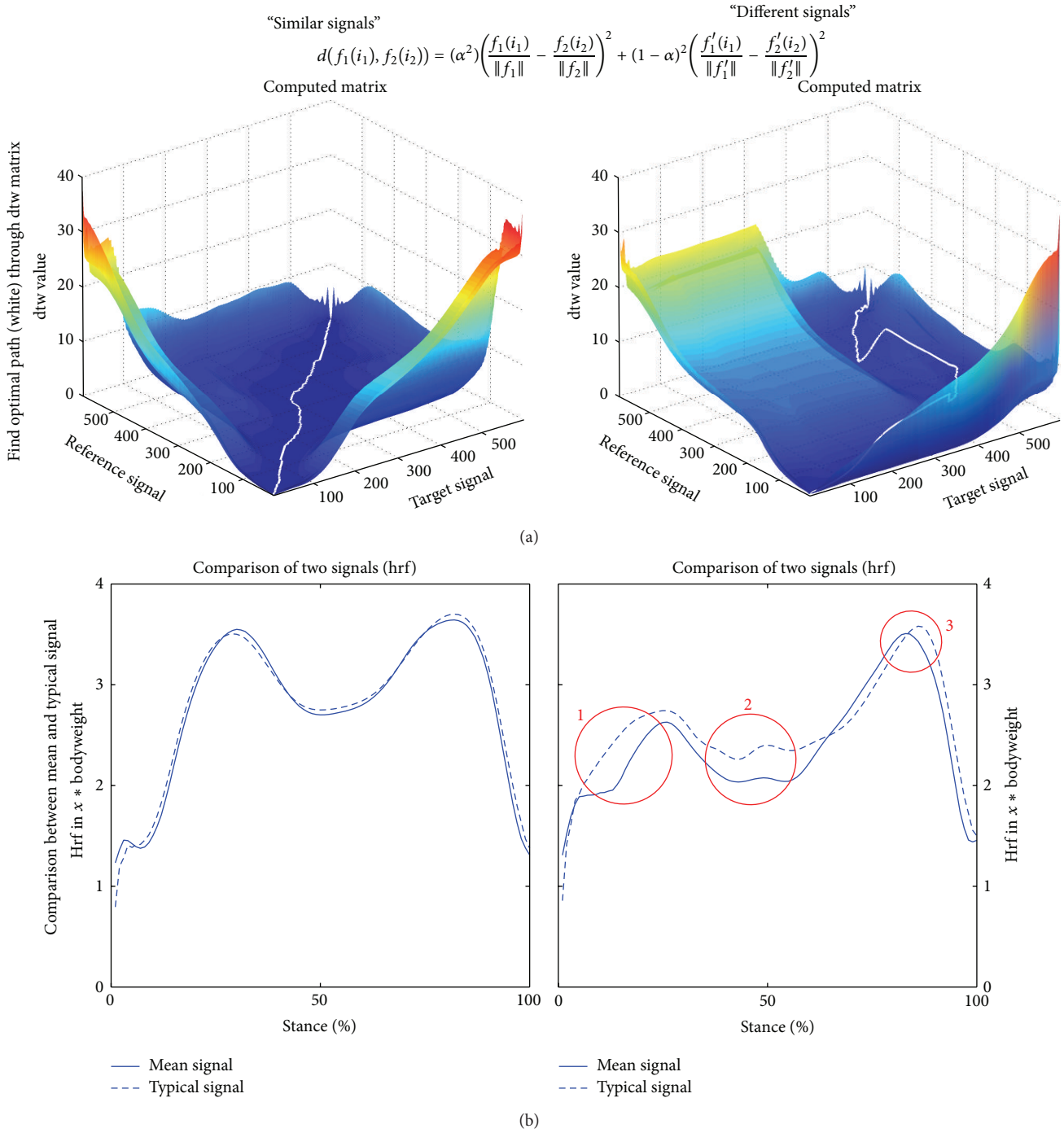

FIGURE 3: Using dtw for computing the TS from "similar" or "different" signals, respectively. (a) dtw matrix with optimized path (white) for similar (left) and varying (right) signals. (b) Comparison of mean signal (full line) and TS (dashed line) from the similar signals (left) and varying signals (right). For similar signals there is practically no difference between the mean signal and the TS. When comparing varying signals the TS yield different characteristics (red circles). Circle 1: no sharp cutoff, appears to be more harmonically, circle 2: peak is underestimated in mean signal, and circle 3: peak values between mean signal and TS are practically the same.

signals" (Figure 3), the strength of dtw is comparing varying signals, as it is often the case when comparing joint reaction forces during walking (Figure 3) [23]. By weighting the signals accordingly, it is also possible to compute the TS from more than two signals, as it was done for the comparison of the CAS FF and CON group.

The path length is a measure of phase shift between two signals (Figure 3). The cumulated cost along the path is

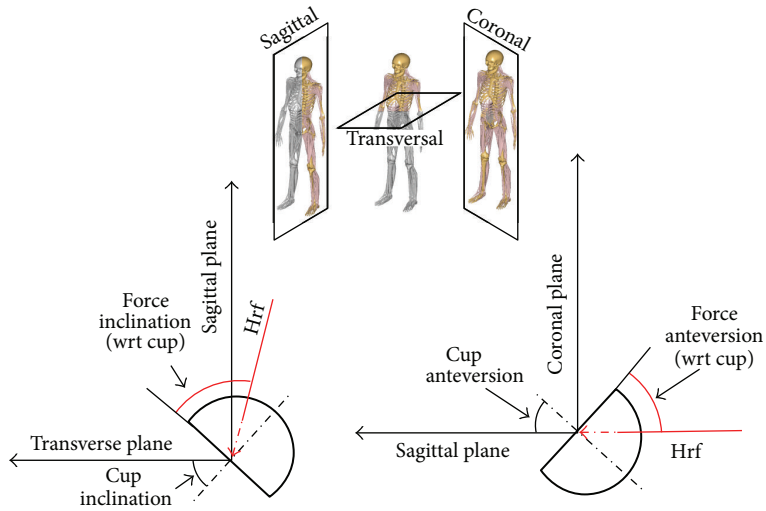

FIGURE 4: The definition of force orientation which is based upon the definition of acetabular orientation in the radiographic coordinate system according to Stansfield and Nicol [35].

a measure of magnitude similarity. Asymmetries are being computed between the operated and not-operated leg at $t0$, $t1$, and $t2$, as well as between the operated leg and a normative dataset at $t0$, $t1$, and $t2$.

2.2.8. Postprocessing. Bagplots are used to visualize the distribution of bivariate statistical data [36]. The greater the area that is being enclosed, the wider the data is scattered and the more asymmetrical the patients walk in terms of hrf. Postprocessing was done using Matlab. Hrf orientations are quantified in the radiographic coordinate system according to Murray (Figure 4) [37].

2.2.9. Statistics. ANOVA tests for unequal sample size ($n_{\text{CASFF}} = 28, n_{\text{CON}} = 32$) including group interactions were performed for all time-points ($t0$, $t1$, $t2$) divided by intervention groups on asymmetry parameters. Significance level was set at 5% ($\alpha = 0.05$). Differences between intervention groups in terms of age, BMI, blood-loss, and operation time were tested using the student's t-test ($\alpha = 0.05$) or with a chi-squared test ($\alpha = 0.05$) for categorical data such as the ASA score.

3. Results

3.1. Patient—Characteristics. The groups showed no significant differences in terms of age, BMI, blood loss, and disease category (ASA-score). The operation time of the CAS FF group was significantly higher.

3.2. Method Verification. Figure 5 displays the verification study results. The mocap-analyst has a negligible influence on the target parameters. Marker Placement has the greatest influence on the target parameters. The repeatability study shows that results are indeed robust, but care must be taken when conducting experiments. A SEM of ±0.25 BW is an estimate of how accurate the hrf during walking can be computed. On the right hand side the maximum hrf of the normal subjects as computed with the aforementioned workflow are compared to literature (normal subjects, computed hrf) [35] (Figure 5). 97.8% of all models compute hrf that lie within the 95% (±1.96SD) confidence interval as published by Stansfield and Nicol [35]. We therefore considered the models valid for this study.

3.3. Model Validation. Figure 6 displays the comparison of computed hrf against measured hrf (hip98, http://www.orthoload.com/). Measured hrf were obtained from four subjects and between 11 and 31 months postop [17]; therefore the measured hrf are shown against the computed hrf at $t2$. The results show good agreement, especially at the first peak. The second peak seems to be overestimated by the computed hrf, but one should note that the measured hrf have been obtained by only four subjects, making valid statistical analysis challenging. The maximum hrf are up to twofold higher than measured ones; however such magnitudes have been reported for healthy subjects [35]. The models were considered valid for this study.

3.4. Typical Signal (TS) of Hrf. The TS as computed by dtw including the normalized walking speed according to Hof are shown in Figure 7 [38]. The dimensionless walking speed increases significantly over all follow-up points, there are no significant differences between the two groups. While the hrf at $t0$ are in the same magnitude and similar shape for both groups, the hrf are increasing over the follow-up period. There are notable differences between the hrf at $t1$ for both groups, the hrf in the CON group are greater when compared to the CAS FF group (0.4 BW), bearing the SEM of ±0.25 BW in mind. At $t2$ the hrf of the CAS FF group are further increasing until becoming more similar to the healthy group in terms of magnitude and shape. At the second hrf peak of

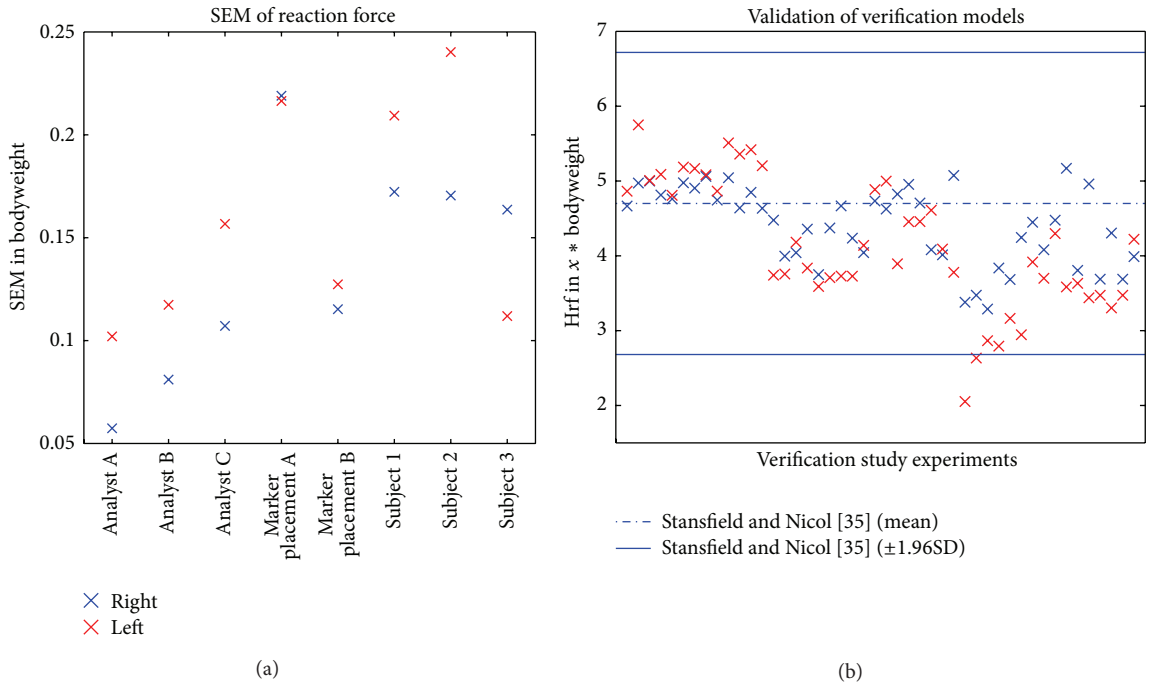

FIGURE 5: Results of the verification experiments. (a) SEM of hrf as computed by different verification studies. (b) Comparison of verification model with literature data [34] including 95% confidence interval (±1.96SD) of the literature data.

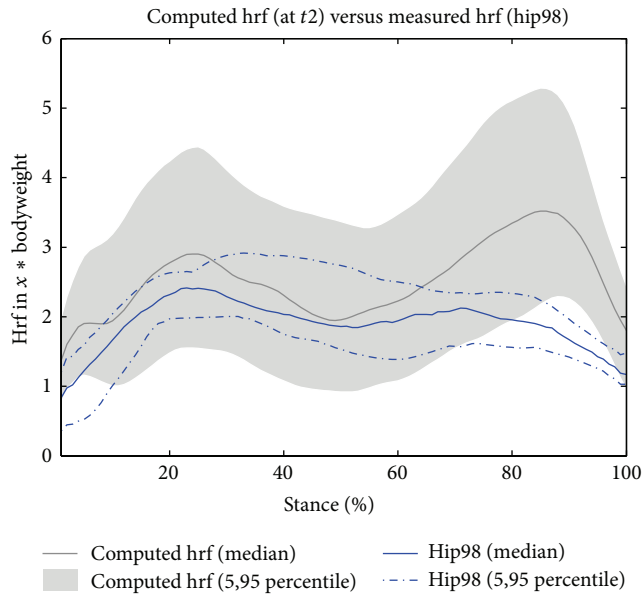

FIGURE 6: Validation study of patient models. The computed hrf are compared to the measured hrf (hip98-data). The hrf in multiples of bodyweight (y-axis) are displayed as a function of stance phase (0–100%, during walking). The gray area indicates the 5 and 95 percentile for (all) hrf (operated side) at $t2$, the dark gray line represents the median thereof. The blue lines represent either the hip98 median hrf (full line) or the 5 and 95 percentile (point-dashed line).

the CAS FF group there is practically no difference to data retrieved from young, healthy adults. The hrf of the CON group do not further increase.

3.5. Symmetries of Hrf. Figure 8 displays the time series similarities of joint reaction forces as computed by dtw by means of bagplots [36]. Figure 8(a) shows the comparison of operated leg versus not-operated leg. Asymmetry measures are the greatest in the CAS FF group at $t0$; thus, those patients were walking preoperative more asymmetrical than patients in the CON group, but this was not significant. During the follow-up period both groups improve significantly in

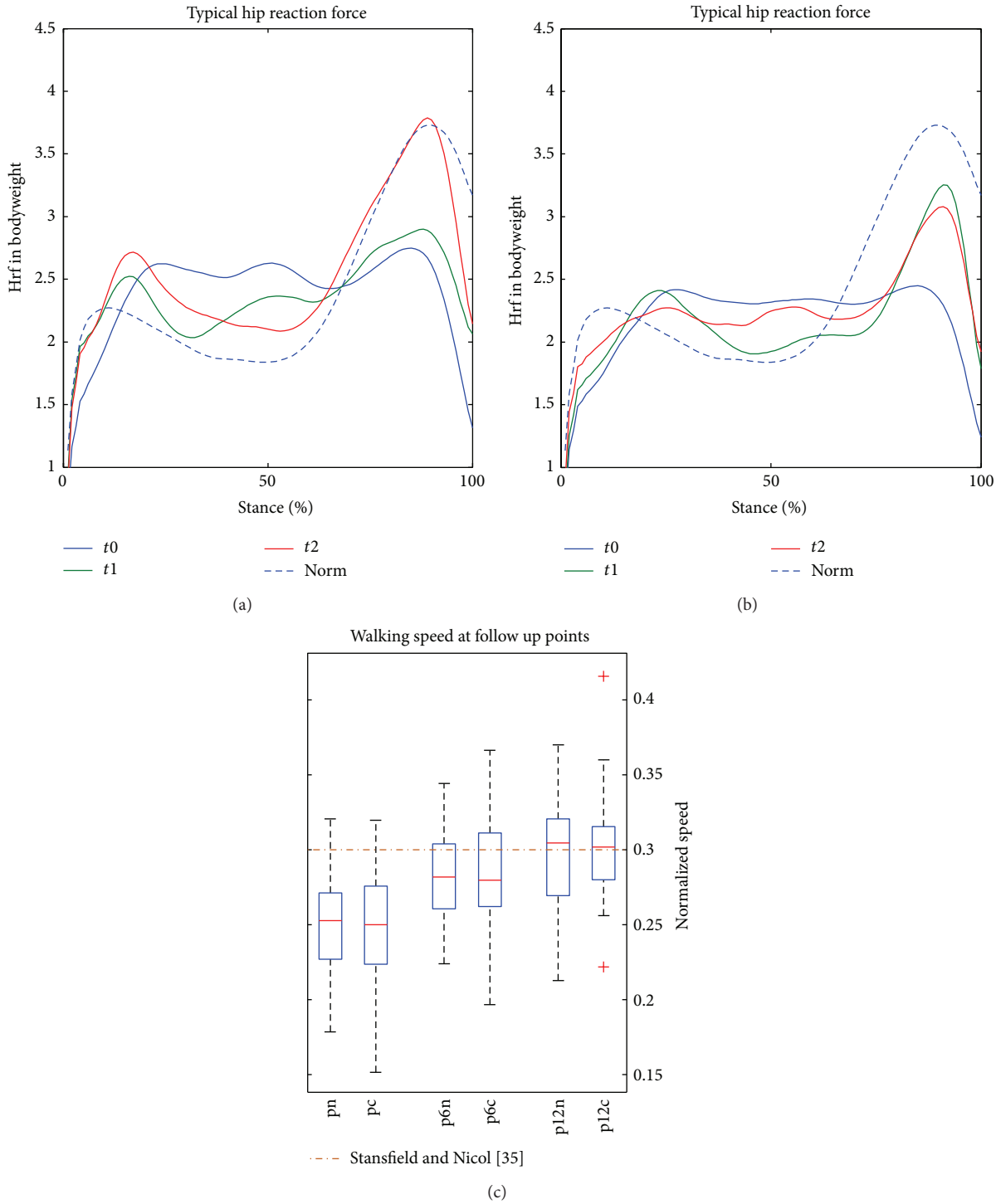

FIGURE 7: The TS of the different THR-groups. (a) The hrf of the CAS FF group at the different follow-up points can be seen (blue: $t0$, green: $t1$, red: $t2$). The x-axis denotes the stance-phase in percent; the y-axis shows the hrf in multiples of bodyweight. The dashed line is the TS of the healthy group as gathered during the method verification experiments. (b) Results for the CON group (blue: $t0$, green: $t1$, red: $t2$). (c) Dimensionless walking speed computed according to Hof [38] at different follow-up points is displayed, as well as literature data for THR patients [35] (point-dashed, dark red line).

phase shift similarity as well as in magnitude similarity, thus patients are walking less asymmetrical at $t2$. Figure 8(b) displays the joint-reaction force time series of the operated leg compared against the normative data. Preoperative values of the CAS FF group are not as scattered as for the CON group, but the difference was not significant. Phase shift and magnitude symmetry increases in both groups significantly, larger improvements can be found for the CAS FF group. In

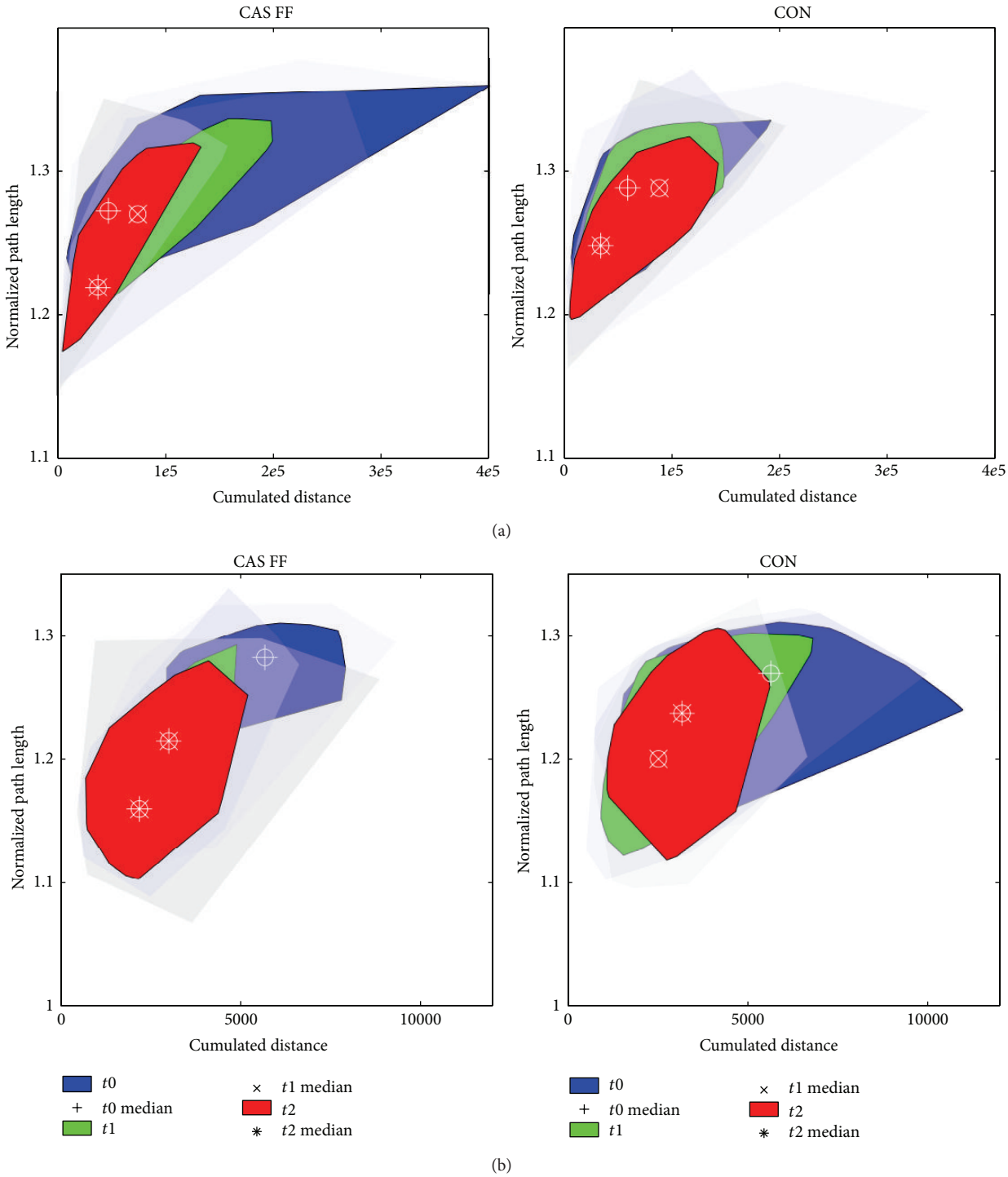

FIGURE 8: Bagplots of the deviation of joint reaction force time series as computed by dtw. On the left row the CAS FF group is displayed whereas on the right side the CON group is shown. On all x-axes one can see the cumulated distance as computed by (4) (magnitude similarity), whereas on all y-axes the normalized path length as computed by (5) (phase shift similarity) is displayed. (a) Comparison of hrf time series for operated versus not operated side at the follow-up points. (b) Comparison of hrf time series for operated versus normative data at the follow-up points.

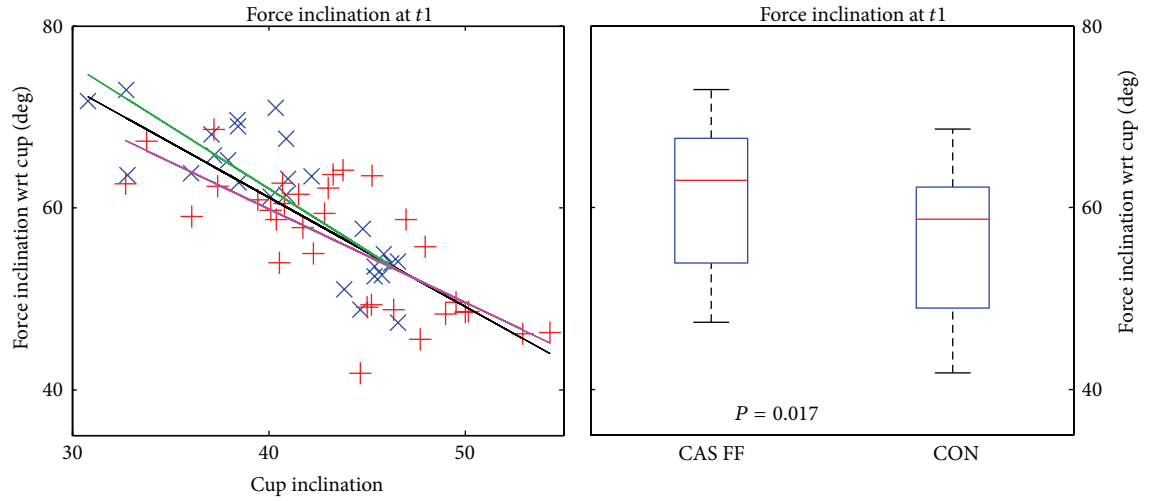

(a)

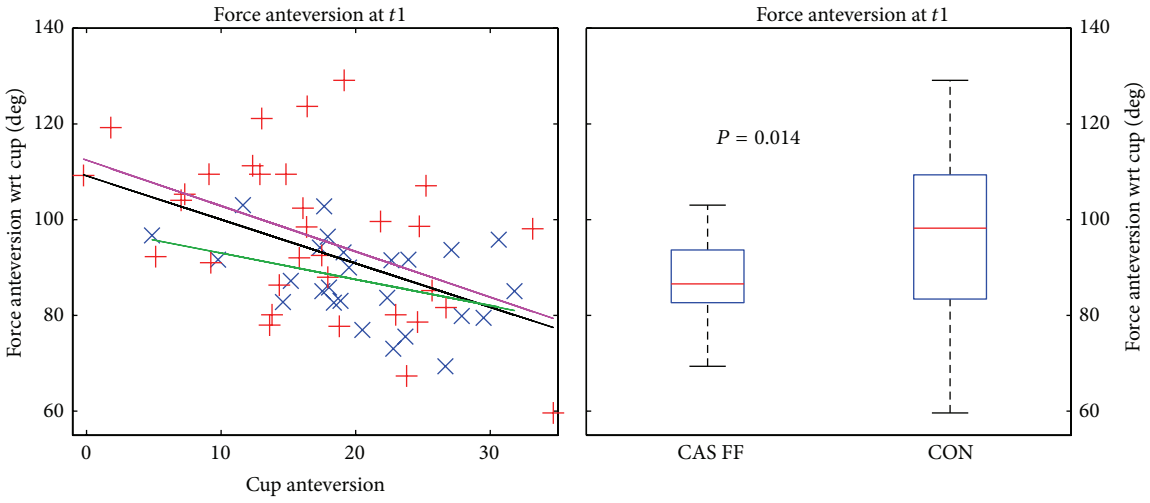

(b)

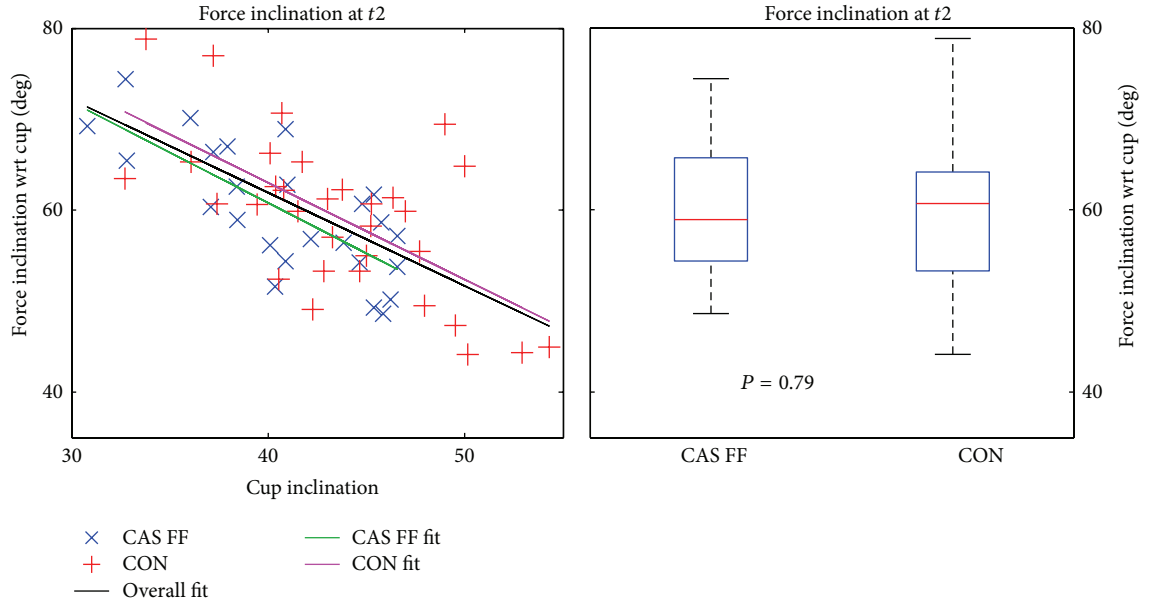

(c)

Figure 9: Continued.

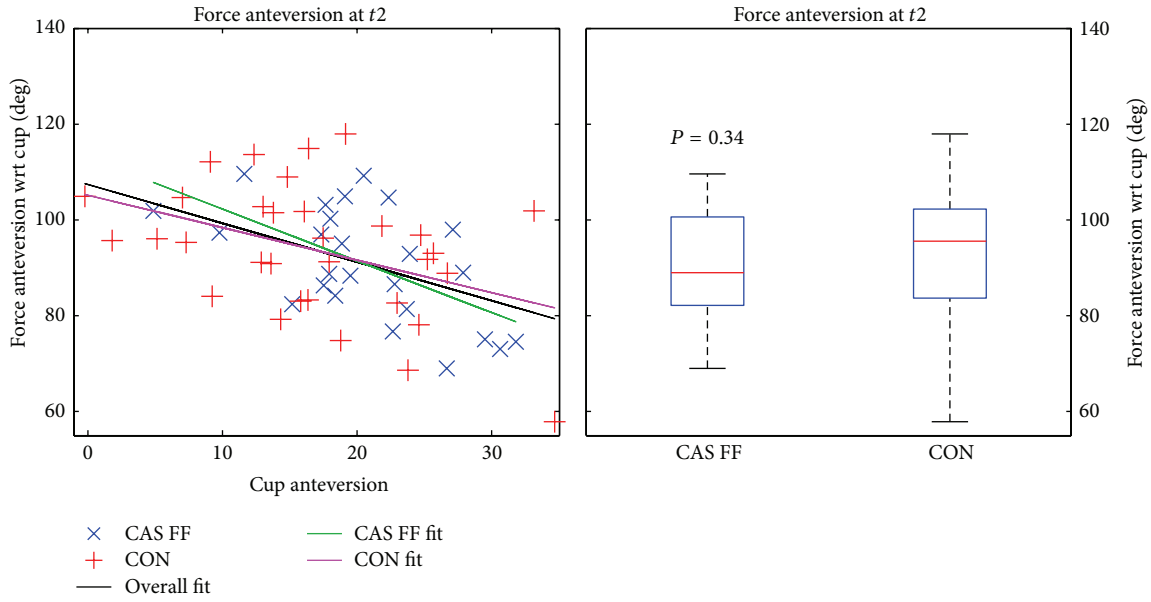

(d)

Figure 9: The hrf orientation at peak loads of the CAS FF and the CON group was compared. Left: hrf orientation as a function of cup orientation, including linear regression lines (black: overall regression; green: regression line for CAS FF group; magenta: regression line for CON group). Blue cross: CAS FF, red plus: CON. Right: boxplot of the hrf orientation at peak loads for the CAS FF and the CON group. (a) Force inclination at $t1$, (b) force anteversion at $t1$, (c) force inclination at $t2$, and (d) force anteversion at $t2$.

Table 3: Measure for the relationship between cup orientation and force orientation wrt cup at $t1$ and $t2$.

	Overall	CAS FF	CON
$t1$			
Inclination			
Pearson correlation coefficient (R)	−0.79	−0.83	−0.74
Significance of correlation (P)	$9.0e-14$	$1.3e-07$	$1.3e-06$
Anteversion			
Pearson correlation coefficient (R)	−0.49	−0.41	−0.48
Significance of correlation (P)	$8.6e-05$	0.039	$5.8e-03$
$t2$			
Inclination			
Pearson correlation coefficient (R)	−0.66	−0.74	−0.64
Significance of correlation (P)	$1.7e-08$	$2.1e-05$	$7.2e-05$
Anteversion			
Pearson correlation coefficient (R)	−0.48	−0.58	−0.41
Significance of correlation (P)	0.0001	0.002	0.019

Table 4: Fit parameters for the linear model $f(x) = a \cdot x + b$ for force orientation wrt cup orientation at $t1$ and $t2$ $x[\text{cup}_{\text{degree}}]$.

	a ($\text{force}_{\text{degree}}/\text{cup}_{\text{degree}}$)	b (degree)
$t1$		
Inclination		
Overall	−1.2	109.3
CAS FF	−1.4	116.8
CON	−1.0	101.1
Anteversion		
Overall	−0.9	109.2
CAS FF	−0.6	98.4
CON	−1.0	112.4
$t2$		
Inclination		
Overall	−1.0	102.9
CAS FF	−1.1	105.2
CON	−1.1	105.6
Anteversion		
Overall	−0.8	107.3
CAS FF	−1.1	113.0
CON	−0.7	105.2

particular, phase shift similarity at $t2$ increased in the CAS FF group more than in the CON group which is also supported by the hrf-TS (Figure 7).

3.6. Orientation of Hrf at Peak Loads. Figure 9 shows the force inclination and force anteversion at $t1$ and $t2$ respectively. The force inclination with respect to cup correlates significantly with the cup inclination in a linear fashion ($f(x) = a \cdot x + b$) as does the anteversion at both follow-up points (Table 3). The coefficient of determination (r^2) is greatest at $t1$ for inclination of the CAS FF group (69% variance explained by linear model—Table 2). Roughly 25% variance is explained by the linear model for the anteversion angle. The variance explained for inclination decreases to 55% at $t2$ as does the correlation coefficient ($-0.83 \rightarrow -0.74$). At all follow-up points we performed a significance test

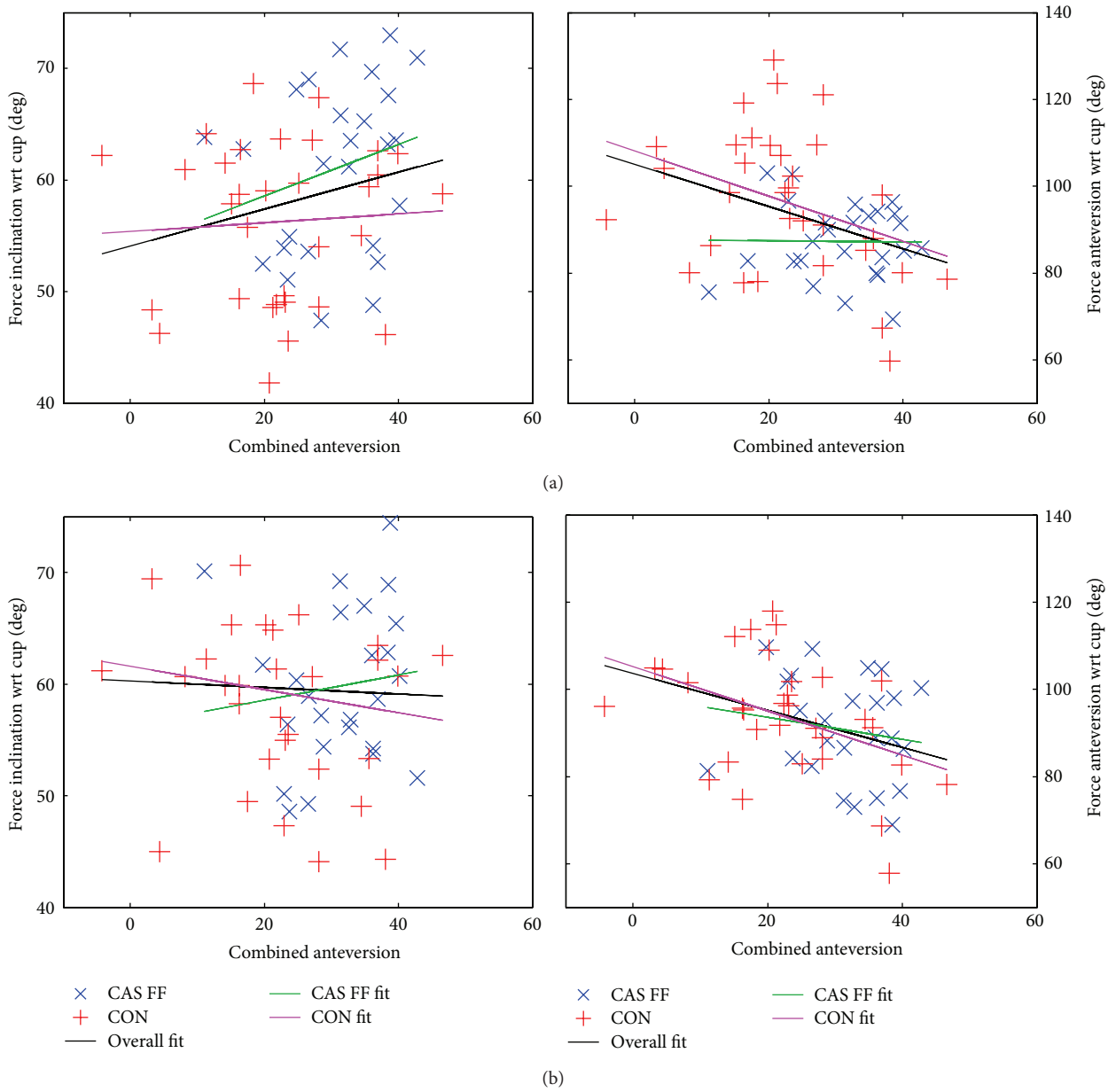

Figure 10: The hrf orientation at peak loads of the CAS FF and the CON group versus the combined anteversion. Left: hrf inclination as a function of combined anteversion, including linear regression lines (black: overall regression; green: regression line for CAS FF group; magenta: regression line for CON group). Blue cross: CAS FF, red plus: CON. Right: hrf inclination as a function of combined anteversion, including linear regression lines (a) force orientation at $t1$ and (b) force orientation at $t2$.

(student's t-test, alpha = 5%) between the CAS FF and the CON group for the force angles. We found significant differences for both angles at $t1$, which vanished at $t2$. Patient that underwent CAS FF surgery showed force-angles closer to optimum (force angle = 90°—force attacks at center of hemisphere). Table 4 lists the coefficients of the linear fit, showing good agreement for inclination angles. Deriving a linear regression line for the anteversion is also possible, but not with the same quality as for inclination (Table 3).

3.7. Orientation of Hrf at Peak Loads with respect to Combined Anteversion. Figure 10 shows the force orientation (force inclination and force anteversion) as a function of the combined anteversion. There is no relationship between the force orientations of the CAS FF group (Table 5). The force anteversion of the CON group shows a significant but weak relationship to the combined anteversion (Table 5). The significant but weak relationship between the combined anteversion and the force anteversion for both groups is a result of the weak correlation for the CON group. Even if there is a relationship between combined anteversion and force orientation for the CON group, only a maximum of 13% of the variance of the data points can be explained, indicating once more influences of other unknown factors.

Table 5: Measure for the relationship between combined anteversion and force orientation wrt cup at $t1$ and $t2$.

	Overall	CAS FF	CON
$t1$			
Force inclination			
Pearson correlation coefficient (R)	0.23	0.24	0.06
Significance of correlation (P)	0.08	0.23	0.74
Force anteversion			
Pearson correlation coefficient (R)	−0.37	−0.01	−0.36
Significance of correlation (P)	0.00	0.95	0.04
$t2$			
Force inclination			
Pearson correlation coefficient (R)	0.03	0.12	0.00
Significance of correlation (P)	0.84	0.56	0.99
Force anteversion			
Pearson correlation coefficient (R)	−0.31	−0.16	−0.35
Significance of correlation (P)	0.02	0.44	0.047

4. Discussion

The purpose of this study was to compare the hrf and their orientation between CAS FF and conventional THR.

The TS of the hrf shows improvement for the CAS FF group at the endpoint $t2$ when compared to normative data. Stansfield and Nicol report similar walking speed for THR patients postoperatively at comparable follow-up points [35]. Both groups performed approximately the same at $t0$, even if the asymmetries were greatest for the CAS FF group at $t0$. The fact that the hrf are decreasing between $t1$ and $t2$ in the CON group can be attenuated to measurement noise. Hrf, as an integral measure for muscle forces, are crucial for bone remodeling and bone in-growth [39, 40]. Therefore restoring the hrf to young healthy adult ones, as we observed it in our study for the CAS FF group, is the benchmark outcome for THR. Asymmetries of operated versus not-operated side in the CAS FF group decrease more than in the CON group, but the effect seems to be insignificant. It is important to also include the asymmetries of operated side versus normative data, since walking can also be symmetrical if both sides perform equally poor. The CAS FF THR group walks closer to a healthy normal, especially at $t2$ in terms of phase shift, meaning local maxima and minima are more likely to occur at the same time of a gait cycle as for a young healthy adult. This indicates a restored ability to walk [41] possibly resulting in a long-term benefit for the patients operated with CAS FF with functional optimization. Such long-term benefit remains to be proven which can only be achieved with additional follow-up points. At $t1$ the TS hrf of the CON group are closer to a healthy normal, but the force orientation for the CAS FF group is closer to optimum than in the CON group. Not only hrf magnitude is crucial for the implant survivorship, but also the orientation of the hrf [21]. Hrf that are closer to the edge of acetabular cup may result in edge or rim-loading, therefore increasing wear and compromising implant-survivorship [16]. While the hrf anteversion and inclination in the CAS FF group appears to be more favorable, the hrf orientation in the CON group is still noncritical, when taking into account that the inlay of the cup gets thinner on the edge (pinnacle/duraloc) due to manufacturing reasons [42]. Measurements taken from Effenberger and Hrsg [43] show that there are indeed cups where force orientation such as presented would result in rim-loading, but especially wear computations are necessary to identify critical regions in the cup [44] to back up this hypothesis. The significant difference in hrf orientation with respect to cup between the CAS FF and CON groups vanishes at $t2$, indicating that over the follow-up period the orientation as found in the CON group adjusts to similar hrf orientations found in the CAS FF group becoming closer to optimum. Our data suggests that the CAS FF procedure with functional optimization is especially beneficial at an early stage and has the potential to decrease the propensity for rim-loading and therefore dislocation and impingement within the first weeks after surgery. We also investigated a possible linear relationship between cup angle and force orientation and found a significant correlation between the force inclination and cup inclination at $t1$ with a high coefficient of correlation (−0.75). The other angles also revealed a nonzero relationship but the explained variance decreases over follow-up period (Table 3). This indicates that with a greater cup inclination and/or anteversion the angle between the resultant hip reaction force and the rim of the cup decreases. Therefore the resultant hip reaction force gets closer to the rim of the cup. This relationship becomes indeed valuable, when thinking of applying these results to either preoperational planning or real-time biomechanical feedback during surgery, which only CAS systems could provide. The fact that the correlation coefficient decreases over the follow-up period shows that other influences may play an important role (implant shaft, gait pattern) and that the relationship is multi-factorial. The weak or nonexistent relationship between the combined anteversion and force orientation supports this assumption. The force orientation cannot only be solely explained with implant orientation. This shows that for the definition of an implant safe-zone based on biomechanical evaluations the patient-specific anatomy and integral motion pattern is of vital importance. Based on such biomechanical evaluations a patient-specific optimal implant safe-zone may exist, which remains to be proven.

To the authors knowledge this is the first study that includes musculoskeletal models of gait in a prospective randomized controlled trial studying the computer-assisted femur first technique in relation to conventional THR. Other studies have been conducted to either study early outcome of standard CAS after THR by means of gait analysis [45] or to study the influence of surgical approach on gait parameters [46, 47]. The results of the gait analysis of these studies are mostly concise with our findings. There are no differences in temporospatial parameters such as walking speed or kinematic parameters. One study also compared muscle activation profiles of patients that underwent either MIS or conventional THR during walking which also did not reveal any significant differences [46]. MM have also been employed to study the outcome of THR but only on an individual basis or with a small, not randomized study population [16, 21, 48]. They all used the same validated musculoskeletal model and

investigated similar parameters (edge-loading, total hrf). No evidence of occurring edge-loading in the studied population was found, which agrees with our findings.

4.1. Strengths. We investigated a rather large patient cohort, speaking for this kind of study (combining gait analysis with MM), which was also patient and observer blinded. To our knowledge this is the first study that has used this specific novel navigation algorithm in clinical practice. To the best of our knowledge this is also the first study ever with a patient- and observer-blinded, prospective randomized controlled study design on navigation in THR that has been published in the literature. The validated MM were highly patient-specific and we are confident that the models reflect the in vivo loads as accurate as possible using such a workflow. Comparing strongly varying signals by means of dtw has the advantage to not only focus on particular time points of signal time series. It rather compares all time-points to all time-points. This makes subjective and observer based decisions obsolete. To our knowledge and based on Bender and Bergmann [23] the TS as computed by dtw is the best representation of typical patterns as they occur in time series.

4.2. Limitations. Since the MM are purely mechanical models, psychological effect are cancelled out. By also analyzing clinical outcome scores (such as the Harris Hip Score (HHS) or the hip osteoarthritis outcome score (HOOS)) we tried to counter such effects; however the scores revealed no differences at $t1$ or $t2$, respectively. The movement of the upper body has not been quantified using motion capture. The measurement volume of the mocap is too small to effectively capture the movement of the body segments above the pelvis. The integral movement of the upper body has been approximated by mechanically balance the center of mass above the pelvis. This does not however reflect the movement, it is rather an approximation. We also did not include the patients' physical activity (PA) particularly. Evaluating the individual PA is very challenging, since the methods to evaluate PA are biased or can be deceived easily [49]. Gait performance in the laboratory may reflect the level of PA in and that is how we included this effect. Patients with higher levels of PA may recover faster than others. Therefore the results may be biased due to PA level of every particular patient. This is an effect that can only be countered by evaluating large patient cohorts. Even though the biomechanics are crucial for the functioning of one of the largest and weight-bearing joints in the human body, it is not completely sure that improved biomechanics also leads to an improved clinical outcome. Current research however shows that improved biomechanics leads to an improved outcome for the patient [50, 51]. Also biomechanical parameters have been found to be clinically relevant [52].

4.3. Clinical Relevance. We suggest practical application for our work such as operational planning based on biomechanical parameters (preop gait pattern, orientation of cup versus hrf orientation) by deriving simple laws and algorithms from the data. The results can also be used for real-time biomechanical feedback during CAS which is a scope for further research. A new safe-zone for implant component position and orientation is also thinkable, which relies on an accurate statistical model. This would draw the focus of implant positioning rather on analytical laws then experience. Future research will also include detailed finite element models based on patient specific medical imaging data and patient-specific muscle forces and boundary conditions. Such modeling will give more insight into implant bone contact stresses and wear in the hip joint, both are important for the prediction of implant survivorship.

5. Conclusion

The computer-assisted THR method following the concept of femur first/combined anteversion does lead to an improved outcome in contrast to conventional THR six month after surgery. In Particular, force orientation is close to optimum for the novel CAS Femur First technique at an early stage. A trend for decreased asymmetries of the gait pattern of the CAS FF group compared to the CON group indicates a restored walking ability and therefore a possible long-term benefit for the patients; however this hypothesis can only be proven by repeating the experiments at additional follow-up points.

Conflict of Interests

The authors declare that there is no conflict of interests regarding the publication of the paper.

Acknowledgments

This work received funding from DePuy International, Leeds, UK, as well as from "Technologie und Wissenstransfer Ostbayern." The authors are also grateful for support from Mr. Süß, Regensburg Center of Biomedical Engineering, for help with the dtw algorithm, Mr. Zeman, Universitätsklinikum Regensburg, Zentrum für klinische Studien, for support in the statistical analysis, and Mr. Waller, Universität Regensburg, British Studies for the revision of this paper.

References

[1] I. D. Learmonth, C. Young, and C. Rorabeck, "The operation of the century: total hip replacement," *The Lancet*, vol. 370, no. 9597, pp. 1508–1519, 2007.

[2] K. J. Bozic, S. M. Kurtz, E. Lau, K. Ong, D. T. P. Vail, and D. J. Berry, "The epidemiology of revision total hip arthroplasty in the united states," *The Journal of Bone & Joint Surgery*, vol. 91, no. 1, pp. 128–133, 2009.

[3] S. Graves, D. Davidson, and A. Tomkins, "Australian Orthopaedic Association National Joint Replacement Registry Annual Report 2013," Adelaide, Australia, 2009.

[4] D. Emsley, J. Martin, C. Newell, and M. Pickford, *National Joint Registry for England and Wales: 5th Annual Report, 2008*, 2012.

[5] A. Malik, A. Maheshwari, and L. D. Dorr, "Impingement with total hip replacement," *Journal of Bone and Joint Surgery A*, vol. 89, no. 8, pp. 1832–1842, 2007.

[6] T. Renkawitz, M. Tingart, J. Grifka, E. Sendtner, and T. Kalteis, "Computer-assisted total hip arthroplasty: coding the next generation of navigation systems for orthopedic surgery," *Expert Review of Medical Devices*, vol. 6, no. 5, pp. 507–514, 2009.

[7] C. S. Ranawat and M. J. Maynard, "Modern technique of cemented total hip arthroplasty," *Techniques in Orthopaedics*, vol. 6, no. 3, pp. 17–25, 1991.

[8] K. H. Widmer and B. Zurfluh, "Compliant positioning of total hip components for optimal range of motion," *Journal of Orthopaedic Research*, vol. 22, no. 4, pp. 815–821, 2004.

[9] L. D. Dorr, A. Malik, M. Dastane, and Z. Wan, "Combined anteversion technique for total hip arthroplasty," *Clinical Orthopaedics and Related Research*, vol. 467, no. 1, pp. 119–127, 2009.

[10] K.-H. Widmer, "Containment versus impingement: finding a compromise for cup placement in total hip arthroplasty," *International Orthopaedics*, vol. 31, supplement 1, pp. S29–S33, 2007.

[11] T. Renkawitz, M. Haimerl, L. Dohmen et al., "Minimally invasive computer-navigated total hip arthroplasty, following the concept of femur first and combined anteversion: design of a blinded randomized controlled trial," *BMC Musculoskeletal Disorders*, vol. 12, article 192, 2011.

[12] T. Renkawitz, M. Haimerl, L. Dohmen et al., "The association between Femoral Tilt and impingement-free range-of-motion in total hip arthroplasty," *BMC Musculoskeletal Disorders*, vol. 13, article 65, 2012.

[13] T. Renkawitz, M. Haimerl, L. Dohmen et al., "Development and evaluation of an image-free computer-assisted impingement detection technique for total hip arthroplasty," *Proceedings of the Institution of Mechanical Engineers Part H*, vol. 226, no. 12, pp. 911–918, 2012.

[14] E. Ingham and J. Fisher, "Biological reactions to wear debris in total joint replacement," *Proceedings of the Institution of Mechanical Engineers Part H: Journal of Engineering in Medicine*, vol. 214, no. 1, pp. 21–37, 2000.

[15] T. P. Culleton, P. J. Prendergast, and D. Taylor, "Fatigue failure in the cement mantle of an artificial hip joint," *Clinical Materials*, vol. 12, no. 2, pp. 95–102, 1993.

[16] S. J. Mellon, G. Grammatopoulos, M. S. Andersen et al., "Individual motion patterns during gait and sit-to-stand contribute to edge-loading risk in metal-on-metal hip resurfacing," *Proceedings of the Institution of Mechanical Engineers Part H: Journal of Engineering in Medicine*, vol. 227, no. 7, pp. 799–810, 2013.

[17] G. Bergmann, G. Deuretzbacher, M. Heller et al., "Hip contact forces and gait patterns from routine activities," *Journal of Biomechanics*, vol. 34, no. 7, pp. 859–871, 2001.

[18] N. W. Rydell, "Forces acting on the femoral head-prosthesis. A study on strain gauge supplied prostheses in living persons," *Acta Orthopaedica Scandinavica*, vol. 37, supplement 88, pp. 1–132, 1966.

[19] S. Dendorfer, T. Weber, and O. Kennedy, "Musculoskeletal modeling for hip replacement outcome analyses and other applications," *Journal of the American Academy of Orthopaedic Surgeons*, vol. 22, no. 4, pp. 268–269, 2014.

[20] M. E. Lund, M. de Zee, M. S. Andersen, and J. Rasmussen, "On validation of multibody musculoskeletal models," *Proceedings of the Institution of Mechanical Engineers Part H: Journal of Engineering in Medicine*, vol. 226, no. 2, pp. 82–94, 2012.

[21] T. Weber, S. Dendorfer, S. Dullien, J. Grifka, G. J. Verkerke, and T. Renkawitz, "Measuring functional outcome after total hip replacement with subject-specific hip joint loading," *Proceedings of the Institution of Mechanical Engineers H: Journal of Engineering in Medicine*, vol. 226, no. 12, pp. 939–946, 2012.

[22] M. S. Andersen, S. J. Mellon, and M. Lund, "The effect of including accurate pelvis bony landmarks in a nonlinearly scaled musculoskeletal lower extremity model," in *Proceedings of the 12th International Symposium on 3D Analysis of Human Movement*, pp. 2–4, 2012.

[23] A. Bender and G. Bergmann, "Determination of typical patterns from strongly varying signals," *Computer Methods in Biomechanics and Biomedical Engineering*, vol. 15, no. 7, pp. 761–769, 2012.

[24] R. A. Zifchock, I. Davis, and J. Hamill, "Kinetic asymmetry in female runners with and without retrospective tibial stress fractures," *Journal of Biomechanics*, vol. 39, no. 15, pp. 2792–2797, 2006.

[25] R. M. Alexander and A. S. Jayes, "A dynamic similarity hypothesis for the gaits of quadrupedal mammals," *Journal of Zoology*, vol. 201, no. 1, pp. 135–152, 2009.

[26] M. Daabiss, "American society of anaesthesiologists physical status classification," *Indian Journal of Anaesthesia*, vol. 55, no. 2, pp. 111–115, 2011.

[27] G. E. Lewinnek, J. L. Lewis, R. Tarr, C. L. Compere, and J. R. Zimmerman, "Dislocations after total hip-replacement arthroplasties," *The Journal of Bone & Joint Surgery*, vol. 60, no. 2, pp. 217–220, 1978.

[28] T. Weber, S. Dullien, J. Grifka, T. Renkawitz, and S. Dendorfer, "Validation of a motion capture laboratory and a new marker placement protocol for clinical applications," *Gait Posture*, vol. 38, pp. S113–S114, 2013.

[29] A. Petrella, J. Rasmussen, A. A. Al-Munajjed, M. Damsgaard, M. Lund, and A. Kiis, "How good is good enough? Lessons in musculoskeletal model validation wit the AnyBody Modeling System," in *Proceedings of the ASME/FDA 1st Annual Frontiers in Medical Devices: Applications of Computer Modeling and Simulation (FMD '13)*, pp. 11–12, Washington, DC, USA, September 2013.

[30] C. Manders, A. New, and J. Rasmussen, "Validation of musculoskeletal gait simulation for use in investigation of total hip replacement," *Journal of Biomechanics*, vol. 41, supplement 1, p. S488, 2008.

[31] C. L. C. Vaughan, B. Davis, and J. O'Connor, *Dynamics of Human Gait*, Human Kinetics, 1992.

[32] F. E. Zajac, "Muscle and tendon: properties, models, scaling, and application to biomechanics and motor control.," *Critical Reviews in Biomedical Engineering*, vol. 17, no. 4, pp. 359–411, 1989.

[33] M. Damsgaard, J. Rasmussen, S. T. Christensen, E. Surma, and M. de Zee, "Analysis of musculoskeletal systems in the AnyBody Modeling System," *Simulation Modelling Practice and Theory*, vol. 14, no. 8, pp. 1100–1111, 2006.

[34] J. M. Bland and D. G. Altman, "Measurement error and correlation coefficients," *British Medical Journal*, vol. 313, no. 7048, pp. 41–42, 1996.

[35] B. W. Stansfield and A. C. Nicol, "Hip joint contact forces in normal subjects and subjects with total hip prostheses: walking and stair and ramp negotiation," *Clinical Biomechanics*, vol. 17, no. 2, pp. 130–139, 2002.

[36] P. Rousseeuw, "The bagplot: a bivariate boxplot," *The. American Statistician*, pp. 37–41, 1999.

[37] D. W. Murray, "The definition and measurement of acetabular orientation," *The Journal of Bone & Joint Surgery B*, vol. 75, no. 2, pp. 228–232, 1993.

[38] A. L. Hof, "Scaling gait data to body size," *Gait and Posture*, vol. 4, no. 3, pp. 222–223, 1996.

[39] C. Bitsakos, J. Kerner, I. Fisher, and A. A. Amis, "The effect of muscle loading on the simulation of bone remodelling in the proximal femur," *Journal of Biomechanics*, vol. 38, no. 1, pp. 133–139, 2005.

[40] R. Huiskes, R. Rulmerman, G. H. van Lenthe, and J. D. Janssen, "Effects of mechanical forces on maintenance and adaptation of form in trabecular bone," *Nature*, vol. 405, no. 6787, pp. 704–706, 2000.

[41] H. Sadeghi, P. Allard, F. Prince, and H. Labelle, "Symmetry and limb dominance in able-bodied gait: a review," *Gait & Posture*, vol. 12, no. 1, pp. 34–45, 2000.

[42] J. Schryver, J. Shea, and D. M. Ryan, *Acetabular Cup Body Prosthesis*, 1994.

[43] Z. Effenberger and R. Hrsg, "Pressfitpfannen. [Gebundene Ausgabe]," MCU—Medical Corporate University, 2004.

[44] T. A. Maxian, T. D. Brown, D. R. Pedersen, and J. J. Callaghan, "The Frank Stinchfield Award. 3-Dimensional sliding/contact computational simulation of total hip wear," *Clinical Orthopaedics and Related Research*, no. 333, pp. 41–50, 1996.

[45] I. H. F. Reininga, M. Stevens, R. Wagenmakers et al., "Comparison of gait in patients following a computer-navigated minimally invasive anterior approach and a conventional posterolateral approach for total hip arthroplasty: a randomized controlled trial," *Journal of Orthopaedic Research*, vol. 31, no. 2, pp. 288–294, 2013.

[46] M. Pospischill, A. Kranzl, B. Attwenger, and K. Knahr, "Minimally invasive compared with traditional transgluteal approach for total hip arthroplasty: a comparative gait analysis," *Journal of Bone and Joint Surgery—Series A*, vol. 92, no. 2, pp. 328–337, 2010.

[47] D. Bennett, L. Ogonda, D. Elliott, L. Humphreys, and D. E. Beverland, "Comparison of gait kinematics in patients receiving minimally invasive and traditional hip replacement surgery: a prospective blinded study," *Gait & Posture*, vol. 23, no. 3, pp. 374–382, 2006.

[48] S. J. Mellon, M. S. Andersen, G. Grammatopoulos, and H. S. Gill, "Mal-positioning alone does not necessarily lead to increased wear in metal-on-metal hip resurfacing," in *Proceedings of the ORS Annual Meeting*, vol. 79 of *Abstract*, p. 2011, San Francisco, Calif, USA.

[49] M. Morlock, E. Schneider, A. Bluhm et al., "Duration and frequency of every day activities in total hip patients," *Journal of Biomechanics*, vol. 34, no. 7, pp. 873–881, 2001.

[50] M. Sliwinski and S. Sisto, "Gait, quality of life, and their association following total hip arthroplasty," *Journal of Geriatric Physical Therapy*, vol. 29, no. 1, pp. 10–17, 2006.

[51] P. J. James, A. C. Nicol, and D. L. Hamblen, "A comparison of gait symmetry and hip movements in the assessment of patients with monarticular hip arthritis," *Clinical Biomechanics*, vol. 9, no. 3, pp. 162–166, 1994.

[52] C. L. Christiansen and J. E. Stevens-Lapsley, "Weight-bearing asymmetry in relation to measures of impairment and functional mobility for people with knee osteoarthritis," *Archives of Physical Medicine and Rehabilitation*, vol. 91, no. 10, pp. 1524–1528, 2010.

Hindawi Publishing Corporation
BioMed Research International
Volume 2015, Article ID 435432, 10 pages
http://dx.doi.org/10.1155/2015/435432

Research Article

Effects of Surface Modification and Bulk Geometry on the Biotribological Behavior of Cross-Linked Polyethylene: Wear Testing and Finite Element Analysis

Kenichi Watanabe,[1,2] Masayuki Kyomoto,[1,2,3] Kenichi Saiga,[1,2] Shuji Taketomi,[4] Hiroshi Inui,[4] Yuho Kadono,[4] Yoshio Takatori,[2] Sakae Tanaka,[4] Kazuhiko Ishihara,[3] and Toru Moro[2,4]

[1] *Research Department, KYOCERA Medical Corporation, Osaka, Japan*
[2] *Division of Science for Joint Reconstruction, Graduate School of Medicine, The University of Tokyo, Tokyo, Japan*
[3] *Department of Materials Engineering, School of Engineering, The University of Tokyo, Tokyo, Japan*
[4] *Orthopaedic Surgery, Sensory and Motor System Medicine, Surgical Sciences, Graduate School of Medicine, The University of Tokyo, Tokyo, Japan*

Correspondence should be addressed to Toru Moro; moro-ort@h.u-tokyo.ac.jp

Received 6 March 2015; Accepted 12 May 2015

Academic Editor: Panagiotis Korovessis

Copyright © 2015 Kenichi Watanabe et al. This is an open access article distributed under the Creative Commons Attribution License, which permits unrestricted use, distribution, and reproduction in any medium, provided the original work is properly cited.

The wear and creep deformation resistances of polymeric orthopedic bearing materials are both important for extending their longevity. In this study, we evaluated the wear and creep deformation resistances, including backside damage, of different polyethylene (PE) materials, namely, conventional PE, cross-linked PE (CLPE), and poly(2-methacryloyloxyethyl phosphorylcholine)- (PMPC-) grafted CLPE, through wear tests and finite element analysis. The gravimetric and volumetric degrees of wear of disks (3 or 6 mm in thickness) of these materials against a cobalt-chromium-molybdenum alloy pin were examined using a multidirectional pin-on-disk tester. Cross-linking and PMPC grafting decreased the gravimetric wear of the PE disks significantly. The volumetric wear at the bearing surface and the volumetric penetration in the backside of the 3-mm thick PE disk were higher than those of the 6-mm thick PE disk, regardless of the bearing material. The geometrical changes induced in the PE disks consisted of creep, because the calculated internal von Mises stress at the bearing side of all disks and that at the backside of the 3-mm thick disks exceeded their actual yield strengths. A highly hydrated bearing surface layer, formed by PMPC grafting, and a cross-linking-strengthened substrate of adequate thickness are essential for increasing the wear and creep deformation resistances.

1. Introduction

Ultra-High-molecular-weight polyethylene (UHMWPE; PE) has conventionally been used for orthopedic bearing materials since the 1960s. In addition, highly cross-linked PE (CLPE) is being used since the 1990s [1]. The degree of wear is one of the important indicators of the clinical performance of the bearing materials used for artificial joints, regardless of whether CLPE is used [2]. The wear particles generated from the acetabular liner used in total hip arthroplasty (THA) induce bone resorption and lead to aseptic loosening [3]. Hence, various strategies have been employed for reducing the number of PE wear particles generated and extending the longevity of polymeric orthopedic bearing materials [4]. To reduce the degree of PE wear and suppress bone resorption, we had previously developed a surface modification technology that involves synthetic phospholipid-polymer poly(2-methacryloyloxyethyl phosphorylcholine [MPC]) (PMPC) grafting. This technology results in increases in the lifetime of the acetabular liners [5, 6]. The polymer MPC is a very common lubricious, hydrophilic, and biologically inert one and is thus suitable for clinical use [7]. The modification of the surface of CLPE with a nanometer-scale layer of PMPC increases the lubricity of CLPE to the same level as that of

articular cartilage under physiological conditions [5]. The grafting of PMPC onto acetabular liners resulted in a drastic reduction in CLPE wear during a long-term hip simulator test [8]; it also yielded good short-term results during clinical tests [9].

Creep deformation resistance is also an important indicator of the clinical performance of acetabular liners [10]. The geometry of the PE part is one of the factors that determine its creep deformation resistance [11, 12]. The dislocation caused by the impingement of the femoral stem neck and the acetabular liner is a common cause of early failure of THAs [13]. A large-diameter femoral head not only allows for an increase in the head/neck ratio, which is directly related to the range of motion prior to the impingement of the femoral stem neck and the acetabular liner, but also increases the jump distance [14]. Hence, large-diameter femoral heads have recently come to be used extensively for improving the stability of bearing surfaces [14, 15]. However, large-diameter femoral heads need to be used with thin acetabular liners, in order to ensure that the acetabular bone is retained, as not doing so can produce higher contact stresses, accelerating the wear and/or fracture of the acetabular liner [16].

Similarly, backside wear as well as the damage caused by volumetric penetration and circular scratching is also a serious problem with respect to the PE acetabular liners used in cementless THA and the PE inserts used in total knee arthroplasty (TKA) [17, 18]. High internal stress occurs in thin PE acetabular liners, and plastic flow is caused by the rubbing of the backside surface against the edge of the screw hole in the metal acetabular shell. A previous study reported that this internal stress as well as the plastic flow of PE increased with a decrease in the thickness of the PE bulk [19]. In contrast, another study reported that the wear of PE and CLPE acetabular liners increases significantly with an increase in the liner thickness [16]. It is therefore thought that the thickness of the PE bulk affects both the wear resistance and the creep deformation resistance. In other words, when evaluating the wear and creep deformation resistances of a polymeric material, the thickness of the test specimen must be taken into account.

The development of new biomaterials requires practical and economical screening methods for identifying the best-suited bearing materials before performing expensive joint simulator tests. A number of wear tests, which are performed under different conditions, have been developed such that they take into account the wear and fatigue mechanisms corresponding to clinical use [20, 21]. The ASTM F732-00 standard has been designed to evaluate bearing couples on the basis of the degree of polymer wear by using a pin-on-disk tester [22]. It also defines a method in which a disk-shaped polymer specimen is loaded with a hemispherical cobalt-chromium-molybdenum (Co-Cr-Mo) alloy pin. If one were to employ this method while using a plate with a screw hole as the backplate of the disk specimen, one could evaluate the damage undergone by the backside of the disk without having to perform an expensive joint simulator test [23]. In addition, this method is suitable for evaluating hydrated polymers because a lubricant is applied on the bearing surface during every loading cycle [24].

The purpose of this study was to evaluate the wear and creep deformation resistances, including the extent of backside damage, of various PE materials using test specimens 3 and 6 mm in thickness. We sought to answer four questions: will the choice of the PE material used affect the (1) wear resistance and (2) creep deformation resistance of the test specimens? Further, will the thickness of the PE test specimens affect their (3) wear resistance and (4) creep deformation resistance?

2. Materials and Methods

2.1. Bearing Materials and PMPC Grafting. Compression-molded bars of PE (GUR1020 resin; Quadrant PHS Deutschland GmbH, Vreden, Germany) were prepared. This material is referred to as untreated PE. A few bars were irradiated with a 50-kGy dose of gamma rays in N_2 gas and annealed at 120°C for 7.5 h in N_2 gas to facilitate cross-linking. This material is referred to as untreated CLPE. PMPC was grafted onto the surfaces of the CLPE samples through photoinduced graft polymerization [5, 6]. Polymerization was performed on the surfaces of the untreated CLPE samples by irradiating them with ultraviolet (UV) radiation with an intensity of 5 mW/cm^2 at 60°C for 90 min in a 0.5 mol/L aqueous solution of MPC (NOF Corp., Tokyo, Japan). Hereafter, this material is referred to as PMPC-grafted CLPE. The samples were then sterilized using gamma rays at a dose of 25 kGy in N_2 gas.

2.2. Cross-Link Density. The cross-link densities of the materials were evaluated using a previously reported method [5, 25]. The specimens (23 × 23 × 1 mm) were weighed (approximately 0.5 g), allowed to swell for 72 h in *p*-xylene containing 0.5 mass% 2-*t*-butyl-4-methylphenol at 130°C, and then reweighed. The samples were then immersed in acetone, dried at 60°C under vacuum, and reweighed. The swelling ratio was determined from the increase in the weights of the samples and densities of the PE used and xylene. The network chain density was calculated using the Flory-Rehner equation [26]. The cross-link density was defined as the mole fraction of the cross-linked units.

2.3. Wettability Test. The contact angle of a static droplet of water on specimens (100 × 10 × 3 mm) of each material was measured using the sessile drop method; an optical bench-type contact angle goniometer (Model DM300; Kyowa Interface Science, Saitama, Japan) was employed for the purpose. Drops of purified water (1 μL) were deposited on the specimens, and the contact angles were measured directly after 60 s using a microscope. Fifteen areas were evaluated on each sample, and the mean values and the standard deviation were calculated.

2.4. Pin-on-Disk Test. The wear and creep deformation resistances of the bearing materials were examined using a pin-on-disk tester (Ortho POD; AMTI, Watertown, MA, USA), in keeping with the ASTM F732-00 standard. The various PE materials were used to fabricate disks with a thickness of 3 or 6 mm, while a Co-Cr-Mo alloy was used for the counter

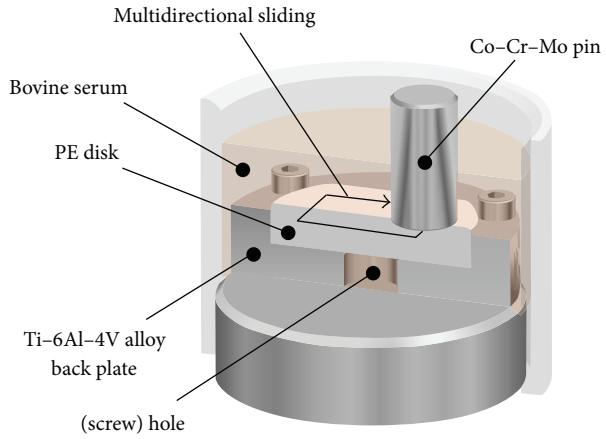

FIGURE 1: Schematic illustration of the multidirectional pin-on-disk test.

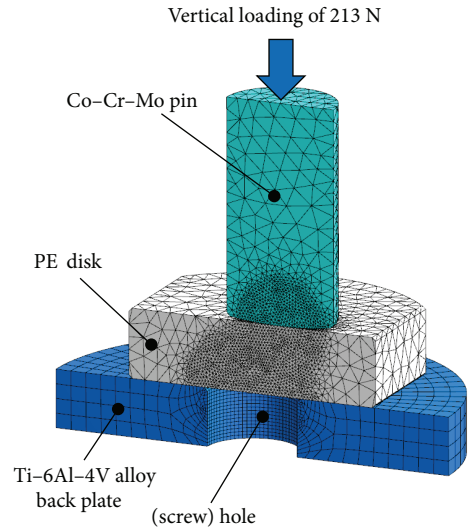

FIGURE 2: Schematic illustration of FEA used to determine the internal stress in the PE disks during the pin-on-disk test.

hemispherical pin (Figure 1). The pin had a surface curvature radius of 30 mm and a surface roughness, R_a, of less than 0.01 μm. Its backplate was made of a titanium alloy and had a sham screw hole with a diameter of 8 mm in the center. A mixture of 27 vol% fetal bovine serum (Biowest, Nuaillé, France), 20 mM/L ethylene diamine-N,N,N′,N′-tetraacetic acid (EDTA), and 0.1 mass% sodium azide was used at 37°C as the lubricant.

Multidirectional pin-on-disk tests were performed; the motion was in the shape of a rectangle with dimensions of 5 × 10 mm. The test conditions were the following: static load of 213 N, motion speed of 30 mm/s, and maximum test duration of 1.0×10^6 cycles. The disks were weighed every 0.25×10^6 cycles to evaluate their gravimetric wear, in keeping with the ISO 14242-2 standard [27]. The lubricant was also replaced every 0.25×10^6 cycles. Soak controls were used to compensate for fluid absorption by the specimens of the same group. Because the gravimetric method was used, the decreases in the weights of the tested specimens were corrected for by subtracting the weight gain resulting from the use of the soak control. The volume of wear was calculated by dividing the individual weight of the disks by the density of the corresponding material: 0.937 g/mm^3 for untreated CLPE, 0.941 g/mm^3 for untreated CLPE, and 0.941 g/mm^3 for PMPC-grafted CLPE. The wear rate was calculated with the least squares linear regression method while using data corresponding to points other than the zero-time point. After the completion of the multidirectional pin-on-disk test, the wear of the bearing surface and the depth of penetration in the backside surface of all the disks were measured using a noncontact optical three-dimensional (3D) profiler (Talysurf CCI Lite; Taylor Hobson Ltd., Leicester, UK).

2.5. Finite Element Analysis. To estimate the internal stress in the PE disks, finite element analysis (FEA) was performed using an FEA software program (ANSYS 14.5; Ansys, Inc., Canonsburg, PA, USA). A computer-aided 3D model of the pin-on-disk test conditions was created using a computer-aided design (CAD) software program (Solid Edge ST3; Siemens PLM Software, Plano, TX, USA). This model was then imported into the FEA program. A static vertical load of 213 N was applied to the disks through the pin (Figure 2). With respect to the physical properties of the different PE materials, Young's moduli of the untreated PE, untreated CLPE, and PMPC-grafted CLPE were taken to be 1.06, 1.05, and 1.10 GPa, respectively, while their Poisson's ratios were assumed to be 0.41, 0.46, and 0.43, respectively.

2.6. Statistical Analysis. The mean values for the three material groups (untreated PE, untreated CLPE, and PMPC-grafted CLPE) were compared using one-factor analysis of variance (ANOVA). The significant differences between the comparable properties were determined through post hoc testing using Tukey-Kramer's method. The mean values of the two thickness groups (3 and 6 mm) for each material were compared by using Student's t-test. All statistical analyses were performed using an add-on (Statcel 3; OMS Publishing, Tokorozawa, Japan) for Microsoft Excel 2007 (Microsoft Corp., Redmond, WA, USA).

3. Results

The cross-link densities of untreated CLPE and PMPC-grafted CLPE were significantly higher ($p < 0.01$) than that of untreated PE (Figure 3(a)). The static water contact angle of PMPC-grafted CLPE was significantly smaller ($p < 0.01$) than those of untreated PE and CLPE (Figure 3(b)).

The gravimetric wear rates for all disks after the end of the pin-on-disk test are shown in Figure 4(a). For the 3-mm thick disk group, the gravimetric wear rates of untreated CLPE and PMPC-grafted CLPE disks were significantly lower ($p < 0.01$) than that of the untreated PE disks; however, the difference between the untreated CLPE and PMPC-grafted CLPE disks was not significant (Figure 4(b)). For the 6-mm thick disk group, the wear rates of untreated CLPE and

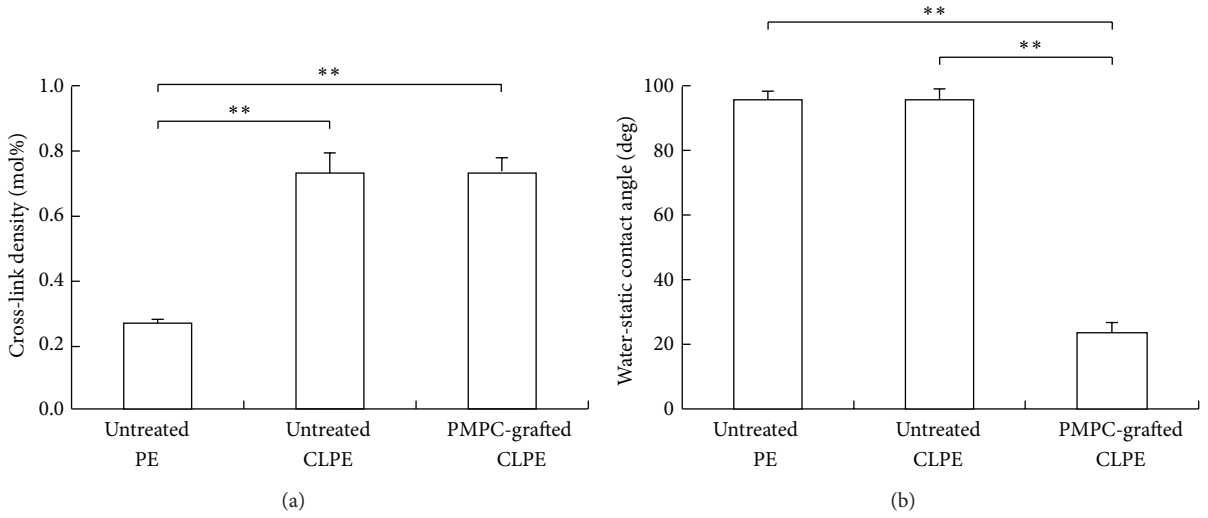

Figure 3: (a) Cross-link densities and (b) static water contact angles of untreated PE, untreated CLPE, and PMPC-grafted CLPE. The bar indicates the standard deviation. ∗∗ indicates $p < 0.01$ as per Tukey-Kramer's test.

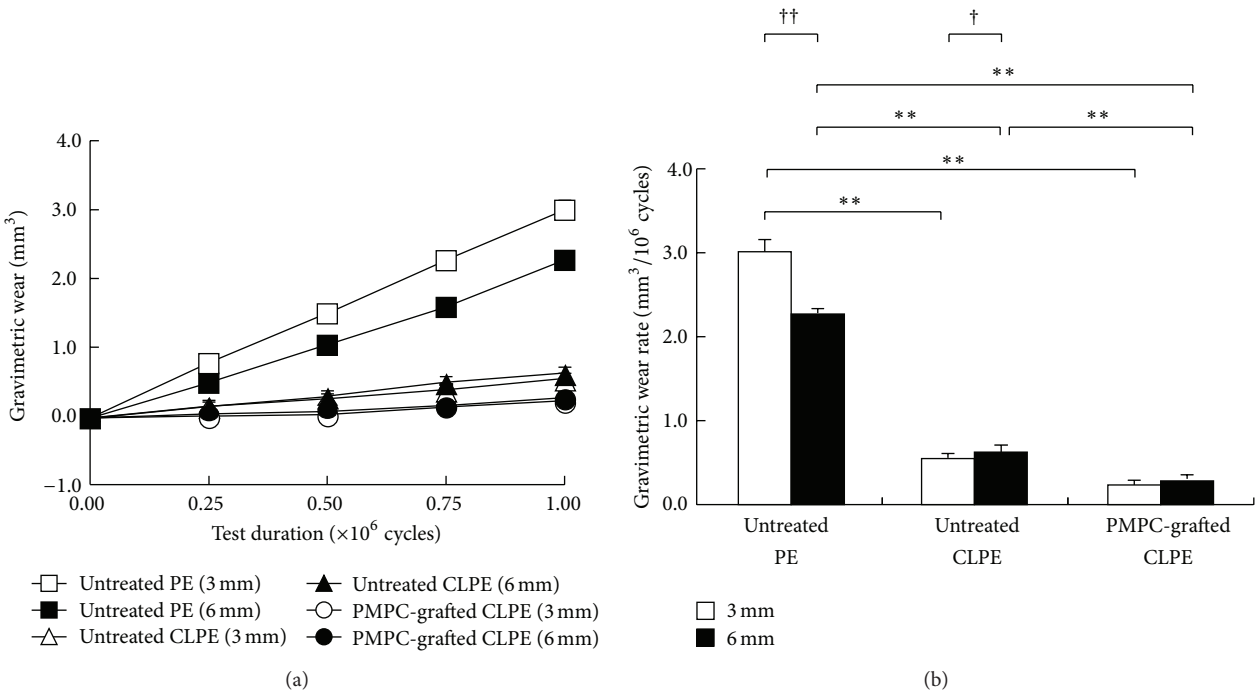

Figure 4: (a) Degrees of gravimetric wear and (b) gravimetric wear rates of untreated PE, untreated CLPE, and PMPC-grafted CLPE, determined using disks 3 and 6 mm in thickness. The bar indicates the standard deviation. ∗∗ indicates $p < 0.01$ as per Tukey-Kramer's test and † indicates $p < 0.05$ and †† indicates $p < 0.01$ as per Student's t-test.

PMPC-grafted CLPE disks were significantly lower ($p < 0.01$) than that of the untreated PE disks. Furthermore, the wear rate of PMPC-grafted CLPE was significantly lower ($p < 0.01$) than that of untreated CLPE. The wear rate of the 3-mm thick untreated PE disks was significantly larger than that of the 6-mm thick disks ($p < 0.01$). On the other hand, the wear rate of the 3-mm thick untreated CLPE disks was significantly lower than that of the 6-mm thick disks ($p < 0.05$). In the case of PMPC-grafted CLPE, there were no significant differences in the wear rates of the 3 and 6 mm disks.

The 3D profile of the disks showed that all the disks exhibited substantial volumetric wear of the bearing surface, with the backside surface penetrating into the sham screw hole (Figures 5 and 6). The differences in the degrees of volumetric wear for the 3-mm thick disks of the different materials were not significant (Figure 7(a)). On the other hand,

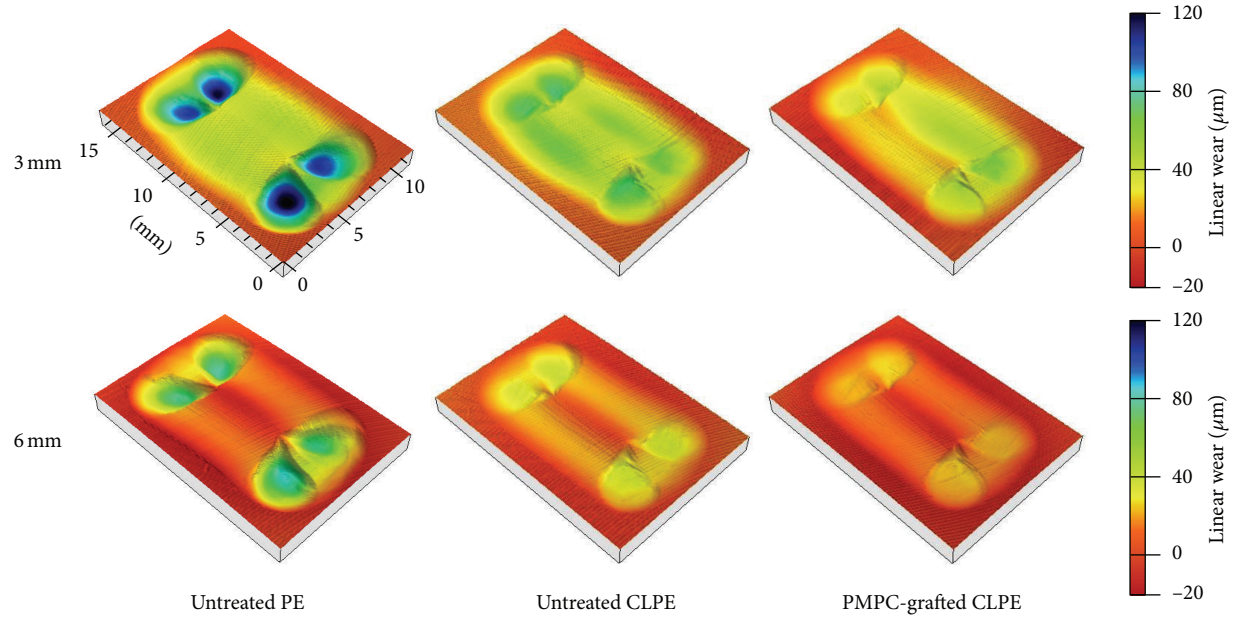

FIGURE 5: Degree of volumetric wear of the bearing surfaces of the untreated PE, untreated CLPE, and PMPC-grafted CLPE disks 3 and 6 mm in thickness.

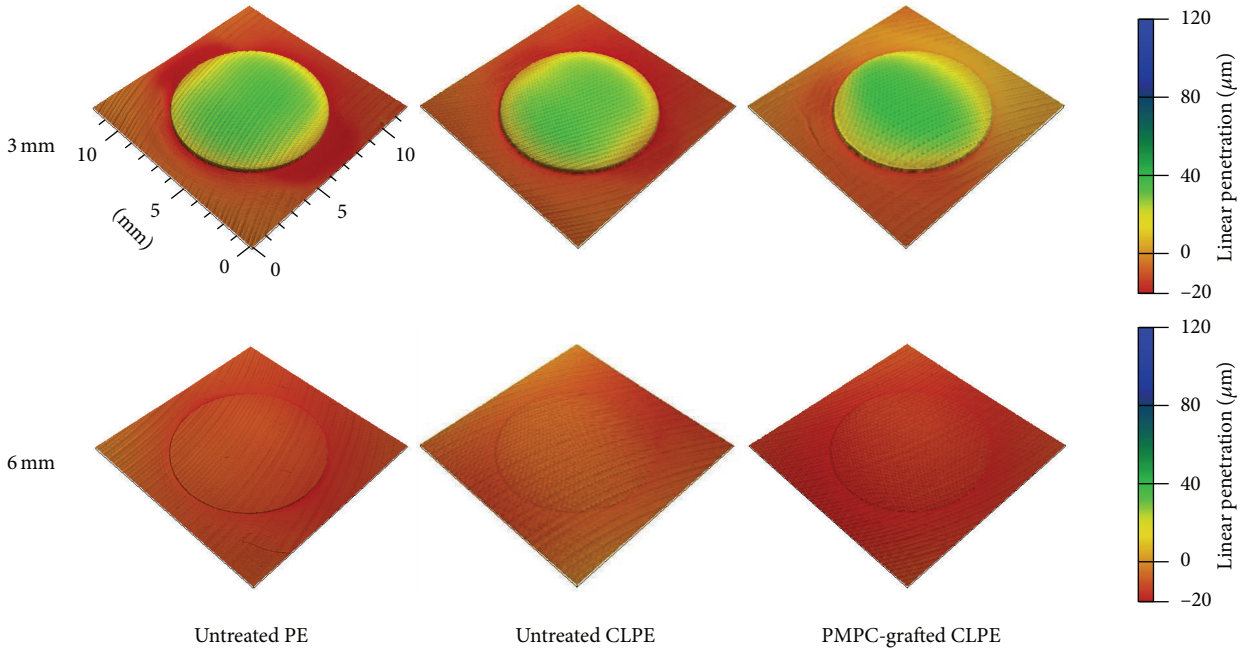

FIGURE 6: Volumetric penetration of the backside surfaces of the untreated PE, untreated CLPE, and PMPC-grafted CLPE disks 3 and 6 mm in thickness.

the volumetric wear of the 6-mm thick disk of untreated PE was significantly larger ($p < 0.01$) than those of the disks of untreated CLPE and PMPC-grafted CLPE. For each material group, the volumetric wear of the 3-mm thick disks was significantly larger ($p < 0.01$) than that of the 6-mm thick disks. The differences in the volumetric penetration for both the 3-mm thick and 6-mm thick disks of the various materials were not significant. For each material group, the volumetric penetration of the 3-mm thick disks was significantly greater ($p < 0.01$) than that of the 6-mm thick disks (Figure 7(b)).

The von Mises stress distribution for all the disks was estimated using FEA (Figure 8). The internal von Mises stress at the bearing side was almost the same for all the materials, as shown in Table 1. Although the stress at the backside was almost the same for all the material groups for both the 3-mm thick and the 6-mm thick disks, the stress in the 3-mm

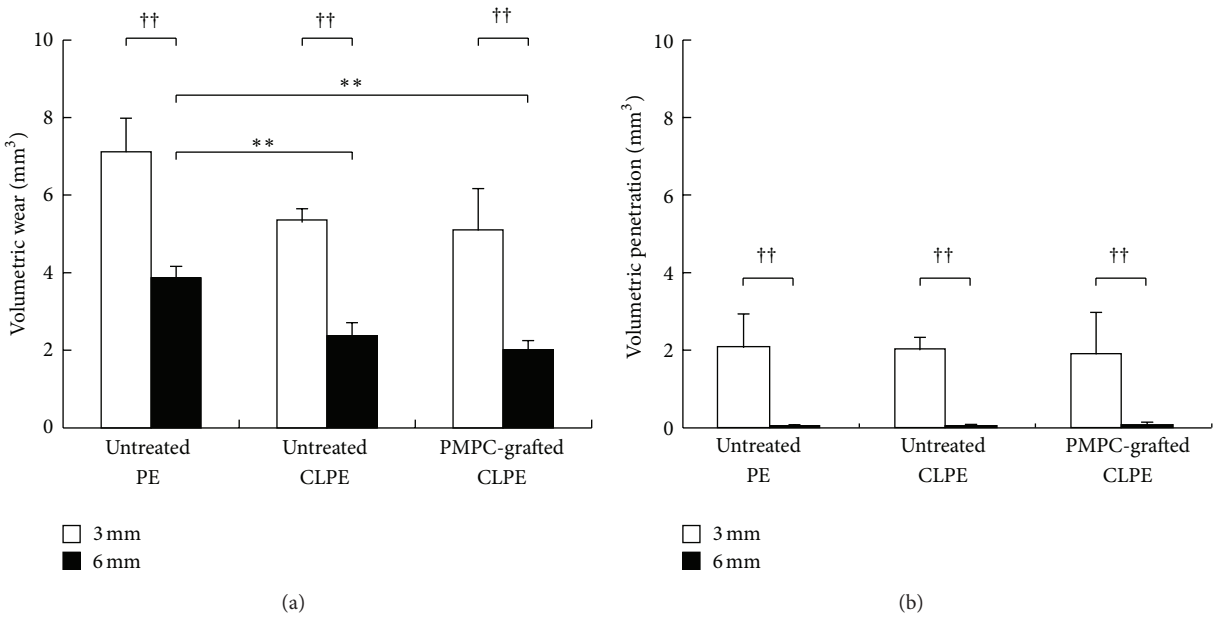

Figure 7: (a) Volumetric wears of the bearing surfaces and (b) volumetric penetration in the backside surfaces of the untreated PE, untreated CLPE, and PMPC-grafted CLPE disks. The bar indicates the standard deviation. ∗∗ indicates $p < 0.01$ as per Tukey-Kramer's test and †† indicates $p < 0.01$ as per Student's t-test.

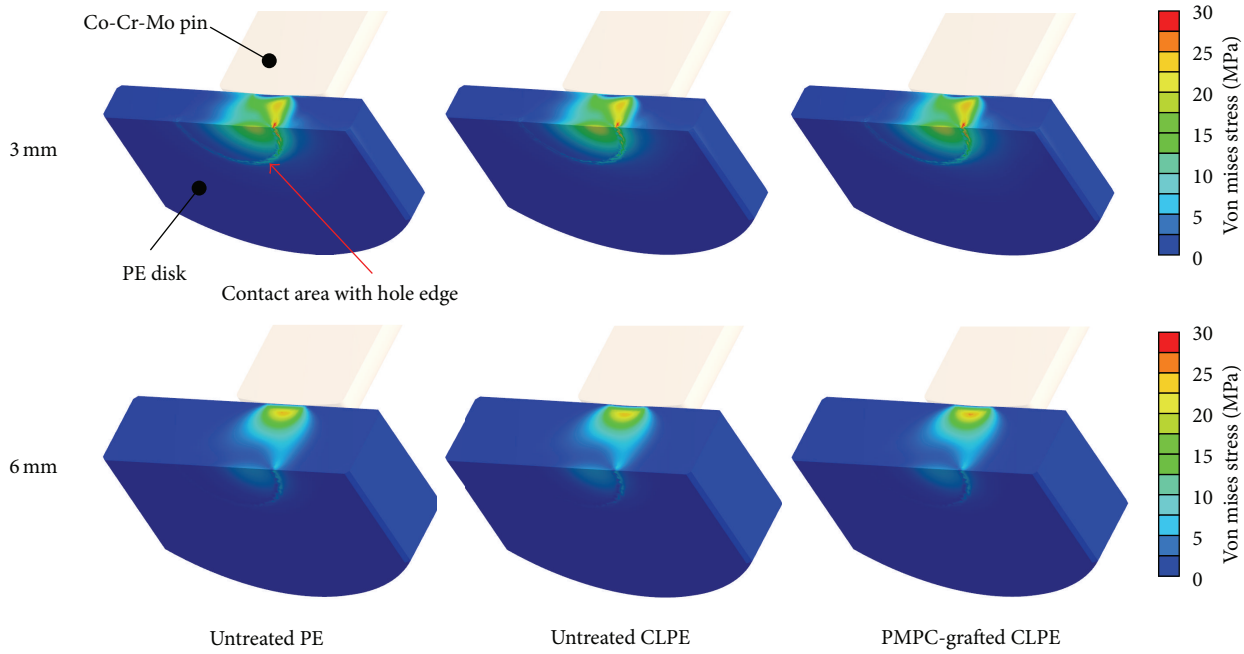

Figure 8: von Mises stress distributions of the untreated PE, untreated CLPE, and PMPC-grafted CLPE disks.

Table 1: Maximum von Mises stresses in the bearing and backside surfaces of the untreated PE, untreated CLPE, and PMPC-grafted CLPE disks.

Thickness (mm)	Maximum von Mises stress (MPa)					
	Bearing surface			Backside surface		
	Untreated PE	Untreated CLPE	PMPC-grafted CLPE	Untreated PE	Untreated CLPE	PMPC-grafted CLPE
3	23.2	23.4	23.9	29.0	28.5	29.0
6	22.7	22.6	23.3	7.3	7.3	7.3

thick disks was computationally much higher than that in the 6-mm thick disks. Further, it exceeded their respective actual yield strengths by a wide margin.

4. Discussion

In this study, we evaluated the wear and creep deformation resistances, including the degree of backside damage, of conventional PE, CLPE, and PMPC-grafted CLPE using disks with thicknesses of 3 and 6 mm. We attempted to answer the following four questions: does the choice of the PE material affect the (1) wear resistance and (2) creep deformation resistance of the test specimens? In addition, will the thickness of the PE specimens affect their (3) wear resistance and (4) creep deformation resistance?

Cross-linking decreased the gravimetric wear of PE significantly, while PMPC grafting decreased it even further. It is known that cross-linking can improve the wear resistance of the acetabular liners used in artificial hip joints [28, 29]. PMPC-grafted CLPE has also been shown to exhibit lower wear than that seen for CLPE [5, 8]; it is thought that the decrease in wear is caused by a surface hydration lubrication mechanism [30]. According to a previous study, the hydrated PMPC layer has a clear effect on the friction response of the polymer; the dynamic coefficient of friction of PMPC-grafted CLPE is significantly lower than that of untreated CLPE [5]. This is attributable to the fluid film formed by the hydrated PMPC layer on the CLPE surface [5]. In the case of natural synovial joints, lubrication is provided by a hydrated layer that consists of chondrocytes; the surrounding matrix macromolecules (e.g., proteoglycans, glycosaminoglycans, and collagens) are also essential for lubrication, while a surface layer of active phospholipids (e.g., phosphatidylcholine derivatives) that covers the surface of the joint cartilage provides hydrophilicity and works as an effective boundary lubricant [31, 32]. Hence, a phospholipid-like layer grafted on the bearing surface of artificial joints may afford ideal hydrophilicity and lubricity, that is, similar to those of physiological joint surfaces.

Even though gravimetric evaluations were performed, measuring the volumetric wear of the bearing surface using an optical 3D profiler did not allow for the detection of significant differences between the three PE material groups in the case of the 3-mm thick disks and between untreated CLPE and PMPC-grafted CLPE in the case of the 6-mm thick disks. The internal von Mises stress at the bearing side for both the 3-mm thick and the 6-mm thick disks reached approximately 23 MPa, which is reportedly the actual yield strength of PE materials [33, 34]. We therefore assumed that the volumetric wear measured in this study consisted of not only the true wear but also the creep deformation of the PE substrate. Since the volume of creep deformation was significantly greater than that of true wear, the differences in the volumetric wear among the three materials for the 3-mm thick disks as well as that between untreated CLPE and PMPC-grafted CLPE for the 6-mm thick disks (which exhibited large creep deformation) might not be significant.

The modification processes investigated, namely, cross-linking and PMPC grafting, did not affect the creep deformation resistance (Figure 7(b)). It has been reported that creep deformation decreases with an increase in the irradiation dose [35]. It was assumed that the effects of an irradiation dose of 50 kGy on creep deformation would be too small to allow for differences in the creep deformations of the PE and CLPE samples to be detected. In the case of PMPC grafting, previous studies have indicated that photoinduced graft polymerization does not affect the mechanical properties of the CLPE substrate [5, 33]. In this study, we used disks 3 or 6 mm in thickness. Thus, the backside surface, where the maximum stress appeared in the case of the 3-mm thick disks (Figure 8), might not be affected by UV irradiation either. Shyichuk et al. reported that UV irradiation affects the mechanical properties of PE, especially on the submillimeter scale [36]. In the present study, UV irradiation was performed with an intensity of $5\,mW/cm^2$ for 90 min; this resulted in an energy of $0.3 \times 10^6\,J/m^2$, which was low compared to that used by Shyichuk et al. ($3.6 \times 10^6\,J/m^2$ for 3 weeks) [36].

Although disk thickness did affect the gravimetric wear rate in the case of the untreated PE and untreated CLPE disks, the effects were not the same. For untreated PE, the gravimetric wear rate increased with a decrease in the thickness of the disk specimens. We assumed that this was attributable to an increase in the contact area, owing to the creep deformation of the bearing surface (Figure 5). For untreated CLPE, in contrast, the gravimetric wear rate increased with an increase in the thickness of the disk specimen. Shen et al. reported that, in an *in vitro* study, the wear rate of a CLPE acetabular liner increased with an increase in the liner thickness [16]. In the present study, the losses in the weights of the untreated CLPE disks (0.043 and −0.070 mg for the 3 and 6-mm thick PE disks, resp.) were much smaller than the increases in their weights owing to fluid absorption (0.487 and 0.673 mg for the 3 and 6-mm thick PE disks, resp.). Thus, these phenomena may not be detectable using the gravimetric method.

The volumetric penetration in the backside surfaces increased with a decrease in disk thickness. The internal von Mises stress in all the 3-mm thick disks was more than 28 MPa in the backside against the edge of the sham screw hole; this was greater than the actual yield strength of the PE materials (Table 1). It is likely that the fact that the internal stress was greater than the actual yield strength is what resulted in the large degree of volumetric penetration. On the other hand, the von Mises stress in all the 6-mm thick disks was less than 8 MPa. This internal stress did not lead to changes in the geometry of the PE disks. However, it affected not only the backside surface but also the bearing surface of the disks. The degree of volumetric wear, which consisted of true wear and creep deformation, was greater in the thinner (3 mm) disks (Figure 7(a)) for every material, regardless of the differences in the degrees of gravimetric wear (Figure 3) and the internal von Mises stress (Table 1). We assumed that the increase in the degree of volumetric wear in thinner (3 mm) disks was partially owing to the volumetric penetration in the backside surface. Oonishi et al. have also reported that the wear rate of PE cups in cemented THA increased with a decrease in the cup thickness [37].

Various wear tester designs and testing conditions have been employed to evaluate the suitability of bearing materials for clinical use [4]. The ASTM F732-00 standard provides the test parameters that are used as guidelines for producing wear rates similar to those observed *in vivo*. In this study, we used PE materials for the disks and a Co-Cr-Mo alloy for the pin, while referring to the Appendix 3 of ASTM F732-00 standard. Baykal et al. reviewed the wear rate data for PE materials obtained using various pin-on-disk testers [38]: the most reviewed studies used PE materials for the pin side and a metal for the disk side, in order to keep the contact area of the bearing interface constant. The test couple employed in the present study, which consisted of PE materials for the disk side and a Co-Cr-Mo alloy for the pin side, has a number of advantages. For example, one can evaluate the effects of the sample geometry (i.e., thickness), backside penetration in the presence and absence of a backplate hole, and the hydration lubrication mechanism, which involves dehydration/rehydration processes. However, it also has a disadvantage in that the contact area does not remain constant. There have been several studies on PE materials involving pin-on-disk tests in which the PE materials were used for the disks [39, 40]. Tomita et al. determined the effectiveness of adding vitamin E to PE for preventing fatigue crack by using metal pin-on-PE disk tests [39]. Saikko et al. developed a test system named Random POD. This system simulated a hip joint in the case of a bearing couple of a PE pin-on-Co-Cr-Mo alloy disk or simulated a knee joint in the case of a bearing couple of Co-Cr-Mo alloy pin-on-PE disk [40, 41]. While they simulated the conditions of knee joints, this bearing couple consisting of a PE disk against a Co-Cr-Mo alloy pin is suitable for simulating not only artificial knee joints, but also artificial hip joints. This is because we could evaluate bearing materials while taking into account sample geometry.

Finally, there were several limitations of the present study. To begin with, we used a small cycling period (1.0×10^6 cycles) for the multidirectional wear test performed using the pin-on-disk tester as a preliminary examination, in keeping with the ASTM F732-00 standard. This duration may not be large enough to correctly simulate the loading and motion conditions associated with physical walking or the daily routine of patients. Nevertheless, we believe that the multidirectional wear test does provide some indication of the wear and fatigue performances of the PE materials [38]. In addition, we calculated the wear rate using data points other than those obtained at the zero-time point; thus, the steady state of the wear process was not known. It has been reported that there are two phases of wear, namely, the run-in state and the steady state, during wear tests [22, 42, 43]. In this study, the steady state of the wear process was not fully known because wear data after 1.0×10^6 cycles is not available; however, the coefficient of determination ranged from 0.94 to 0.99. We assumed that the run-in state might be over after 0.25×10^6 cycles [42]. However, we are in the process of conducting longer hip simulator studies using PMPC-grafted CLPE liners and have been able to confirm that the PMPC-grafted liners exhibit almost no wear after 20×10^6 cycles [8]. Second, the conditions under which the pin-on-disk wear test, in which a disk-shaped polymer specimen is loaded with a hemispherical pin, increases is performed, the contact area increases owing to an increase in the volumetric wear. While this is a limitation, it probably reflects the actual clinical conditions. Third, during the FEA, we simulated static conditions and used only a vertical load. In actuality, the pin-on-disk test involves dynamic conditions, and the disk is subjected to not only vertical loads but also multidirectional kinetic forces. In addition, the FEA was a linear analysis, while creep deformation should be simulated using a nonlinear analysis [44].

5. Conclusions

The main conclusions of the present study can be listed as follows: (1) the cross-linking of PE improved its wear resistance, while PMPC grafting improved the resistance even further. (2) Cross-linking through irradiation at a dose of 50 kGy and PMPC grafting did not affect creep deformation. (3) An increase in disk thickness tended to decrease the gravimetric wear for untreated PE; however, the effect was too small to detect in the case of untreated and PMPC-grafted CLPE. (4) The thickness of the test samples had an effect on the creep deformation resistance; this was true for both the bearing and the backside surfaces.

A hydrated bearing surface and a bearing substrate of the appropriate thickness are essential for improving the wear and creep deformation resistances. We believe that PMPC-grafted CLPE is a promising bearing material for increasing the longevity of artificial joints. Further, the pin-on-disk test is a useful one for evaluating bearing biomaterials in a practical and economical manner.

Conflict of Interests

One or more of the authors or institutions received outside funding or grants from KYOCERA Medical Corporation. One or more of the authors (Kenichi Watanabe, Masayuki Kyomoto, and Kenichi Saiga) are employed by KYOCERA Medical Corporation.

Acknowledgments

This research was supported in part by a Health and Welfare Research Grant for Research on Publicly Essential Drugs and Medical Devices (H23-007) and by the Research on Development of New Medical Devices (H26-006) Program of the Ministry of Health, Labour and Welfare, Japan. The authors thank Dr. Fumiaki Miyaji, Mr. Mikio Iwamoto, and Ms. Shihori Yamane (KYOCERA Medical Corporation) for their technical assistance.

References

[1] S. M. Kurtz, O. K. Muratoglu, M. Evans, and A. A. Edidin, "Advances in the processing, sterilization, and crosslinking of ultra-high molecular weight polyethylene for total joint arthroplasty," *Biomaterials*, vol. 20, no. 18, pp. 1659–1688, 1999.

[2] C. H. Geerdink, B. Grimm, W. Vencken, I. C. Heyligers, and A. J. Tonino, "Cross-linked compared with historical polyethylene in THA: an 8-year clinical study," *Clinical Orthopaedics and Related Research*, vol. 467, no. 4, pp. 979–984, 2009.

[3] W. H. Harris, "The problem is osteolysis," *Clinical Orthopaedics and Related Research*, vol. 311, pp. 46–53, 1995.

[4] S. M. Kurtz, *UHMWPE Biomaterials Handbook: Ultra-High Molecular Weight Polyethylene in Total Joint Replacement and Medical Devices*, Academic Press, Burlington, Wash, USA, 2nd edition, 2009.

[5] M. Kyomoto, T. Moro, S. Yamane, M. Hashimoto, Y. Takatori, and K. Ishihara, "Effect of UV-irradiation intensity on graft polymerization of 2-methacryloyloxyethyl phosphorylcholine on orthopedic bearing substrate," *Journal of Biomedical Materials Research Part A*, vol. 102, no. 9, pp. 3012–3023, 2014.

[6] T. Moro, Y. Takatori, K. Ishihara et al., "Surface grafting of artificial joints with a biocompatible polymer for preventing periprosthetic osteolysis," *Nature Materials*, vol. 3, no. 11, pp. 829–836, 2004.

[7] Y. Iwasaki and K. Ishihara, "Phosphorylcholine-containing polymers for biomedical applications," *Analytical and Bioanalytical Chemistry*, vol. 381, no. 3, pp. 534–546, 2005.

[8] T. Moro, Y. Takatori, M. Kyomoto et al., "Long-term hip simulator testing of the artificial hip joint bearing surface grafted with biocompatible phospholipid polymer," *Journal of Orthopaedic Research*, vol. 32, no. 3, pp. 369–376, 2014.

[9] Y. Takatori, T. Moro, K. Ishihara et al., "Clinical and radiographic outcomes of total hip replacement with poly(2-methacryloyloxyethyl phosphorylcholine)-grafted highly cross-linked polyethylene liners: three-year results of a prospective consecutive series," *Modern Rheumatology*, vol. 25, no. 2, pp. 286–291, 2015.

[10] O. K. Muratoglu, E. S. Greenbaum, C. R. Bragdon, M. Jasty, A. A. Freiberg, and W. H. Harris, "Surface analysis of early retrieved acetabular polyethylene liners," *The Journal of Arthroplasty*, vol. 19, no. 1, pp. 68–77, 2004.

[11] S. L. Bevill, G. R. Bevill, J. R. Penmetsa, A. J. Petrella, and P. J. Rullkoetter, "Finite element simulation of early creep and wear in total hip arthroplasty," *Journal of Biomechanics*, vol. 38, no. 12, pp. 2365–2374, 2005.

[12] J. R. Penmetsa, P. J. Laz, A. J. Petrella, and P. J. Rullkoetter, "Influence of polyethylene creep behavior on wear in total hip arthroplasty," *Journal of Orthopaedic Research*, vol. 24, no. 3, pp. 422–427, 2006.

[13] K. J. Bozic, S. M. Kurtz, E. Lau, K. Ong, D. T. P. Vail, and D. J. Berry, "The epidemiology of revision total hip arthroplasty in the United States," *The Journal of Bone and Joint Surgery—American Volume*, vol. 91, no. 1, pp. 128–133, 2009.

[14] J. A. Rodriguez and P. A. Rathod, "Large diameter heads: is bigger always better?" *Journal of Bone and Joint Surgery: Series B*, vol. 94, no. 11, supplement A, pp. 52–54, 2012.

[15] S. S. Jameson, D. Lees, P. James et al., "Lower rates of dislocation with increased femoral head size after primary total hip replacement: a five-year analysis of NHS patients in England," *The Journal of Bone and Joint Surgery—British Volume*, vol. 93, no. 7, pp. 876–880, 2011.

[16] F.-W. Shen, Z. Lu, and H. A. McKellop, "Wear versus thickness and other features of 5-mrad crosslinked UHMWPE acetabular liners," *Clinical Orthopaedics and Related Research*, vol. 469, no. 2, pp. 395–404, 2011.

[17] A. H. Krieg, B. M. Speth, and P. E. Ochsner, "Backside volumetric change in the polyethylene of uncemented acetabular components," *The Journal of Bone and Joint Surgery—British Volume*, vol. 91, no. 8, pp. 1037–1043, 2009.

[18] M. A. Conditt, M. T. Thompson, M. M. Usrey, S. K. Ismaily, and P. C. Noble, "Backside wear of polyethylene tibial inserts: mechanism and magnitude of material loss," *The Journal of Bone and Joint Surgery—American Volume*, vol. 87, no. 2, pp. 326–331, 2005.

[19] D. C. M. Chang, J. C. H. Goh, S. H. Teoh, and K. Bose, "Cold extrusion deformation of UHMWPE in total knee replacement prostheses," *Biomaterials*, vol. 16, no. 3, pp. 219–223, 1995.

[20] V. Saikko, "A multidirectional motion pin-on-disk wear test method for prosthetic joint materials," *Journal of Biomedical Materials Research*, vol. 41, no. 1, pp. 58–64, 1998.

[21] O. K. Muratoglu, C. R. Bragdon, D. O. O'Connor et al., "Unified wear model for highly crosslinked ultra-high molecular weight polyethylenes (UHMWPE)," *Biomaterials*, vol. 20, no. 16, pp. 1463–1470, 1999.

[22] ASTM, "Standard test method for wear testing of polymeric materials used in total joint prostheses," ASTM F732-00, ASTM International, 2011.

[23] M. F. Shepard, J. R. Lieberman, and J. M. Kabo, "Ultra-high-molecular weight polyethylene wear. An in vitro comparison of acetabular metal types and polished surfaces," *The Journal of Arthroplasty*, vol. 14, no. 7, pp. 860–866, 1999.

[24] M. Kyomoto, T. Moro, Y. Takatori, S. Tanaka, and K. Ishihara, "Multidirectional wear and impact-to-wear tests of phospholipidpolymer-grafted and vitamin E-blended cross-linked polyethylene: a pilot study," *Clinical Orthopaedics and Related Research*, vol. 473, no. 3, pp. 942–951, 2015.

[25] F.-W. Shen, H. A. McKellop, and R. Salovey, "Irradiation of chemically crosslinked ultrahigh molecular weight polyethylene," *Journal of Polymer Science, Part B: Polymer Physics*, vol. 34, no. 6, pp. 1063–1077, 1996.

[26] P. J. Flory, *Principles of Polymer Chemistry*, Cornell University Press, Ithaca, NY, USA, 1953.

[27] ISO, "Implants for surgery—wear of total hip-joint prostheses—part 2: methods of measurement," ISO 14242-2:2000, International Organization for Standardization, London, UK, 2000.

[28] H. Oonishi, Y. Takayama, and E. Tsuji, "Improvement of polyethylene by irradiation in artificial joints," *International Journal of Radiation Applications and Instrumentation C*, vol. 39, no. 6, pp. 495–504, 1992.

[29] H. McKellop, F.-W. Shen, B. Lu, P. Campbell, and R. Salovey, "Development of an extremely wear-resistant ultra high molecular weight polyethylene for total hip replacements," *Journal of Orthopaedic Research*, vol. 17, no. 2, pp. 157–167, 1999.

[30] Y. Ishikawa, K.-I. Hiratsuka, and T. Sasada, "Role of water in the lubrication of hydrogel," *Wear*, vol. 261, no. 5-6, pp. 500–504, 2006.

[31] R. Goldberg, A. Schroeder, G. Silbert, K. Turjeman, Y. Barenholz, and J. Klein, "Boundary lubricants with exceptionally low friction coefficients based on 2D close-packed phosphatidylcholine liposomes," *Advanced Materials*, vol. 23, no. 31, pp. 3517–3521, 2011.

[32] G. W. Stachowiak, A. W. Batchelor, and L. J. Griffiths, "Friction and wear changes in synovial joints," *Wear*, vol. 171, no. 1-2, pp. 135–142, 1994.

[33] M. Kyomoto, T. Moro, S. Yamane et al., "Poly(2-methacryloyloxyethyl phosphorylcholine) grafting and vitamin E blending for high wear resistance and oxidative stability of orthopedic bearings," *Biomaterials*, vol. 35, pp. 6677–6686, 2014.

[34] A. A. Edidin and S. M. Kurtz, "Influence of mechanical behavior on the wear of 4 clinically relevant polymeric biomaterials in a hip simulator," *The Journal of Arthroplasty*, vol. 15, no. 3, pp. 321–331, 2000.

[35] Y. Ikada, K. Nakamura, S. Ogata et al., "Characterization of ultrahigh molecular weight polyethylene irradiated with γ-rays and electron beams to high doses," *Journal of Polymer Science A: Polymer Chemistry*, vol. 37, no. 2, pp. 159–168, 1999.

[36] A. V. Shyichuk, J. R. White, I. H. Craig, and I. D. Syrotynska, "Comparison of UV-degradation depth-profiles in polyethylene, polypropylene and an ethylene-propylene copolymer," *Polymer Degradation and Stability*, vol. 88, no. 3, pp. 415–419, 2005.

[37] H. Oonishi, S. Wakitani, N. Murata et al., "Clinical experience with ceramics in total hip replacement," *Clinical Orthopaedics and Related Research*, no. 379, pp. 77–84, 2000.

[38] D. Baykal, R. S. Siskey, H. Haider, V. Saikko, T. Ahlroos, and S. M. Kurtz, "Advances in tribological testing of artificial joint biomaterials using multidirectional pin-on-disk testers," *Journal of the Mechanical Behavior of Biomedical Materials*, vol. 31, pp. 117–134, 2014.

[39] N. Tomita, T. Kitakura, N. Onmori, Y. Ikada, and E. Aoyama, "Prevention of fatigue cracks in ultrahigh molecular weight polyethylene joint components by the addition of vitamin E," *Journal of Biomedical Materials Research*, vol. 48, no. 4, pp. 474–478, 1999.

[40] V. Saikko, "in vitro wear simulation on the RandomPOD wear testing system as a screening method for bearing materials intended for total knee arthroplasty," *Journal of Biomechanics*, vol. 47, pp. 2774–2778, 2014.

[41] V. Saikko and J. Kostamo, "Random POD—a new method and device for advanced wear simulation of orthopaedic biomaterials," *Journal of Biomechanics*, vol. 44, no. 5, pp. 810–814, 2011.

[42] H. Oonishi, I. C. Clarke, V. Good, H. Amino, and M. Ueno, "Alumina hip joints characterized by run-in wear and steady-state wear to 14 million cycles in hip-simulator model," *Journal of Biomedical Materials Research: Part A*, vol. 70, no. 4, pp. 523–532, 2004.

[43] V. Saikko and T. Ahlroos, "Type of motion and lubricant in wear simulation of polyethylene acetabular cup," *Proceedings of the Institution of Mechanical Engineers Part H: Journal of Engineering in Medicine*, vol. 213, no. 4, pp. 301–310, 1999.

[44] M. B. Kanchi, O. C. Zienkiewicz, and D. R. J. Owen, "The visco-plastic approach to problems of plasticity and creep involving geometric non-linear effects," *International Journal for Numerical Methods in Engineering*, vol. 12, no. 1, pp. 169–181, 1978.

Hindawi Publishing Corporation
BioMed Research International
Volume 2015, Article ID 946215, 8 pages
http://dx.doi.org/10.1155/2015/946215

Clinical Study

Occult Infection in Aseptic Joint Loosening and the Diagnostic Role of Implant Sonication

J. T. Kempthorne,[1] R. Ailabouni,[1] S. Raniga,[1] D. Hammer,[2] and G. Hooper[3]

[1]*Department of Orthopaedic Surgery, Christchurch Hospital, Private Bag 4710, Christchurch 8140, New Zealand*
[2]*Department of Microbiology, Northland DHB, Private Bag 9742, Whangarei 0148, New Zealand*
[3]*Department of Orthopaedic Surgery and Musculoskeletal Medicine, University of Otago, Christchurch 8140, New Zealand*

Correspondence should be addressed to J. T. Kempthorne; jkempthorne@ihug.co.nz

Received 1 April 2015; Revised 6 July 2015; Accepted 7 July 2015

Academic Editor: Michiaki Takagi

Copyright © 2015 J. T. Kempthorne et al. This is an open access article distributed under the Creative Commons Attribution License, which permits unrestricted use, distribution, and reproduction in any medium, provided the original work is properly cited.

Our aim was to determine the incidence of occult infection and to examine the role of ultrasound sonication of the implants in cases of presumed aseptic loosening in a prospective trial. Joint swabs, aspirates, and deep tissue samples were obtained from around the prosthesis for routine microbiology. Each prosthesis was sonicated and the sonicate examined with Gram staining and extended cultures. There were 106 joints in the study of which 54 were revised for aseptic loosening and 52 were assigned to the control revision group. There were 9 positive cultures with 8/54 positive cultures in the aseptic loosening group and 1/52 in the control revision group ($p = 0.017$, associated OR 47.7). We found concordant results between sonication fluid culture and conventional samples in 5/9 cultures. Preoperative inflammatory markers were not prognostic for infection. *Coagulase-negative Staphylococcus* was the most commonly cultured organism (7/9). Previously unrecognised infection was present in 15% of patients undergoing revision for aseptic loosening. Ultrasound sonication of the removed prosthesis was less sensitive than conventional sampling techniques. We recommend routine intraoperative sampling for patients having revision for aseptic loosening, but we do not support the routine use of ultrasound sonication for its detection.

1. Introduction

New Zealand has an increasing aging active population with increasing rates of primary and revision joint arthroplasty surgery. In 2009, 1467 hip and knee revision arthroplasty operations were conducted nationwide, which represented 11% of all hip and knee arthroplasty operations performed during that time period. Aseptic loosening was one of the most common indications for revision, being the cause for revision in 35% and 23% of total hip and knee joints, respectively [1]. Differentiating between prosthetic joint infection (PJI) and aseptic loosening is important, as the treatment of the two groups is significantly different. Despite attempts to differentiate between the two, no single investigation has been identified as being reliable in determining the presence of infection.

The American Academy of Orthopaedic Surgeons guidelines for the diagnosis of PJI of the hip and knee recommend risk stratification on the basis of preoperative C-reactive protein and erythrocyte sedimentation rates and selective hip aspiration in patients where infection is suspected or likely [2]. On the basis of current evidence, they do not recommend intraoperative Gram stain, but they do recommend intraoperative frozen section and cultures in cases of likely infection.

Some microorganisms, especially *Staphylococcus* species, are able to attach to implants in a glycocalyx biofilm [3, 4]. These biofilms make the identification and treatment of the microorganism more difficult. Unrecognized or occult infection has been implicated in contributing to "aseptic" loosening of joint prostheses [3, 5, 6]. Recent literature has suggested that sonication (ultrasonic cleaning submersed in a solution) and culture of extracted implants may be a reliable method of improving the sensitivity in the detection of PJI and may be superior to standard tissue cultures [6–10].

The first aim of this study was to determine the prevalence of occult or unrecognized infection in a local sample of

patients undergoing joint revision surgery for presumed aseptic loosening. The second aim was to determine whether ultrasound sonication of the removed implants improved the detection of microorganisms over conventional sampling methods, in patients with low risk preoperative risk of deep infection. Our hypothesis was that sonication and subsequent culture of retrieved implants would be more sensitive at detecting occult infection than conventional culture techniques in cases of presumed aseptic loosening.

2. Methods

Prior to the initiation of the trial, we undertook quality control studies to ensure that we did not have false culture growths secondary to contamination or false negative results due to organism destruction. First we used 15 sterilized and unused joint prostheses that were removed directly from their packaging and processed through the sonication protocol, adhering to sterile surgical technique. There were no positive culture results from these implants. The effect of the study's sonication protocol on microorganism viability was also assessed in a series of *in vitro* experiments where the colony counts were compared between sonicated and nonsonicated *Staphylococcus aureus* and *Escherichia coli* standardized colonies. There were no differences between the two groups, which confirmed that there were no detrimental effects of the sonication protocol on both Gram positive and Gram negative microorganism viability.

We undertook a prospective case-control study, from 2008 until 2011, at two tertiary referral hospitals in Christchurch, New Zealand. Participation in the study was dependent on surgeons' and patient's wishes. Verbal and written consent was obtained from the patient by their orthopaedic consultant surgeon or registrar. The only exclusion criteria were a refusal by a patient to participate in the study or a failure to adhere to the study protocol. The study design was assessed and approved by the Upper South Island Regional Ethics Committee (URA/08/03/EXP).

The indication for revision surgery was used to divide the patients into two groups. The first was an aseptic loosening (study) group. These patients had a loose prosthesis and a clinically determined unlikely infection based on routine preoperative investigations. Cases were defined as infected if there were any of the following: (1) presence of a sinus tract to the joint, (2) a positive culture sample from the affected joint preoperatively, (3) an acutely unwell patient with elevated inflammatory markers, and (4) gross purulence at the time of revision surgery. The second was a control revision group, which included patients undergoing revision surgery for isolated polyethylene wear with liner exchange, dislocation, periprosthetic fracture, and mechanical failure of an implant.

All patients had preoperative blood tests that included a full blood count with white cell differential. We had incomplete acquisition of erythrocyte sedimentation rate (ESR) and C-reactive protein (CRP) for the patients in the study. Preoperative joint aspirates were not routinely performed unless there was clinical concern for acute or low grade infection. Prophylactic antibiotics were administered as per the surgeons' wishes, as a requirement for ethical approval, and therefore some patients received these at induction.

At the time of revision surgery, once the joint capsule was entered, one swab, a joint fluid aspirate, and several deep tissue samples from around the prosthesis were obtained. Any presence of frank purulence or lack of it was documented. The samples were sent to the laboratory for gram staining and conventional culture on chocolate and sheep blood agar. Once a prosthetic component was extracted, any gross contamination with tissue, bone fragments, and/or cement was gently cleaned off by rinsing the implant in a bowl of sterile saline. Handling of the implant was minimized. It was then placed into a sterile leak proof plastic container by the surgical team. The implant was fully submersed in sterile saline and then the container closed and sealed with adhesive tape. This was done to eliminate leakage and contamination in transit to the laboratory where all the processing of the removed prostheses occurred.

Each prosthesis was sonicated, in the original surgical container, for 10 minutes at 67 kHz using a Cavitator Ultrasonic Cleaner (Mettler Electronics, Anaheim, CA, USA). After sonication, a 50 mL aliquot of the sonicated fluid was centrifuged at 3000 rpm for 15 minutes. The supernatant was discarded and the pellet was cultured aerobically on blood and chocolate agar and anaerobically on blood agar. A gram stain alcohol washed slide was then prepared for review and extended cultures performed for 14 days.

A review of the patient's electronic records was used to collect data on patient demographics and historical details of the joint undergoing revision and data on the following risk factors: smoking status, history of diabetes mellitus, prolonged steroid use (more than 6 months), and obesity (BMI >40). The preoperative radiographs were reviewed to determine whether the implants were uncemented, hybrid, or cemented joints.

Statistical analysis was performed using a PASW SPSS 18.0.0 Statistical Software package (IBM, Chicago, IL, USA). Pearson's Chi-square test was used for tests of association. Mann-Whitney nonparametric tests were used to compare the time to revision surgery, as this data did not have a normal distribution. Odds ratios were calculated from 2×2 contingency tables.

Statistical significance was defined as a p value ≤ 0.05 with a 2-sided hypothesis.

3. Results

During the study period, 109 patients were enrolled, from a total of 202 patients who underwent hip and knee joint revision surgery involving the exchange of at least one component. We excluded 3 patients for breach of protocol, because their larger implants were sent to the lab in plastic bags. Sonication of implants in plastic bags has been shown to have a high risk of contamination and therefore false positive results [7].

The final study population was 106 joints from 106 patients. Fifty-four joints were revised for aseptic loosening of the implant (aseptic study group), and fifty-two joints underwent revision for other reasons (control revision group) such

Table 1: Comparison between the study groups (comparison by Chi-square test and ANOVA means comparison).

Factor	Aseptic loosening $n = 54$	Control $n = 52$	p value	Odds ratio
Male sex	33 (61%)	21 (40%)	0.033	
Mean age at index arthroplasty (yrs)	57.4	60.4	0.274	
Mean age at revision arthroplasty (yrs)	72.3	70.7	0.452	
Mean number of years since index operation (95% CI)	14.0 (11.2–16.8)	10.3 (8.1–12.5)	0.054	
Joint type				
Hip	37 (70%)	40 (75%)	0.51	
Knee	16 (30%)	13 (25%)		
Cemented implants	25 (46%)	22 (42%)	0.073	
Smoking history	7 (13%)	1 (2%)	0.007	7.6
Indication for index replacement				
Degenerative	45 (83%)	42 (81%)	0.823	
Inflammatory arthritis	3 (6%)	3 (6%)		
Posttraumatic arthritis	4 (7%)	3 (6%)		
Other	2 (4%)	4 (8%)		

as isolated polyethylene wear (16/106), dislocation (12/106), periprosthetic fracture (8/106), and finally mechanical failure (16/106).

There were no significant differences between our groups in the type of joint revised ($p = 0.51$) or the indication for index arthroplasty ($p = 0.832$). Furthermore, there was no difference in the patients' age at either index or revision surgery ($p = 0.274$ and $p = 0.452$). Finally there was no difference in the use of cement between the groups ($p = 0.073$). There was a significant difference ($p = 0.033$) in the gender distribution between the groups with females overrepresented in the control revision group ($p = 0.033$) and those patients with a history of smoking ($p = 0.007$). There was no significant difference in the lifespan of the implant prior to revision between aseptic loosening (14 years) and control revision (10.3 years) groups ($p = 0.054$) (Table 1).

There were 9 positive cultures in the study, eight (15%) positive cultures in the aseptic loosening group and 1 (2%) in our control revision group ($p = 0.017$, associated odds ratio of 47.7). Any positive culture on swab, aspirate, or deep tissue was taken to represent a positive culture on conventional sampling technique. These nine patients had an average post-op documented clinic follow-up in the medical records of 9.7 months (range 3–22 months) and 19.3 months (range 8–31 months) of survivorship at writing of the manuscript without known representation. Four patients were treated in consultation with a specialist infectious diseases team with oral and/or intravenous antibiotics. All patients underwent a single stage revision and none have had any ongoing complications, repeat admissions, or operations due to infection of their prosthesis.

Out of the 8 cases in the aseptic loosening group with positive conventional cultures, 3 cases had positive cultures from a single sampling technique. Those cultures were from deep tissue samples, where multiple specimens from different regions around the joint undergoing revision were positive with the same organism.

We found concordant results between sonication fluid culture and conventional samples in 5 of the 9 cultures (56%). Sonicated fluid culture was positive in one case where conventional cultures were negative. Three patients from the aseptic loosening group had concordant growths from both conventional and sonication cultures (Table 3). We found more cultures to be positive on conventional sampling alone than on sonicated fluid culture alone (4 compared to 1). Conventional sampling techniques provided more positive cultures than sonication. Examination of the conventional sampling techniques indicated that deep tissue sampling was the most likely to be positive with synovial fluid aspirates the least likely to be positive (Table 4).

The microorganisms cultured were mainly *Staphylococci* with coagulase-negative *Staphylococci* (CONS) the most commonly cultured organisms in the aseptic loosening group and the only species cultured from the only positive control case. *S. aureus* was the other cultured organism, being positive in 2 cultures from the aseptic loosening group. *Staphylococci* were the only microorganisms to be cultured from the sonicated fluid samples in this study (Table 2).

We compared the results of those who returned a positive culture with the previously recorded risk factors and found that none of these factors were associated with an increased risk of returning a positive culture. There was also no statistically significant association between having raised or abnormal preoperative neutrophil differential counts, CRP or ESR, and having a positive culture result (Table 5). There were three patients in the aseptic loosening group and four patients in the control revision group who had an isolated elevated preoperative CRP. In the aseptic loosening group, two of the three patients had a CRP within 2 mg/L of the cutoff point of 10 mg/L. There were no other features to suggest infection at the time of workup. One of these patients returned positive cultures of CONS at revision from all methods and was treated as an occult infection. The third patient had a negative preoperative radiologically guided aspirate for a significantly elevated CRP and hence was included in the aseptic loosening group. Of the four in the control group, one had a CRP within 1 mg of the cutoff point, two had a background of rheumatoid arthritis and were receiving steroids, and one

Table 2: Positive culture case series.

Patient number	Aseptic loosening (AL) or control (C)	Joint involved	Conventional culture	Sonication culture	Organism	Treatment	Clinical follow-up	Months since index procedure	Infection related complication
2	A.L	Uncemented THA	N	Y	*S. aureus*	Oral Abs.	22	31	No
7	A.L	Hybrid THA	Y	N	CONS	NIL	3	27	No
18	A.L	Cemented THA	Y	N	CONS	NIL	15	24	No
19	A.L	Uncemented THA	Y	Y	CONS	ID/Abs.	5	23	No
32	C	Uncemented THA	Y	Y	CONS	NIL	10	13	No
70	A.L	Uncemented THA	Y	N	CONS	NIL	12	18	No
96	A.L	Cemented THA	Y	Y	CONS	ID/Abs.	3	13	No
107	A.L	TKA	Y	N	*S. aureus*	ID/Abs.	8	9	No
110	A.L	TKA	Y	N	CONS	NIL	6	8	No

Table 3: Breakdown of positive cultures into sampling technique.

Study group	Conventional only	Sonication and conventional	Conventional	Total (%)	Odds ratio	p value
Aseptic loosening ($n = 54$)	4	1	3	8 (15%)	7.7	0.017
Control revision ($n = 52$)	0	0	1	1 (2%)		

Table 4: Frequency of sampling method returning a positive culture.

Study group	Aspirate	Swab	Tissue	Conventional combined	Ultrasonication
Aseptic loosening	2	3	5	7	4
Control revision	1	1	1	1	1

Table 5: Preoperative blood tests (Chi-Square test).

Blood test		Any positive cultures		Totals	p values
		Y	N		
CRP (normal <10 mg/L)	Normal	6	43	49	0.89
	High	1	6	7	
ESR (normal 1–20 mm/hr)	Normal	8	46	54	1
	High	0	0	0	
WCC (normal 4–11 $\times 10^9$/L)	Normal	7	41	48	0.181
	Abnormal	1	1	2	
Neutrophils (normal 1.7–7.5 $\times 10^9$/L)	Normal	7	41	48	0.407
	Abnormal	1	2	3	

had a periprosthetic fracture and concomitant lower limb cellulitis at the time of admission. None of these patients had positive cultures from the revision procedure.

4. Discussion

Although we found a significant positive culture rate from patients undergoing revision for presumed aseptic loosening, our study did not support the sonication of retrieved implants at revision surgery for aseptic loosening despite the literature suggesting that implant sonication is a more sensitive technique for the detection of infection. We consistently had more positive cultures from conventional sampling methods combined than on sonication. This reduced sensitivity of detection is out of keeping with the published literature around the use of sonication [6–10]. Our implants were placed into a sterile sealed solid container as opposed to sealed plastic bags given the concerns about contamination. Trampuz et al. found that there was clear evidence of bag leakage after sonication and showed reduced specificity with some growths of water related bacterial organisms [11]. To our knowledge, most other sonication protocols looked at sonication in bags which therefore could be subject to the same issues of contamination. Our methodology aimed to obviate that risk; however, it may be that the solid container decreased the efficacy of energy transmission and therefore cavitation between the sonicated fluid and metal interface, leading to our seemingly reduced sensitivity as compared with conventional sampling techniques. As part of the study design, we undertook a viability study to ensure that the sonication and culturing process was not compromising microorganism viability. Nevertheless, our *in vitro* assessment did not directly assess the ability of our sonication protocol to work on implants in a solid container.

To our knowledge, this study is the first to use a control revision arthroplasty group for comparison when assessing the rate of infection in revision for aseptic loosening whereas prior literature has focused on the aseptic loosening and infection groups exclusively. Our study groups were very similar despite being an unmatched prospective case-control series. The gender discrepancy between groups could relate to higher proportion of female patients who underwent revision for periprosthetic fracture and dislocation. Nguyen et al. studied the role of sonication in 21 femoral component revisions from both hip and knee replacement surgeries for aseptic loosening [8]. They had an intraoperative control implant opened at the time of surgery and processed concurrently to validate their sonication protocol. They had stringent criteria for excluding cases from their aseptic group such as any derangement in preoperative inflammatory markers. They found 4.7% (1/21) positive growth from sonicated fluid in this group of patients but also had one case of contamination.

We found a 15% positive culture rate in our presumed aseptic loosening group. This was significantly higher than the recent literature that has directly or indirectly examined this problem [7, 8, 11, 12], but well below earlier work by

Tunney et al. [10, 13]. Tunney et al. had a 10% positive sonicated culture rate in 120 implants and 73% PCR positive rate (mainly *Staphylococcus* and *Propionibacterium* species). However, in their work, Tunney et al. did not screen for clinical infection. Trampuz et al. documented a 9% culture rate from conventional sampling in a series of 54 patients [9], but later research demonstrated a much lower rate of 2% in a larger series of 252 revisions for aseptic loosening [11].

By comparing the aseptic loosening group to those undergoing revision for isolated polyethylene wear, dislocation, and fracture, respectively, without implant loosening, the results clearly show that loosening is associated with higher rates of occult infective process. Whether the higher rates of bacterial growth are indicative of occult infection being the cause of loosening or whether loosening creates a favourable environment for bacterial growth is difficult to determine. Regardless, according to the current Musculoskeletal Infection Society definition, the isolation of the same pathogen from two separate tissue samples obtained from a prosthetic joint constitutes a PJI and therefore the patients would receive treatment [14]. Coagulase-negative *Staphylococcus* was our most commonly cultured organism. Because of the multiple processes used to validate our methodology, we are confident that our results are not false positives (contamination).

Despite having incomplete preoperative inflammatory marker testing, we have also shown that there still remain a significant number of patients who are likely to have occult infection at revision for aseptic loosening despite normal preoperative ESR and CRP. The best method to confirm or exclude infection was deep tissue samples at the time of surgery. We had three patients in the aseptic loosening group with an elevated CRP preoperatively, but only one of them had a positive culture from deep tissues. Conversely, four patients in the control group had elevated inflammatory markers preoperatively and none of them had evidence of occult infection. Our results indicate that a negative preoperative workup with inflammatory markers should not replace adequate microbiological sampling at the time of revision surgery especially for cases of aseptic loosening as compared to other causes of revision. One should use inflammatory markers to stratify the risk of infection in their patients before proceeding with revision surgery as per international guidelines [2].

The rate of clinical infection developing in cases with unexpected positive culture results at the time of revision surgery in the literature has varied from 0 to 11% depending on the length of follow-up and on the initiation of therapeutic antibiotics after positive results [10, 12, 13]. Our approach has been to treat any deep tissue cultures which are multiply positive with appropriate antibiotic therapy in consultation with an infectious diseases team as this meets the current diagnosis of PJI and we felt that the benefits outweighed the potential downsides of treatment with antibiotics. We consider the possibility of the positive result being a contaminant is unlikely in this study because of our control group, and the quality control tests, which validated our methodology.

There are several limitations to our study, for example, the variability of use of prophylactic antibiotics on induction of anaesthesia. However, we were unable to control this as it was a restriction required to get ethical approval for the study. Furthermore, given the premise that bacteria in biofilms are more resistant to antibiotic administration, this would, if anything, underestimate the prevalence of occult infection in the aseptic loosening group. This would add further credence to the utility of microbiological sampling at the time of revision for patients with loose implants.

A further methodological weakness includes an incomplete set of inflammatory markers for all patients undergoing revision. Within that context, however, we were able to find significant *Staphylococcus* growths in patients who had negative preoperative inflammatory markers. Given our study design, we can not comment on the specificity or sensitivity of the preoperative blood workup on the diagnosis of PJI other than to say that negative preoperative assessment does not always indicate lack of infection or the converse.

Another limitation was the lack of histopathological review of tissues in our study. A comparison between the positive culture patients and their routine microscopic histological assessment would have been beneficial as added evidence of the presence of infection. Previous literature however has shown that deep tissue culture when positive is highly specific for PJI [15, 16]. We did not undertake frozen section intraoperatively. Tsaras et al. showed that the presence of 5 neutrophils (PMN) in five high power fields (HPF, 400x magnification) increased the likelihood of infection 12-fold [17]. Furthermore, they showed that there was no significant difference between 5 and 10 PMN/HPF cutoffs. However, it is our experience that frozen section is highly subjective and its utility in PJI sampling is unpredictable. In their study, Tunney et al. found that histopathology could only be suitably assessed on 67.5% (81/120) of their cases [10]. Based on a cutoff of >10 PMN/HPF, only 4/26 patients with positive cultures had an abnormal frozen section suggestive of infection. Furthermore, 7/94 culture negative cases had frozen section features to suggest infection but no positive cultures despite their increased sensitivity using sonication. We therefore feel that our results are valid despite the lack of histopathological comparison.

Finally, we did not undertake PCR analysis on the sonicated fluid cultures in our study. PCR of the 16S rRNA segment of the bacterial genome offers a highly sensitive assessment for the presence of bacteria. Ince et al. found one positive culture on PCR of tissue samples in a series of 24 revision procedures for aseptic loosening, but they did not assess the role of sonication [6]. Tunney et al. had an overall 72% positive rate of PCR in their study of sonicated fluid culture [13]. This comprised a 100% PCR positive rate in their culture positive group and 40% rate in their culture negative group. This led them to assume that occult infection is present at a much higher rate than previously thought. However, they only excluded skin contamination from the staff at the laboratory undertaking the analysis and not the operating room personnel or environment. Kobayashi et al. undertook an assessment of ultrasonication and real time intraoperative PCR in 23 patients undergoing 30 reoperations of a large joint prosthesis [18]. They do not give a clear indication of the reasons for reoperation but the sample included operations for the treatment of infection. They

found that intraoperative PCR was positive in 13/15 patients who had conventional positive cultures. The sensitivity and specificity of their sonicated fluid PCR were 0.8 and 0.87, respectively, when compared to conventional cultures and histopathology combined.

The presence of bacterial 16S rRNA material on PCR does not equate with the presence of active or indolent bacterial infection. It merely indicates the presence of bacterial genetic material rather than bacterial material viability or pathogenicity. The test is also highly sensitive, which makes any potential contamination more likely to be detected. The 16S rRNA segment is very common to most bacteria known to cause PJI; therefore, its use is reportedly associated with increased sensitivity [19]. PCR targeted at organisms such as Methicillin Resistant *Staphylococcus aureus* was more specific but lacked sensitivity [18]. In a meta-analysis of 14 articles looking at PCR, Qu et al. found that PCR had a sensitivity of 0.86 and specificity of 0.91 for PJI [19]. They also noted a heterogeneity of the study materials and that quantitative PCR was more accurate compared to nonquantitative assessments. Currently, the role of PCR is not part of the standard definition of PJI but may be a useful adjunct in the management of culture negative overt PJI.

5. Conclusion

We found a positive culture from intraoperative sampling in patients undergoing revision for aseptic loosening group of 15%, and as such previously unrecognised infection was present in a clinically significant proportion of this group. Ultrasound sonication of the removed prosthesis was less sensitive than conventional sampling techniques in our study. This could be due to ultrasonication in solid containers as opposed to bags to reduce contamination risk. We suggest that unrecognised infection may be present in a significant proportion of aseptic loosening cases undergoing revision surgery and that routine intraoperative sampling is recommended, but our results do not support the routine use of ultrasound sonication for its detection. The question remains whether loosening is caused by low grade infection or whether infection is promoted in the environment of loosening.

Conflict of Interests

There was no internal or external professional financial conflict for all researchers and no external funding for this research project.

Acknowledgments

The authors would like to acknowledge the excellent support and services provided by Professor David Murdock, the Microbiology Lab staff at Canterbury Health Laboratories, and the theatre team at Burwood Hospital (Christchurch).

References

[1] New Zealand Orthopaedic Association (NZOA), *New Zealand Joint Registry Ten Year Report*, New Zealand Orthopaedic Association (NZOA), Christchurch, New Zealand, 2009.

[2] "AAOS clinical practice guideline: diagnosis of periprosthetic joint infections of the hip and knee," *Journal of the American Academy of Orthopaedic Surgeons*, vol. 18, no. 12, pp. 771–772, 2010.

[3] K. R. Berend, A. V. Lombardi Jr., and J. B. Adams, "Unexpected positive intraoperative cultures and gram stain in revision total hip arthroplasty for presumed aseptic failure," *Orthopedics*, vol. 30, no. 12, pp. 1051–1053, 2007.

[4] A. G. Gristina and J. W. Costerton, "Bacterial adherence to biomaterials and tissue. The significance of its role in clinical sepsis," *The Journal of Bone & Joint Surgery—American Volume*, vol. 67, no. 2, pp. 264–273, 1985.

[5] J. A. Dupont, "Significance of operative cultures in total hip arthroplasty," *Clinical Orthopaedics and Related Research*, vol. 211, pp. 122–127, 1986.

[6] A. Ince, J. Rupp, L. Frommelt, A. Katzer, J. Gille, and J. F. Löhr, "Is 'aseptic' loosening of the prosthetic cup after total hip replacement due to nonculturable bacterial pathogens in patients with low-grade infection?" *Clinical Infectious Diseases*, vol. 39, no. 11, pp. 1599–1603, 2004.

[7] C. L. Nelson, A. C. McLaren, S. G. McLaren, J. W. Johnson, and M. S. Smeltzer, "Is aseptic loosening truly aseptic?" *Clinical Orthopaedics and Related Research*, no. 437, pp. 25–30, 2005.

[8] L. L. Nguyen, C. L. Nelson, M. Saccente, M. S. Smeltzer, D. L. Wassell, and S. G. McLaren, "Detecting bacterial colonization of implanted orthopaedic devices by ultrasonication," *Clinical Orthopaedics and Related Research*, vol. 403, pp. 29–37, 2002.

[9] A. Trampuz, K. E. Piper, M. J. Jacobson et al., "Sonication of removed hip and knee prostheses for diagnosis of infection," *The New England Journal of Medicine*, vol. 357, no. 7, pp. 654–663, 2007.

[10] M. M. Tunney, S. Patrick, S. P. Gorman et al., "Improved detection of infection in hip replacements. A currently underestimated problem," *The Journal of Bone and Joint Surgery—British Volume*, vol. 80, no. 4, pp. 568–572, 1998.

[11] A. Trampuz, K. E. Piper, A. D. Hanssen et al., "Sonication of explanted prosthetic components in bags for diagnosis of prosthetic joint infection is associated with risk of contamination," *Journal of Clinical Microbiology*, vol. 44, no. 2, pp. 628–631, 2006.

[12] K. E. Piper, M. J. Jacobson, R. H. Cofield et al., "Microbiologic diagnosis of prosthetic shoulder infection by use of implant sonication," *Journal of Clinical Microbiology*, vol. 47, no. 6, pp. 1878–1884, 2009.

[13] M. M. Tunney, S. Patrick, M. Curran et al., "Detection of prosthetic hip infection at revision arthroplasty by immunofluorescence microscopy and PCR amplification of the bacterial 16S rRNA gene," *Journal of Clinical Microbiology*, vol. 37, no. 10, pp. 3281–3290, 1999.

[14] J. Parvizi, B. Zmistowski, E. F. Berbari et al., "Workgroup Convened by the Musculoskeletal Infection Society. New definition for periprosthetic joint infection," *Journal of Arthroplasty*, vol. 26, Article ID 1136e8, 2011.

[15] V. K. Aggarwal, C. Higuera, G. Deirmengian, J. Parvizi, and M. S. Austin, "Swab cultures are not as effective as tissue cultures for diagnosis of periprosthetic joint infection," *Clinical Orthopaedics and Related Research*, vol. 471, no. 10, pp. 3196–3203, 2013.

[16] D. E. Padgett, A. Silverman, F. Sachjowicz, R. B. Simpson, A. G. Rosenberg, and J. O. Galante, "Efficacy of intraoperative cultures obtained during revision total hip arthroplasty," *The Journal of Arthroplasty*, vol. 10, no. 4, pp. 420–426, 1995.

[17] G. Tsaras, A. Maduka-Ezeh, C. Y. Inwards et al., "Utility of intraoperative frozen section histopathology in the diagnosis of periprosthetic joint infection: a systematic review and meta-analysis," *The Journal of Bone & Joint surgery—American Volume*, vol. 94, no. 18, pp. 1700–1711, 2012.

[18] N. Kobayashi, Y. Inaba, H. Choe et al., "Simultaneous intraoperative detection of methicillin-resistant *Staphylococcus* and pan-bacterial infection during revision surgery use of simple DNA release by ultrasonication and real-time polymerase chain reaction," *The Journal of Bone & Joint Surgery—American Volume*, vol. 91, no. 12, pp. 2896–2902, 2009.

[19] X. Qu, Z. Zhai, H. Lin et al., "OCR-based diagnosis of prosthetic joint infection," *Journal of Clinical Microbiology*, vol. 51, no. 8, pp. 2742–2746, 2013.

Hindawi Publishing Corporation
BioMed Research International
Volume 2015, Article ID 283038, 10 pages
http://dx.doi.org/10.1155/2015/283038

Research Article

Does Metal Transfer Differ on Retrieved Ceramic and CoCr Femoral Heads?

Eliza K. Fredette,[1] Daniel W. MacDonald,[1] Richard J. Underwood,[1,2] Antonia F. Chen,[3] Michael A. Mont,[4] Gwo-Chin Lee,[5] Gregg R. Klein,[6] Clare M. Rimnac,[7] and Steven M. Kurtz[1,2]

[1] *Implant Research Center, School of Biomedical Engineering, Science and Health Systems, Drexel University, Philadelphia, PA 19104, USA*
[2] *Exponent, Inc., Philadelphia, PA 19104, USA*
[3] *Rothman Institute at Thomas Jefferson University Hospital, Philadelphia, PA 19107, USA*
[4] *Center for Joint Preservation and Replacement, The Rubin Institute of Advanced Orthopedics, Sinai Hospital of Baltimore, Baltimore, MD 21215, USA*
[5] *The University of Pennsylvania, Philadelphia, PA 19104, USA*
[6] *Hartzband Center for Hip and Knee Replacement, Paramus, NJ 07652, USA*
[7] *Center for the Evaluation of Implant Performance, Departments of Orthopaedics and Mechanical and Aerospace Engineering, Case Western Reserve University, Cleveland, OH 44106, USA*

Correspondence should be addressed to Eliza K. Fredette; ekf35@drexel.edu

Received 3 April 2015; Revised 13 July 2015; Accepted 28 July 2015

Academic Editor: Kengo Yamamoto

Copyright © 2015 Eliza K. Fredette et al. This is an open access article distributed under the Creative Commons Attribution License, which permits unrestricted use, distribution, and reproduction in any medium, provided the original work is properly cited.

Metal transfer has been observed on retrieved THA femoral heads for both CoCr and ceramic bearing materials. *In vitro* wear testing has shown increased wear to polyethylene acetabular liners with the presence of metal transfer. This study sought to investigate the extent of metal transfer on the bearing surface of CoCr and ceramic femoral heads and identify prevalent morphologies. Three bearing couple cohorts: M-PE ($n = 50$), C-PE ($n = 35$), and C-C ($n = 15$), were derived from two previously matched collections ($n = 50$/group) of CoCr and ceramic femoral heads. From the three cohorts, 75% of the femoral heads showed visual evidence of metal transfer. These femoral heads were analyzed using direct measurement, digital photogrammetry, and white light interferometry. Surface area coverage and curved median surface area were similar among the three cohorts. The most prevalent metal transfer patterns observed were random stripes ($n = 21/75$), longitudinal stripes ($n = 17/75$), and random patches ($n = 13/75$). Metal transfer arc length was shorter in the M-PE cohort. Understanding the morphology of metal transfer may be useful for more realistic recreation of metal transfer in *in vitro* pin-on-disk and joint simulators studies.

1. Introduction

Metal transfer has been observed on the femoral head components of revised total hip replacements for decades, appearing dark and metallic in color [1, 2]. The mechanisms of metal transfer to the bearing surface are thought to include femoral head dislocation, closed reduction procedures, impingement, or third body entrapment in the articulating zone [3–5]. Long longitudinal stripes have been observed when the femoral head and metal shell come into contact, referred to in past reports as "longitudinal scraping" on the bearing surface with both metal transfer and femoral head material loss [3, 6]. Additionally, debris entrapped in the counterface has been linked to patterned markings on the bearing surface [5, 7]. Metal transfer markings may consist of titanium (Ti) or cobalt chromium (CoCr) alloy and have been shown to increase the surface roughness of both ceramic and CoCr femoral heads [1, 8]. Metal transfer is a concern because some studies have correlated this increased surface roughness of the femoral head to an increased wear rate of the (conventional, i.e., not highly cross-linked) polyethylene counterface [8, 9].

Table 1: Patient demographics were similar between the three cohorts with the exception of patient age. All data is reported as median, IQR, with the exceptions of gender (reported as percent female).

	CoCr-on-polyethylene femoral heads	Ceramic-on-polyethylene femoral heads	Ceramic-on-ceramic femoral heads	p value
Age (years)	57 (16.0)	53 (15.3)	49 (11.4)	0.02
Gender (% female)	50%	37%	27%	0.21
Body mass index (kg/m^2)	29.1 (11.7)	28.2 (11.9)	30.7 (7.3)	0.54
Weight (kg)	185 (71.5)	189 (75.0)	200 (82.8)	0.37
Head size [median] (mm)	32 (8.0)	32 (4.0)	32 (0.0)	0.47
Max UCLA activity score	6 (4)	6 (3)	6 (3)	0.64
Implantation time (years)	1.9 (2.7)	2.1 (4.4)	1.7 (1.4)	0.77

Little is known about the morphology of metal transfer on ceramic or CoCr femoral heads or whether clinical and material factors influence either the extent or the morphology of metal transfer. Previous studies of metal transfer consisted of visual observation, semiquantitative scoring, and surface roughness measurements but failed to distinguish among the different morphologies of the metal transfer observed [1, 3, 8]. A recent set of case studies with six analyzed components described global patterns observed on the bearing surface of CoCr femoral heads for revised total hip replacements, but the patterns noted were not specific to metal transfer [7]. Recent studies have also established methods to ascertain global positions of wear patterns on CoCr femoral heads for computer-generated models simulating conventional polyethylene wear and liner positioning [6, 9]. These studies focused only on scratches and material removal of CoCr femoral heads, disregarding ceramic heads, alternative bearings, and metal transfer onto the bearing surface. To our knowledge, metal transfer evaluation has yet to be performed on ceramic femoral heads or on a large cohort of retrieved implants.

In this study, we asked the following questions: (1) what is the extent of metal transfer on the bearing surface of ceramic and CoCr femoral heads, and (2) does one bearing couple have a higher incidence of metal transfer? Additionally, we asked: (3) is there a specific pattern and morphology of metal transfer that occurs most often, and (4) does the metal transfer pattern or morphology differ between ceramic and CoCr femoral heads?

2. Methods

2.1. Cohort Selection. From 2001 to 2014, over 3,000 total hip replacement systems were collected at revision surgery as part of a multi-institutional, institutional review board-approved orthopaedic implant retrieval program, including six medical centers and three biomedical engineering laboratories. We utilized two previously matched groups of CoCr and ceramic heads. The CoCr femoral heads articulated with conventional polyethylene ($n = 11$) and HXLPE ($n = 39$). The ceramic femoral heads were a mix of alumina on alumina ($n = 15$), alumina on conventional polyethylene ($n = 12$), alumina on highly cross-linked polyethylene (HXLPE) ($n = 8$), zirconia-toughened-alumina (ZTA) on conventional polyethylene ($n = 3$), and zirconia-toughened-alumina (ZTA) on HXLPE ($n = 12$). The bearing couples were grouped into three cohorts overall: CoCr-on-polyethylene (M-PE), ceramic-on-polyethylene (C-PE), and ceramic-on-ceramic (C-C).

The M-PE components were implanted for a median of 1.9 years (Interquartile Range [IQR]: 2.7 years), the C-PE components for 2.1 years (IQR: 4.4 years), and the C-C components for 1.7 years (IQR: 1.4 years; $p = 0.77$). Although not specifically matched for, head size was similar among the three cohorts with a median head size of 32 mm ($p = 0.47$). Components in all cohorts were revised primarily for loosening and infection. Only one implant from the C-PE (ZTA on HXLE) cohort was revised for instability. Gender, body mass index (BMI), University of California Los Angeles activity score (UCLA), and implantation time were similar among all cohorts ($p > 0.05$; Table 1). The C-PE and C-C cohorts were slightly younger than the M-PE cohort (mean difference = 3 and 10 years, resp.; $p = 0.02$; Table 1).

All components were cleaned using the same institutional procedure. Specifically, the CoCr and ceramic femoral heads were individually soaked in 10 : 1 water : Discide solution (Alimed; Dedham, Massachusetts, USA) for twenty minutes. The components were scrubbed with a soft nylon brush to remove loose debris and soaked again in 10 : 1 water : Discide solution for twenty minutes. The femoral heads were then placed in an ultrasonication bath for two twenty-minute sessions to remove loose debris. Following cleaning, the femoral heads were air-dried and stored in air until inspection was performed.

2.2. Visual Scoring of Metal Transfer. The extent of metal transfer on the femoral heads was scored using a 3-point semiquantitative scale adapted from Kim et al. [1] and a diffused lighting technique established by Heiner et al. [10]. Three independent observers (EKF, JSJ, and JTS) scored each femoral head, discussing dissimilar visual scores until a consensus was reached. Resting on the taper surface, the heads were viewed while being shrouded in an opaque tube. The tube diffused the room lighting, replacing any reflections with a smooth white background. Only the portion of the head that would articulate with the acetabular liner in a normal gait pattern was observed and scored in this manner (i.e., the upper hemisphere) [6, 11]. A score of 1 was given when no metal transfer was observed. A score of 2 was

given when minimal metal transfer was observed, defined as isolated marks, a few marks in concentrated areas, or markings very light in color. A score of 3 was given for severe metal transfer, that is, when a longitudinal, concentrated metal transfer stripe was observed or when metal transfer of any type was observed over the majority of the upper hemisphere [1]. We used the visual score of metal transfer as a screening process to identify femoral heads suitable for quantitative analysis.

2.3. Image Acquisition. Femoral heads were photodocumented using the same diffused lighting technique developed by Heiner et al. [10]. Each femoral head was wiped with water and isopropyl alcohol to remove any dust that accumulated during storage and then positioned above a dark blue background in the opaque tube to remove background reflection artifacts and diffuse the external lighting from the photography lights, respectively. The upper hemisphere of each femoral head was photographed using a Nikon D800 digital SLR camera (Nikon Inc.; Melville, New York, USA) mounted on an overhead stand and remote accessed from a computer. In order to increase our depth of field and to obtain an in-focus image of the entire upper hemisphere, we utilized focus-bracketing using commercial software (Helicon Focus 6, Kharkov, Ukraine). Ten images per femoral head were captured at different equidistant focal points and digitally stacked to achieve an extended depth of field.

2.4. Metal Transfer Surface Area Calculations. We quantitatively analyzed components with visual evidence of metal transfer (corresponding to a transfer score ≥ 2), using a customized MATLAB (Mathworks; Natick, Massachusetts, USA) algorithm applied to all images of the femoral heads. All photographs were enhanced using a standard MATLAB monochromatic photograph filter. Metal transfer was identified using an edge detection filter (Canny Edge Detection) to isolate metal transfer using pixel segmentation [6, 10, 12]. Outlines of the transfer were filled in using a customized Nearest-Neighbor algorithm. The two-dimensional image was projected onto an idealized half-sphere using a reverse azimuthal projection (Figure 1). Metal transfer was reported as a percentage of the surface area of the upper hemisphere covered by metal transfer and then converted to the surface area in mm^2 for a half sphere based on the femoral head size. A repeatability study was conducted in accordance with ASTM International Designation: E 691-08 [13]. It was determined that this procedure, when repeated three times consecutively under similar conditions by the same operator, allowed for an average repeatability standard deviation (s_r) of 0.348% across the cohorts. This was derived from the standard deviation of the percentages produced three consecutive times per head, over an entire population of 74 analyzed heads ($s_r = \sqrt{\sum_1^p (s^2/p)}$; $p = 74$).

2.5. Pattern Classification. The upper hemispheres of femoral heads with evidence of metal transfer (transfer score ≥ 2) were inspected to determine different patterns of transfer through visual examination and digital microscopy (Keyence; Itasca, Illinois, USA). Seven pattern categories were discerned by three independent observers (EKF, JSJ, and JTS): solid patch, directional scratches, longitudinal stripe, random stripe, random patches, patterned coverage, and miscellaneous (Table 2). In the case of discrepancies between the observers, the differences were discussed until consensus was obtained.

The dimensions of the three most frequently observed patterns (longitudinal stripe, random stripe, and random patches) were measured. The most prominent mark (i.e., largest metal transfer surface area, darkest, and most consistent in color) was measured for total length and width using calibrated calipers. Length was considered to be the main exhibited direction, and each mark was measured only to the upper hemisphere boundary at the head equator. Arc length was calculated from the chord length measured with the calipers (Arc Length = Diameter $*$ $\sin^{-1}$(Measured Chord Length/Diameter)). Metal transfer height was measured using white light interferometry (WLI) (NewView 5000, Zygo; Middlefield, Connecticut, USA). A total of 5 WLI measurements per femoral head were taken for visually identified regions of metal transfer. Using commercial three-dimensional surface analysis software (TalyMap Platinum, Taylor Hobson, Leicester, United Kingdom), the spherical form was removed from each surface scan and converted into a series of two-dimensional height profiles encompassing the entire measured surface (Figure 2). The maximum metal transfer peak height for each femoral head was calculated as the mean peak areal height (SR_{pm}): the single maximum mean-to-peak height per each measurement location averaged over all scanned regions (Figure 2).

2.6. Statistical Analysis. Nonparametric statistical analysis was performed using commercially available software (SPSS Statistics 22; Chicago, Illinois) due to the nonnormal nature of the data. To determine differences between bearing couples, we used the Kruskal Wallis analysis of variance with *post hoc* Dunn's test, where appropriate. For correlations between continuous variables, Spearman's Rank Correlation test was used. Alpha was set to 0.05 for all tests. All results are reported as median, IQR.

3. Results

Metal transfer was a common observation for all bearing couples; however, it occurred in different proportions among the three cohorts ($p < 0.001$; Pearson Test). Metal transfer (transfer score ≥ 2) on the upper hemisphere was observed in 64% ($n = 32/50$) of M-PE heads, 83% ($n = 29/35$) of C-PE heads, and 93% ($n = 14/15$) of C-C heads (Figure 3). Altogether, 75 of 100 femoral heads had a metal transfer score ≥ 2. Within these 75 femoral heads, severe or concentrated metal transfer (transfer score = 3) was observed on 20% ($n = 10/50$) of M-PE heads, 23% ($n = 8/35$) of C-PE heads, and 80% ($n = 12/15$) of C-C heads.

For the 75 femoral heads that exhibited metal transfer with a visual score ≥ 2, the metal transfer surface area

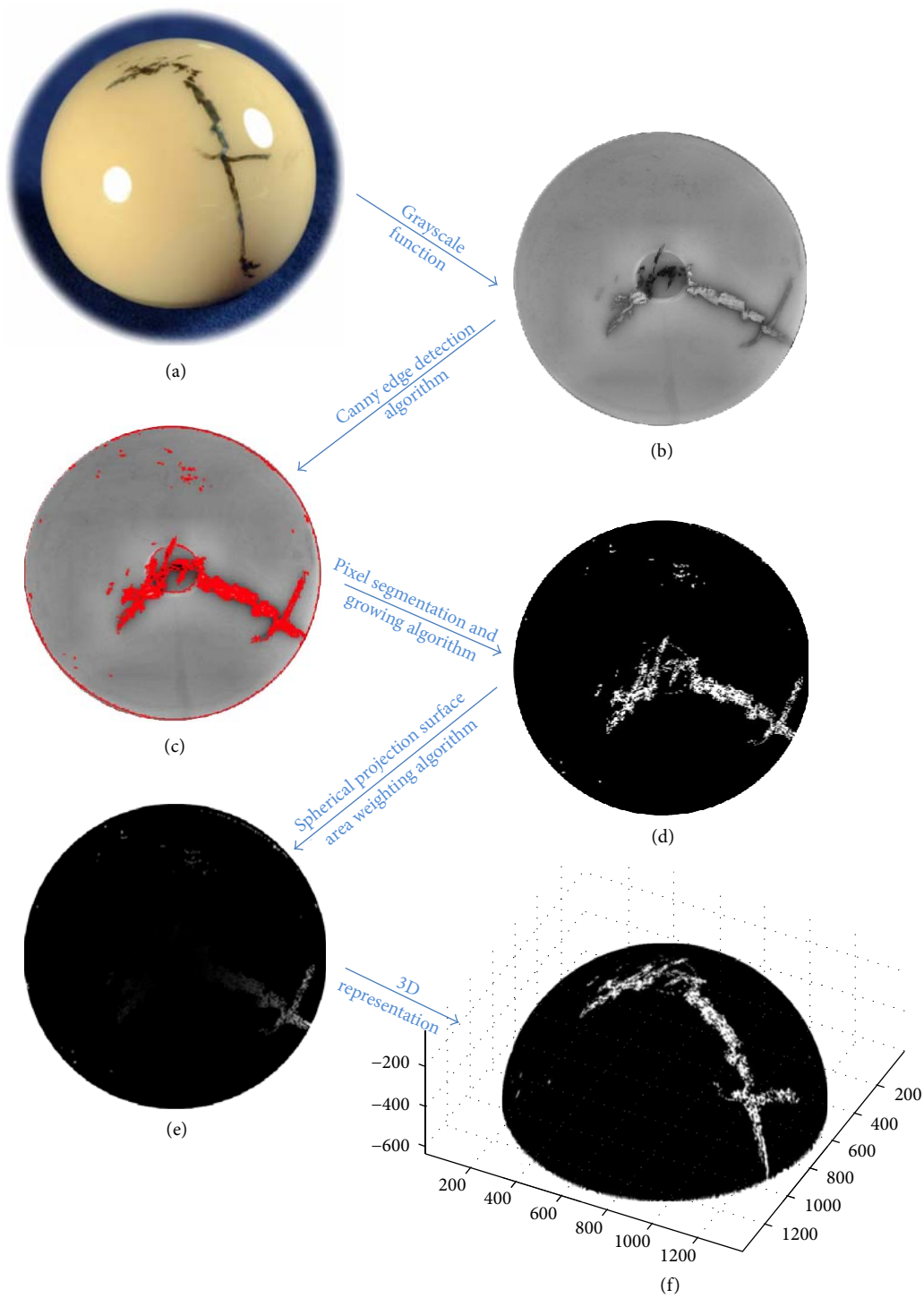

Figure 1: Procedure for analyzing metal transfer damage on a ceramic femoral head. (a) Initial photo documentation of a ceramic femoral head with metal transfer damage. (b) Photo documentation with grayscale enhancement applied. (c) Canny edge detection defining the edges of the metal transfer. (d) Pixel segmentation isolating metal transfer from the femoral head for the upper hemisphere, expanded to full metal transfer surface area using a Nearest-Neighbor growing algorithm. (e) Reverse azimuthal projection producing a weighted two-dimensional image of the total upper hemisphere featuring metal transfer, and the percent coverage. (f) An equivalent 3D representation of the isolated metal transfer.

Table 2: Summarized pattern categories of observed metal transfer on the bearing surface of the analyzed femoral heads. Patterns are presented by type, description, and an exemplar photograph for each cohort (images taken with a digital microscope (Keyence; Itasca, Illinois, USA)).

Pattern observed	Description	CoCr	Ceramic
Solid patch	Similar in length and width, with a rough dark gray appearance. Often only one per femoral head, and commonly the only metal transfer on the bearing surface. Occasionally accompanied by one or two random patches		
Directional scratches	Multiple thin lines of transfer with similar macrodirectionality. Typically clustered in groups or in a circular ring around the apex of the femoral head		
Longitudinal stripe	Longitudinal dark marks appearing black on ceramic and dark gray, brown, or dull gray on CoCr. Often extending from taper to apex of the femoral head with strong macrodirectionality, opposing microdirectionality, and one or both longitudinal edges straight and well defined. Often only one mark of this type per head, accompanied by additional transfer patterns (see random patches, patterned coverage)		
Random stripe	Similar coloring to a longitudinal stripe, with a high length : width ratio and no preferred orientation (lateral or longitudinal). It can be straight, curved, or looped; one to two seen per upper hemisphere		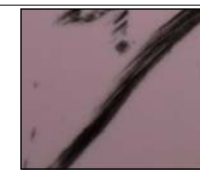
Random patches	No overall directionality, often overlapping marks. Found in clustered groups or independently with no location preference. Typically one to a few marks, either the only pattern observed or a secondary pattern		
Patterned coverage	Small straight lines or pinpoints markings, evenly distributed over the entire upper hemisphere. Spaced approximately 1 mm apart in every direction. Most often a secondary pattern to a longitudinal transfer stripe		
Miscellaneous	Iatrogenic damage, stripe wear accompanied by metal transfer, additional surface damage, or unconfirmed metal transfer	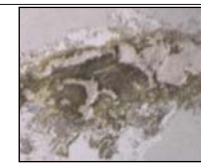	

coverage was similar among the 3 cohorts, with an overall median coverage of 2.3% of the upper hemisphere (IQR: 4.1%; $p = 0.90$) (Figure 4). The median metal transfer surface area coverage was 2.2% (IQR: 4.3%) for the M-PE cohort, 2.2% (IQR: 2.9%) for the C-PE cohort, and 3.4% (IQR: 5.3%) for the C-C cohort. Similarly, the curved surface area of metal transfer was similar among the three cohorts (overall median surface area = 39.8 mm^2 (IQR: 67.5 mm^2); $p = 0.98$). The surface area of metal transfer was 38.6 mm^2 (IQR: 70.9 mm^2) for the M-PE cohort, 35.7 mm^2 (IQR: 50.0 mm^2) for the C-PE cohort, and 54.7 mm^2 (IQR: 99.7 mm^2) for the C-C cohort. There was no difference in metal transfer surface area coverage between ZTA and alumina heads in the C-PE cohort ($p = 0.27$) or between conventional and HXLPE for the M-PE and C-PE cohorts ($p = 0.44$, $p = 0.53$, resp.). Patient weight, implantation time, BMI, head size, age, and gender were not correlated with the metal transfer surface area coverage in any of the cohorts ($p > 0.16$).

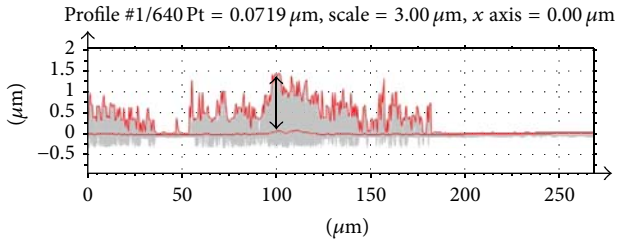

Figure 2: Optical microscopy surface scan converted into a series of profiles with profile envelopes for the maximum and mean values. Distance between the mean line and the highest peak was measured per scan and averaged per head (SR_{pm}).

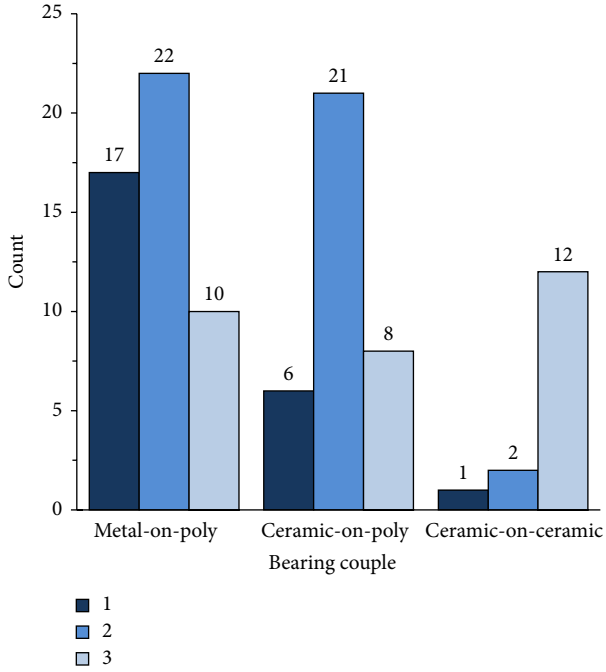

Figure 3: Count of femoral heads in each material cohort (M-PE, C-PE, and C-C) belonging to each visual score classification. Scores ≥ 2 were analyzed further for having visual metal transfer.

Seven metal transfer patterns were observed on the 75 analyzed femoral heads across all three cohorts, occurring in different proportions ($p = 0.02$; Figure 5).

For femoral heads with evidence of metal transfer, the three most common primary patterns observed were random stripe ($n = 21/75$), longitudinal stripe ($n = 17/75$), and random patches ($n = 13/75$) (Figure 6). For 72% ($n = 54/75$) of the femoral heads, only one of the seven metal transfer patterns was observed on the upper hemisphere. A secondary metal transfer pattern (lighter in color, less surface area coverage, and more sporadic in appearance) was observed for 28% ($n = 21/75$) of the femoral heads: 12% ($n = 9/75$) of the M-PE cohort; 9% ($n = 7/75$) of the C-PE cohort; and 7% ($n = 5/75$) of the C-C cohort. The most common secondary pattern observed was patterned coverage ($n = 6/21$) accompanying a longitudinal stripe ($n = 5/21$).

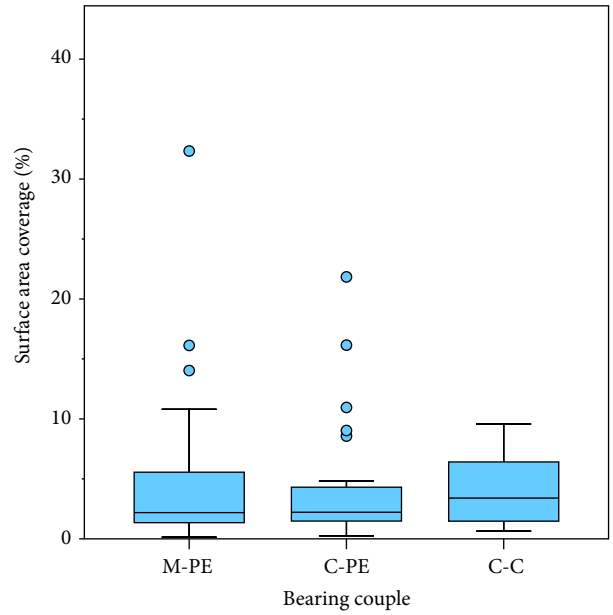

Figure 4: The distribution of metal transfer surface coverage was similar across the three material cohorts ($p = 0.90$).

Although the surface area coverage of the upper hemisphere was similar among the cohorts, we did observe differences in morphology of the three most prevalent primary patterns (Table 3). In particular, the arc length of the predominant pattern was shorter in the M-PE cohort than both the C-PE cohort and the C-C cohort (mean difference = 5.7 mm and 7.11 mm; $p = 0.006$, $p = 0.001$, resp.). In addition, the arc width was also smaller for the M-PE cohort compared to the C-C cohort (mean difference = 0.78 mm, $p = 0.001$), and the height of the metal transfer was significantly taller in the M-PE cohort than the C-C cohort (mean difference = 0.84 mm, $p = 0.022$). With the numbers available, we could not detect a difference in arc length, arc width, or metal transfer height between the two cohorts with ceramic heads ($p = 0.805$, $p = 0.138$ and 1.000 for the arc length, arc width, and transfer height, resp.).

4. Discussion

Metal transfer has been observed on retrieved femoral heads in total hip replacements. *In vitro* studies have observed increased wear of the polyethylene acetabular liner with the presence of metal transfer [8]. Although this has been observed in retrieved components, little is known about the effect (if any) of the bearing surface material on the morphology of the metal transfer. This study investigated whether observed metal transfer was more prominent on one bearing surface couple over another, and if metal transfer on these surfaces had a common morphology. We found that metal transfer was a common observation on the femoral heads for the bearing surface couples investigated in this study. Moreover, for heads that did have evidence of metal transfer, we found that amount of surface area covered by

Table 3: Dimensions of the most prominent mark for the three most prevalent primary transfer patterns. Sample size was determined by the amount of femoral heads per cohort exhibiting each pattern (longitudinal stripe, random stripe, and random patches, resp.). Data is reported as the mean ± standard deviation.

	M-PE			C-PE			C-C		
	Length (mm)	Width (mm)	Height (μm)*	Length (mm)	Width (mm)	Height (μm)	Length (mm)	Width (mm)	Height (μm)*
Longitudinal stripe	12.3 (11.7)	1.9 (1.3)	1.2*	9.1 (10.3)	1.5 (0.9)	0.5 (0.2)	16.2 (5.0)	2.2 (1.7)	0.4 (0.6)
Random stripe	7.3 (5.0)	0.7 (0.5)	1.8 (1.9)	14.5 (2.9)	1.2 (1.9)	1.0 (1.1)	5.9*	1.2*	2.3*
Random patches	2.6 (2.1)	1.2 (1.0)	1.9*	3.6 (3.8)	1.2 (2.9)	0.7 (0.9)	6.2*	3.1*	0.9*

*Height only available for 10 C-C heads and 13 M-PE heads, with insufficient data to present and interquartile range in some cases.

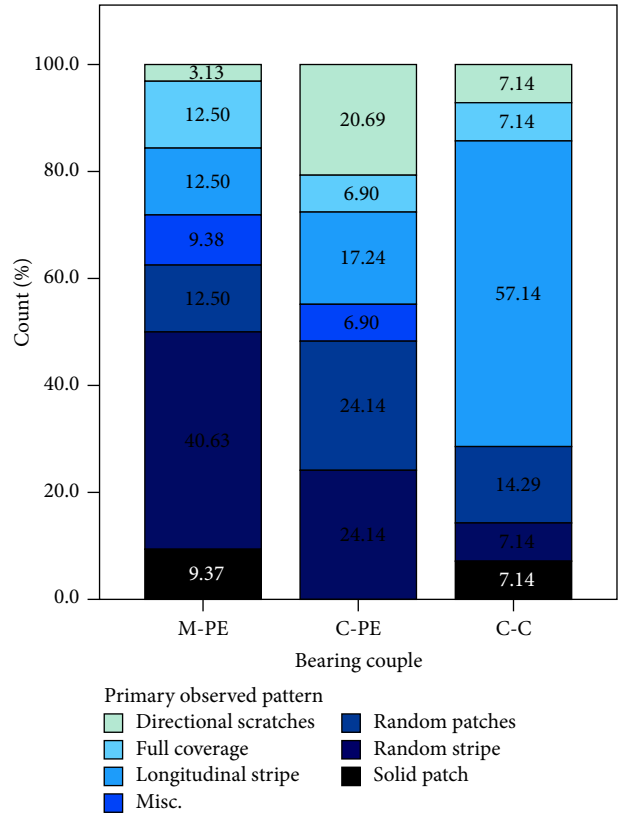

Figure 5: Distribution of identified metal transfer patterns across the three cohorts.

metal transfer was similar among the M-PE, C-PE, and C-C cohorts. However, observed metal transfer was greater in height and shorter in length on CoCr compared to ceramic femoral heads. Clinical factors (weight, BMI, implantation time, etc.) were not predictors of the amount of metal transfer observed on the upper hemisphere.

There were limitations to this study. We only measured damage on the upper hemisphere. Although we did observe damage on the heads outside of this area, these marks were excluded from our analysis in order to only capture transfer that would likely have an impact on the bearing surface of the acetabular liner during normal use. This study only addressed revised hip replacements, and thus the findings may not be reflective of functioning implants that are *in vivo*. We did not consider if femoral heads articulated in extreme positions, such as acetabular cups with a highly vertical placement, which could lead to a very different articulating zone. The opposing articulating surface was also not examined, which could give additional information about causation mechanisms. Although metal transfer has been observed in unstable implants that have undergone dislocations and closed reductions, only one implant in this study was revised for instability. According to a community registry study performed in the past year on 6,801 revision cases over twenty years, instability/dislocation was the cause of failure for 1.7% of total hip replacements [14]. The cohorts in the current study likely underrepresent components revised for instability, making it likely that this study underestimated the amount of metal transfer across our retrieval collection of revised hips. Also, the metal transfer was visually more apparent in the ceramic cohort when compared to the CoCr cohort. Although the diffuse lighting technique made by Heiner et al. [10] for viewing CoCr femoral heads helped define the areas of metal transfer, it is possible that we underestimated the amount of transfer in the CoCr cohort due to the similarity in color.

The original CoCr and ceramic femoral head cohorts were matched for flexural rigidity of the implant stem, with no consideration of bearing surface characteristics. This ensured a random sampling of femoral heads when examining the bearing surface. To the author's knowledge, this is the largest sample size to date to be examined for metal transfer on the bearing surface, the next largest sample size being 27 explanted ZTA femoral heads studied by Elpers et al. [11]. Additionally, the height profiles for each WLI measurement were cumulative of the entire scanned region (365 linear profiles for both the longitudinal and lateral directions), rather than a representative orthogonal profile. Using SR_{pm} was an advantage over commonly used roughness parameters (Sa, Ra) that average both material loss (depth) and material gain (height) from the bearing surface center line [1, 5, 8]. SR_{pm} provided the height of just the metal transfer above the bearing surface center line (representing the unworn femoral head), achieving more accurate height dimensions. Furthermore, batch processing performed in MATLAB on the profiles and photographs allowed for high throughput on a large cohort.

The results reported here are consistent with the work of past reports that identified metal transfer on the bearing surface of CoCr and ceramic femoral heads.

(a) (b) (c)

Figure 6: Digital photographs of the three most common patterns: (a) random stripe, (b) longitudinal stripe, and (c) random patches. Both the longitudinal stripe and the random stripe also feature the most common secondary pattern: patterned coverage over the entire upper hemisphere.

In the Elpers et al. [11] study of ZTA femoral heads, metal transfer was observed on 60% of the femoral heads at the apex and 95.6% of the femoral heads at the equator. Similarly, the current study observed metal transfer on 75% of the femoral heads examined, over the region of apex to equator. The surface area percentages reported here are also similar to the work of Kim et al. [1], where they observed areas identified as metallic-like "smearing" covering 1 to 10% of the total head surface in a study of 15 retrieved ceramic heads. An additional retrieval study performed by Müller et al. [5] found metal transfer surface areas on the total bearing surface of 5 mm^2 to 8 mm^2 per metal transfer mark. In this study the results are generally an order of magnitude higher than the other studies. This may be because we considered the entire curved surface area of the upper hemisphere. It is unclear how the previous studies calculated the surface area, or if they accounted for the spherical form in the calculation. With the numbers available, we were unable to detect a difference in metal transfer surface area coverage among the cohorts. However, the implications of this finding on the clinical performance of ceramic femoral heads (particularly wear) are unknown at this point. In a hip simulator study of zirconia and CoCr heads on conventional polyethylene disks, Eberhardt et al. [8] reported higher levels of polyethylene wear for both materials that had induced transfer when compared to undamaged femoral heads. However, the femoral heads with induced transfer showed a postsimulation positive skewness (R_{sk}) more than twice that of the femoral head retrievals in their study. On the bearing surface of a femoral head, a positive skewness suggests material build-up whereas a negative skewness suggests material loss. The high positive values reported suggest that the induced metal transfer height for simulation did not replicate the induced metal transfer height *in vivo*, warranting simulator studies with more accurate generation of metal transfer morphology. In addition, Kim et al. [1] found in a retrieval study that femoral heads with severe "smearing" had significantly higher polyethylene wear rates than femoral heads with slight "smearing" on conventional polyethylene. Thus, a future retrieval study documenting conventional and HXLPE wear in the context of metal transfer surface area on the femoral head is warranted.

Of the seven distinct patterns identified within the three cohorts, random stripes and random patches were the most common for both the M-PE and C-PE cohorts. These are hypothesized to be from 3rd body debris trapped in the articulating space, such as particles of porous coatings on acetabular shells, or material removed from impingement of the shell and neck [8]. These markings are also consistent with those noted in other reports, although in most reports there is no form of pattern classification system presented except for the six case studies performed by Heiner et al. [7, 11]. Previous studies suggest that the most common cause of metal transfer is impingement and dislocation, exhibiting broad regions of micro and macro scraping and longitudinal directionality (here represented by the longitudinal stripe pattern) [6, 7]. In the current study, 23% (n = 17/75) of the patterns identified had longitudinal stripes. Most of the previous work investigating metal transfer was performed on selected cohorts from patients who were unstable or had multiple dislocations [1, 8, 9]. Therefore, the differences may be a result of selection bias. In this study the longitudinal stripe pattern was less common for the M-PE cohort (13%, n = 4/32) than the C-PE and C-C cohorts (26%, n = 9/35; 44%, n = 4/9, resp.). In previous literature, longitudinal stripes on ceramic bearings have been attributed to direct contact between the raised Ti acetabular shell rim and the femoral head during dislocation or the closed reduction process [5, 7]. However, only 4 out of 13 ceramic heads with a longitudinal stripe pattern of transfer had a ceramic liner with a raised Ti edge. The longitudinal stripe height was greater for the M-PE cohort compared to both of the ceramic cohorts. This height difference could be attributed to the hardness of modern-day ceramic femoral heads, resulting in the softer transferred metal to be worn down by the normal gait cycle more easily than on CoCr femoral heads [5, 15]. Nevertheless, the mean height differences observed between the M-PE and the two

ceramic cohorts (C-PE and C-C) were less than one micron. Therefore, the clinical impact of these observed differences remains unclear.

Miscellaneous and unusual metal transfer patterns that did not fall into the seven pattern groups were noted on two ceramic and four CoCr femoral heads of the 75 analyzed. Both of the ceramic heads had extreme metal transfer. One head showed tooling marks originating at the taper and extending towards the apex of the femoral head, indicative of iatrogenic damage. The other ceramic femoral head had extensive metal transfer occurring both on the unworn portion (appearing shiny) and significantly worn portion (appearing dull and rough to the touch) of the bearing surface [16]. This head had completely worn through the polyethylene liner and had been articulating solely against the Ti alloy acetabular shell, resulting in gross amounts of Ti transfer to the bearing surface. Two of the miscellaneous CoCr heads showed varying degrees of brown coloring with a cloudy surface finish. Although the cause of this is unclear, the pattern was similar to the circumferential discoloration pattern observed by Heiner et al. from Ti corrosion, albeit to a lesser degree. The two other CoCr heads showed highly roughened areas similar to the visual characteristics noted by Heiner at al. [7] as pitting underneath metal transfer deposits, possibly causing the original deposits to detach from the bearing surface.

5. Conclusion

This retrieval study compared metal transfer presence on CoCr and ceramic femoral heads and established a categorization method to describe the morphology of the common forms of observed metal transfer. Understanding the morphology of metal transfer may be useful for more accurate polyethylene wear studies through more realistic recreation of metal transfer in *in vitro* pin-on-disk and joint simulators studies. This would allow for metal transfer and its correlation to polyethylene wear to be more accurately studied under normal and adverse activities and for predictive wear studies of failure mechanisms to be performed on HXLPE.

Ethical Approval

Each author certifies that his or her institution approved the human protocol for this investigation, that all investigations were conducted in conformity with ethical principles of research, and that informed consent for participation in the study was obtained.

Disclosure

This work was performed at the Implant Research Center, Drexel University, Philadelphia, PA, USA.

Conflict of Interests

All statements have been approved by their respective authors. Ms. Eliza K. Fredette declares that there is no conflict of interests in this paper. Mr. Daniel W. MacDonald declares that there is no conflict of interests in this paper. Dr. Richard J. Underwood, Ph.D., reports that he is an employee of Exponent, Inc. Dr. Antonia F. Chen, M.D., M.B.A., declares that there is no conflict of interests in this paper. Dr. Michael A. Mont, M.D., reports that he is a paid consultant of DJ Orthopaedics, Medical Compression Systems, Sage Products, Inc., Stryker, and Tissue Gene, and that he receives research support from DJ Orthopaedics, National Institutes of Health (NIAMS & NICHD), Sage Products, Inc., Stryker, and Tissue Gene. Dr. Gwo-Chin Lee, M.D., reports that he is a paid consultant for Depuy, Iroko pharmaceuticals, Mallinckrodt Pharmaceuticals, Pacira, and Stryker; that he is a paid presenter for Ceramtec, Depuy, Medtronic; and that he receives research support from CD Diagnostics, Smith and Nephew, and Zimmer. Dr. Gregg R. Klein, M.D., receives institutional support from Zimmer and is a consultant for Zimmer. Dr. Clare M. Rimnac, Ph.D., reports that institutional support is received as a PI from Exponent, Depuy Synthes, and Medtronic, and that she is a Senior Associate Editor for Clinical Orthopaedics and Related Research. Dr. Steven M. Kurtz, Ph.D., reports that he is an employee and shareholder of Exponent, Inc., and that institutional support is received as a PI from Smith & Nephew; Stryker; Zimmer Biomet; Depuy Synthes; Medtronic; Invibio; Stelkast; Formae; Kyocera Medical; Wright Medical Technology; Ceramtec; DJO; Celanese; Aesculap; Spinal Motion; Active Implants; and Ferring Pharmaceuticals.

Authors' Contribution

Each author has read and approved the content of the submitted paper.

Acknowledgments

This study was supported by the National Institutes of Health (NIAMS) R01 AR47904. Institutional support has been received from Active implants, Aesculap/B. Braun, Smith & Nephew, Simplify Medical, Stryker, Zimmer, Biomet, Depuy Synthes, Medtronic, Stelkast, Celanese, Invibio, Formae, Kyocera Medical, Wright Medical, Ceramtec, and DJO. The authors would like to thank Rebecca Moore of Case Western Reserve University and Michael Beeman, Justin San Juan, Jackie Schachtner, and Michael Koerner, of Drexel University, for their contributions.

References

[1] Y.-H. Kim, A. Ritchie, and C. Hardaker, "Surface roughness of ceramic femoral heads after in vivo transfer of metal: correlation to polyethylene wear," *The Journal of Bone and Joint Surgery—Series A*, vol. 87, no. 3, pp. 577–582, 2005.

[2] B. S. Bal, M. N. Rahaman, T. Aleto, F. S. Miller, F. Traina, and A. Toni, "The significance of metal staining on alumina femoral heads in total hip arthroplasty," *The Journal of Arthroplasty*, vol. 22, no. 1, pp. 14–19, 2007.

[3] C. B. Chang, J. J. Yoo, W. S. Song, D. J. Kim, K.-H. Koo, and H. J. Kim, "Transfer of metallic debris from the metal

surface of an acetabular cup to artificial femoral heads by scraping: comparison between alumina and cobalt-chrome heads," *Journal of Biomedical Materials Research Part B: Applied Biomaterials*, vol. 85, no. 1, pp. 204–209, 2008.

[4] C. Chevillotte, R. T. Trousdale, Q. Chen, O. Guyen, and K.-N. An, "The 2009 frank stinchfield award: 'hip squeaking': a biomechanical study of ceramic-on-ceramic bearing surfaces," *Clinical Orthopaedics and Related Research*, vol. 468, no. 2, pp. 345–350, 2010.

[5] F. A. Müller, M. Hagymási, P. Greil, G. Zeiler, and A. Schuh, "Transfer of metallic debris after dislocation of ceramic femoral heads in hip prostheses," *Archives of Orthopaedic and Trauma Surgery*, vol. 126, no. 3, pp. 174–180, 2006.

[6] K. M. Kruger, N. M. Tikekar, A. D. Heiner et al., "Encoding scratch and scrape features for wear modeling of total joint replacements," *Computational and Mathematical Methods in Medicine*, vol. 2013, Article ID 624267, 12 pages, 2013.

[7] A. D. Heiner, N. M. Tikekar, K. M. Kruger, J. J. Lannutti, and T. D. Brown, "Distinctive damage patterns on THA metal bearing surfaces: case studies," *The Iowa Orthopaedic Journal*, vol. 34, pp. 84–93, 2014.

[8] A. W. Eberhardt, R. T. McKee, J. M. Cuckler, D. W. Peterson, P. R. Beck, and J. E. Lemons, "Surface roughness of CoCr and ZrO_2 femoral heads with metal transfer: a retrieval and wear simulator study," *International Journal of Biomaterials*, vol. 2009, Article ID 185456, 6 pages, 2009.

[9] K. M. Kruger, N. M. Tikekar, A. D. Heiner, J. J. Lannutti, J. J. Callaghan, and T. D. Brown, "Modeling polyethylene wear acceleration due to femoral head dislocation damage," *Journal of Arthroplasty*, vol. 29, no. 8, pp. 1653.e1–1657.e1, 2014.

[10] A. D. Heiner, K. M. Kruger, T. E. Baer, and T. D. Brown, "Enhancing damage visibility on metallic bearing surfaces: a simple technique for photography and viewing," *The Journal of Arthroplasty*, vol. 28, no. 3, pp. 543.e9–543.e12, 2013.

[11] M. Elpers, D. Nam, S. Boydston-White, M. P. Ast, T. M. Wright, and D. E. Padgett, "Zirconia phase transformation, metal transfer, and surface roughness in retrieved ceramic composite femoral heads in total hip arthroplasty," *The Journal of Arthroplasty*, vol. 29, no. 11, pp. 2219–2223, 2014.

[12] D. Yang, "Canny edge detection for 2d black and white images," in *Canny Edge Detection 2D. Matlab*, Central Washington University, St. Louis, Mo, USA, 2012.

[13] ASTM International, *Standard Practice for Conducting an Interlaboratory Study to Determine the Precision of a Test Method 1. Designation: E691-08*, ASTM International, West Conshohocken, Pa, USA, 2008.

[14] T. Salassa, D. Hoeffel, S. Mehle, P. Tatman, and T. J. Gioe, "Efficacy of revision surgery for the dislocating total hip arthroplasty: report from a large community registry," *Clinical Orthopaedics and Related Research*, vol. 472, no. 3, pp. 962–967, 2014.

[15] B. E. Bierbaum, J. Nairus, D. Kuesis, J. C. Morrison, and D. Ward, "Ceramic-on-ceramic bearings in total hip arthroplasty," *Clinical Orthopaedics and Related Research*, no. 405, pp. 158–163, 2002.

[16] J.-M. Dorlot, P. Christel, and A. Meunier, "Wear analysis of retrieved alumina heads and sockets of hip prostheses," *Journal of Biomedical Materials Research*, vol. 23, no. 3, pp. 299–310, 1989.

Hindawi Publishing Corporation
BioMed Research International
Volume 2015, Article ID 690539, 7 pages
http://dx.doi.org/10.1155/2015/690539

Clinical Study

Total Hip Arthroplasty Using the S-ROM-A Prosthesis for Anatomically Difficult Asian Patients

Akira Hozumi, Kyousuke Kobayashi, Nobuhisa Tsuru, Chikara Miyamoto, Jyunichiro Maeda, Ko Chiba, Hisataka Goto, and Makoto Osaki

Department of Orthopaedic Surgery, Nagasaki University Hospital, 1-7-1 Sakamoto, Nagasaki 852-8501, Japan

Correspondence should be addressed to Akira Hozumi; akira45512@gmail.com

Received 22 March 2015; Accepted 21 June 2015

Academic Editor: Panagiotis Korovessis

Copyright © 2015 Akira Hozumi et al. This is an open access article distributed under the Creative Commons Attribution License, which permits unrestricted use, distribution, and reproduction in any medium, provided the original work is properly cited.

Background. The S-ROM-A prosthesis has been designed for the Asian proximal femur with a small deformed shape and narrow canal. In this study, the clinical and radiological results using the S-ROM-A prosthesis for Japanese patients with severe deformity due to dysplasia and excessive posterior pelvic tilt were examined. *Methods*. 94 hips were followed up for a mean of 55 months, with a mean age at surgery of 61 years. The primary diagnoses were 94 coxarthritis cases, including 51 dysplasia and 37 primary OA, 1 avascular necrosis, 2 traumatic arthritis, and 3 Perthes disease. Thirty-one hips had been treated with osteotomy of the hip joints. Preoperative intramedullary canal shapes were stovepipe in 23 hips, normal in 51 hips, and champagne-flute in 5 hips. The maximum pelvic inclination angle was 56°. *Results*. The mean JOA score improved from 46 points preoperatively to 80 points at final follow-up. On radiological evaluation of the fixation of the implants according to the Engh classification, 92 (97%) hips were classified as "bone ingrown fixation." *Conclusion*. In primary THA, using the S-ROM-A prosthesis for Asian patients with proximal femoral deformity, even after osteotomy and with posterior pelvic tilt, provided good short- to midterm results.

1. Introduction

Total hip arthroplasty (THA) has excellent long-term outcomes with low rates of complications. However, it is difficult to treat patients with anatomic deformities of the hip joints, including developmental dysplasia of the hip (DDH), previous femoral and acetabular osteotomy, or severe posterior pelvic tilt with porotic bone. Treatment outcomes with cementless stems are inconsistent in these patients, and there is concern regarding the difficulties of treatment, such as frequent dislocation from early loosening or malpositioning of the implant used. In 1984, the S-ROM system (DePuy, Warsaw, IN) was developed as a stem for patients with these various types of anatomic deformities. This stem has a modular mechanism with a high degree of freedom. It consists of two parts, the sleeve and stem body. In addition, the stem and sleeve have various combinations and independent reaming in the proximal metaphyseal region of the femur and the diaphyseal region enables robust fixation with respect to various intramedullary canal shapes. Good results have been reported [1–4].

Compared with other races, Asian patients with hip diseases are of smaller stature, have less bone stock, and have a higher rate of DDH. Jingushi et al. [5] and Nakamura et al. [6] reported that more than 80% of primary diagnoses of osteoarthritis of the hip joints in Japan were related to DDH.

The S-ROM-A femoral prosthesis (DePuy) was developed in 2004 as a modification of the S-ROM based on the anatomical data of 270 Japanese hips. It has a shorter stem (5–25 mm shorter) with bullet tips, which reduce impingement with the femoral shaft and contribute to reducing the thigh pain and periprosthetic fracture. Furthermore, it has more neck offset options with a smaller diameter (changed from 11/13 to 9/10 neck taper) compared with the S-ROM femoral prosthesis.

It is important to select femoral stems that are suited for individual cases based on the patient's physique and anatomical and clinical state. For a case with severe deformities of the proximal femur, retroverted acetabulum, and posterior pelvic tilt in Japanese patients, we use the S-ROM-A prosthesis.

In this study, the clinical and radiological results using the S-ROM-A prosthesis for Japanese patients with severe

Table 1: Preoperative diagnoses and etiologies of anatomical abnormalities of the hip.

Preoperative diagnosis		Previous operation	
Primary osteoarthritis	37		
Developmental dysplasia	51	Rotational acetabular osteotomy	13
		Chiari and/or femoral osteotomy	14
Osteonecrosis	1	Sugioka's osteotomy	1
Perthes disease	3	Varus osteotomy	3
Traumatic arthritis	2	Osteosynthesis	2
Total	94		33

posterior pelvic tilt, DDH with proximal femoral deformity, and postosteotomy hip joint were evaluated.

2. Materials and Method

2.1. Patients Status. A total of 115 primary cementless THAs using the S-ROM-A femoral component were performed in 120 patients by 5 hip surgeons between March 2005 and December 2011; the subjects were 89 patients (94 joints) who could be followed for at least 3 years and who had no rheumatoid arthritis or obvious metabolic bone disease such as renal osteodystrophy.

Ninety-four hips were followed up for a mean of 55 (range, 36 to 121) months, with a mean age at surgery of 61 (range, 42 to 84) years. There were 79 women and 10 men. Mean of patient height was 152 (range, 135 to 173) cm, of weight was 55 (range, 34 to 81) kg, and of body mass index was 23.4 (range, 17.2 to 34.9) kg/m^2. The primary diagnoses were 94 coxarthritis (DDH: 51, primary OA: 37, traumatic arthritis: 2, avascular necrosis: 1, and Perthes disease: 3) including 33 postosteotomy hips. According to Crowe's classification [7], the degree of dislocation on preoperative X-rays was Group I in 53 hips, Group II in 25 hips, Group III in 12 hips, and Group IV in 4 hips.

The etiologies of the anatomical abnormalities of the hip are summarized in Table 1.

2.2. Surgical Procedure and Postoperative Protocol. Surgery was performed through a direct lateral approach in 82 hips, posterolateral approach in 6 hips, and subtrochanteric osteotomy in 6 hips. All operations were performed in a lateral position without trochanteric osteotomy. The acetabular component was used with a Pinnacle-A (DePuy, Warsaw, IN) in 73 hips, Duraloc in 15 hips (DePuy), and STD-CP (cemented cup, JMM, Osaka, Japan) in 6 hips. The average outer diameter of the cups was 50.1 (range, 44–56) mm. The inner head diameters were 22 mm in 1 hip, 26 mm in 8 hips, 28 mm in 51 hips, 32 mm in 30 hips, and 36 mm in 3 hips. The bearing surface was cobalt-chromium on polyethylene in 91 hips (cross-linked: 66, conventional: 25) and metal on metal in 3 hips.

The femoral diaphysis was reamed to the minor diameter of the stem. Hip joint stability was confirmed by the intraoperative dislocation test. When hip joint stability was insufficient, stem anteversion or cup anteversion was adjusted to achieve maximum stability of the hip joint. Subsequently, the final neck rotational angle against the sleeve was examined by the method similar to Kindsfater et al. [8]. Patients were allowed full weight-bearing on the day after surgery, except for subtrochanteric osteotomy cases.

2.3. Clinical and Radiographic Evaluations. Patients were examined preoperatively, postoperatively at 3 months and 6 months, and then yearly and at the final follow-up. Functional outcomes were evaluated using the Japanese Orthopaedic Association scoring system (JOA score), which has a total of 100 points, consisting of 40 points for pain, 20 for range of motion, 20 for ability to walk, and 20 for activities of daily living [9]. Preoperative morphology was assessed in terms of posterior pelvic tilt angle (PTA), femoral neck anteversion angle on CT scan, and the canal-flare index (CFI) [10], except in patients with some kind of osteotomy of the proximal femoral bone. PTA was defined as the angle formed by a vertical line drawn from the superior margin of the pubic symphysis and sacral promontory on lateral plain X-ray (Figure 2).

Stem fixation was classified as bony ingrowth, being fibrous stable, or being unstable according to the Engh classification [11–13]. Bone ingrowth was defined as apertures with no subsidence and no or less than 50% radiolucent lines around the sleeve. The presence of spot welds around the sleeve was considered bony ingrowth. Stable fibrous ingrowth was defined as a stem with no progressive subsidence and extensive radiolucent lines around the sleeve. Unstable fixation was defined as a stem with either progressive subsidence or migration and widely radiolucent lines around the sleeve. The stem position was classified as neutral, valgus, and varus according to 2 degrees more compared to the femoral shaft axis.

The intraoperative stem rotation angle against the sleeve was also examined [3, 8]. Intraoperative complications, such as femoral fracture, and postoperative complications, such as infection, dislocation, symptomatic pulmonary embolus, bone union of subtrochanteric osteotomy cases, and other implant-related complications such as thigh pain, were examined.

All radiological data were evaluated separately by three different surgeons (Akira Hozumi, Kyousuke Kobayashi, and Nobuhisa Tsuru).

In the statistical analysis, the Mann-Whitney U test was used to compare the difference in the mean JOA score between before operation and the latest follow-up, femoral anteversion angle, and CFI between DDH patients and primary OA patients. Statistical significance was established at $p < 0.05$.

3. Results

3.1. Clinical Outcome. The mean JOA score (pain/ROM/ambulation/ADL) improved from 46.1 points (14.0/11.7/8.1/12.3) preoperatively to 79.7 points (35.4/15.6/13.0/15.7) at final follow-up. In patients with a history of an osteotomy of the hip joint, the mean JOA score at final follow-up was 74.1

Table 2: Preoperative and postoperative Japanese orthopaedic association score.

(a) Preoperative and postoperative JOA score with history of osteotomy of the hip

	Preop	Postop
Pain	11.7	32.9
Range of motion	13.0	15.1
Walk	9.1	11.4
Activity of daily living	12.0	14.6
Total	45.8	74.1*

(b) Preoperative and postoperative JOA score without history of osteotomy of the hip

	Preop	Postop
Pain	14.9	36.4
Range of motion	11.1	16.0
Walk	7.7	13.6
Activity of daily living	12.4	16.1
Total	46.1	82.1*

(c) Preoperative and postoperative JOA score in all patients

	Preop	Postop
Pain	14.0	35.4
Range of motion	11.7	15.6
Walk	8.1	13.0
Activity of daily living	12.3	15.7
Total	46.1	79.7

*$P < 0.05$ (Mann-Whitney U test).

Table 3: The preoperative CFI of femoral bone and the number of intraoperative fractures.

Femoral bone shape (CFI)	Number of hips*	Number of fractures (%)	Mean CFI of fracture patients
Stovepipe (<3.0)	23	7 (30.4%)	2.51
Normal (3.0–4.7)	51	8 (15.4%)	3.43
Champagne-flute (>4.7)	5	0 (0%)	—
Total	79	15	2.97

*Number of hips without a history of osteotomy of the proximal femoral bone.

points. This was significantly lower than in patients without osteotomy of the hip joint ($p < 0.05$) (Tables 2(a)–2(c)).

There were 15 hip-related complications. A longitudinal calcar fracture around the sleeve in 9 hips and a greater trochanteric fracture in 6 hips occurred as intraoperative complications, and the CFI of these patients was relatively low (Table 3). Previous osteotomy did not affect intraoperative fracture (data not shown).

Thirteen cases were successfully treated by cerclage wiring procedures. Two cases of greater trochanteric fracture had nonunion.

Postoperative dislocation was not observed in any cases. Infection and symptomatic PE were not observed. Persistent groin pain after THA was observed in one hip with severe posterior pelvic tilt, which was diagnosed as iliopsoas impingement, but the patient preferred to continue with conservative management.

3.2. Preoperative Femoral Anteversion Angle, the Canal-Flare Index, and Posterior Pelvic Tilt. The femoral anteversion angle at the level of the osteotomy varied from −6° to 86°, with a mean of 28.4°. Mean posterior pelvic tilt was 20.6°. Femoral anteversion angle of DDH cases were significantly strong in comparison with the primary OA; adversely, the posterior pelvic tilt angle was significantly stronger in primary OA than DDH cases. According to preoperative CFI, there was no significant difference due to the primary diagnoses (Table 4). The preoperative CFI of femoral bone (without a history of osteotomy of the proximal femoral bone) was stovepipe in 23 hips, normal in 52 hips, and champagne-flute in 5 hips (Table 3).

3.3. Stem-Sleeve Rotation Angle. Overall, femoral component version was changed in 67 hips (71%). The rotational angle of the stem ranged from 60° retroversion to 35° anteversion against the sleeve. The stem rotational angle against the sleeve according to preoperative diagnoses is shown in Figure 1.

3.4. Radiological Evaluation. Alignment of the stem was neutral in 88 hips (94%) and varus in 6 hips (6%). For fixation of implants according to the Engh classification, 91 hips (97%) were classified as "stable fixation." None of the hips required revision surgery. Two hips were classified as "fibrous stable," showing radiolucent lines around the sleeve, and one hip had unstable status. Spot welds around the sleeve were observed in 81 hips (88%). Second-degree stress shielding was observed in 57 hips (61%), and more than third-degree stress shielding was observed in 7 hips (7%). Stem subsidence was observed in 7 hips, including fibrous fixation cases, but it was not progressive except in the unstable case.

The overall radiological results according to the Noble classification, the filling rate of the distal part of the canal by the stem, and alignment of the stem are summarized in Table 5.

4. Discussion

The use of the S-ROM stem for primary THA in patients with DDH has been reported by Biant et al. [1]. They reported 0% aseptic loosening in 55 hips with anatomically difficult cases, of which 28 were severe DDH cases. Regarding the use of the S-ROM-A prosthesis, Kido et al. [2] and Tamegai et al. [3] reported that it was well-fitted for Asian DDH patients with short stature, a narrow canal, and severe proximal femoral deformity, showing favorable short- to midterm results. Zhao and Sun [4] reported good short-term results in elderly patients with poor bone quality containing Dorr type C using the S-ROM system. In the present study, stable bone ingrowth fixation was seen in 92 of 95 hips (96.8%). Furthermore,

Table 4: Femoral anteversion angle, CFI, and pelvic tilt angle (PTA) according to preoperative diagnoses.

	Femoral anteversion	CFI	PTA
DDH	30.2 (17.6, −6–86)*	3.56 (0.96, 1.62–6.2)	16.3, (8.1, −2.3–31.5)*
Primary OA	21.5 (10.6, −1–42)*	3.41 (0.89, 1.61–4.69)	27.3 (14.6, 14.1–55.6)*
Others	23 (16.5, 2–48)	4.21 (1.24, 2.93–6.17)	26.35 (6.67, 17.05–32.9)
Total	28.4 (17.8, −6–86)	3.49 (0.97, 1.61–6.27)	20.59 (11.9, −2.3–55.6)

*$P < 0.05$ (Mann-Whitney U test).

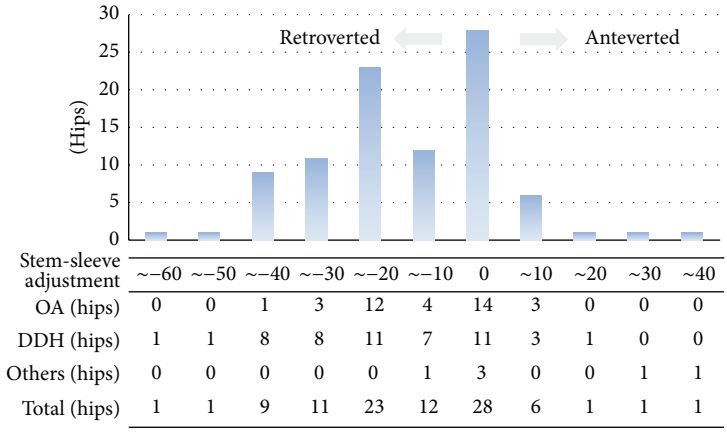

Stem-sleeve adjustment	~−60	~−50	~−40	~−30	~−20	~−10	0	~10	~20	~30	~40
OA (hips)	0	0	1	3	12	4	14	3	0	0	0
DDH (hips)	1	1	8	8	11	7	11	3	1	0	0
Others (hips)	0	0	0	0	0	1	3	0	0	1	1
Total (hips)	1	1	9	11	23	12	28	6	1	1	1

Figure 1: Adjustment of the rotation angle of the stem against the sleeve.

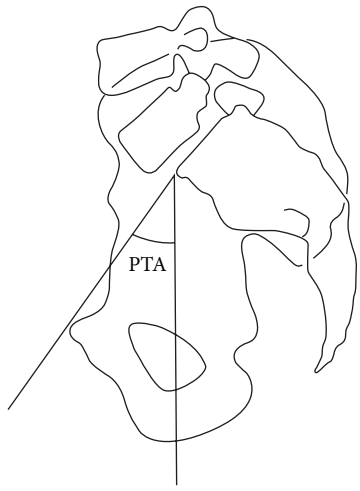

Figure 2: PTA was defined as the angle formed by a vertical line drawn from the superior margin of the pubic symphysis and sacral promontory on lateral plain X-ray.

especially in stovepipe cases, all cases were stable fixation (Table 5). The reason for this depends on the fixation manner of S-ROM system. The S-ROM modular stem was designed to generate maximal contact between the metaphysis and diaphysis by independent reaming. Furthermore, proximal sleeve which has up to seven-size variation for each stem size and porous coated step surface generate good fit and fill and vertical stability, whereas, in the distal part, distal flute structure generates torsional stability and scratch fit. [14]. In particular, in the S-ROM A stem, it has a reduced stem length (5–25 mm shorter than the standard stem) and a bullet tip, which contribute to more fit and fill for the shorter Asian femur.

However, when large diameter stems are implanted, proximal stress shielding and thigh pain have sometimes been concerns [15, 16]. In the present series, no case had thigh pain at final follow-up. To explain this, we think that the hollow cylindrical stem with a coronal slot, shorter stem length, and bullet tip contribute greatly to decreasing the stiffness difference between the implant and the host bone, which is an important reason for postoperative thigh pain.

Second-degree stress shielding was radiographically detected in 57 hips (61%). Most of these occurred due to the formation of spot welds in the distal part of the sleeve, and this finding is consistent with trends seen in previous studies [17, 18]. Stress shielding of ≥3 degrees was observed in 7 hips (7%), of which 5 hips occurred in conjunction with some form of bone reaction to the distal part of the stem. The mean CFI in these patients was low at 2.2, and the stem had a high canal fill ratio or was varus inserted. However, bone ingrowth was ultimately achieved at the sleeve site for all patients, so these events were deemed to be temporary stress concentrations. In terms of their clinical course, patients tended to complain of femoral pain soon after surgery, but it resolved over time.

Table 5: Radiological results according to femoral canal shape and implant positioning.

	N	Spot welding	Stress shielding (>III)	Bone ingrowth	Bone reaction around the distal part of the stem
Dorr classification					
Stove pipe	23	20	5	23	8
Normal	51	46	2	48	11
Champagne-flute	5	0	0	5	0
Postfemoral osteotomy	15	15	0	15	0
Filling rate of the distal part of the canal by the stem					
<80	10	7	1	8	4
80–90	40	38	4	40	6
90–100	44	39	2	43	7
Alignment of stem					
Neutral	88	79	6	85	15
Varus	6	6	1	6	4
Valgus	0	0	0	0	0

However, in the case of excessive stovepipe and champagne-flute cases, careful implant selection and consideration of other stems (such as the well-documented cemented stem) should be considered because of the mismatch of fitting between the proximal and distal medulla even with this system.

Intraoperative fracture was seen in 15 hips (16%), higher than in previous reports [1–3]. The reason for this may have been that the mean CFI of this group was 2.97, indicating osteoporotic bone. In these cases, strong stress was added to the greater trochanter by the retractor in the Hardinge approach, and excessive reaming was done for large sleeve insertion. For these osteoporotic cases, preventive cerclage wiring should be done in the calcar portion, in addition to careful reaming.

Kindsfater et al. [8] reported that they needed stem-sleeve adjustment for 47.9% of cases, in which 79.3% of stems were anteverted. Tamegai et al. [3] reported that they needed anteversion for 18% and retroversion for 56% of their 196 DDH cases, and, furthermore, the postoperative dislocation rate was 0.9%. In the present study, stem-sleeve adjustment was needed in 71% (anteversion: 9%, retroversion: 61%), a higher rate, and there was no dislocation. We think that the Hardinge approach was one factor for the high rate of retroversion cases, and another factor was that the posterior pelvic tilt cases (≥30 degree) accounted for 23%. No postoperative dislocation was seen in the present study. In many past reports, the dislocation rate was around 1% [3, 8]. Many of these cases used a posterior approach. In the present study, a Hardinge approach, with which the short rotator can be preserved and good access to the acetabulum is possible for patients with strong anatomic deformities, was used. It is thought that this approach enables not only preservation of the short rotator but also accurate cup positioning, so that a high resistance to dislocation can be achieved.

We used S-ROM-A proactively for THA in posterior pelvic tilt cases (Figure 3(b)). Change of pelvic inclination from lying position to standing position is frequently seen in aged patients. Furthermore, in these cases optimal adjustment of the acetabular cup is of utmost importance but is very difficult for ensuring stability and maximum range of motion of the prosthetic joint, without causing impingement on neck-liner or iliopsoas tendon. Thus, we think that it is advantageous for joint stability and prevention of implant-related complications to set the cup anatomically and to adjust rotation in the stem side as much as possible. Therefore, the use of S-ROM-A system is desirable for severe pelvic tilt cases.

In addition, this system is useful for patients with a high risk of dislocation with wide range of motion (alcoholic osteonecrosis, psychiatric disorders, paralytic disease, etc.) because of easy adjustment of stem version without removing the sleeve with bone ingrowth. On the other hand, there were several reports of catastrophic complications related to the S-ROM modular stem-sleeve junction [19–21]. In the present series, although there were no modularity-associated complications, such as fretting wear, corrosion, and breakage at the modular joint, longer-term follow-up is necessary. Furthermore, care is needed for young patients with high activity and severely obese patients when using the modular system.

Finally, in the present study, the JOA score at the final follow-up was relatively low (80 points) compared to previous reports [2, 3]. The high rate of patients who had postosteotomy hip joint likely affected the functional results.

5. Conclusions

Excellent short- to midterm results were obtained in anatomically difficult Asian patients with DDH, postosteotomy hip

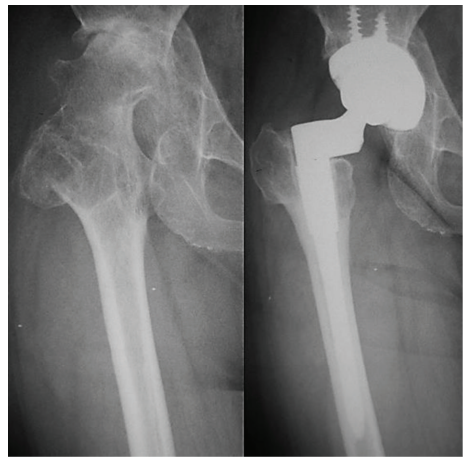

(a)

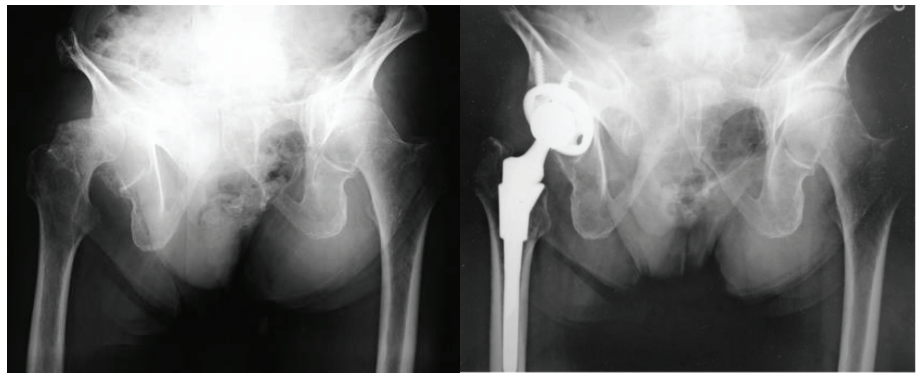

(b)

Figure 3: (a) 58-year-old female after pelvic and femoral osteotomy. Preoperative JOA was 52 points. Final follow-up (4Y) JOA was 74, stable fixation. (b) 84-year-old man with severe posterior pelvic tilt (50 degrees) 5 years after THA.

joints, and posterior pelvic tilt using the S-ROM-A system. The S-ROM-A prosthesis provides high stability of hip joints and reliable fixation for Asian patients.

Conflict of Interests

The authors declare that there is no conflict of interests regarding the publication of this paper.

Acknowledgment

The authors would like to thank Professor Emeritus, Dr. Shindo, for his help in preparing this paper.

References

[1] L. C. Biant, W. J. M. Bruce, J. B. Assini, P. M. Walker, and W. R. Walsh, "Primary total hip arthroplasty in severe developmental dysplasia of the hip. Ten-year results using a cementless modular stem," *Journal of Arthroplasty*, vol. 24, no. 1, pp. 27–32, 2009.

[2] K. Kido, M. Fujioka, K. Takahashi, K. Ueshima, T. Goto, and T. Kubo, "Short-term results of the S-ROM-A femoral prosthesis. Operative strategies for Asian patients with osteoarthritis," *Journal of Arthroplasty*, vol. 24, no. 8, pp. 1193–1199, 2009.

[3] H. Tamegai, T. Otani, H. Fujii, Y. Kawaguchi, T. Hayama, and K. Marumo, "A modified s-rom stem in primary total hip arthroplasty for developmental dysplasia of the hip," *Journal of Arthroplasty*, vol. 28, no. 10, pp. 1741–1745, 2013.

[4] Z.-S. Zhao and J.-Y. Sun, "Total hip arthroplasty using S-ROM prosthesis in elder patients with type C and B bone," *Journal of Orthopaedics*, vol. 10, no. 2, pp. 65–69, 2013.

[5] S. Jingushi, S. Ohfuji, M. Sofue et al., "Multiinstitutional epidemiological study regarding osteoarthritis of the hip in Japan," *Journal of Orthopaedic Science*, vol. 15, no. 5, pp. 626–631, 2010.

[6] S. Nakamura, S. Ninomiya, and T. Nakamura, "Primary osteoarthritis of the hip joint in Japan," *Clinical Orthopaedics and Related Research*, no. 241, pp. 190–196, 1989.

[7] J. F. Crowe, V. J. Mani, and C. S. Ranawat, "Total hip replacement in congenital dislocation and dysplasia of the hip," *The Journal of Bone and Joint Surgery—American Volume*, vol. 61, no. 1, pp. 15–23, 1979.

[8] K. A. Kindsfater, J. Politi, D. Dennis, and C. Sychterz Terefenko, "The incidence of femoral component version change in primary THA using the S-ROM femoral component," *Orthopedics*, vol. 34, no. 4, article 11, 2011.

[9] R. Ogawa and S. Imura, "Evaluation chart of hip joint functions," *Nippon Seikeigeka Gakkai Zasshi*, vol. 69, p. 860, 1995 (Japanese).

[10] P. C. Noble, J. W. Alexander, L. J. Lindahl, D. T. Yew, W. M. Granberry, and H. S. Tullos, "The anatomic basis of femoral component design," *Clinical Orthopaedics and Related Research*, no. 235, pp. 148–165, 1988.

[11] C. A. Engh, J. D. Bobyn, and A. H. Glassman, "Porous-coated hip replacement. The factors governing bone ingrowth, stress shielding, and clinical results," *The Journal of Bone & Joint Surgery Series B*, vol. 69, no. 1, pp. 45–55, 1987.

[12] C. A. Engh, P. Massin, and K. E. Suthers, "Roentgenographic assessment of the biologic fixation of porous-surfaced femoral components," *Clinical Orthopaedics and Related Research*, no. 257, pp. 107–128, 1990.

[13] L. C. Biant, W. J. Bruce, J. B. Assini, P. M. Walker, and W. R. Walsh, "The anatomically difficult primary total hip replacement: medium- to long-term results using a cementless odular stem," *The Journal of Bone & Joint Surgery—British Volume*, vol. 90, no. 4, pp. 430–435, 2008.

[14] J. S. Kang, K. H. Moon, R. S. Kim, S. R. Park, J. S. Lee, and S. H. Shin, "Total hip arthroplasty using S-ROM prosthesis for dysplastic hip," *Yonsei Medical Journal*, vol. 52, no. 4, pp. 655–660, 2011.

[15] A. C. L. Campbell, C. H. Rorabeck, R. B. Bourne, D. Chess, and L. Nott, "Thigh pain after cementless hip arthroplasty. Annoyance or ill omen," *The Journal of Bone & Joint Surgery—British Volume*, vol. 74, no. 1, pp. 63–66, 1992.

[16] R. L. Barrack, M. Jasty, C. Bragdon, T. Haire, and W. H. Harris, "Thigh pain despite bone ingrowth into uncemented femoral stems," *The Journal of Bone & Joint Surgery—British Volume*, vol. 74, no. 4, pp. 507–510, 1992.

[17] D. Le, K. Smith, D. Tanzer, and M. Tanzer, "Modular femoral sleeve and stem implant provides long-term total hip survivorship," *Clinical Orthopaedics and Related Research*, vol. 469, no. 2, pp. 508–513, 2011.

[18] M. Tanzer, S. Chan, C. E. Brooks, and J. D. Bobyn, "Primary cementless total hip arthroplasty using a modular femoral component: a minimum 6-year follow-up," *Journal of Arthroplasty*, vol. 16, no. 8, supplement 1, pp. 64–70, 2001.

[19] C. R. Fraitzl, L. E. Moya, L. Castellani, T. M. Wright, and R. L. Buly, "Corrosion at the stem-sleeve interface of a modular titanium alloy femoral component as a reason for impaired disengagement," *Journal of Arthroplasty*, vol. 26, no. 1, pp. 113.e1–119.e1, 2011.

[20] N. Mehran, T. North, and M. Laker, "Failure of a modular hip implant at the stem-sleeve interface," *Orthopedics*, vol. 36, no. 7, pp. e978–e981, 2013.

[21] A. Patel, J. Bliss, R. P. Calfee, J. Froehlich, and R. Limbird, "Modular femoral stem-sleeve junction failure after primary total hip arthroplasty," *The Journal of Arthroplasty*, vol. 24, no. 7, pp. 1143.e1–1143.e5, 2009.

Hindawi Publishing Corporation
BioMed Research International
Volume 2015, Article ID 368124, 6 pages
http://dx.doi.org/10.1155/2015/368124

Clinical Study

Iodine-Supported Hip Implants: Short Term Clinical Results

Tamon Kabata, Toru Maeda, Yoshitomo Kajino, Kazuhiro Hasegawa, Daisuke Inoue, Takashi Yamamoto, Tomoharu Takagi, Takaaki Ohmori, and Hiroyuki Tsuchiya

Department of Orthopaedic Surgery, Kanazawa University Graduate School of Medical Science, 13-1 Takara-machi, Kanazawa 920-8641, Japan

Correspondence should be addressed to Tamon Kabata; tamonkabata@yahoo.co.jp

Received 23 April 2015; Revised 4 July 2015; Accepted 5 July 2015

Academic Editor: Paul M. Tulkens

Copyright © 2015 Tamon Kabata et al. This is an open access article distributed under the Creative Commons Attribution License, which permits unrestricted use, distribution, and reproduction in any medium, provided the original work is properly cited.

We developed a new povidone iodine coating technology for titanium hip implants and performed a clinical trial to assess its usefulness in suppressing postoperative infection. Results indicate that iodine-supported titanium has favorable antibacterial activity, biocompatibility, and no cytotoxicity. Thirty joints in 28 patients were treated using iodine-supported implants. Fourteen joints were revision total hip arthroplasty (THA) after periprosthetic infection, 13 were primary THA for immunosuppressive conditions or pyogenic arthritis, and 3 were conversions from hemiarthroplasty to THA for immunosuppressive conditions. Two examinations were conducted sequentially until final follow-up: white blood cell (WBC) and C-reactive protein (CRP) were measured pre- and postoperatively and thyroid hormone levels in the blood were examined. The mean follow-up period was 33 months (14–78). There were no signs of infection in any patient at the last follow-up. WBC and CRP levels returned to normal within several weeks. No abnormalities of thyroid gland function were detected. Loosening of the implants did not occur in any patient. Excellent bone ingrowth and ongrowth were found around prostheses. No cytotoxicity or adverse effects were detected. These results suggest that iodine-supported THA implants can be highly effective in preventing and treating postoperative infections.

1. Introduction

Total hip arthroplasty (THA) is frequently used to treat degenerative hip joint diseases and is widely recognized as one of the most successful orthopedic surgeries. The increase in average life span has resulted in a dramatic increase in the number of THAs, which is estimated to exceed 500,000 per year by the year 2020 [1]. This will also mean an increase in the number of periprosthetic joint infections (PJI). PJI is a common complication after THA. The incidence is approximately 1% after primary cases and about 4% in revision cases, despite strict antiseptic operative procedures which include systemic prophylaxis [2, 3]. Currently, PJI is the second or third most common cause for revision hip arthroplasty [4, 5].

Postoperative PJIs are thought to be the result of bacterial adhesion to the implant surface and subsequent biofilm formation at the implantation site. In order to decrease bacterial infection, it is crucial to inhibit bacterial adhesion to the implant surface since biofilm can be very resistant to immune response and antibiotics. To prevent bacterial colonization and biofilm formation, several antibacterial coatings have been proposed, including vancomycin [6], gentamicin [7], carbonated hydroxyapatite (HA) [8], nitric oxide-releasing xerogel [9], and silver [10]. However, available technologies are far from ready for large-scale application, due to various limitations such as questionable long-term effects on bacterial resistance, osseointegration, regulatory issues, and cost.

We recently developed a new procedure for the anodization of povidone-iodine-containing surfaces that could be directly supported on existing implants [11, 12]. Iodine is a component of thyroid hormones and is the heaviest essential element needed by all living organisms. Our previous studies indicate that iodine-supported titanium has antibacterial activity, biocompatibility, and no cytotoxicity [11].

In this study, we performed a clinical trial of the newly invented technology of povidone iodine-supported THA implants.

2. Materials and Methods

A consecutive single-center series of 30 joints in 28 patients treated with iodine-supported hip implants was reviewed.

(a) (b)

Figure 1: An uncoated hip prosthesis (a) and an iodine-supported hip prosthesis (b).

The study group consisted of 13 men and 15 women with a mean age of 56 years (range, 17–81 years). Follow-up after surgical intervention averaged 33 months (range, 14–78 months). Fourteen joints were revision THA after PJI, and 13 joints were primary THA for compromised immune system conditions (severe diabetes mellitus, high dose glucocorticoid administration, under chemotherapy, inactive infections in other organs, and so on) or pyogenic arthritis. Three joints were conversions from hemiarthroplasty (bipolar in two, monopolar in one) to THA for immunosuppressive conditions. In the revision THAs after PJI, only one case underwent single-stage revision, while the other 13 needed two-stage revisions using antibiotic-loaded acrylic cement spacers (ALAC). In primary THA for pyogenic arthritis, 4 cases needed two-stage surgery using ALAC, while one case underwent single-stage implantation. Postoperatively, all patients received antibiotics intravenously tailored to the sensitivities of intraoperative cultures for at least 3–7 days, followed by oral administration until inflammatory markers (CRP, ESR) return to stable limits.

In all cases in this series we used titanium hip implants with iodine-containing surfaces (Figure 1). Two weeks before surgery, all implants were selected according to the preoperative plan using a 3D templating system (ZedHip, Lexi Co., Tokyo, Japan), and iodine-containing surface treatments were applied by the Chiba Institute of Technology (Narashino, Japan) using the technique described by Hashimoto et al. [13]. The thickness of the anodic oxide film was 5–10 μm with >50,000 pores/mm^2, with the capacity to support 10–12 μg/cm^2 of iodine (Figure 2) [11, 12]. Twenty-six acetabular sockets (Trilogy, Zimmer, Warsaw, USA; Converge, Zimmer, Warsaw, USA; Tritanium, Stryker, Mahwah, USA), 4 acetabular reinforcement cages (KT-plate, Kyocera, Osaka, Japan; Contour, Smith & Nephew, Memphis, USA), and 26 femoral stems (Allo-classic, Zimmer, Warsaw, USA; CLS, Zimmer, Warsaw, USA; Mayo conservative hip, Zimmer, Warsaw, USA; S-ROM-A, DePuy-Synthes Warsaw, USA) were iodine-supported and implanted.

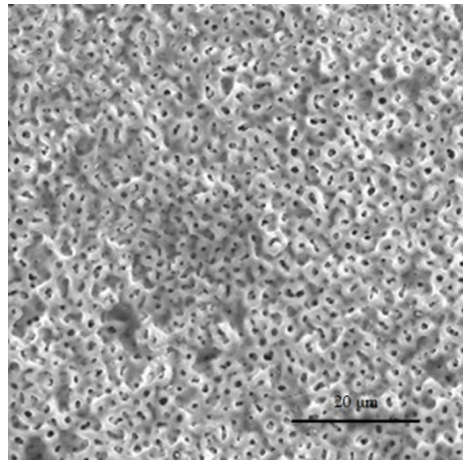

Figure 2: Electron micrograph of the oxide layer: more than 50,000 pores/mm^2.

Perioperatively, white blood cell (WBC) counts and C-reactive protein (CRP) levels were analyzed. To assess the influence of iodine from the implant, thyroid hormone levels in the blood, including thyroid-stimulating hormone (TSH), free triiodothyronine (FT3), and free thyroxine (FT4), were examined. Postoperative radiological evaluations were performed regularly, during which time loosening and failure of the implants were checked.

This study was approved by the ethics committee of our university. Written informed consent was obtained from all 28 patients.

3. Results

In the series of revision THAs after PJI, isolated microorganisms included methicillin-resistant coagulase-negative *Staphylococci* (MRCNS) in 6 patients, methicillin-resistant *Staphylococcus aureus* (MRSA) in 1 patient, and unknown

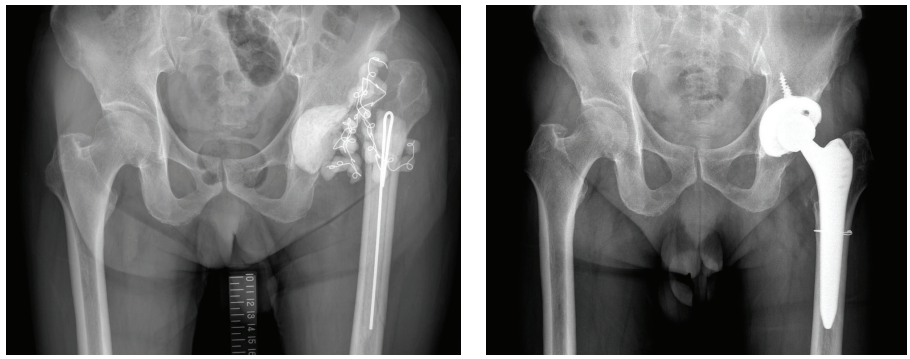

(a) (b)

Figure 3: Case of a 65-year-old man. PJI with methicillin-resistant coagulase-negative staphylococcus. Previous treatments including single-stage revision, implant removal, several irrigation, debridement, and ALAC treatments were performed by former surgeon, but suppression of PJI could not be obtained (a). Before iodine-supported prosthesis implantation, inflammation was still active, but the infection was cured after thorough debridement and implantation of iodine-supported hip prosthesis. CRP was 0.1 mg/dL and WBC was 4,400/ll 12 months later (b).

organisms in 6. One case underwent single-stage revision because of the patient's advanced age and general status. Thirteen cases underwent a two-stage ALAC treatment before implantation, which was effective in 10 cases but could not control PJI in the remaining 3 (Figure 3). Regardless of the preoperative treatment for PJI, complete suppression of PJI was obtained at the final evaluation in all cases except one pelvic tumor reconstruction case, which showed a slight elevation of CRP levels at 24 months after temporary suppression was obtained.

In the series of primary THAs for compromised immune conditions, PJI was prevented in all 11 cases. In the series of pyogenic arthritis, isolated microorganisms included methicillin-sensitive *Staphylococcus aureus* (MSSA) in 3 patients, *Pseudomonas aeruginosa* in 1, and *Streptococcus agalactiae* in 1. Although 1 case with *Pseudomonas aeruginosa* needed additional wound irrigation because of continuous wound discharge, all 5 cases successfully underwent primary THA without recurrence of infectious arthritis (Figure 4).

As for postoperative complications, three cases had postoperative dislocation, all of which were conservatively treated. None of the implants loosened during the follow-up period. Radiography revealed excellent bone ingrowth and ongrowth around the prostheses except for two acetabular sockets which showed slight radiolucent lines.

In the antibacterial treatment cases (14 cases of PJI and 5 cases of pyogenic arthritis), the preoperative median WBC counts and median CRP levels were 5,670/mm^3 (range, 3,630–8,690/mm^3) and 0.2 mg/dL (range, 0.0–2.6, reference value 0.3), respectively. Although the WBC counts tended to be high one week after surgery, they returned to normal by the final evaluation (median 5,860/mm^3, range 3,490–9,040/mm^3; median 0.2 mg/dL, range 0.0–1.5) (Figures 5 and 6).

In all cases, the preoperative FT3 (pg/mL), FT4 (ng/dL), and TSH levels (μIU/mL) were almost normal ranges (median 2.68 pg/mL, range 2.07–3.43; 1.14 ng/dL, range 0.8–1.42; 1.98 μIU/mL, range 0.3–8.54, resp.). One year postoperatively, the levels were still within the normal ranges (median 2.87 pg/mL, range 2.17–3.73; 1.14 ng/dL, range 0.81–1.59; 2.9 μIU/mL, range 0.86–19.9, resp.) (Figure 7). There was no case of thyroid gland malfunction with the use of iodine-supported implants.

4. Discussion

PJI represents one of the most severe complications in joint arthroplasty. Once severe PJI occurs, the cure rate by conservative treatment is low, and some kind of surgical intervention, such as removal of the implants, is usually required. However, an extremely effective prophylaxis or effective treatment for PJI has not yet been established. Systemic administration of antibiotics for bacterial infection is the most common therapy but is not effective for the resistant bacteria. Also, the local soft tissue surrounding implant cannot supply an effective amount of antibiotics for the bacteria present in the implant surface because of the lack of blood flow. Therefore, it would be meaningful from the viewpoint of PJI prevention and treatment for the surface of the implant to possess local antibacterial activity. Various strategies to provide implants with an antibacterial coating have been proposed recently [6–12].

In this study, we used iodine-supported titanium hip implants. Clinically, the iodine coating has several advantages. First, the antibacterial spectrum of iodine is very broad, acting not only on general bacteria but also on certain viruses, tubercle bacilli, and fungi [12]. Second, iodine does not cause drug resistance as it might be induced by the administration of antibiotics [12]; it has been noted that PJI due to antibiotic resistant bacteria is increasing [14], and antibiotic coating implants, such as gentamicin, may not sufficiently prevent PJI. Third, iodine is a trace metal and an essential component of the thyroid hormone. Iodine released from the implant is biologically safe because it can be excreted by the kidneys. In this study, TSH, FT3, and FT4 levels were in the normal range during the study period, postoperative WBC and CRP levels had returned to normal by the end of the study period, and no abnormalities of thyroid gland function were detected

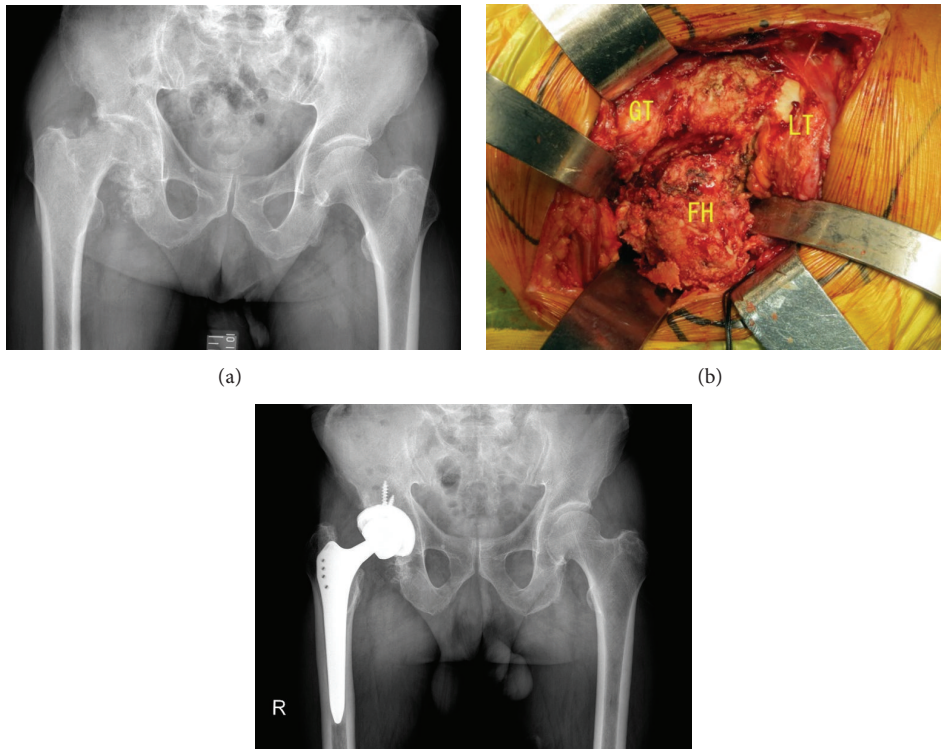

(a) (b)

(c)

Figure 4: Case of an 82-year-old man. Pyogenic arthritis of the right hip joint with methicillin-sensitive *Staphylococcus aureus* (MSSA). Irrigation and antibiotics treatment in former hospital could not suppress infection, which resulted in femoral head destruction (a). Right hip joint was filled with infected scar tissue and debris of the destructed femoral head. Single-stage implantation was performed after thorough debridement (b). GT: greater trochanter, LT: lesser trochanter, and FH: femoral head. One year after surgery, his hip function was almost normal, and iodine-supported hip prosthesis was well fixed. CRP was 0.2 mg/dL and WBC was 3,810/ll 12 months later (c).

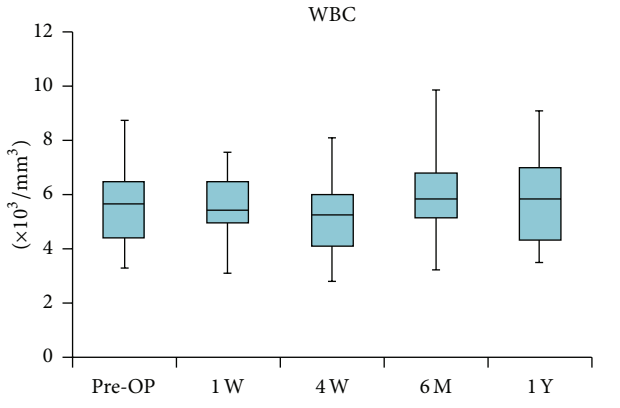

Figure 5: Changes in white blood cell (WBC) counts (/mm^3). WBC counts tended to be high several days after the surgery but returned to normal by 1 or 2 weeks.

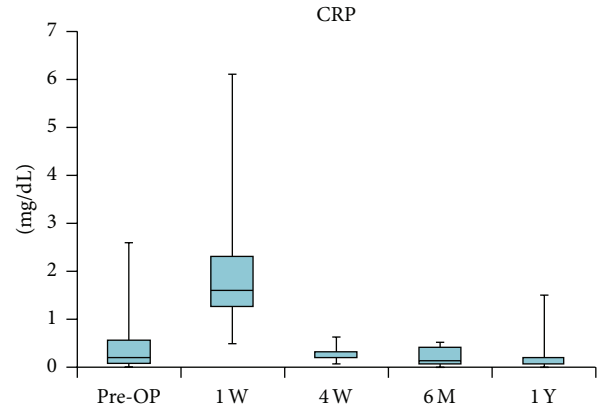

Figure 6: Changes in C-reactive protein (CRP; mg/dL). CRP level returned to normal level within 4 weeks after implantation.

(Figure 7). Fourth, duration of the antibiotic effect is relatively long. The biological half-life of an antibiotics coating or silver coating is said to be only several hours or days [15, 16]. On the other hand, recent data showed that the amount of iodine on the titanium pin in patients with external fixation was maintained, with approximately 40% remaining after 1 year [17]. Fifth, iodine-supported implants have excellent osteoconduction and good biocompatibility [11]; bone conduction is reportedly not possible on certain materials such as silver [10]. In this study, radiography showed excellent bone ingrowth and ongrowth. There were no signs of bone absorption or inhibition of bone formation. We think that the osteoconductive effects were reinforced according to the

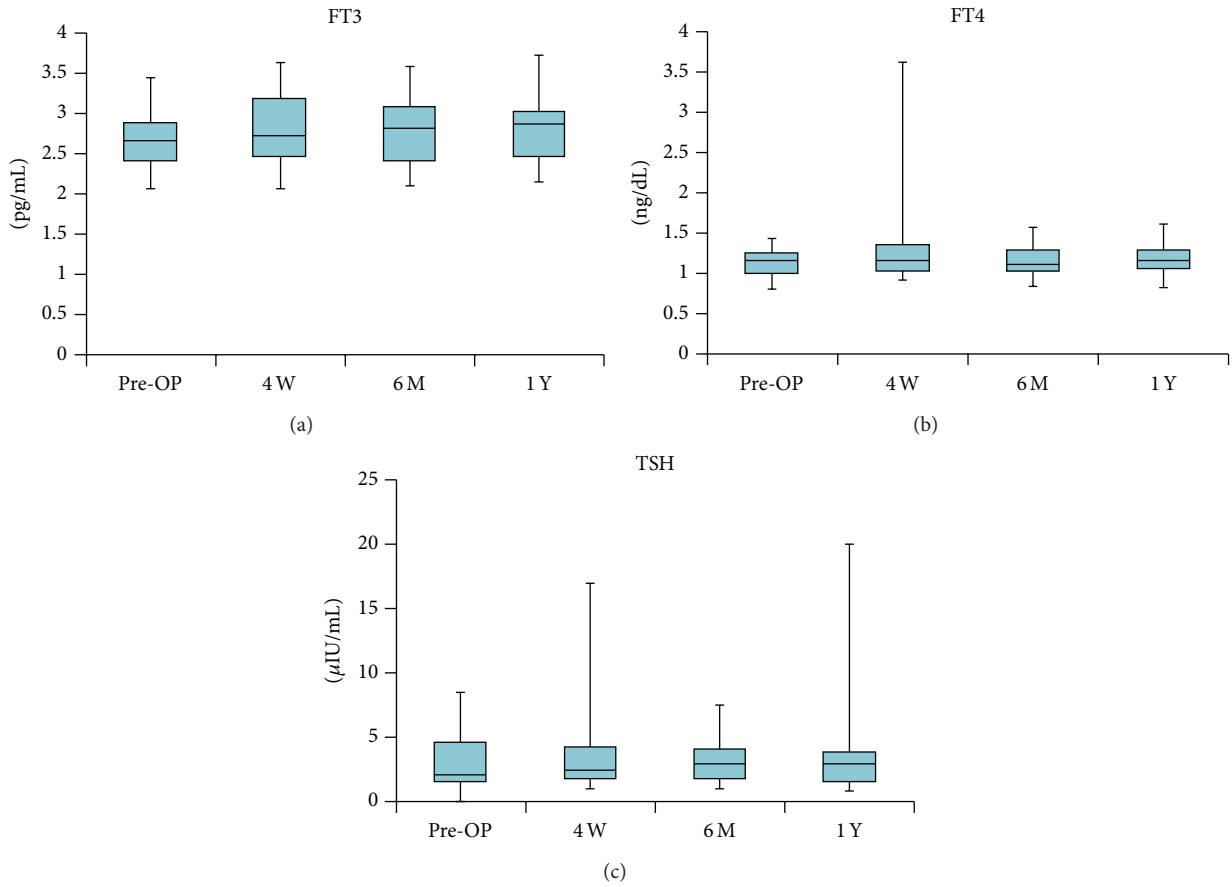

Figure 7: The free triiodothyronine (FT3; pg/mL), free thyroxine (FT4; ng/dL), and thyroid-stimulating hormone (TSH; μIU/mL) levels were within the normal ranges during the study period.

porous structure of the oxide layer. The characteristics of these iodine prosthesis coatings are extremely advantageous for PJI treatment. Although the number of cases was small, the results of this clinical trial suggest that iodine-supported titanium hip implants can be very effective in the prevention and treatment of PJIs after hip arthroplasty.

We think that the introduction of iodine coating for hip implants could result in a paradigm shift in current treatment strategies for PJI of the hip. Today two-stage revision arthroplasty is regarded as the gold standard treatment method for severe PJI [18]. Nevertheless, this procedure is costly and time-consuming and may affect the patient's mental condition. In contrast to two-stage revision, single-stage revision offers a shorter hospital stay, the avoidance of complications associated with a second operation, improved postoperative function and pain, and lower cost. However, this procedure is usually applied for highly selected patients. Using a reimplanted hip prosthesis that is iodine-supported could broaden the single-stage revision options. In this series, we successfully performed a single-stage revision for a PJI case in an elderly patient and a single-stage implantation for pyogenic arthritis. Our recent report demonstrated the efficacy of iodine-supported titanium implants in the management of active pyogenic vertebral osteomyelitis [19].

This case series does not have a sufficient number of cases or a long enough follow-up period. However, no infection recurred during the follow-up period in the series of revision THAs after PJI, and in the series of primary THAs for patients with compromised immune conditions, PJI was prevented in all cases. For comparison, a meta-analysis of 36 articles has reported that the infection recurrence rate in two-stage revision for PJI is 10.3%, while the infection rate for single-stage revision is 13.1% [20]. Also, it is well-known that joint replacement surgery for compromised immune conditions has a higher rate of PJI than for healthy patients. The reality is that, in these cases we cannot completely prevent PJI. However, the iodine coated implant is thought to have significant potential for reducing those rates of infection.

On the other hand, it must be recognized that there are several disadvantages to iodine-supported implants. The iodine coating procedure is costly and time-consuming (about 10 days for preparation). It cannot be applied to implants made from CoCr or ceramics, so the joint surface usually remains noncoated material. The implant size must be selected before surgery, which requires perfect preoperative planning. We routinely use a 3D templating system in the preoperative planning to select the appropriate implant design and size. The coating makes polished surfaces rough,

which may influence the original implant design concepts of each implant. We prefer to select an implant with a fully rough surface, like a Zweymuller type stem with a grit-blasted surface.

The present study has several limitations, including the uncontrolled retrospective design, small sample size, and diversity of patient background. Therefore, a prospective randomized clinical trial on a large scale is necessary to demonstrate the statistical significance of the infection rate. Although the small patient size limits the significance of the present study, the positive effect of iodine-supported implants in the prevention or treatment of PJI after THA is encouraging and merits further investigation.

5. Conclusion

The results of this clinical trial suggest that iodine-supported THA implants can be very effective and show great promise in the prevention and treatment of PJIs.

Conflict of Interests

None of the authors of this paper received any type of support, benefits, or funding from a commercial party related directly or indirectly to the subject of this paper.

References

[1] S. M. Kurtz, K. L. Ong, E. Lau, and K. J. Bozic, "Impact of the economic downturn on total joint replacement demand in the United States: updated projections to 2021," *The Journal of Bone & Joint Surgery*, vol. 96, no. 8, pp. 624–630, 2014.

[2] S. Ridgeway, J. Wilson, A. Charlet, G. Katafos, A. Pearson, and R. Coello, "Infection of the surgical site after arthroplasty of the hip," *The Journal of Bone & Joint Surgery—British Volume*, vol. 87, no. 6, pp. 844–850, 2005.

[3] C. Perka and N. Haas, "Periprosthetic infection," *Chirurg*, vol. 82, no. 3, pp. 218–226, 2011.

[4] T. W. Bauer, J. Parvizi, N. Kobayashi, and V. Krebs, "Diagnosis of periprosthetic infection," *The Journal of Bone & Joint Surgery—American Volume*, vol. 88, no. 4, pp. 869–882, 2006.

[5] K. J. Bozic, S. M. Kurtz, E. Lau, K. Ong, D. T. P. Vail, and D. J. Berry, "The epidemiology of revision total hip arthroplasty in the united states," *The Journal of Bone & Joint Surgery Series A*, vol. 91, no. 1, pp. 128–133, 2009.

[6] V. Antoci Jr., S. B. King, B. Jose et al., "Vancomycin covalently bonded to titanium alloy prevents bacterial colonization," *Journal of Orthopaedic Research*, vol. 25, no. 7, pp. 858–866, 2007.

[7] D. Neut, R. J. B. Dijkstra, J. I. Thompson, H. C. van der Mei, and H. J. Busscher, "A gentamicin-releasing coating for cementless hip prostheses-longitudinal evaluation of efficacy using *in vitro* bio-optical imaging and its wide-spectrum antibacterial efficacy," *Journal of Biomedical Materials Research Part A*, vol. 100, no. 12, pp. 3220–3226, 2012.

[8] M. Stigter, J. Bezemer, K. de Groot, and P. Layrolle, "Incorporation of different antibiotics into carbonated hydroxyapatite coatings on titanium implants, release and antibiotic efficacy," *Journal of Controlled Release*, vol. 99, no. 1, pp. 127–137, 2004.

[9] B. J. Nablo, H. L. Prichard, R. D. Butler, B. Klitzman, and M. H. Schoenfisch, "Inhibition of implant-associated infections via nitric oxide release," *Biomaterials*, vol. 26, no. 34, pp. 6984–6990, 2005.

[10] A. Ewald, S. K. Glückermann, R. Thull, and U. Gbureck, "Antimicrobial titanium/silver PVD coatings on titanium," *BioMedical Engineering Online*, vol. 5, article 22, 2006.

[11] T. Shirai, T. Shimizu, K. Ohtani, Y. Zen, M. Takaya, and H. Tsuchiya, "Antibacterial iodine-supported titanium implants," *Acta Biomaterialia*, vol. 7, no. 4, pp. 1928–1933, 2011.

[12] H. Tsuchiya, T. Shirai, H. Nishida et al., "Innovative antimicrobial coating of titanium implants with iodine," *Journal of Orthopaedic Science*, vol. 17, no. 5, pp. 595–604, 2012.

[13] K. Hashimoto, M. Takaya, A. Maejima et al., "Antimicrobial characteristics of anodic oxidation coating of aluminum impregnated with lodine compound," *Inorganic Materials*, vol. 6, pp. 457–462, 1999.

[14] D. J. Anderson, D. J. Sexton, Z. A. Kanafani, G. Auten, and K. S. Kaye, "Severe surgical site infection in community hospitals: epidemiology, key procedures, and the changing prevalence of methicillin-resistant *Staphylococcus aureus*," *Infection Control and Hospital Epidemiology*, vol. 28, no. 9, pp. 1047–1053, 2007.

[15] L. Zhang, J. Yan, Z. Yin et al., "Electrospun vancomycin-loaded coating on titanium implants for the prevention of implant-associated infections," *International Journal of Nanomedicine*, vol. 9, no. 1, pp. 3027–3036, 2014.

[16] M. Tsukamoto, H. Miyamoto, Y. Ando et al., "Acute and subacute toxicity *in vivo* of thermal-sprayed silver containing hydroxyapatite coating in rat tibia," *BioMed Research International*, vol. 2014, Article ID 902343, 8 pages, 2014.

[17] T. Shirai, K. Watanabe, H. Matsubara et al., "Prevention of pin tract infection with iodine-supported titanium pins," *Journal of Orthopaedic Science*, vol. 19, no. 4, pp. 598–602, 2014.

[18] M. C. Parry and C. P. Duncan, "The challenge of methicillin resistant staphylococcal infection after total hip replacement," *Bone and Joint Journal*, vol. 96, no. 11, supplement A, pp. 60–65, 2014.

[19] S. Demura, H. Murakami, T. Shirai et al., "Surgical treatment for pyogenic vertebral osteomyelitis using iodine-supported spinal instruments: initial case series of 14 patients," *European Journal of Clinical Microbiology and Infectious Diseases*, vol. 34, no. 2, pp. 261–266, 2014.

[20] J. Lange, A. Troelsen, R. W. Thomsen, and K. Søballe, "Chronic infections in hip arthroplasties: comparing risk of reinfection following one-stage and two-stage revision: a systematic review and meta-analysis," *Clinical Epidemiology*, vol. 4, no. 1, pp. 57–73, 2012.

Hindawi Publishing Corporation
BioMed Research International
Volume 2015, Article ID 164206, 6 pages
http://dx.doi.org/10.1155/2015/164206

Research Article

An In Vivo Study of Low-Dose Intra-Articular Tranexamic Acid Application with Prolonged Clamping Drain Method in Total Knee Replacement: Clinical Efficacy and Safety

Paphon Sa-ngasoongsong,[1] Pongsthorn Chanplakorn,[1] Siwadol Wongsak,[1] Krisorn Uthadorn,[1] Tanapong Panpikoon,[2] Paisan Jittorntam,[3] Katcharin Aryurachai,[4] Pantap Angchaisukisiri,[4] and Viroj Kawinwonggowit[1]

[1]*Department of Orthopedics, Faculty of Medicine Ramathibodi Hospital, Mahidol University, Bangkok, Thailand*
[2]*Department of Radiology, Faculty of Medicine Ramathibodi Hospital, Mahidol University, Bangkok, Thailand*
[3]*Section of Research, Education, and Innovation, Faculty of Medicine Ramathibodi Hospital, Mahidol University, Bangkok, Thailand*
[4]*Department of Medicine, Faculty of Medicine Ramathibodi Hospital, Mahidol University, Bangkok, Thailand*

Correspondence should be addressed to Pongsthorn Chanplakorn; pongsthornc@yahoo.com

Received 24 April 2015; Accepted 21 June 2015

Academic Editor: Kengo Yamamoto

Copyright © 2015 Paphon Sa-ngasoongsong et al. This is an open access article distributed under the Creative Commons Attribution License, which permits unrestricted use, distribution, and reproduction in any medium, provided the original work is properly cited.

Background. Recently, combined intra-articular tranexamic acid (IA-TXA) injection with clamping drain method showed efficacy for blood loss and transfusion reduction in total knee replacement (TKR). However, until now, none of previous studies revealed the effect of this technique on pharmacokinetics, coagulation, and fibrinolysis. *Materials and Methods*. An experimental study was conducted, during 2011-2012, in 30 patients undergoing unilateral TKR. Patients received IA-TXA application and then were allocated into six groups regarding clamping drain duration (2-, 4-, 6-, 8-, 10-, and 12-hours). Blood and drainage fluid were collected to measure tranexamic acid (TXA) level and related coagulation and fibrinolytic markers. Postoperative complication was followed for one year. *Results*. There was no significant difference of serum TXA level at 2 hour and 24 hour among groups ($p < 0.05$). Serum TXA level at time of clamp release was significantly different among groups with the highest level at 2 hour ($p < 0.0001$). There was no significant difference of TXA level in drainage fluid, postoperative blood loss, blood transfusion, and postoperative complications ($p < 0.05$). *Conclusions*. Low-dose IA-TXA application in TKR with prolonged clamping drain method is a safe and effective blood conservative technique with only minimal systemic absorption and without significant increase in systemic absorption over time.

1. Introduction

Total knee replacement (TKR) is a major orthopaedic operation that significantly associates with large amount of perioperative blood loss (PBL) and the need of blood transfusion. Therefore, perioperative blood loss management, in order to prevent bleeding related complication and transfusion-related morbidity [1, 2], is one of the most important factors for successful postoperative outcome. Regarding the proven methods used for reducing PBL in TKR, intra-articular tranexamic acid (IA-TXA) application together with 1-hour or 2-hour drain clamp has been demonstrated as ability to decrease PBL and proportion of patients requiring postoperative blood transfusion [3–8]. However, there was no consensus regarding the time that drain should be clamped for maximum benefit of intra-articular clot stabilization and minimize systemic absorption, and the recent studies also supported that prolonged clamping drain up to 12 hours is safe and effective for blood loss reduction [9–13]. Through our knowledge, none of the previous studies has been shown about pharmacokinetics of tranexamic acid (TXA) within joint space after intra-articular application with drain clamping in TKR and its effect on systemic homeostasis. Therefore, this study aimed to evaluate the serum TXA level

and the TXA concentration in drainage fluid after IA-TXA with specific time after drain clamp, in order to understand the pharmacodynamics of TXA within joint space and ability of systemic absorption and correlate with the other related postoperative outcomes.

2. Patients and Methods

A prospective experimental study was conducted, between 2011 and 2012, in 30 patients who underwent unilateral TKR in Ramathibodi Hospital. The study was approved by Committee on Human Right Related to Researches Involving Human Subjects (Protocol number ID 09-54-28). Informed consent was obtained from all participants, before the surgery was scheduled in accordance with the Declaration of Helsinki.

The inclusion criteria were (1) the patients who diagnosed as primary knee osteoarthritis and underwent primary unilateral cemented conventional TKR and (2) osteoarthritis grades II-III according to Ahlbäck classification [14]. The exclusion criteria were (1) risk of abnormal bleeding tendency or bleeding disorder (normal coagulogram, serum creatinine < 2.0 mg/dL, stopping nonsteroidal anti-inflammatory drugs and antiplatelet drugs more than 7 days), and (2) contraindication for TXA use (active intravascular clotting process, acquired defective colour vision, subarachnoid hemorrhage, hypersensitivity to TXA, and any of history of serious adverse effects, thrombotic disorder, and hematuria).

The blocked-randomization was generated by STATA 11.0 software (Stata Corp, College Station, Texas, USA) and further concealed with sealed envelopes in the sequentially numbered container. The surgery was performed by one of the authors (Viroj Kawinwonggowit), who was an experienced arthroplasty surgeon, under spinal anesthesia. The prostheses used in this present study were Nexgen total knee system (Zimmer Inc., Warsaw, Indiana, USA). Due to awareness of sex-related difference in anteroposterior diameter of the distal femur, Nexgen Gender prosthesis was specifically used in female patient while Nexgen Flex prosthesis was used in male patient. The pneumatic tourniquet was applied at proximal thigh with pressure as 350 mmHg. The surgical approach was midline skin incision, medial parapatellar arthrotomy, and midvastus incision. After the bony structure was prepared, all prosthesis components were inserted with full cementation (Palacos, Hevaeus Medical GmbH, Germany). Two standard drain tubes (size 8 Redon drain, B-Braun Ltd.) were placed deep into knee joint, which exited superolaterally. No superficial drain was used in this study. One drain tube was used to apply 500 mg intra-articular tranexamic acid injection and then connected to vacuum drains (Drainobag 600V Lock, B-Braun, Melsungen AG, Germany) [7]. Another drain was connected to smaller vacuum drains (Drainobag 150V Lock, B-Braun, Melsungen AG, Germany) in order to collect the drainage fluid to measure TXA level. Subcutaneous and skin closure was performed subsequently. Bulky compressive dressing was applied and both drains were clamped before tourniquet was deflated.

After the operation, the research assistant, who was not involved with the surgery, was responsible for opening the envelopes, opening the drain at the setting time, and recording the amount of drain volume as data collection protocol. Then the patients were randomly allocated into six groups regarding clamping drain duration (2-, 4-, 6-, 8-, 10-, and 12-hour). Postoperative blood samples were collected preoperatively, at the time of clamp release, 24-hour, 3-day, and 2-week postoperatively. Drainage fluid was collected at the time of clamp release by one of the authors (Krisorn Uthadorn) by standard protocol. The clamp of the smaller vacuum drain was released first to collect 50 mL of drainage fluid and then this drain was removed. Then, the clamp of larger vacuum drain was then fully opened later. Standard postoperative care protocol was applied to all patients. Blood transfusion was considered according to American Society of Anesthesiologists (ASA) guideline [15]. The amount of blood loss and transfusion was recorded. All patients were sent to document deep vein thrombosis (DVT) by duplex ultrasound, performed by an experienced radiologist (Tanapong Panpikoon) on the fourth postoperative day. If the patients who developed postoperative clinical presentation suspected pulmonary embolism (PE) such as acute dyspnea or unexplained hypoxemia, the computer tomographic angiogram was then performed to confirm the diagnosis by the same radiologist. All patients were followed for clinical outcome for one year.

Patients' demographic data and preoperative laboratory values were collected. Serum TXA level at 2 hours, time of clamp release, and 24 hours postoperatively and drainage TXA level were measured with mass spectrometry [16, 17], by one of the authors (Paisan Jittorntam). Total hemoglobin loss (THL) was calculated from the difference between preoperative Hb and postoperative Hb on the third postoperative day. Calculated total blood loss (CTBL) was calculated by using specific method [18, 19].

Blood samples were taken from all patients for measuring the coagulation and fibrinolytic markers with the standard technique using calibrated machine (as platelet count, prothrombin time (PT), partial thromboplastin time (PTT), thrombin time (TT), international normalized ratio (INR), D-dimer, and fibrinogen) at the time before operation, 2 hours, time of clamp release, 24 hours, 3 days, and 14 days postoperatively. Specific fibrinolytic markers, as plasmin inhibitor (PI), plasminogen (PLG), plasminogen activator inhibitor type 1 (PAI-1), and tissue plasminogen activator (t-PA) were all measured with standard kit, by one of the authors (Katcharin Aryurachai), at, preoperatively, 2 hours, time of clamp release, 24 hours, and 3 days postoperatively (tPA (Asserachrom tPA kit; Diagnostica Stago, Asnières-Sur-Seine, France), Plasma PAI-1 (Asserachrom PAI-1, Diagnostica Stago), Plasmin inhibitor (HemosIL Plasmin inhibitor, Instrumentation Laboratory), and Plasminogen (HemosIL Plasminogen, Instrumentation Laboratory)).

Statistical analysis was performed using Stata software version 11.0 (Stata Corp, College Station, Texas, USA). Normality of data was tested by Kolmogorov-Smirnov test. Continuous data were presented as mean and standard deviation and compared with one-way analysis of variance (ANOVA). The comparison of serial laboratory values between groups according to time was performed by repeated measurement

Table 1: Patients' characteristics data.

	Group						p value
	2 h	4 h	6 h	8 h	10 h	12 h	
Female gender■	4 (80)	2 (40)	4 (80)	4 (80)	5 (100)	3 (60)	0.36
Age, year◆	69 ± 7	72 ± 6	68 ± 7	67 ± 9	68 ± 4	74 ± 9	0.58
Height, cm◆	152 ± 5	155 ± 7	162 ± 11	153 ± 10	150 ± 5	158 ± 4	0.38
Weight, kg◆	61 ± 6	62 ± 6	67 ± 5	66 ± 10	67 ± 7	63 ± 4	0.68
BMI, kg/m^2◆	27 ± 2	26 ± 2	27 ± 3	29 ± 3	30 ± 3	25 ± 1	0.16
ASA physical status, grade I/II	2/3	3/2	3/2	3/2	1/4	1/4	0.56
Right side■	2 (40)	3 (60)	3 (60)	5 (100)	4 (80)	2 (40)	0.32
Preoperative laboratory values◆							
Hemoglobin, g/dL	13.5 ± 0.8	13.5 ± 1.5	12.7 ± 1.3	12.3 ± 1.4	12.1 ± 0.7	14.0 ± 2.0	0.26
Platelet count, ×10^3/mm^3	267 ± 48	275 ± 70	267 ± 84	251 ± 40	283 ± 72	255 ± 83	0.97
Prothrombin time, sec	11.7 ± 0.5	11.6 ± 0.8	11.5 ± 0.2	11.7 ± 0.7	11.9 ± 1.3	11.6 ± 0.4	0.96
Partial thromboplastin time, sec	28.1 ± 2.4	32.4 ± 0.8	27.7 ± 4.6	27.7 ± 4.6	24.4 ± 1.8	28.3 ± 8.9	0.53
Thrombin time, sec	10.7 ± 0.3	10.8 ± 0.5	10.5 ± 0.5	10.8 ± 1.1	10.3 ± 0.5	10.4 ± 0.5	0.60
INR	1.02 ± 0.04	1.01 ± 0.07	1.00 ± 0.02	1.01 ± 0.06	1.04 ± 0.10	1.01 ± 0.03	0.95
D-dimer, ng/mL	209 ± 64	348 ± 253	190 ± 70	184 ± 84	289 ± 176	335 ± 183	0.37
Fibrinogen, mg/dL	310 ± 37	310 ± 79	357 ± 68	338 ± 108	434 ± 122	442 ± 138	0.21

■: value presented as number of subjects (percentage), ◆: value presented as mean ± standard deviation.

Table 2: Serum tranexamic acid (TXA) level and TXA level in drainage fluid.

	Group						p value
	2 h	4 h	6 h	8 h	10 h	12 h	
Serum TXA level, μg/mL◆							
2 hours	12.8 ± 1.6	12.2 ± 2.6	15.0 ± 2.4	11.3 ± 2.1	13.2 ± 1.9	12.1 ± 2.3	0.16
Clamp release	12.8 ± 1.6	9.4 ± 3.3	6.4 ± 2.4	2.3 ± 0.5	2.0 ± 0.7	1.7 ± 1.0	**<0.0001**∗
24 hours	0.3 ± 0.1	0.5 ± 0.6	0.4 ± 0.2	0.2 ± 0.1	0.3 ± 0.1	0.3 ± 0.2	0.51
Drainage TXA level, μg/mL◆	461.9 ± 181.3	856 ± 505.8	282.8 ± 142.9	530.9 ± 839.4	560.5 ± 466.7	736.5 ± 621.6	0.59

◆: value presented as mean ± standard deviation.
∗: significant difference among groups with $p < 0.05$.

with Scheffe test post hoc analysis. Categorical data were presented as proportion and compared with Chi-square test.

3. Results

A total of 30 patients (8 males and 22 females) were recruited into this study and then were allocated into six groups according the blocked randomization. The average age and BMI were 69.7 ± 6.9 years (range 50–78 years) and 26.8 ± 2.9 kg/m^2 (range 22.5–33.3 kg/m^2). The mean preoperative Hb was 13.0 ± 1.4 g/dL (range 10.7–15.6 g/dL). There was no significant difference in gender, age, height, weight, BMI, ASA physical status, side of operation, and preoperative laboratory values among groups as shown in Table 1.

There was no significant difference between groups in serum TXA level at 2 hours and 24 hours postoperatively; however, the serum TXA level at the clamp release time was significantly lower according to time period of drain clamp (Figure 1) ($p < 0.0001$). The TXA concentration in drainage fluid was not significantly different between groups as shown in Table 2. No significant difference was found in DBL, THL, and CTBL between groups (Table 3).

No significant difference was found between groups in platelet count, PT, PTT, TT, INR, D-dimer, fibrinogen, PI, PLG, and t-PA preoperatively ($p > 0.05$); however there was a significant difference between groups in preoperative PAI-1 ($p = 0.01$). After surgery, there were significant differences between groups in D-dimer (14 d, $p = 0.01$), fibrinogen (time of clamp release, $p = 0.02$), PAI-1 (time of clamp release, 24 hours, and 3 days, $p = 0.002$, 0.03, and 0.03 resp.), and t-PA (2 hours and time of clamp release, $p = 0.05$ and 0.02) (Table 4).

Neither deep vein thrombosis nor infection nor wound complication was found immediately after operation and during 1-year follow-up period.

4. Discussion

Regarding the perioperative blood loss management in TKR, intra-articular tranexamic acid (IA-TXA) application has recently become a popular method due to its excellent efficacy for reducing PBL and transfusion requirement. However, through our knowledge, previous studies demonstrated ability to reduce postoperative blood loss with a variety of techniques and mostly using 1-2-hour clamp drain technique

Table 3: Blood loss outcome.

	Group						p value
	2 h	4 h	6 h	8 h	10 h	12 h	
Drainage blood loss, mL◆	418 ± 216	210 ± 117	266 ± 111	278 ± 118	238 ± 140	276 ± 163	0.35
Total hemoglobin loss, g/dL◆	2.5 ± 0.7	2.4 ± 0.8	2.0 ± 0.8	2.0 ± 0.5	2.2 ± 0.9	3.0 ± 0.8	0.37
Calculated total blood loss, mL◆	236 ± 105	245 ± 61	196 ± 106	154 ± 55	208 ± 112	277 ± 95	0.39

◆: value presented as mean ± standard deviation.

Table 4: p value of coagulation and fibrinolytic markers between each groups.

	p value between groups					
	Preop.	2 hours	C.R.	24 hours	3 days	14 days
Platelet count	0.97	0.77	0.69	0.52	0.68	0.92
Prothrombin time	0.96	0.92	0.83	0.86	0.12	0.62
Partial thromboplastin time	0.53	0.62	0.66	0.89	0.13	0.90
Thrombin time	0.60	0.99	0.75	0.64	0.47	0.91
INR	0.95	0.95	0.30	0.95	0.12	0.66
D-dimer	0.37	0.21	0.64	0.53	0.62	**0.01***
Fibrinogen level	0.21	0.28	**0.02***	0.13	0.38	1.00
Plasmin inhibitor	0.78	0.42	0.71	0.38	0.71	NA
Plasminogen	0.75	0.11	0.41	0.27	0.61	NA
Plasminogen activator inhibitor	**0.02***	0.20	**0.004***	**0.05***	0.06	NA
Tissue plasminogen activator	0.23	**0.05***	**0.02***	0.08	0.09	NA

Preop.: preoperative, C.R.; clamp release, and INR; international normalized ratio.
∗; Significant difference among groups with $p < 0.05$, NA; not available.

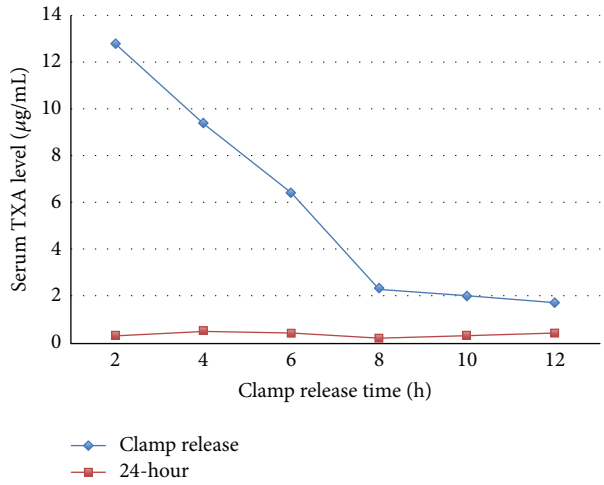

Figure 1: Serum tranexamic acid (TXA) level at time of clamp release and 24 hours in each group.

[3–8]. Moreover, several recent studies showed that the clamp drain technique up to 12 hours was safe and effective for blood loss reduction [9–13]. Therefore, in this prospective experimental study, we aimed to evaluate the effect of IA-TXA application with prolonged clamp drain technique on pharmacokinetics and systemic hemostasis.

Our data showed the systemic absorption after IA-TXA was independently affected with prolonged clamping drain method. Based on our findings, the systemic absorption of TXA was highest at 2 hours after application with drain clamp and gradually declined until 12 hours (Figure 1). Therefore, the drain-clamping time did not affect the systemic absorption in this study. This could be explained by blockage of TXA absorption due to an increase of clot formation on surgical bed and by consumption of the small concentration of IA-TXA (500 mg of TXA) into the intra-articular blood clot. The peak of serum concentration that was found in 2 hours after application of IA-TXA should be due to the absorption of TXA before the intra-articular clot formation and further metabolized in systemic circulation. After the clot formation was maximally established, an only minimal or no systemic absorption then occurred and, consequently, none of serum TXA level spikes was observed even with longer drain clamping applied. Moreover, this study also demonstrated that the TXA level in drainage fluid at the time of clamp release was not significantly different among groups (Table 2). This may imply that the synovial tissue did not play a role in the metabolism of IA-TXA for at least 12 hours, and low-dosage IA-TXA application was sufficient for inducing clot formation within joint space and stabilizing clot for at least 12 hours comparable with intravenous TXA administration [20].

Concerning the postoperative blood loss, there was no significant difference in any parameters on postoperative blood loss (Table 3). However, even without statistical significance, the lowest total hemoglobin loss and calculated total blood loss were found in 8 hours clamping drain group. Therefore, we concluded that, with our protocol, the small dose of IA-TXA for 500 mg of TXA with prolonged drain

clamp up to 8 hours should be safe protocol in order to minimize blood loss without significant increase in systemic absorption.

Venous thrombosis becomes a main concern immediately after major orthopedic surgery. During TKR with tourniquet, venous stasis and endothelial injuries may also cause venous thrombosis [21]. The use of TXA may increase this risk. Several studies have measured biological markers of fibrinolysis (such as D-Dimers, plasmin, antiplasmin, and t-PA) and coagulation (e.g., prothrombin fragment 1.2, PAI-1) perioperatively in major orthopedic surgery. A reduced fibrinolytic activity may be associated with increased thrombotic risk [22, 23]. In this study, we used coagulation and fibrinolytic markers (as D-dimer, fibrinogen, plasmin inhibitor (PI), plasminogen (PLG), plasminogen activator inhibitor type 1 (PAI-1), and tissue plasminogen activator (t-PA)) to evaluate the systemic event after application of IA-TXA. Our results showed significant differences between groups in D-dimer (14 d, $p = 0.01$) and fibrinogen (time of clamp release, $p = 0.02$) (Table 4). However, none of radiographic evidences as detected by duplex ultrasonography on postoperative day 4 and clinical evidences of venous thrombosis during 1-year follow-up period was observed in this study. Therefore, this phenomenon should be caused by majority of intra-articular clot formation and clot lysis process.

PAI-1 and t-PA had also found a significant difference between groups, PAI-1 (time of clamp release, 24 hours, and 3 days, $p = 0.002$, 0.03, and 0.03, resp.) and t-PA (2 hours and time of clamp release, $p = 0.05$ and 0.02) (Table 4). This might be explained by a significant preoperative higher value due to patients' baseline status [24]. In fact, fibrinolysis with t-PA synthesis was located at the surgical site (lower limb), while venous samples were taken from the upper limbs. Theoretically, in the operated limb, fibrinolysis is activated by a local increase in t-PA released by the endothelium, leading in turn to clot destruction. As t-PA not bound to fibrin is rapidly inhibited by PAI, an increase in active t-PA should not be observed in the nonoperated limb.

This present study had some limitations. This study was carried out on a relatively small population; although our result showed no significant difference in systemic absorption related to prolonged clamp drain period, it still needed more study population to demonstrate the effect of prolonged clamping drain to any rare possible postoperative complications such as DVT or PE.

In conclusion, IA-TXA application in TKR with a small dose of 500 mg together with prolonged drain clamp up to 8 hours should be a safe protocol in order to minimize blood loss without significant increase in systemic absorption. The peak of serum concentration that was found in 2 hours after application of IA-TXA should be due to the absorption of TXA before the intra-articular clot formation and further metabolized in systemic circulation and no effect in intravascular clot formation.

Conflict of Interests

All of the authors declare that they have no conflict of interests.

Acknowledgments

The authors wish to thank Professor Suphaneewan Jaovisidha, M.D., as a senior radiology consultant in their study, and thank Department of Orthopedics, Faculty of Medicine Ramathibodi Hospital, Mahidol University, for all of the kind help and permission to carry out this study.

References

[1] J. Allain, S. L. Stramer, A. Carneiro-Proietti et al., "Transfusion-transmitted infectious diseases," *Biologicals*, vol. 37, no. 2, pp. 71–77, 2009.

[2] E. C. Vamvakas and M. A. Blajchman, "Transfusion-related mortality: the ongoing risks of allogeneic blood transfusion and the available strategies for their prevention," *Blood*, vol. 113, no. 15, pp. 3406–3417, 2009.

[3] K. Ishida, N. Tsumura, A. Kitagawa et al., "Intra-articular injection of tranexamic acid reduces not only blood loss but also knee joint swelling after total knee arthroplasty," *International Orthopaedics*, vol. 35, no. 11, pp. 1639–1645, 2011.

[4] R. N. Maniar, G. Kumar, T. Singhi, R. M. Nayak, and P. R. Maniar, "Most effective regimen of tranexamic acid in knee arthroplasty: a prospective randomized controlled study in 240 patients," *Clinical Orthopaedics and Related Research*, vol. 470, no. 9, pp. 2605–2612, 2012.

[5] T. Onodera, T. Majima, N. Sawaguchi, Y. Kasahara, T. Ishigaki, and A. Minami, "Risk of deep venous thrombosis in drain clamping with tranexamic acid and carbazochrome sodium sulfonate hydrate in total knee arthroplasty," *The Journal of Arthroplasty*, vol. 27, no. 1, pp. 105–108, 2012.

[6] P. Sa-Ngasoongsong, T. Channoom, V. Kawinwonggowit et al., "Postoperative blood loss reduction in computer-assisted surgery total knee replacement by low dose intra-articular tranexamic acid injection together with 2-hour clamp drain: a prospective triple-blinded randomized controlled trial," *Orthopedic Reviews*, vol. 3, no. 2, article e12, 2011.

[7] P. Sa-Ngasoongsong, S. Wongsak, P. Chanplakorn et al., "Efficacy of low-dose intra-articular tranexamic acid in total knee replacement; a prospective triple-blinded randomized controlled trial," *BMC Musculoskeletal Disorders*, vol. 14, no. 1, article 340, 2013.

[8] J.-G. Seo, Y.-W. Moon, S.-H. Park, S.-M. Kim, and K.-R. Ko, "The comparative efficacies of intra-articular and IV tranexamic acid for reducing blood loss during total knee arthroplasty," *Knee Surgery, Sports Traumatology, Arthroscopy*, vol. 21, no. 8, pp. 1869–1874, 2013.

[9] N. Kiely, M. Hockings, and A. Gambhir, "Does temporary clamping of drains following knee arthroplasty reduce blood loss? A randomised controlled trial," *Knee*, vol. 8, no. 4, pp. 325–327, 2001.

[10] F. Madadi, A. S. Mehrvarz, F. Madadi, M. Boreiri, K. Abachizadeh, and A. Ershadi, "Comparison of drain clamp after bilateral total knee arthroplasty," *The Journal of Knee Surgery*, vol. 23, no. 4, pp. 215–221, 2010.

[11] P.-C. Shen, I.-M. Jou, Y.-T. Lin, K.-A. Lai, C.-Y. Yang, and T.-C. Chern, "Comparison between 4-hour clamping drainage and nonclamping drainage after total knee arthroplasty," *Journal of Arthroplasty*, vol. 20, no. 7, pp. 909–913, 2005.

[12] J. Stucinskas, S. Tarasevicius, A. Cebatorius, O. Robertsson, A. Smailys, and H. Wingstrand, "Conventional drainage versus

four hour clamping drainage after total knee arthroplasty in severe osteoarthritis: a prospective, randomised trial," *International Orthopaedics*, vol. 33, no. 5, pp. 1275–1278, 2009.

[13] N. Roy, M. Smith, M. Anwar, and C. Elsworth, "Delayed release of drain in total knee replacement reduces blood loss. A prospective randomised study," *Acta Orthopaedica Belgica*, vol. 72, no. 1, pp. 34–38, 2006.

[14] S. Ahlbäck, "Osteonecrosis of the knee," *Calcified Tissue Research*, vol. 2, no. 1, p. 36, 1968.

[15] American Society of Anesthesiologists Task Force on Perioperative Blood Transfusion and Adjuvant Therapies, "Practice guidelines for perioperative blood transfusion and adjuvant therapies: an updated report by the American society of anesthesiologists task force on perioperative blood transfusion and adjuvant therapies," *Anesthesiology*, vol. 105, no. 1, pp. 198–208, 2006.

[16] Q. Chang, O. Q. Yin, and M. S. S. Chow, "Liquid chromatography-tandem mass spectrometry method for the determination of tranexamic acid in human plasma," *Journal of Chromatography B*, vol. 805, no. 2, pp. 275–280, 2004.

[17] S. G. Delyle, E. Abe, A. Batisse et al., "A validated assay for the quantitative analysis of tranexamic acid in human serum by liquid chromatography coupled with electrospray ionization mass spectrometry," *Clinica Chimica Acta*, vol. 411, no. 5-6, pp. 438–443, 2010.

[18] J. D. Robinson, S. M. Lupkiewicz, L. Palenik, L. M. Lopez, and M. Ariet, "Determination of ideal body weight for drug dosage calculations," *American Journal of Hospital Pharmacy*, vol. 40, no. 6, pp. 1016–1019, 1983.

[19] P. Seeber and A. Shander, *Basics of Blood Management*, Blackwell Publishing, Malden, Mass, USA, 1st edition, 2007.

[20] A. Blanié, L. Bellamy, Y. Rhayem et al., "Duration of postoperative fibrinolysis after total hip or knee replacement: a laboratory follow-up study," *Thrombosis Research*, vol. 131, no. 1, pp. e6–e11, 2013.

[21] A. Abdel-Salam and K. S. Eyres, "Effects of tourniquet during total knee arthroplasty. A prospective randomised study," *The Journal of Bone and Joint Surgery—British Volume*, vol. 77, no. 2, pp. 250–253, 1995.

[22] B. I. Eriksson, E. Hultman, S. Martinell, E. Eriksson, L. Tengborn, and B. Risberg, "Regional fibrinolysis following total hip replacement," *Thrombosis Research*, vol. 62, no. 5, pp. 441–447, 1991.

[23] J. V. Sørensen, L. C. Borris, M. R. Lassen et al., "Association between plasma levels of tissue plasminogen activator and postoperative deep vein thrombosis-influence of prophylaxis with a low molecular weight heparin," *Thrombosis Research*, vol. 59, no. 1, pp. 131–138, 1990.

[24] A. Festa, K. Williams, R. P. Tracy, L. E. Wagenknecht, and S. M. Haffner, "Progression of plasminogen activator inhibitor-1 and fibrinogen levels in relation to incident type 2 diabetes," *Circulation*, vol. 113, no. 14, pp. 1753–1759, 2006.

Hindawi Publishing Corporation
BioMed Research International
Volume 2015, Article ID 413839, 15 pages
http://dx.doi.org/10.1155/2015/413839

Research Article

Assessment of Hip Fracture Risk Using Cross-Section Strain Energy Determined by QCT-Based Finite Element Modeling

Hossein Kheirollahi[1] and Yunhua Luo[1,2]

[1]*Department of Mechanical Engineering, Faculty of Engineering, University of Manitoba, Winnipeg, MB, Canada R3T 5V6*
[2]*Department of Anatomy, Southern Medical University, Guangzhou 510515, China*

Correspondence should be addressed to Yunhua Luo; yunhua.luo@umanitoba.ca

Received 24 April 2015; Revised 28 June 2015; Accepted 29 June 2015

Academic Editor: Kengo Yamamoto

Copyright © 2015 H. Kheirollahi and Y. Luo. This is an open access article distributed under the Creative Commons Attribution License, which permits unrestricted use, distribution, and reproduction in any medium, provided the original work is properly cited.

Accurate assessment of hip fracture risk is very important to prevent hip fracture and to monitor the effect of a treatment. A subject-specific QCT-based finite element model was constructed to assess hip fracture risk at the critical locations of femur during the single-leg stance and the sideways fall. The aim of this study was to improve the prediction of hip fracture risk by introducing a novel failure criterion to more accurately describe bone failure mechanism. Hip fracture risk index was defined using cross-section strain energy, which is able to integrate information of stresses, strains, and material properties affecting bone failure. It was found that the femoral neck and the intertrochanteric region have higher fracture risk than other parts of the femur, probably owing to the larger content of cancellous bone in these regions. The study results also suggested that women are more prone to hip fracture than men. The findings in this study have a good agreement with those clinical observations reported in the literature. The proposed hip fracture risk index based on strain energy has the potential of more accurate assessment of hip fracture risk. However, experimental validation should be conducted before its clinical applications.

1. Introduction

Two of the major determinants of proximal femur fractures among the elderly are osteoporosis and sideways fall. The most common serious injury associated with the fall of an elderly person is hip fracture. Furthermore, hip fracture is associated with an up to 20% chance of death, a 25% chance of long term institutionalization, and less than a 50% chance of full recovery [1]. The total number of hip fractures in men and women in 1990 was estimated to be 338,000 and 917,000, respectively, over the world [2]. Assuming no change in the age- and sex-specific incidence, the number of hip fractures is estimated to approximately double to 2.6 million by the year 2025 and 4.5 million by the year 2050 over the world [2]. By the increasing trend in hip fractures because of the aging of the population, the worldwide annual costs of hip fractures in the year 2050 have been estimated to be $131.5 billion [3]. So, hip fracture risk should be assessed in individuals who are at a risk for an osteoporotic hip fracture to provide proper plans to prevent future probable fractures.

Statistical models and bone mineral density (BMD) captured by Dual-Energy X-ray Absorptiometry (DXA) are used for in vivo osteoporotic fracture risk assessment [4, 5]. However, their accuracy in assessment of fractures is limited; most osteoporotic fractures actually occur with BMD measurements that are above the conventional osteoporotic threshold [6]. Fracture Risk Assessment Tool (FRAX) is a tool to evaluate an individual's fracture probability in the next 10 years, adopted by the WHO in 2008 [7]. FRAX does not take into account fall-induced impact force that is critically important in the hip fracture risk assessment [8, 9]. The main limitations of the FRAX include the following: it is a statistical model and fracture risk is not consistent within 10 years with some of the treatment results [10]. Hip structure analysis (HSA) program is now commercially available and is used to automatically assess the geometric and structural parameters of the femur. Whereas HSA is based on a beam model, the deformation of bone is oversimplified, especially in the femoral neck and the intertrochanteric region where osteoporotic femoral fractures most often occur; therefore

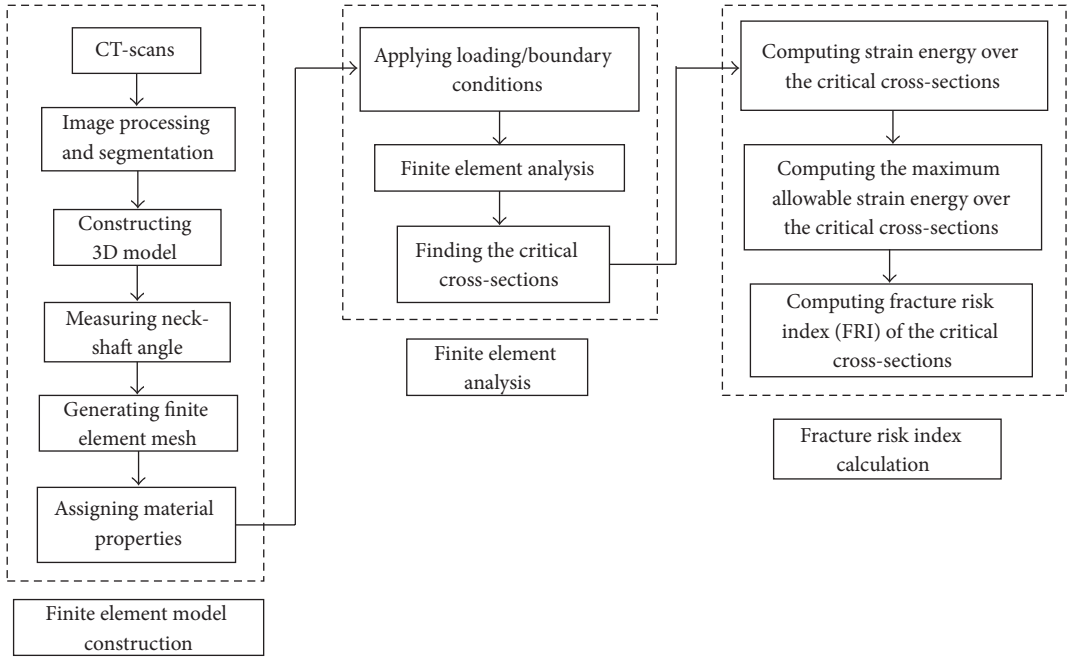

Figure 1: The proposed methodology for calculating hip fracture risk index using the strain energy criterion.

the deformation is too complicated to be described as a beam model [11].

Finite element models constructed from quantitative computed tomography (QCT) are very helpful in assessing hip fracture risk, as they are based on well-established biomechanical principles and theories. In QCT-based finite element modeling, choosing a proper failure criterion is very important to accurate assessment of hip fracture risk. Commonly used bone failure criteria include von Mises stress and strain criteria [12–15], maximum principle stress and strain criteria [16–19], maximum shear stress criterion [20], and maximum distortion energy criterion [20]. The femur consists of inhomogeneous (porous) cancellous bone and nearly homogenous cortical bone, and their failure mechanisms are different due to their different microstructure. Failure mechanism of the cancellous bone is mostly in the form of spicule (trabecula) buckling, and the failure of denser cancellous bone and the cortical bone is mostly characterized by local cracking [21, 22]. Cortical and cancellous bone have different properties. Cortical bone is usually more brittle [23], while cancellous bone is more ductile. The current failure criteria are not convenient in describing their properties. Therefore, the total strain energy, which integrates all information of stress, strain, and material properties, is a better option [21]. Mirzaei et al. [21, 24] predicted failure strength and failure patterns of human proximal femur and human vertebrae using the strain energy criterion with a QCT-based FE model. Their predictions of the failure loads and failure locations were in a good agreement with the experimental findings. The strain energy criterion is widely used in fracture analysis of engineering materials. It is usually used in crack problems [25–27], composite laminates [28, 29], and bone cement analysis [30]. Therefore, computation of hip fracture risk index (FRI) over a region of interest (ROI) based on the strain energy criterion theoretically should be more accurate for assessing hip fracture risk. To the best of our knowledge, there are currently no published studies that use the strain energy criterion for the hip fracture risk assessment. The objective of this study is to improve the hip fracture risk assessment procedure previously developed by Luo et al. [11] by introducing the strain energy criterion.

2. Materials and Methods

The proposed methodology for assessment of hip fracture risk in the critical regions of femur using the strain energy criterion determined from QCT-based finite element model is shown in Figure 1. The procedure is explained in detail in the following.

2.1. QCT-Based Finite Element Model

2.1.1. QCT-Scan of Femur. The purpose of this study is to accurately assess hip fracture risk, so, a 3D finite element model of subject's femur is required to achieve it. The 3D model can be constructed from the subject's femur QCT images. QCT slices are produced using multiple scanners with a set of proper acquisition and reconstruction parameters (Figure 2(a)). Slice thickness of 1 mm is commonly used. The scanned QCT images are stored in the format of Digital Imaging and Communications in Medicine (DICOM), which can be used for the construction of a 3D FE model. A proper segmentation is done to separate the femur for constructing the 3D model. Each voxel in the QCT-scan has an intensity (or grey scale) that is expressed as Hounsfield Unit (HU), which is correlated to bone density [31, 32]. Threshold value

Table 1: Statistical information of the 60 clinical cases.

Gender		Age (years)	Height (cm)	Body weight (kg)	BMI (kg/m^2)
Female	Range	50–82	149–174.7	51.7–110.9	21.01–43.36
	Average	65	163.92	77.58	28.81
Male	Range	50–78	163.4–193.2	61.5–126.6	18.83–40.96
	Average	64.71	175.74	86.22	27.9

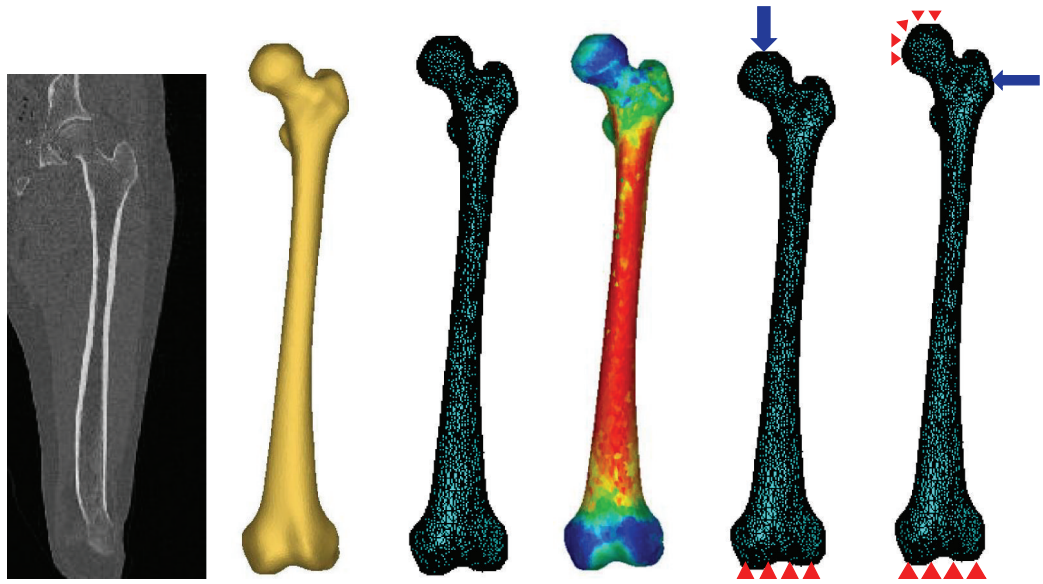

Figure 2: QCT-based finite element modeling: (a) QCT-scan of the subject's femur; (b) 3D model generated from the QCT images; (c) 3D finite element model; (d) distribution of elasticity modulus; (e) single-leg stance configuration; and (f) sideways fall configuration.

for the cancellous bone is from 100 HU to 200 HU and for the cortical bone is between 200 HU and 2000 HU. QCT images of 60 clinical cases (30 females and 30 males) were acquired from the Winnipeg Health Science Centre in an anonymous way under a human research ethics approval. The subjects are in the age scope from 50 to 82 years (average of 65 years). Statistical information of the clinical cases is listed in Table 1.

2.1.2. Generation of Finite Element Mesh. In the first step, the geometrical model of the femur is generated from clinical QCT images using Mimics (Materialise, Leuven, Belgium). QCT images (in DICOM format) are imported to Mimics for segmentation (Figure 2(a)) and construction of 3D geometric model of the femur (Figure 2(b)). With the 3D geometric model, a FE mesh is generated using the 3-matic module in Mimics (Figure 2(c)). The 4-node linear tetrahedral element SOLID72 in ANSYS was used in this study. To investigate model convergence, FE models with different maximum element edge lengths were created. For each FE model, displacement was calculated under the same loading and boundary conditions. The maximum element edge length that produced converged finite element solutions was obtained and used in all the rest of FE simulations. The number of elements for each case is assigned based on the maximum element edge length that provided converged FE solution, meaning that the number of elements is different from case to case.

2.1.3. Assignment of Material Properties. To construct a more faithful FE model, bone material properties are considered inhomogeneous and isotropic in this study. Information on the inhomogeneous isotropic mechanical properties of the bone can be derived from the CT data using a mathematical relationship between the CT numbers and the mechanical properties of bone. The following empirical equation was used to determine bone ash density (ρ_{ash}) from HU number [33, 34]:

$$\rho_{\text{ash}} = 0.04162 + 0.000854\,\text{HU} \quad \left(\text{g/cm}^3\right). \tag{1}$$

Equations (2) and (3), derived by Keller [35], were, respectively, used to assign Young's modulus (E) and yield stress (σ_Y) according to the bone ash density:

$$E = 10500\rho_{\text{ash}}^{2.29} \quad (\text{MPa}) \tag{2}$$

$$\sigma_Y = 116\rho_{\text{ash}}^{2.03} \quad (\text{MPa}). \tag{3}$$

A constant Poisson's ratio ($\nu = 0.4$) was considered as suggested in the literature [13, 36, 37]. To assign material properties, elements are grouped into a number of discrete

material bins using Mimics (Materialise, Leuven, Belgium), to approximately represent the continuous distribution of the inhomogeneous bone mechanical properties. To determine the maximum number of material bins, convergence study was performed. Models with different material bins were created for convergence study. For each FE model, displacement was calculated under the same loading and boundary conditions. The maximum number of material bins that generated converged finite element solutions was obtained. Figure 2(d) shows the isotropic inhomogeneous distribution of material properties.

2.2. Finite Element Analysis Using ANSYS. The finite element model of femur with the assigned material properties was output from Mimics and then imported to ANSYS for finite element analysis. For a precise assessment of hip fracture risk during the single-leg stance and the sideways fall, loading and boundary conditions simulating the single-leg stance and the sideways fall configurations are required in the FE model. To simulate the single-leg stance configuration, 2.5 times the patient's body weight was applied as a distributed load on the femoral head in direction of femoral shaft axis [38] and femur was fixed at the distal end [13, 39]; see Figure 2(e). Consider

$$F_{\text{Stance}} = 2.5w \quad (\text{N}), \tag{4}$$

where w is the subject's body weight in Newton (N). To simulate sideways fall, the distal end of femur was completely fixed and the surface of femoral head was fixed in the loading direction (Figure 2(f)) [40, 41]. The impact force during the sideways fall acting on the greater trochanter perpendicularly (Figure 2(f)) is given by [38, 42]:

$$F_{\text{Impact}} = 8.25w\left(\frac{h}{170}\right)^{1/2} \quad (\text{N}), \tag{5}$$

where h is the height of the subject in centimeter (cm). Loading and boundary conditions on the greater trochanter, the femoral head, and the distal end of femur were applied to a group of nodes using APDL codes (Figures 2(e) and 2(f)). After importing the QCT-based FE model and applying the loading and boundary conditions, finite element analysis was performed and finite element solutions were obtained. In all the analysis, the nodal displacements, stresses, and strains were obtained for each subject.

2.3. Detection of the Three Critical Cross-Sections on the Femur. Hip fractures usually occur at one of the anatomical locations: the femoral neck, the intertrochanter, and the subtrochanter as illustrated in Figure 3. According to clinical observations, 49 percent of hip fractures are intertrochanteric, 37 percent are at femoral neck, and 14 percent are subtrochanteric [43]. Therefore, the smallest femoral neck cross-section (SFN CS), the intertrochanteric cross-section (IntT CS), and the subtrochanteric cross-section (SubT CS) are the three critical cross-sections of femur that usually have the highest fracture risk (Figure 3). To determine the smallest femoral neck cross-section and the intertrochanteric cross-section, neck-shaft angle is needed. The neck-shaft angle is the angle

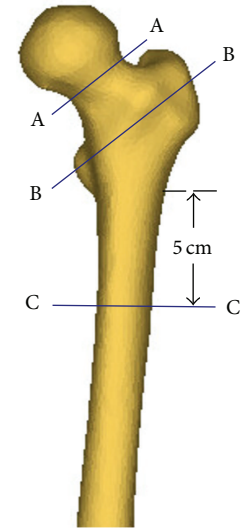

Figure 3: Three critical cross-sections of femur: the smallest femoral neck cross-section (A-A), the intertrochanteric cross-section (B-B), and the subtrochanteric cross-section (C-C).

between the femoral neck axis and the femoral shaft axis. This angle traditionally is measured on conventional radiography images, or using 2D images projected from CT/MRI data. In spite of their popularity, these methods are based on oversimplification of the real 3D anatomy and may lead to large errors due to the inaccuracies in selection of the measurement plane [44–46]. In this study, the neck-shaft angle was measured using a 3D measurement technique based on fitting functions. In this technique, the shapes of particular parts of the femur are approximated using geometric entities such as circle, cylinder, and sphere, which are well fitted to the actual anatomy, and the geometrical relationships between these entities are obtained to estimate the neck-shaft angle.

First, a sphere was fitted to the femoral head, to obtain the position of the joint's centre of rotation, which is also the femoral head centre. Then, the femoral neck axis and the femoral shaft axis are identified by applying the "fit ruled surface direction" function on the femoral neck and shaft. All fitting functions were applied using the 3-matic module in Mimics. The neck-shaft angle was also measured by 3-matic module of Mimics (Figure 4). With the femoral neck-shaft angle, the intertrochanteric cross-section and the smallest femoral neck cross-section were found using in-house computer codes. The smallest femoral neck cross-section is chosen as the cross-section with the smallest area in the neck region and the intertrochanteric cross-section is chosen as the cross-section that has the largest area in the intertrochanteric region [47]. By using APDL codes, perpendicular planes on the femoral neck axis were determined and then areas of the cross-sections were calculated. The planes with the smallest and the largest areas were chosen, respectively, as the smallest femoral neck cross-section and the intertrochanteric cross-section. The subtrochanteric cross-section is considered five centimeters below the lesser trochanter [48] (Figure 3).

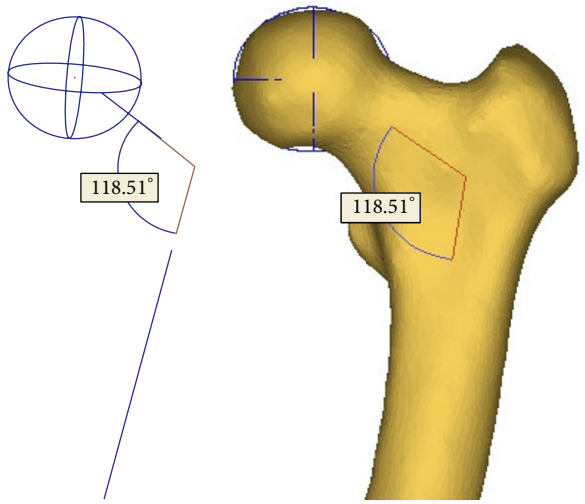

Figure 4: Neck-shaft angle measured by the fitting functions in the 3-matic module of Mimics.

2.4. Hip Fracture Risk Index Definition Using the Strain Energy Criterion. Based on the previous discussion of the bone failure mechanism and microstructure, the strain energy criterion is theoretically more favourable for hip fracture risk assessment. The strain energy at the three critical cross-sections of femur induced by the applied forces was computed using in-house developed MATLAB codes and the data extracted by APDL codes from the obtained finite element solutions. The plane boundaries of the three critical cross-sections, extracted from the finite element mesh, were imported to MATALB to generate a 2D mesh for calculating the cross-section strain energy. Figure 5 shows the generated triangle elements over the smallest femoral neck cross-section, the intertrochanteric cross-section, and the subtrochanteric cross-section.

The strain energy at the three critical cross-sections induced by the applied forces is the sum of strain energy in all the triangle elements; that is,

$$U = \sum_{i=1}^{m} U_e, \tag{6}$$

where U_e is the strain energy in Element e induced by the applied forces and m is the number of triangle elements created over the concerned cross-section. Gaussian integration method was used to calculate the strain energy in elements. Integration points in each triangle element were determined using in-house MATLAB codes. By using Gaussian integration method, the strain energy of Element e induced by the applied forces is calculated as

$$U_e = \iint \widehat{U}_e \, dA \approx \sum_{i=1}^{n} W_i \, |J| \, \widehat{U}_i, \tag{7}$$

where $\widehat{U}_e$ is the strain energy density of Element e; $\widehat{U}_i$ is the strain energy density at the integration point i of in Element e; W_i is the weight at the integration point; $|J|$ is the determinant of the Jacobean matrix of the triangle element; and n is the number of integration points over the triangle element. The strain energy density at an integration point (i) was determined from the finite element solutions obtained by the QCT-based FE model; that is,

$$\widehat{U}_i = \frac{1}{2} \{\sigma\}^T \{\varepsilon\}, \tag{8}$$

where $\{\sigma\} = [D]\{\varepsilon\}$ and $\{\varepsilon\} = [B]\{d\}$. The strain energy density at each integration point can be expressed by the finite element solutions as

$$\widehat{U}_i = \frac{1}{2} \{d\}_e^T [B]_e^T [D]_e [B]_e \{d\}_e, \tag{9}$$

where $\{d\}$ is the displacement vector consisting of displacements at the nodes of Element e; matrix $[B]$ consists of the derivatives of shape functions of the element; and $[D]$ is the material property matrix. Consider

$$[D]_e = \frac{E}{(1+\nu)(1-2\nu)} \cdot \begin{bmatrix} 1-\nu & \nu & \nu & 0 & 0 & 0 \\ \nu & 1-\nu & \nu & 0 & 0 & 0 \\ \nu & \nu & 1-\nu & 0 & 0 & 0 \\ 0 & 0 & 0 & \frac{1}{2}-\nu & 0 & 0 \\ 0 & 0 & 0 & 0 & \frac{1}{2}-\nu & 0 \\ 0 & 0 & 0 & 0 & 0 & \frac{1}{2}-\nu \end{bmatrix}, \tag{10}$$

where Poisson's ratio is constant ($\nu = 0.4$) and Young's modulus is a function of the bone density as given in (2). For each integration point, its Young's modulus is determined by the bone density at the point.

The maximum allowable strain energy over a critical cross-section of the femur was also computed from the obtained finite element solutions using in-house MATLAB codes. The maximum allowable strain energy (or the yield strain energy) over a critical cross-section is obtained as

$$U_Y = \sum_{i=1}^{m} U_Y^e, \tag{11}$$

where U_Y^e is the yield strain energy in Element e and m is the number of triangle elements over the concerned cross-section. The Gaussian integration method was also used to calculate the maximum allowable strain energy in each triangle element. The maximum allowable strain energy that a triangle element (e) can sustain is given by

$$U_Y^e = \iint \widehat{U}_Y^e \, dA \approx \sum_{i=1}^{n} W_i \, |J| \, \widehat{U}_{Yi}, \tag{12}$$

where $\widehat{U}_Y^e$ is the yield strain energy density in Element e; n is the number of integration points; and $\widehat{U}_{Yi}$ is the yield strain energy density at integration point i and is calculated as

$$\widehat{U}_{Yi} = \frac{1}{2} \sigma_{Yi} \varepsilon_{Yi} = \frac{\sigma_{Yi}^2}{2E_i}, \tag{13}$$

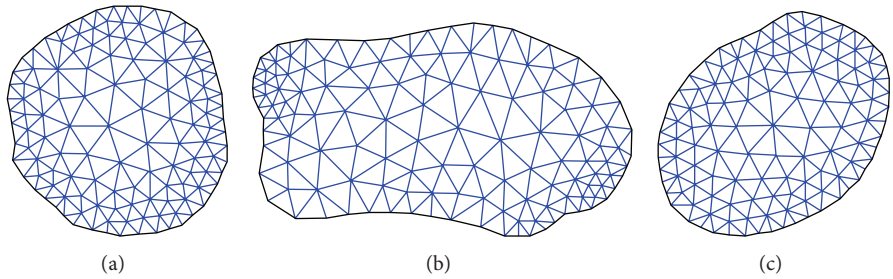

Figure 5: Generated triangle elements over (a) the smallest femoral neck cross-section, (b) the intertrochanteric cross-section, and (c) the subtrochanteric cross-section.

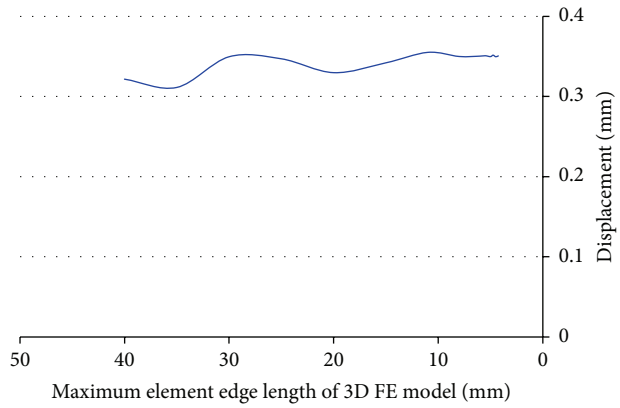

Figure 6: Convergence of finite element solutions with element size.

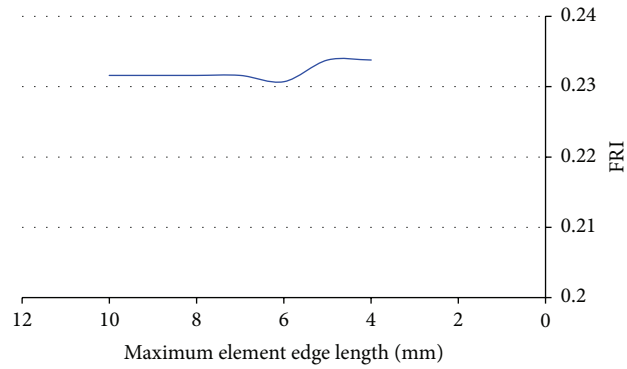

Figure 7: Convergence of FRI.

where σ_{Yi} and E_i are, respectively, the yield stress and Young's modulus at the integration point. Both of them are function of bone density, as given in (2) and (3).

Hip fracture risk index (η) at a critical cross-section is defined as

$$\eta = \frac{U}{U_Y}, \tag{14}$$

where U and U_Y are, respectively, obtained from (6) and (11).

3. Results

3.1. Convergence Studies

3.1.1. Element Size in Femur Finite Element Analysis. The convergence of finite element solutions in a representative case is shown in Figure 6. The convergence study showed that the finite element displacements converged with the maximum element edge length smaller than 8 mm. Therefore, in construction of the rest of femur FE models, the maximum element edge length was set to 8 mm.

3.1.2. Assignment of Inhomogeneous Material Properties. For convergence study in assigning the inhomogeneous material properties, 3D femur FE models with different material bins were created. For each FE model with different material bins, the maximum displacement at the smallest femoral neck cross-section was monitored under the same loading and boundary conditions. Data on the displacement were compared among the FE models with different material bins. The results of the convergence study showed that the displacement did not change significantly with the number of material bins larger than 50. Therefore, in the assignment of material properties for all the cases, 50 discrete material bins were considered.

3.1.3. Element Size in Calculating Cross-Section Strain Energy. Convergence study was also performed to determine the element size used in integrating cross-section strain energy, as it affects the calculated fracture risk index (FRI). The FRI at the concerned cross-section was calculated with different maximum element edge lengths. The results are plotted in Figure 7. The FRI did not change significantly with the maximum element edge length smaller than 5 mm. Therefore, the maximum element edge length was set to 5 mm in calculating cross-section strain energy.

3.1.4. The Number of Integration Points in Calculating Cross-Section Strain Energy. The effect of the number of integration points on the calculated FRI was investigated. FRI at the smallest femoral neck cross-section was computed for 5 clinical cases with different number of integration points. The relative errors between FRIs obtained with 3 and 7 integration points are shown in Table 2. As it can be seen, the errors are not significant. Therefore, the 3-point integration rule was used in this study to reduce computational time.

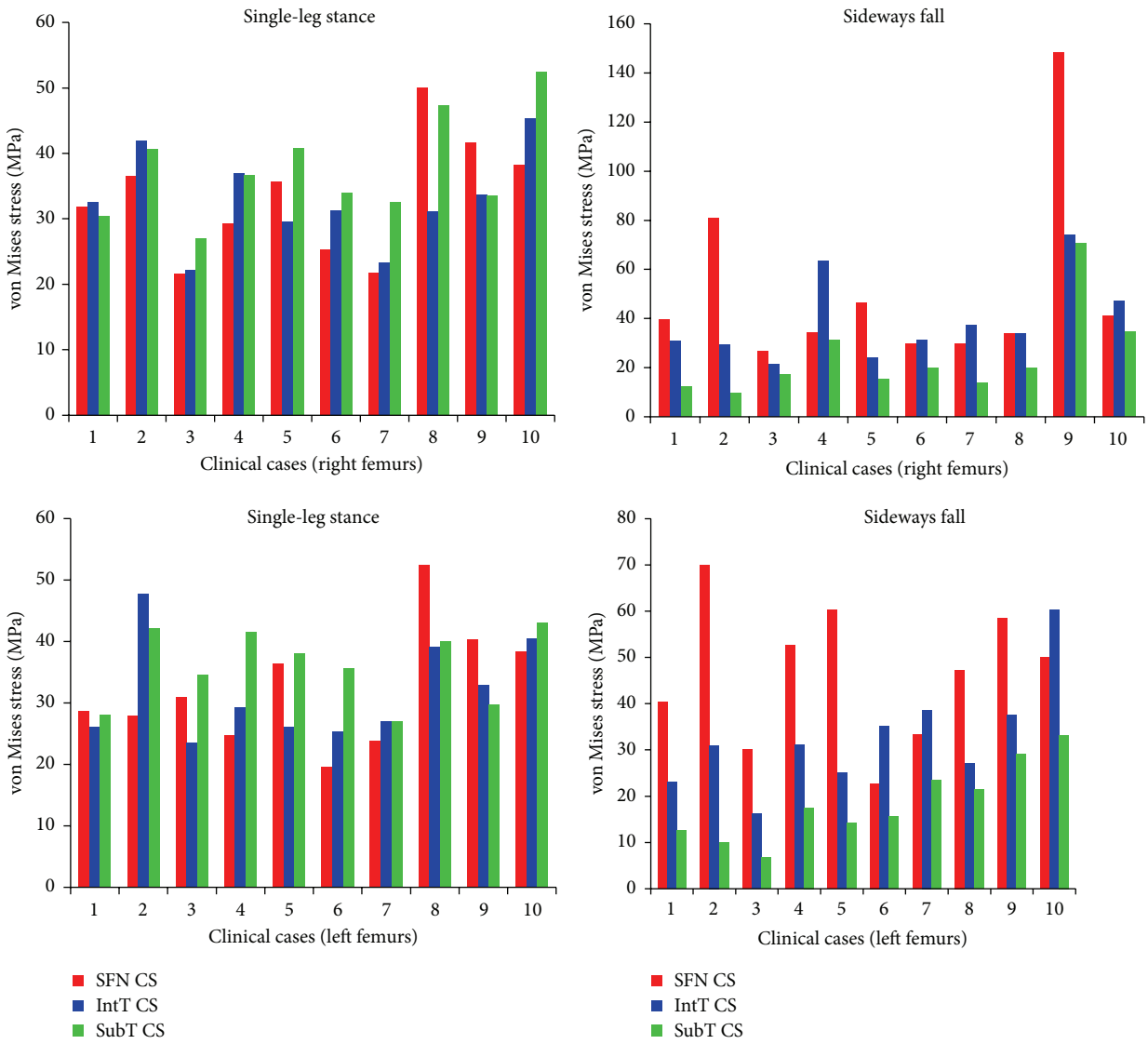

Figure 8: The maximum von Mises stress (Mpa) at the smallest femoral neck cross-section (SFN CS), the intertrochanteric cross-section (IntT CS), and the subtrochanteric cross-section (SubT CS) of right and left femurs of 10 clinical cases during the single-leg stance and the sideways fall.

Table 2: Femoral neck FRI obtained with different number of integration points.

Case number	FRI		Relative error (%)
	3 integration points	7 integration points	
1	0.239	0.2416	1.07
2	0.6898	0.6975	1.1
3	0.2966	0.2976	0.33
4	0.8885	0.899	1.16
5	1.1482	1.1701	1.87

3.2. Stress and Strain Patterns at the Three Critical Cross-Sections. For the 10 clinical cases (5 females and 5 males, totally 20 right and left femurs), the maximum von Mises stress and strain at the three critical cross-sections of femur during both the single-leg stance and the sideways fall are shown in Figures 8 and 9. It can be observed that, during the sideways fall, the femoral neck and the intertrochanteric region received higher stresses than the subtrochanteric region (Table 4). But during the single-leg stance, the patterns in the stresses are different (Table 3); first, the differences between the stresses over the three regions are much smaller; for some cases, the stresses at the subtrochanteric region are higher than those in the other two regions (Figure 8). Strains in the three regions have similar patterns during both the single-leg stance and the sideways fall (Tables 5 and 6).

3.3. Comparison of Hip Fracture Risk at the Three Critical Cross-Sections. For the 60 clinical cases (30 females and 30 males), hip fracture risk indices based on the strain energy

Table 3: Average maximum von Mises stress (MPa) at the smallest femoral neck cross-section (SFN CS), the intertrochanteric cross-section (IntT CS), and the subtrochanteric cross-section (SubT CS) of right and left femurs of 10 clinical cases during the single-leg stance.

	Maximum von Mises stress (MPa)					
	Right femurs			Left femurs		
	SFN CS	IntT CS	SubT CS	SFN CS	IntT CS	SubT CS
Range	21.7–49.96	22.23–45.37	26.93–52.47	19.56–52.38	23.55–47.8	27.09–43.04
Average	33.63	32.97	37.89	32.93	32.41	35.84

Table 4: Average maximum von Mises stress (MPa) at the smallest femoral neck cross-section (SFN CS), the intertrochanteric cross-section (IntT CS), and the subtrochanteric cross-section (SubT CS) of right and left femurs of 10 clinical cases during the sideways fall.

	Maximum von Mises stress (MPa)					
	Right femurs			Left femurs		
	SFN CS	IntT CS	SubT CS	SFN CS	IntT CS	SubT CS
Range	26.69–148.53	21.57–74.3	9.8–70.63	22.78–69.97	16.2–60.3	6.73–33.2
Average	57.22	40.74	27.08	46.52	33.48	18.66

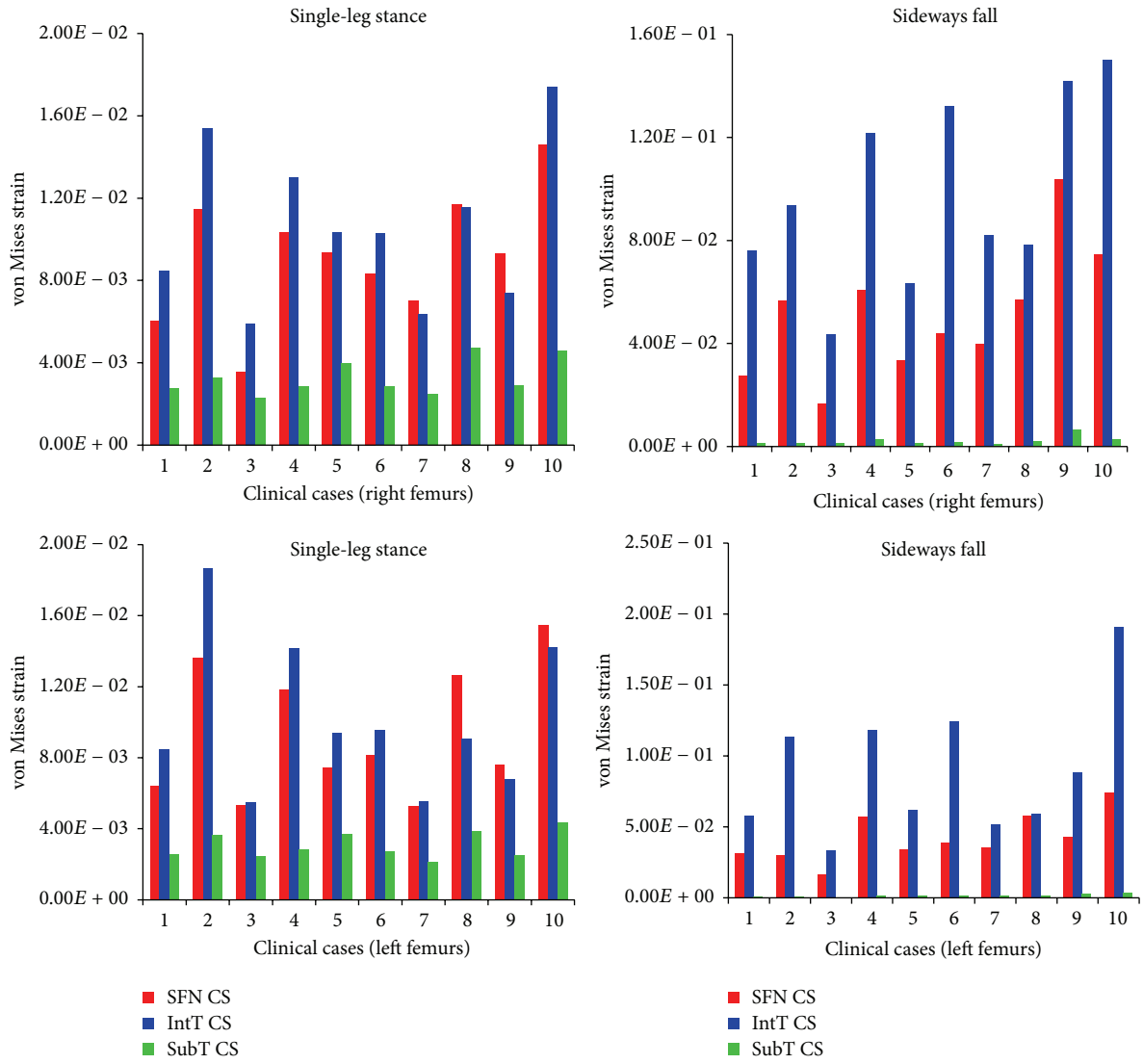

Figure 9: The maximum von Mises strain at the smallest femoral neck cross-section (SFN CS), the intertrochanteric cross-section (IntT CS), and the subtrochanteric cross-section (SubT CS) of right and left femurs of 10 clinical cases during the single-leg stance and the sideways fall.

Table 5: Average maximum von Mises strain at the smallest femoral neck cross-section (SFN CS), the intertrochanteric cross-section (IntT CS), and the subtrochanteric cross-section (SubT CS) of right and left femurs of 10 clinical cases during the single-leg stance.

		Range	Average
Maximum von Mises strain	Right femurs		
	SFN CS	$3.54E-03$–$1.46E-02$	$9.15E-03$
	IntT CS	$5.89E-03$–$1.74E-02$	$1.08E-02$
	SubT CS	$2.3E-03$–$4.75E-03$	$3.32E-03$
	Left femurs		
	SFN CS	$5.25E-03$–$1.55E-02$	$9.55E-03$
	IntT CS	$5.49E-03$–$1.87E-02$	$1.05E-02$
	SubT CS	$2.14E-03$–$4.34E-03$	$3.11E-03$

Table 6: Average maximum von Mises strain at the smallest femoral neck cross-section (SFN CS), the intertrochanteric cross-section (IntT CS), and the subtrochanteric cross-section (SubT CS) of right and left femurs of 10 clinical cases during the sideways fall.

		Range	Average
Maximum von Mises strain	Right femurs		
	SFN CS	$1.67E-02$–$1.04E-01$	$5.29E-02$
	IntT CS	$4.34E-02$–$1.50E-01$	$9.80E-02$
	SubT CS	$12E-03$–$6.38E-03$	$2.44E-03$
	Left femurs		
	SFN CS	$1.67E-02$–$7.43E-02$	$4.26E-02$
	IntT CS	$3.35E-02$–$1.91E-01$	$9.37E-02$
	SubT CS	$5.08E-04$–$3.31E-03$	$1.74E-03$

criterion were calculated for the smallest femoral neck, the intertrochanteric, and the subtrochanteric cross-section of femur during the single-leg stance and the sideways fall. The calculated fracture risk indices are shown in Figures 10 and 11.

As shown in Tables 7, 8, 9, and 10 and Figures 12 and 13, the average FRI at the smallest femoral neck was higher than those at the intertrochanteric and the subtrochanteric cross-section during both the single-leg stance and sideways fall.

For the single-leg stance, FRIs for all cases at the three critical cross-sections are much lower than one (FRI $\ll 1$), indicating that the possibility of hip fracture incidence in the single-leg stance was low. For the sideways fall, FRIs of 8 right femurs and 7 left femurs at the smallest femoral neck cross-section and FRIs of 7 right femurs and 5 left femurs at the intertrochanteric cross-section were higher than one (FRI $>$ 1), meaning that there is possibility for fracture occurring in these regions; but the FRIs at the subtrochanteric cross-section in all cases were much lower than one (FRI $\ll 1$), indicating that there is lower possibility of fracture in this region. Figure 14 shows the number of possible fractures at the three critical cross-sections of femur during the sideways fall, that is, the cases that have FRI larger than one (FRI > 1) at one of the three critical cross-sections.

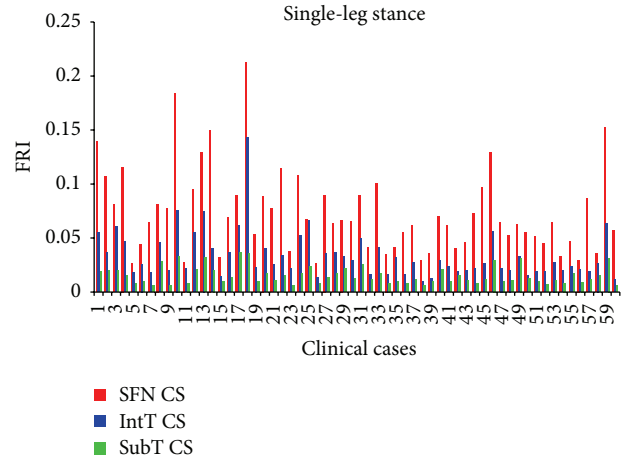

Figure 10: Fracture risk index in single-leg stance configuration.

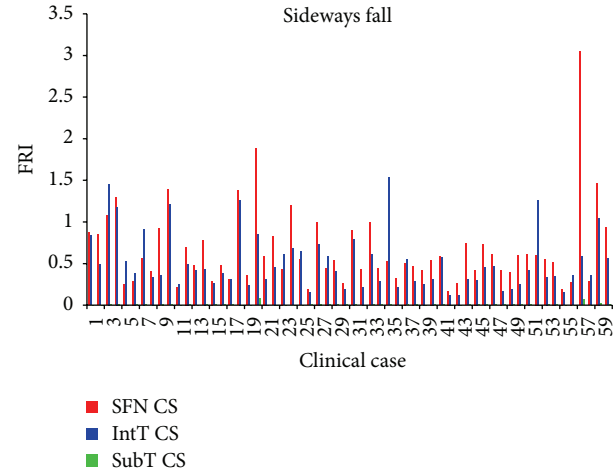

Figure 11: Fracture risk index in sideways fall configuration.

3.4. Comparison of Hip Fracture Risk in Women and Men. In this study, hip fracture risk for the 30 females and 30 males was assessed. The average hip fracture risk of females was generally higher than that of males. As it can be seen from Tables 11–13 and Figures 15 and 16, the average FRI at the smallest femoral neck cross-section, the intertrochanteric cross-section, and the subtrochanteric cross-section of the 30 females is higher than that of the 30 males for both the single-leg stance and the sideways fall. Figure 17 shows the number of possible hip fractures in women and men during the sideways fall for the studied cases.

4. Discussion

Hip fracture may occur anywhere from the articular cartilage of the hip joint to the femur shaft [48]. Not only the location of the fracture types but also the etiology differs. It was reported that women with the intertrochanteric fracture have significantly lower BMD than those with the femoral neck fracture [49–51]. On the other hand, the femoral neck fracture

Table 7: Average FRI at the three critical cross-sections of 60 right femurs during the single-leg stance.

	FRI		
	Smallest femoral neck cross-section	Intertrochanteric cross-section	Subtrochanteric cross-section
Range	0.0261–0.2124	0.0099–0.143	0.0058–0.0363
Average	0.0752	0.0351	0.0155

Table 8: Average FRI at the three critical cross-sections of 60 left femurs during the single-leg stance.

	FRI		
	Smallest femoral neck cross-section	Intertrochanteric cross-section	Subtrochanteric cross-section
Range	0.023–0.1936	0.0095–0.1078	0.0037–0.0337
Average	0.0681	0.0329	0.0142

Table 9: Average FRI at the three critical cross-sections of 60 right femurs during the sideways fall.

	FRI		
	Smallest femoral neck cross-section	Intertrochanteric cross-section	Subtrochanteric cross-section
Range	0.1725–3.0448	0.1226–1.534	0.0004–0.0812
Average	0.6944	0.5245	0.0091

Table 10: Average FRI at the three critical cross-sections of 60 left femurs during the sideways fall.

	FRI		
	Smallest femoral neck cross-section	Intertrochanteric cross-section	Subtrochanteric cross-section
Range	0.1599–1.8301	0.116–1.5493	0.0004–0.0585
Average	0.6395	0.4864	0.0083

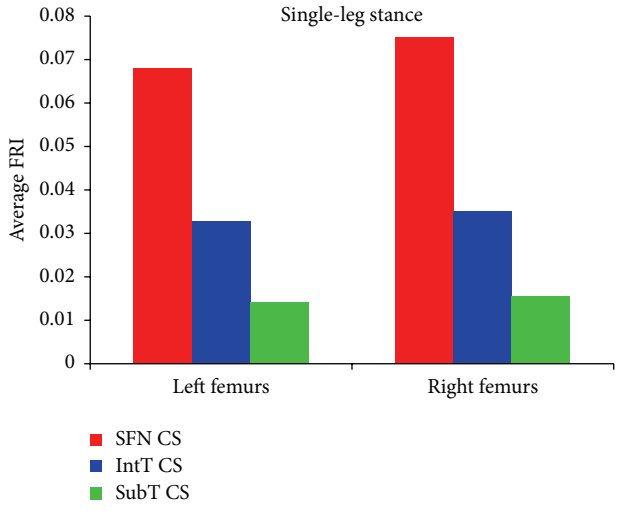

Figure 12: Average FRI at the smallest femoral neck cross-section (SFN CS), the intertrochanteric cross-section (IntT CS), and the subtrochanteric cross-section (SubT CS) of 60 right femurs and 60 left femurs during the single-leg stance.

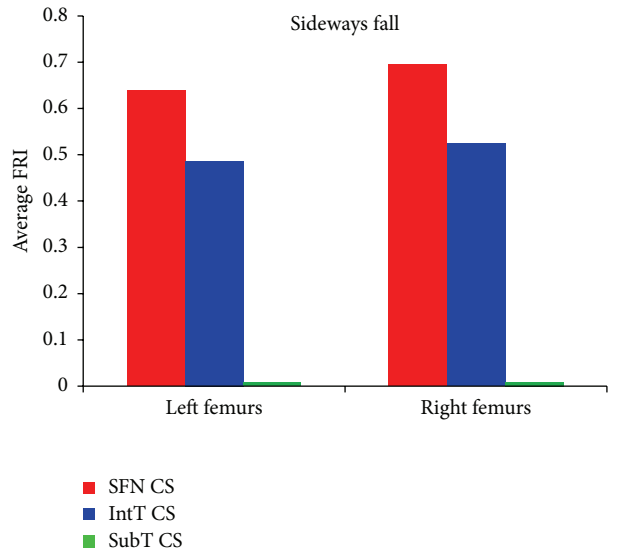

Figure 13: Average FRI at the smallest femoral neck cross-section (SFN CS), the intertrochanteric cross-section (IntT CS), and the subtrochanteric cross-section (SubT CS) of 60 right femurs and 60 left femurs during the sideways fall.

may not be mainly attributed to low BMD but may be related to external causes such as sideways fall [52]. Femoral neck and intertrochanteric fractures are often the result of falls from standing height and impact onto the greater trochanter, particularly for the elderly. The subtrochanteric fractures, on the other hand, are typically the result of high energy impacts such as motor vehicle accidents and falls from a height [53].

The selection of bone failure criterion is challenging. In literatures, stress and strain based failure criteria such as

Table 11: Average FRI at the smallest femoral neck cross-section of 30 females and 30 males during the single-leg stance and the sideways fall.

	FRI at the smallest femoral neck cross-section			
	Single-leg stance		Sideways fall	
	Female	Male	Female	Male
Range	0.023–0.2124	0.0231–0.1628	0.1826–1.8809	0.1599–3.0448
Average	0.0816	0.0611	0.7035	0.6315

Table 12: Average FRI at the intertrochanteric cross-section of 30 females and 30 males during the single-leg stance and the sideways fall.

	FRI at the intertrochanteric cross-section			
	Single-leg stance		Sideways fall	
	Female	Male	Female	Male
Range	0.0138–0.143	0.0095–0.0637	0.1398–1.4572	0.116–1.5493
Average	0.042	0.0253	0.5666	0.4433

Table 13: Average FRI at the subtrochanteric cross-section of 30 females and 30 males during the single-leg stance and the sideways fall.

	FRI at the subtrochanteric cross-section			
	Single-leg stance		Sideways fall	
	Female	Male	Female	Male
Range	0.0037–0.0363	0.0053–0.0315	0.0004–0.0812	0.0004–0.0694
Average	0.0167	0.0129	0.0087	0.0088

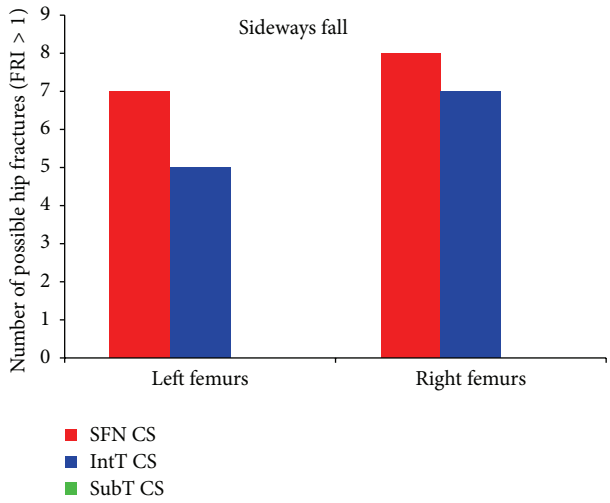

Figure 14: Number of possible hip fractures occurring at the smallest femoral neck cross-section (SFN CS), the intertrochanteric cross-section (IntT CS), and the subtrochanteric cross-section (SubT CS) of 60 right femurs and 60 left femurs during the sideways fall, that is, cases that have the FRI higher than one (FRI > 1) at one of the three critical cross-sections.

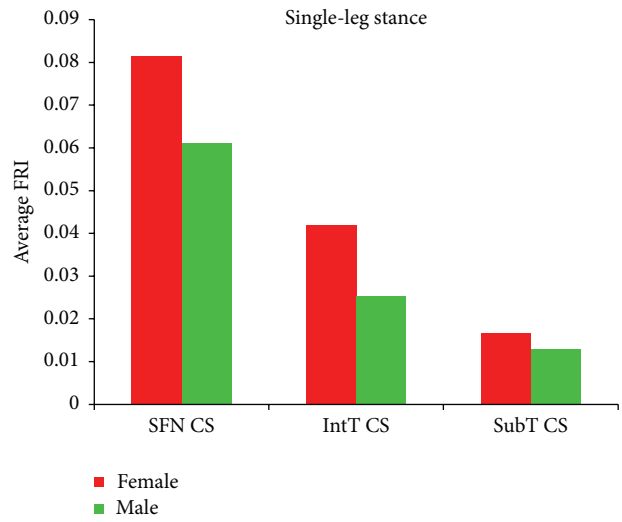

Figure 15: Average FRI at the smallest femoral neck cross-section (SFN CS), the intertrochanteric cross-section (IntT CS), and the subtrochanteric cross-section (SubT CS) of 30 females and 30 males during the single-leg stance.

the von Mises stress and strain criteria and the maximum principle stress and strain criteria were commonly used to assess hip fracture risk. To the best of our knowledge, the strain energy based failure criterion has not been used yet for hip fracture risk assessment. Whereas the cancellous bone failure is in the form of buckling and deformation (strain intensity) and the cortical bone failure is related to its local cracking (stress intensity), strain energy failure criterion, which is a combination of both stress and strain intensities, is theoretically more reasonable than other failure criteria for hip fracture risk assessment. The differences between the strains in the three critical regions of femur during both the single-leg stance and the sideways fall (Figure 9, Tables 5 and 6) are much higher than the differences between

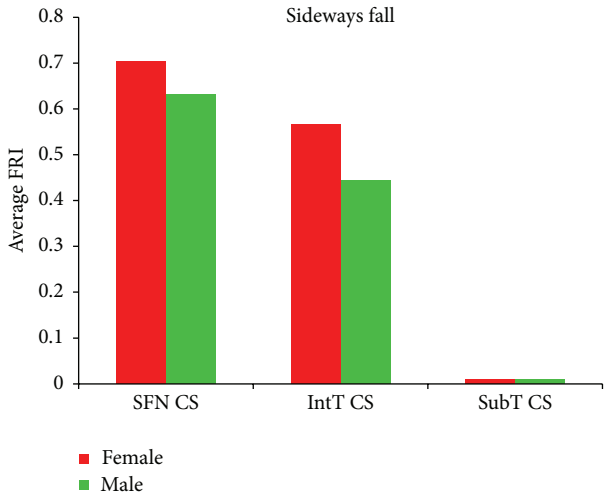

Figure 16: Average FRI at the smallest femoral neck cross-section (SFN CS), the intertrochanteric cross-section (IntT CS), and the subtrochanteric cross-section (SubT CS) of 30 females and 30 males during the sideways fall.

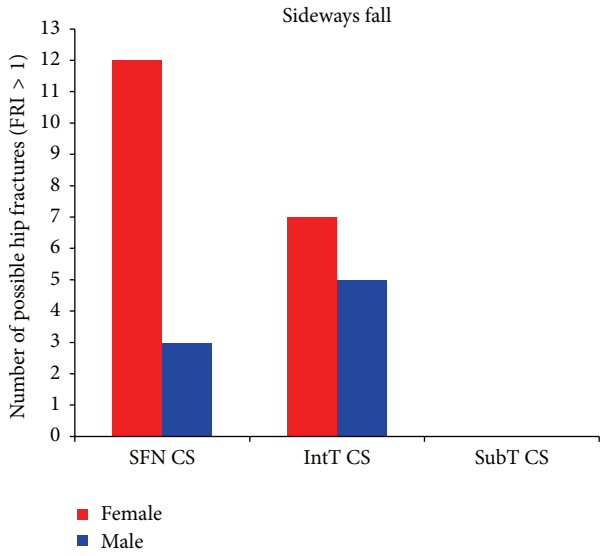

Figure 17: Number of possible hip fractures occurring at the smallest femoral neck cross-section (SFN CS), the intertrochanteric cross-section (IntT CS), and the subtrochanteric cross-section (SubT CS) of 30 females and 30 males during the sideways fall.

the corresponding stresses (Figure 8, Tables 3 and 4), indicating that bone failure is more sensitive to the strains because of its fragility property and the effects of strains should also be considered in bone fracture risk assessment.

Results of this study show that the femoral neck and the intertrochanteric region have higher fracture risk than the subtrochanteric region (Figures 12 and 13 and Tables 7–10), which is consistent with the fact that the femoral neck and the intertrochanteric region have a larger proportion of cancellous bone than the subtrochanteric region; and the cancellous bone is generally weaker than the cortical bone. Therefore, hip fracture is most likely to initiate first at the femoral neck and then in the intertrochanteric region or in the subtrochanteric region. For all subjects, there is very low hip fracture risk during the single-leg stance (FRI < 1). Among all the cases, during the sideways fall, 15 femurs at the femoral neck and 12 femurs at the intertrochanteric region have FRI higher than one (FRI > 1), while there is very low fracture risk at the subtrochanteric region for all the subjects (FRI < 1) (Figure 14). Our findings have a good agreement with the previous clinical observations. According to the clinical observations, the femoral neck is the most common location for a hip fracture, accounting for 45% to 53% of hip fractures; the intertrochanteric fractures account for approximately 38% to 50% of all hip fractures; and the subtrochanteric fractures are less common than the femoral neck and intertrochanteric fractures, accounting for approximately 5% to 15% of hip fractures [54, 55]. Also it was observed that, in old people with age between 65 and 99, femoral neck and intertrochanteric fractures occurred with approximately the same frequency [56]. Data on 176 geriatric patients with hip fractures showed that 59% were the intertrochanteric fractures while the rest (41%) were the intracapsular neck fractures [57]. In another study by Michelson et al. [43], it was observed that 37% of hip fractures are in the femoral neck, 49% are intertrochanteric, and 14% are subtrochanteric. Therefore, the femoral neck and the intertrochanteric region are more disposed to fracture than the subtrochanteric region.

Both the fracture risk level and the potential fracture location are patient-dependent and depend on BMD and other conditions that have not been studied in this paper. We have found that women generally have lower bone strength than men and thus are exposed to higher hip fracture risk during both the single-leg stance and the sideways fall (Figures 15 and 16 and Tables 11–13). Based on the calculated FRI, in the 30 women potentially there are 12 femoral neck fractures and 7 intertrochanteric fractures, while for the 30 men there are only 3 potential femoral neck and 5 potential intertrochanteric fractures (Figure 17). Our finding is consistent with other studies that have found that hip fracture risk in women is generally higher than in men. The results of a worldwide study by Dhanwal et al. [58] on incidence and epidemiology of hip fractures in Asia, Africa, Europe, Latin America, North America, and Oceania show that women are more disposed to the hip fracture risk than men in different countries over the world. In the study by Jacobsen et al. [59], the age-adjusted hip fracture incidence rates in white US males and females were 4.3 and 8.1 per 1,000 per year, respectively. Higher hip fracture risk in women may be related to their lower BMD.

5. Conclusion

A reliable methodology to assess hip fracture risk in individuals is crucially important for preventing hip fracture and initiating a treatment. The purpose of this study is to propose a more effective hip fracture risk index that is based on the

strain energy failure criterion, and it is able to better describe bone failure mechanism and microstructure. The proposed fracture risk index can predict not only the fracture risk level, but also the potential fracture location. The results of this study showed that there is a very low hip fracture risk during the single-leg stance, while, during the sideways fall, there is a high fracture risk at the femoral neck and the intertrochanteric region, compared to the subtrochanteric region. Based on the results obtained from this study, women are more prone to hip fracture than men. The procedure described in this study can be implemented into computer programming and used in hip fracture prevention and monitoring of osteoporosis treatments in the elderly. The method may also help design more effective hip protectors by providing feedback information such as stresses/strains in the hip for adjusting the design parameters. The main limitation of this study is that no experiment has been conducted to validate the predicted fracture risk levels and potential fracture locations, which has been set as future work.

Conflict of Interests

The authors declare that there is no conflict of interests regarding the publication of this paper.

References

[1] N. M. Resnick and S. L. Greenspan, "'Senile' osteoporosis reconsidered," *Journal of the American Medical Association*, vol. 261, no. 7, pp. 1025–1029, 1989.

[2] B. Gullberg, O. Johnell, and J. A. Kanis, "World-wide projections for hip fracture," *Osteoporosis International*, vol. 7, no. 5, pp. 407–413, 1997.

[3] O. Johnell, "The socioeconomic burden of fractures: today and in the 21st century," *The American Journal of Medicine*, vol. 103, no. 2, pp. 20S–26S, 1997.

[4] J. S. Bauer and T. M. Link, "Advances in osteoporosis imaging," *European Journal of Radiology*, vol. 71, no. 3, pp. 440–449, 2009.

[5] D. M. Albertsson, D. Mellström, C. Petersson, and R. Eggertsen, "Validation of a 4-item score predicting hip fracture and mortality risk among elderly women," *Annals of Family Medicine*, vol. 5, no. 1, pp. 48–56, 2007.

[6] D. Marshall, O. Johnell, and H. Wedel, "Meta-analysis of how well measures of bone mineral density predict occurrence of osteoporotic fractures," *British Medical Journal*, vol. 312, no. 7041, pp. 1254–1259, 1996.

[7] J. A. Kanis, H. Johansson, A. Oden, and E. V. McCloskey, "Assessment of fracture risk," *European Journal of Radiology*, vol. 71, no. 3, pp. 392–397, 2009.

[8] S. Kaptoge, L. I. Benevolenskaya, A. K. Bhalla et al., "Low BMD is less predictive than reported falls for future limb fractures in women across Europe: results from the European Prospective Osteoporosis Study," *Bone*, vol. 36, no. 3, pp. 387–398, 2005.

[9] T. L. N. Järvinen, H. Sievänen, K. M. Khan, A. Heinonen, and P. Kannus, "Shifting the focus in fracture prevention from osteoporosis to falls," *British Medical Journal*, vol. 336, no. 7636, pp. 124–126, 2008.

[10] M. R. McClung, "To FRAX or not to FRAX," *Journal of Bone and Mineral Research*, vol. 27, no. 6, pp. 1240–1242, 2012.

[11] Y. Luo, Z. Ferdous, and W. D. Leslie, "A preliminary dual-energy X-ray absorptiometry-based finite element model for assessing osteoporotic hip fracture risk," *Proceedings of the Institution of Mechanical Engineers Part H: Journal of Engineering in Medicine*, vol. 225, no. 12, pp. 1188–1195, 2011.

[12] Y. Luo, Z. Ferdous, and W. D. Leslie, "Precision study of DXA-based patient-specific finite element modeling for assessing hip fracture risk," *International Journal for Numerical Methods in Biomedical Engineering*, vol. 29, no. 5, pp. 615–629, 2013.

[13] J. H. Keyak, S. A. Rossi, K. A. Jones, and H. B. Skinner, "Prediction of femoral fracture load using automated finite element modeling," *Journal of Biomechanics*, vol. 31, no. 2, pp. 125–133, 1997.

[14] J. C. Lotz, E. J. Cheal, and W. C. Hayes, "Fracture prediction for the proximal femur using finite element models: part I—linear analysis," *Journal of Biomechanical Engineering*, vol. 113, no. 4, pp. 353–360, 1991.

[15] J. C. Lotz, E. J. Cheal, and W. C. Hayes, "Fracture prediction for the proximal femur using finite element models: part II—nonlinear analysis," *Journal of Biomechanical Engineering*, vol. 113, no. 4, pp. 361–365, 1991.

[16] D. Testi, M. Viceconti, F. Baruffaldi, and A. Cappello, "Risk of fracture in elderly patients: a new predictive index based on bone mineral density and finite element analysis," *Computer Methods and Programs in Biomedicine*, vol. 60, no. 1, pp. 23–33, 1999.

[17] T. Ota, I. Yamamoto, and R. Morita, "Fracture simulation of the femoral bone using the finite-element method: how a fracture initiates and proceeds," *Journal of Bone and Mineral Metabolism*, vol. 17, no. 2, pp. 108–112, 1999.

[18] E. Schileo, F. Taddei, L. Cristofolini, and M. Viceconti, "Subject-specific finite element models implementing a maximum principal strain criterion are able to estimate failure risk and fracture location on human femurs tested in vitro," *Journal of Biomechanics*, vol. 41, no. 2, pp. 356–367, 2008.

[19] H. Gong, M. Zhang, Y. Fan, W. L. Kwok, and P. C. Leung, "Relationships between femoral strength evaluated by nonlinear finite element analysis and BMD, material distribution and geometric morphology," *Annals of Biomedical Engineering*, vol. 40, no. 7, pp. 1575–1585, 2012.

[20] J. H. Keyak and S. A. Rossi, "Prediction of femoral fracture load using finite element models: an examination of stress- and strain-based failure theories," *Journal of Biomechanics*, vol. 33, no. 2, pp. 209–214, 2000.

[21] M. Mirzaei, M. Keshavarzian, and V. Naeini, "Analysis of strength and failure pattern of human proximal femur using quantitative computed tomography (QCT)-based finite element method," *Bone*, vol. 64, pp. 108–114, 2014.

[22] J. S. Stölken and J. H. Kinney, "On the importance of geometric nonlinearity in finite-element simulations of trabecular bone failure," *Bone*, vol. 33, no. 4, pp. 494–504, 2003.

[23] J. Cordey and E. Gautier, "Strain gauges used in the mechanical testing of bones. Part I: theoretical and technical aspects," *Injury*, vol. 30, no. 1, pp. SA7–SA13, 1999.

[24] M. Mirzaei, A. Zeinali, A. Razmjoo, and M. Nazemi, "On prediction of the strength levels and failure patterns of human vertebrae using quantitative computed tomography (QCT)-based finite element method," *Journal of Biomechanics*, vol. 42, no. 11, pp. 1584–1591, 2009.

[25] G. C. Sih, "Strain-energy-density factor applied to mixed mode crack problems," *International Journal of Fracture*, vol. 10, no. 3, pp. 305–321, 1974.

[26] G. C. Sih, *Mechanics of Fracture Initiation and Propagation*, Springer, Dordrecht, The Netherlands, 1991.

[27] Y. Wei, "An extended strain energy density failure criterion by differentiating volumetric and distortional deformation," *International Journal of Solids and Structures*, vol. 49, no. 9, pp. 1117–1126, 2012.

[28] W. E. Wolfe and T. S. Butalia, "A strain-energy based failure criterion for non-linear analysis of composite laminates subjected to biaxial loading," *Composites Science and Technology*, vol. 58, no. 7, pp. 1107–1124, 1998.

[29] T. S. Butalia and W. E. Wolfe, "A strain-energy-based non-linear failure criterion: comparison of numerical predictions and experimental observations for symmetric composite laminates," *Composites Science and Technology*, vol. 62, no. 12-13, pp. 1697–1710, 2002.

[30] R. Vasu, D. R. Carter, and W. H. Harris, "Evaluation of bone cement failure criteria with applications to the acetabular region," *Journal of Biomechanical Engineering*, vol. 105, no. 4, pp. 332–337, 1983.

[31] J. H. Keyak, J. M. Meagher, H. B. Skinner, and C. D. Mote Jr., "Automated three-dimensional finite element modelling of bone: a new method," *Journal of Biomedical Engineering*, vol. 12, no. 5, pp. 389–397, 1990.

[32] T. M. Keaveny, R. E. Borchers, L. J. Gibson, and W. C. Hayes, "Trabecular bone modulus and strength can depend on specimen geometry," *Journal of Biomechanics*, vol. 26, no. 8, pp. 991–1000, 1993.

[33] C. M. Les, J. H. Keyak, S. M. Stover, K. T. Taylor, and A. J. Kaneps, "Estimation of material properties in the equine metacarpus with use of quantitative computed tomography," *Journal of Orthopaedic Research*, vol. 12, no. 6, pp. 822–833, 1994.

[34] D. Dragomir-Daescu, J. O. D. Buijs, S. McEligot et al., "Robust QCT/FEA models of proximal femur stiffness and fracture load during a sideways fall on the hip," *Annals of Biomedical Engineering*, vol. 39, no. 2, pp. 742–755, 2011.

[35] T. S. Keller, "Predicting the compressive mechanical behavior of bone," *Journal of Biomechanics*, vol. 27, no. 9, pp. 1159–1168, 1994.

[36] D. T. Reilly and A. H. Burstein, "The elastic and ultimate properties of compact bone tissue," *Journal of Biomechanics*, vol. 8, no. 6, pp. 393–405, 1975.

[37] W. C. van Buskirk and R. B. Ashman, "The elastic moduli of bone," *Transaction of American Society of Mechanical Engineers*, vol. 45, pp. 131–143, 1981.

[38] T. Yoshikawa, C. H. Turner, M. Peacock et al., "Geometric structure of the femoral neck measured using dual-energy x-ray absorptiometry," *Journal of Bone and Mineral Research*, vol. 9, no. 7, pp. 1053–1064, 1994.

[39] M. Bessho, I. Ohnishi, T. Matsumoto et al., "Prediction of proximal femur strength using a CT-based nonlinear finite element method: differences in predicted fracture load and site with changing load and boundary conditions," *Bone*, vol. 45, no. 2, pp. 226–231, 2009.

[40] J. E. M. Koivumäki, J. Thevenot, P. Pulkkinen et al., "Ct-based finite element models can be used to estimate experimentally measured failure loads in the proximal femur," *Bone*, vol. 50, no. 4, pp. 824–829, 2012.

[41] K. K. Nishiyama, S. Gilchrist, P. Guy, P. Cripton, and S. K. Boyd, "Proximal femur bone strength estimated by a computationally fast finite element analysis in a sideways fall configuration," *Journal of Biomechanics*, vol. 46, no. 7, pp. 1231–1236, 2013.

[42] S. N. Robinovitch, W. C. Hayes, and T. A. McMahon, "Prediction of femoral impact forces in falls on the hip," *Journal of Biomechanical Engineering*, vol. 113, no. 4, pp. 366–374, 1991.

[43] J. D. Michelson, A. Myers, R. Jinnah, Q. Cox, and M. Van Natta, "Epidemiology of hip fractures among the elderly: risk factors for fracture type," *Clinical Orthopaedics and Related Research*, no. 311, pp. 129–135, 1995.

[44] J. S. Kim, T. S. Park, S. B. Park, J. S. Kim, I. Y. Kim, and S. I. Kim, "Measurement of femoral neck anteversion in 3D. Part 1: 3D imaging method," *Medical and Biological Engineering and Computing*, vol. 38, no. 6, pp. 603–609, 2000.

[45] B. Atilla, A. Oznur, O. Cağlar, M. Tokgözoğlu, and M. Alpaslan, "Osteometry of the femora in Turkish individuals: a morphometric study in 114 cadaveric femora as an anatomic basis of femoral component design," *Acta orthopaedica et Traumatologica Turcica*, vol. 41, no. 1, pp. 64–68, 2007.

[46] E. Sariali, A. Mouttet, G. Pasquier, and E. Durante, "Three-dimensional hip anatomy in osteoarthritis: analysis of the femoral offset," *Journal of Arthroplasty*, vol. 24, no. 6, pp. 990–997, 2009.

[47] R. Nikander, P. Kannus, P. Dastidar et al., "Targeted exercises against hip fragility," *Osteoporosis International*, vol. 20, no. 8, pp. 1321–1328, 2009.

[48] B. Abrahamsen, T. van Staa, R. Ariely, M. Olson, and C. Cooper, "Excess mortality following hip fracture: a systematic epidemiological review," *Osteoporosis International*, vol. 20, no. 10, pp. 1633–1650, 2009.

[49] E. Vega, C. Mautalen, H. Gómez, A. Garrido, L. Melo, and A. O. Sahores, "Bone mineral density in patients with cervical and trochanteric fractures of the proximal femur," *Osteoporosis International*, vol. 1, no. 2, pp. 81–86, 1991.

[50] N. Nakamura, T. Kyou, K. Takaoka, K. Ohzono, and K. Ono, "Bone mineral density in the proximal femur and hip fracture type in the elderly," *Journal of Bone and Mineral Research*, vol. 7, no. 7, pp. 755–759, 1992.

[51] S. L. Greenspan, E. R. Myers, L. A. Maitland, T. H. Kido, M. B. Krasnow, and W. C. Hayes, "Trochanteric bone mineral density is associated with type of hip fracture in the elderly," *Journal of Bone and Mineral Research*, vol. 9, no. 12, pp. 1889–1894, 1994.

[52] C. A. Mautalen, E. M. Vega, and T. A. Einhorn, "Are the etiologies of cervical and trochanteric hip fractures different?" *Bone*, vol. 18, no. 3, supplement, pp. 133S–137S, 1996.

[53] R. B. Birrer, *Field Guide to Fracture Management*, Lippincott Williams & Wilkins, 2005.

[54] K. J. Koval and J. D. Zuckerman, "Hip fractures: I. Overview and evaluation and treatment of femoral-neck fractures," *Journal of the American Academy of Orthopaedic Surgeons*, vol. 2, no. 3, pp. 141–149, 1994.

[55] Fixing Hip Fractures, March 2015, http://www.hopkinsmedicine.org/gec/series/fixing_hip_fractures.

[56] M. R. Karagas, G. L. Lu-Yao, J. A. Barrett, M. L. Beach, and J. A. Baron, "Heterogeneity of hip fracture: age, race, sex, and geographic patterns of femoral neck and trochanteric fractures among the US elderly," *American Journal of Epidemiology*, vol. 143, no. 7, pp. 677–682, 1996.

[57] V. Trikha and S. Rastogi, "Epidemiology and rehabilitation of hip fractures in the geriatric population," *Indian Journal of Physical Medicine and Rehabilitation*, vol. 16, no. 1, pp. 16–19, 2005.

[58] D. K. Dhanwal, E. M. Dennison, N. C. Harvey, and C. Cooper, "Epidemiology of hip fracture: worldwide geographic variation," *Indian Journal of Orthopaedics*, vol. 45, no. 1, pp. 15–22, 2011.

[59] S. J. Jacobsen, J. Goldberg, T. P. Miles, J. A. Brody, W. Stiers, and A. A. Rimm, "Hip fracture incidence among the old and very old: a population-based study of 745,435 cases," *The American Journal of Public Health*, vol. 80, no. 7, pp. 871–873, 1990.

Hindawi Publishing Corporation
BioMed Research International
Volume 2015, Article ID 485975, 9 pages
http://dx.doi.org/10.1155/2015/485975

Review Article

Titanium-Nitride Coating of Orthopaedic Implants: A Review of the Literature

Ruud P. van Hove,[1] Inger N. Sierevelt,[2] Barend J. van Royen,[3] and Peter A. Nolte[2,4]

[1]*Department of Orthopaedics, Catharina Hospital, 5623 EJ Eindhoven, Netherlands*
[2]*Research Centre Linnaeus Institute, Spaarne Hospital, 2134 TM Hoofddorp, Netherlands*
[3]*Department of Orthopaedics, VU University Medical Centre, 1081 HZ Amsterdam, Netherlands*
[4]*Department of Orthopaedics, Spaarne Hospital, 2134 TM Hoofddorp, Netherlands*

Correspondence should be addressed to Ruud P. van Hove; ruud.v.hove@catharinaziekenhuis.nl

Received 20 April 2015; Accepted 24 May 2015

Academic Editor: Hiroshi Ito

Copyright © 2015 Ruud P. van Hove et al. This is an open access article distributed under the Creative Commons Attribution License, which permits unrestricted use, distribution, and reproduction in any medium, provided the original work is properly cited.

Surfaces of medical implants can be enhanced with the favorable properties of titanium-nitride (TiN). In a review of English medical literature, the effects of TiN-coating on orthopaedic implant material in preclinical studies were identified and the influence of these effects on the clinical outcome of TiN-coated orthopaedic implants was explored. The TiN-coating has a positive effect on the biocompatibility and tribological properties of implant surfaces; however, there are several reports of third body wear due to delamination, increased ultrahigh molecular weight polyethylene wear, and cohesive failure of the TiN-coating. This might be due to the coating process. The TiN-coating process should be optimized and standardized for titanium alloy articulating surfaces. The clinical benefit of TiN-coating of CoCrMo knee implant surfaces should be further investigated.

1. Introduction

Titanium-nitride (TiN) is a ceramic which has general properties such as great hardness (2000 kg/mm^2), high decomposition temperature (2949°C), defect structure, that is, deviation from stoichiometry, chemical stability at room-temperature, superconductivity, and a gold-yellow color [1]. TiN can be prepared by direct reaction of titanium or titanium hydrogen powder with nitrogen at 1200°C [1]. Using nitrogen ion implantation, physical vapor deposition, and plasma ion nitriding, titanium surfaces can be enhanced with a TiN layer [2]. Single crystals of TiN can also be vapor deposited on other metals [1]. Recently newer techniques have been introduced for TiN-coating of titanium alloys, such as powder immersion reaction assisted coating (PIRAC) [3], nitrogen plasma immersion ion implantation (PIII) [4], and Hardion+ nitrogen implantation technique [5], to improve the adhesion of the TiN-coating to the implant material.

TiN is mainly used as a coating to enhance other materials with the properties of TiN. TiN showed encouraging blood tolerability properties with a hemolysis percentage near to zero [6]. Therefore, TiN-coatings are used in cardiology for ventricular assist devices for patients with heart failure [7] and for pacemaker leads [8]. In neurology, TiN-coated electrodes are investigated for the development of chronically implanted devices for the treatment of, for example, spinal cord injury [9]. TiN-coating is applied in dentistry to dental implants, because of the excellent biological properties of TiN, such as the reduction of the release of cobalt-chromium-molybdenum (CoCrMo) ions, and the aesthetic aspect of the "golden color" [10, 11].

In 1972, Steinemenan patented the "use of implants of titanium or a titanium alloy for the surgical treatment of bones" [12]. This included a surface layer, for example, nitride, to prevent abrasion and corrosion of the implant and to prevent fretting of contacting implants [12]. In 1997, Buechel and Pappas patented the "prosthesis with biologically inert wear resistant surface" [13]. The load bearing surfaces are coated with biologically inert abrasion resistant material, such as TiN, preferably 8–10 microns thick, harder than the substrate for preventing wear and leaching of ions [13]. Besides the suggested beneficial effect of TiN-coating of

the bearing surfaces in cemented and uncemented prosthesis, the TiN-coating might also be beneficial at the bone-implant surface of uncemented prosthesis because it is biologically inert.

Untreated titanium-aluminum-vanadium alloy (Ti6Al4V) showed excessive wear of femoral heads, and surface treatment of Ti6Al4V by TiN-coating was discussed as a possibility to enhance the Ti6Al4V surface [14]. The purpose of this review is to identify the effects of TiN-coating of orthopaedic implant material in preclinical studies and whether these effects influence the clinical outcome of TiN-coated orthopaedic implants.

2. Method

This study focuseson preclinical and clinical studies using TiN-coated orthopaedic implants and implant material. Inclusion criteria were clinical studies on TiN-coated orthopaedic implants and preclinical studies on wear and biocompatibility of TiN-coated implant material. To identify all relevant studies on TiN-coated orthopaedic implants and implant material in English scientific literature, the following databases were searched: Medline (1947 to January 2015), Embase Classic and Embase (1947 to January 2015). No restrictions were made to the type of studies. Papers outside the English language, abstracts from scientific meetings, and unpublished reports were excluded. References of retrieved publications were used to add studies meeting the inclusion criteria that were missed by the electronic search. The Medline search is defined in Appendix. The query was checked for inconsistencies using PubMed Query Editor 0.1. Selection of studies was first performed by screening titles and abstracts. In case of insufficient information in the title or abstract, full text copies were retrieved to make a decision for the article selection. References of retrieved publications were used to add studies meeting the inclusion criteria that were missed by the electronic search.

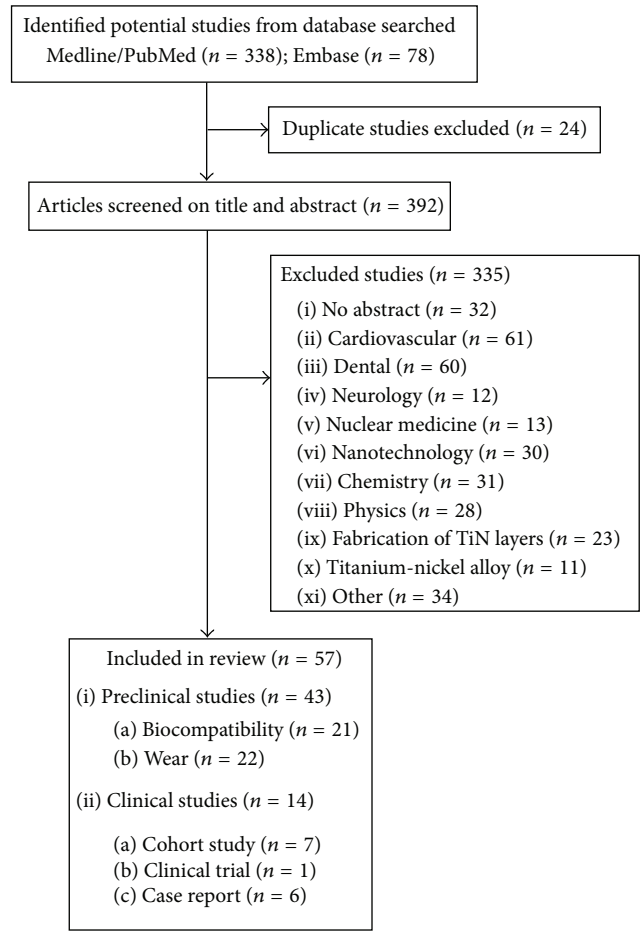

Figure 1: Flow diagram of the search process. Duplicate studies were excluded as well as studies of which there was no abstract. Studies on cardiovascular, dental, and neurological titanium-nitride coated implant material and other studies were excluded. Four studies on dental titanium-nitride coated implant material were included in this study in Section 3.1.

3. Results

The results of the combined Medline and Embase search are shown in Figure 1. After examining titles and abstracts, a total of 335 out of 394 studies were excluded, due to the absence of abstracts ($n = 32$), research in medical fields other than orthopaedic (61 cardiovascular, 60 dental, 12 neurological, and 13 nuclear medicine), or other reasons ($n = 157$). No additional studies were identified from reference lists of the identified articles.

3.1. Preclinical Studies: Biocompatibility. A high variety of cell types were used for cell culture on TiN-coated implant materials: human bone marrow stem cells [15–17], human primary osteoblasts [18], Saos-2 osteoblast-like cells [19], human fibroblasts [20], human fetal osteoblasts [5, 21], U937 macrophages and L929 fibroblasts [22], mouse fibroblasts [23–25], murine monocytes [26], and murine calvarial osteoblasts [4, 27]. Studies on proliferation and differentiation of cells cultured on TiN-coated materials compared with control material are shown in Table 1. In several studies, no difference in proliferation of cells was found on TiN-coated materials compared with their controls [5, 15, 16, 19, 20]; however, an increase in proliferation of cells on TiN-coated materials compared with their controls was observed in other studies [4, 18, 23, 27, 28]. No differences were found on TiN-coated materials compared with their controls in differentiation of cells [15, 16, 18, 19, 27, 28], cell morphology [20, 24, 29], cell adhesion [15, 16, 29, 30], viability [21], and metabolic activity [24]. One study showed a higher number of cells adhered to TiN-coated material compared with the control [17]. Cell viability of cells cultured in the presence of Ti6Al4V, CoCrMo, and TiN-particles decreased after 4 hours to 58%, 44%, and 44%, respectively, but recovered after 24 hours to 78%, 51%, and 65%, respectively [26]. Viability of other cells cultured in the presence of different concentrations of TiN-debris was foremost influenced by the concentration of 50 μm^3 per cell [22].

TiN-coated materials were implanted in the femurs of dogs [31], rats [3], and rabbits [32]. In dog femurs, some

Table 1: Preclinical studies on proliferation and differentiation of cells cultured on TiN-coated materials compared with control material.

Study	Cell type	TiN-coated material	Proliferation	Differentiation
van Raay et al. (1995) [20]	Human fibroblasts	Glass cover slips	~	
Groessner-Schreiber et al. (2003) [23]	Mouse fibroblasts	cpTi	+	
Yeung et al. (2007) [4]	Mouse osteoblasts	NiTi; SS; Ti6Al4V	+	
Annunziata et al. (2008) [15]	BMSC	Ti6Al4V	~	~
Annunziata et al. (2011) [16]	BM-MSC	TPS	~	~
Czarnowska et al. (2011) [19]	Saos-2	Ti6Al4V	~	~
Durual et al. (2011) [18]	hOB	cpTi	+	~
Gordin et al. (2012) [5]	hFOB 1.19	cpTi; Ti6Al4V	~	
Rieder et al. (2012) [28]	hOB	cpTi; SS	+	~
van Hove et al. (2013) [27]	MC3T3-E1	CoCrMo	+	~

~: no difference between TiN-coated material and the control; +: higher on TiN-coated material than the control; −: lower on TiN-coated material than the control. TiN: titanium-nitride; BMSC: human bone marrow stromal cells; BM-MSC: human bone marrow mesenchymal stem cells; Saos-2: sarcoma osteogenic, human osteoblast-like cells; hOB: human primary osteoblasts; hFOB 1.19: human fetal-osteoblastic cell line; MC3T3-E1: mouse calvarial osteoblast-like cell; cp Ti: commercially pure titanium; NiTi: nickel-titanium; SS: stainless steel; Ti6Al4V: titanium-aluminum-vanadium alloy; TPS: titanium plasma sprayed.

regions of the TiN-coated implants showed no bone opposition at 4 weeks, but from 24 weeks some specimens showed direct bone opposition [31]. The affinity of bone to the implant index of TiN-coated stainless steel was comparable with alumina, but not significantly better than uncoated stainless steel [31]. TiN-coated Ti6Al4V rods were implanted in rat femurs and showed similar biocompatibility and bone-bonding properties compared with uncoated Ti6Al4V [3]. Relative bone area and bone-implant contact of TiN-coated commercially pure (cp) titanium threaded implants in rabbits was similar compared with TiO_2-coated cp titanium [32].

Results of three independent experiments showed a lower adhesion and proliferation ($P < 0.05$) over 24 hours of bacteria cultures *S. pyogenes* and *S. sanquinis* on TiN-coated titanium plasma sprayed surfaces (TPS) compared with uncoated TPS [16].

3.2. Preclinical Studies: Wear. TiN-coated Ti6Al4V showed a high scratch resistance [33, 34] and low coefficient of friction [33, 35], reduction of abrasive particle formation and less ultrahigh molecular weight polyethylene (UHMWPE) wear [35], more resistance to fretting and corrosion [5, 36, 37], reduction of wear [38], lower ion release rates [5, 39], and low fatigue cycle [40] compared with uncoated Ti6Al4V. Studies on wear of TiN-coated materials compared with their controls are shown in Table 2. The TiN-coating of Ti6Al4V showed minor to no signs of surface delamination, surface scratching, or coating failure in simulator tests [35, 37, 41–43]. However, in one study, a high incidence of adhesive coating failure was found in PVD TiN-coated Ti6Al4V, and the TiN-coating was prone to pitting and blistering at small coating defects [44]. Also, the wear behavior is affected heavily by pinholes in the PVD TiN-coating of CoCrMo [45, 46]. In a pin-on-plate test, TiN-coated CoCrMo showed a fourfold increase in wear rate compared with CoCrMo due to catastrophic adhesive failure of the TiN-coating [22]. In a metal-on-UHMWPE hip simulator test, minimal abrasive wear without signs of pitting, delamination, or overheating of the UHMWPE was found when in contact with TiN-coated Ti6Al4V [42]. TiN-coated Ti6Al4V showed lower UHMWPE wear rates compared with Ti6Al4V [35] and 316L stainless steel [41]. TiN-coated CoCrMo showed less adhesion to polyethylene compared with CoCrMo, and CoCrMo showed a catalytic effect on the degradation of polyethylene whereas TiN is inert [46]. Although the volumetric wear rate of UHMWPE was reduced with 42% using a hybrid process for the TiN-film compared with commercialized CoCrMo [47], in another study, the average volumetric wear rate of UHMWPE to TiN-coated CoCrMo was not superior to CoCrMo or alumina [33]. Also, in a multidirectional wear test using UHMWPE specimens, no significant differences were found between TiN-coated CoCrMo and uncoated CoCrMo in coefficient of friction, and wear rate on damaged and undamaged surfaces [48]. Furthermore, friction and wear of the UHMWPE counterface was dependent of the lubricant used [24]. In the presence of protein, wear is very low independently of the surface roughness in the TiN/UHMWPE contact pair [49].

In a metal-on-metal hip simulator test, TiN-coated CoCrMo showed a lower wear rate compared with uncoated CoCrMo [50, 51]. The average wear of the uncoated insert articulating with a TiN-coated femoral head was greater compared with the uncoated femoral heads [51].

3.3. Clinical Studies. Clinical studies on survival of TiN-coated orthopaedic implants are presented in Table 3. In a cohort of 76 patients who received a cemented hip prosthesis, 60 received a CoCrMo head and 16 received a TiN-coated titanium head [52]. Loosening of the femoral component occurred in 44.4% of the hips with a TiN-coated titanium head and in 21.6% of the hips with a CoCrMo head ($P = 0.11$) with a 26-month follow-up [52].

In a postmortem retrieval analysis of a cementless TiN-coated Ti6Al4V THA one year after index surgery, the TiN-coated Ti6A14V femoral head showed circular voids without TiN-coating and voids filled with circular droplets of pure titanium [53]. Adhered to the TiN-coating, pure titanium and Ti6Al4V debris was found [53]. In an analysis of four TiN-coated Ti6Al4V femoral heads retrieved at revision after a period of in vivo articulation against UHMWPE liners,

Table 2: Preclinical studies on wear of TiN-coated materials compared with control material.

Study	Test	TiN-coated material	TiN-coating process	Control	Findings	TiN-coating related problems
Coll and Jacquot (1988) [35]	UHMWPE pin on disc	Ti6Al4V	AVID	Ti6Al4V	Reduction of UHMWPE wear*	
Maurer et al. (1993) [2]	Screws on plates	Ti6Al4V	PVD/PIII/NII	Ti6Al4V	Reduction of weight loss and metal release*	
Venugopalan et al. (2000) [34]	Pin-cylinder scratch test	Ti6Al4V	N	Ti6Al4V	Better scratch resistance*	
Hendry and Pilliar (2001) [37]	Fretting test	Ti6Al4V	PVD	Ti6Al4V	No evidence of significant wear*	Microparticles and pinholes
Komotori et al. (2001) [44]	Multidirectional scratch testing	Ti6Al4V/SP-700	AIP	TO-Ti6Al4V/SP-700	More mechanical damage*	Adhesive coating failure; pitting and blistering
Fisher et al. (2002) [51]	MOM hip simulator	CoCrMo	AEPVD	CoCrMo	Lower wear*	Relatively high wear inserts
Williams et al. (2003) [22]	Multidirectional pin on plate	CoCrMo	AEPVD	CoCrMo	Fourfold increase of wear*	Cohesive failure
Gutmanas and Gotman (2004) [41]	UHMWPE hip simulator	cpTi/Ti6Al4V	PIRAC	SS	Lower UHMWPE wear rate*	
Fisher et al. (2004) [50]	MOM hip simulator	CoCrMo	AEPVD	CoCrMo	Lower wear*	Some localized damage
Galvin et al. (2008) [33]	UHMWPE hip simulator	CoCrMo	AEPVD	CoCrMo	Higher UHMWPE volumetric wear rate*	
Galetz et al. (2010) [45]	Station-wheel-on-flat testing	CoCrMo	PVD	CoCrMo	No scratches*	Polyethylene in pinholes
Kim et al. (2010) [38]	Pin on disc	Ti6Al4V	AIP	Ti6Al4V	Lower wear*	Higher wear of TiN compared with TiAlN
Lee et al. (2010) [47]	UHMWPE pin on disc	SS	PIII	CoCrMo	Lower UHMWPE volumetric wear rate*	

*: of titanium-nitride coated material compared with the control; TiN: titanium-nitride; UHMWPE: ultrahigh molecular weight polyethylene; MOM: metal-on-metal; SS: stainless steel; Ti6Al4V: titanium-aluminum-vanadium alloy; TO-Ti6Al4V: titanium-oxide coated Ti6Al4V; SP-700: Ti4.5Al3V2Fe2Mo, titanium-aluminum-vanadium-iron-molybdenum alloy; CoCrMo: cobalt-chromium-molybdenum alloy; cp Ti: commercially pure titanium; TiAlN: titanium-aluminum-nitride coating; PIII: plasma immersion ion implantation; AIP: arc ion plating; AVID: arc vapor ion deposition; PVD: physical vapor deposition; NII: nitrogen ion implantation; N: nitrogen diffusion hardening; AEPVD: arc evaporative physical vapor deposition; PIRAC: powder immersion reaction assisted coating.

Table 3: Clinical studies on survival of TiN-coated orthopaedic implants.

Study	Type	Prosthesis	TiN-coated material	Number	Fixation	Follow-up	Survival	Reasons for revision
Buechel and Pappas (1992) [64]	Cohort	TAP	Ti6Al4V	14	Cementless	15 (5–24)	100%	None
Massoud et al. (1997) [52]	Cohort	THP	Ti nos	16	Cemented	26	56%	Aseptic loosening
Buechel et al. (2003) [63]	Cohort	TAP	Ti6Al4V	50	Cementless	60 (24–120)	93.5%	Malalignment; PE wear; component subsidence
Buechel et al. (2004) [62]	Cohort	THP	Ti6Al4V	130	Cementless	77 (27–134)	95.5%	Aseptic loosening; bearing dissociation
Buechel and Pappas (2011) [55]	Cohort	RHP	Ti6Al4V	60	Cementless	36 (8–70)	91.8%	Not specified
Mohammed et al. (2014) [58]	Cohort	TKP	CoCrMo	305	Cementless	79 (36–122)	95.1%	Prosthetic fractures; aseptic loosening; alignment
van Hove et al. (2015) [61]	RCT	TKP	CoCrMo	50	Cementless	60	96%	Aseptic loosening

All prosthetic joint articulations were TiN-coated implant material to UHMWPE. Follow-up is presented as mean (range) in months. RCT: randomized clinical trial; TAP: total ankle prosthesis; THP: total hip prosthesis; RHP: resurfacing total hip prosthesis; TKP: total knee prosthesis; Ti6Al4V: titanium-aluminum-vanadium alloy; CoCrMo: cobalt-chromium-molybdenum alloy; Ti nos: titanium not otherwise specified.

TiN-coating breakthrough and fretting occurred in 2 out of 4 retrieved prostheses [54].

Failures of a cementless TiN-coated titanium alloy-on-UHMWPE resurfacing THA were suggested to be due to the use of conventional UHMWPE instead of highly cross-linked UHMWPE [55]. In a case of a failed cementless TiN-coated titanium alloy-on-UHMWPE resurfacing THA eleven years after index surgery, severe wear of the polyethylene liner with erosion of the femoral head into the metal acetabular shell was reported [56].

In the radiological follow-up (16.6 months, range 12–39 months) of 330 hips with a press-fit polyethylene cup with TiN-coated stainless steel mesh (Sulmesh, Sulzer, Winterthur, Switzerland) for the bone-implant interface, there was one case showing a radiolucent line around the cup; however, this was without clinical problems [57]. There was insufficient stability of the mesh in 4 of the 330 cases [57].

In a retrospective study of mainly cementless TiN-coated CoCrMo mobile bearing TKAs, revision surgery was performed in 4.9% [58]. Prosthetic fractures were found in four knees and involved the posteromedial flange of right-sided, size 5, femoral components only [58]. A case report on the fracture of a cementless TiN-coated CoCrMo femoral component met with these findings [59]. Another case, which concerned the fracture of the medial flange posterior to the peg of a TiN-coated Ti6Al4V TKA, was also reported [60].

In a recently published RCT, no differences in postoperative pain, KSS, revision surgery, knee flexion and knee flexion contracture, knee circumference, and knee skin temperature were observed between the TiN-coated CoCrMo TKA (n = 51) and a CoCrMo TKA (n = 50) [61]. In both groups two knees were revised for reasons unrelated to the TiN-coating, which resulted in a 5-year survival of 96% [61].

4. Discussion

In preclinical studies, TiN-coating of implant materials showed to be biocompatible with mainly favorable tribological properties. Several cohort studies of TiN-coated implants showed an overall survival exceeding 90% with a follow-up of 15 to 77 months and good clinical results [55, 58, 62–64]. There were no clinical studies that compared TiN-coated Ti6Al4V implants with uncoated Ti6Al4V implants. One study compared a TiN-coated CoCrMo implant with an uncoated CoCrMo implant and found no difference in clinical outcome or survival [61]. Although preclinical studies showed that TiN-coating of implant material supplies the implant surface with favorable properties, there is insufficient evidence that the TiN-coating affects the clinical outcome and survival of implants in clinical studies. Nonetheless, concerns were raised in a preclinical study about PVD TiN-coated Ti6Al4V because of adhesive coating failure due to coating defects [44]. In retrieved PVD TiN-coated Ti6Al4V femoral heads, the TiN-coating was damaged [53, 54]. Delaminated surface asperities of the TiN-coated femoral head might result in wear debris and lead to adhesive wear on the articular surface [53]. It was suggested that the underlying substrate is prone for third body wear, in case of coating breakthrough [53, 54, 65]. Also, it was advised to handle TiN-coated implants carefully with proper soft instruments, because the thin coating may be easily cracked or scratched by hard surgical tools due to high local stresses at contact points between hard materials opening direct pathways for corrosion leading to delamination [65]. There were no reports of failures of other surface treatments which result in a TiN layer on Ti6Al4V, such as PIRAC [3, 41], PIII [4], and Hardion+ [5].

In a pins-and-plate test of polished PVD TiN-coated CoCrMo a higher surface roughness, catastrophic cohesive failure within the layers of the TiN-coating and a fourfold increase in wear was found [22]. Higher surface roughness of PVD TiN-coated CoCrMo was due to small pits and pinholes related to the PVD process [45]. These pits and pinholes were filled with UHMWPE debris [45, 46]. Although this could be a reason for implant failure, there was no report of failure of a TiN-coated CoCrMo implant in contrast to TiN-coated Ti6Al4V implant. This could be due to a worse TiN-coating layer performance on Ti6Al4V than on CoCrMo [45]. Although the hardness of Ti6Al4V and CoCrMo is similar, Ti6Al4V has a higher difference in elastic modulus with the TiN-coating compared with CoCrMo [45]. It is suggested that this difference in elastic modulus leads to failure of the bonding layer between the TiN-coating and Ti6Al4V [45]. This might induce a cascade of wear and failure of the implant.

A high incidence of aseptic loosening was found with a new design of cemented THA using CoCrMo and TiN-coated titanium heads on UHMWPE liner [52]. There was no significant difference in aseptic loosening of the femoral stem with either the CoCrMo or TiN-coated titanium heads [52]. Furthermore, two brands of cement were used, but no multivariate analysis was performed [52]. Of the cases revised the polyethylene had no visible wear [52]. It remains unclear in this study whether TiN-coated titanium heads have a negative effect on the survival of the implant. That particular implant has been taken off the market.

Prosthetic fractures of the medial flange of size 5 right-sided TiN-coated CoCrMo femoral component of a TKA were found [58, 59]. It is unclear if all size 5 right-sided TiN-coated CoCrMo femoral components in that study fractured. However, the junction of the posterior and the distal chamfer at the medial flange of the implant had a narrow surface cross section, which resulted in a high stress concentration [58]. Adjustments were made to the design and there have been no reports of prosthetic fractures ever since [58]. It is unlikely that the TiN-coating was a cause for these prosthetic fractures.

Noteworthy is that of the 7 clinical studies, case reports not included, 4 studies [55, 62–64] on survival and results of TiN-coated implants were performed by researchers, who patented one of the implants [13] and who also founded the company which produced the implant. This might imply a conflict of interests and might be of influence on the results.

5. Conclusion

Titanium alloys used for articulating surfaces require surface treatment to increase hardness and reduce wear. TiN-coating has a favorable effect on the biocompatibility and

tribological properties of implant surfaces. However, there are reports of third body wear due to delamination of the PVD TiN-coating on Ti6Al4V, increased UHMWPE wear and cohesive failure of the PVD TiN-coating on CoCrMo of hip implants in preclinical studies, and TiN-coating breakthrough and fretting in a retrieval study of TiN-coated Ti6Al4V femoral heads. These adverse effects might be related to the various coating processes of titanium alloys. The TiN-coating process of titanium alloy articulating surfaces should be optimized and standardized. There were no reports of adverse effects related to TiN-coating of CoCrMo knee implants. Clinical benefit of TiN-coating of CoCrMo knee implant articulating surfaces should be investigated further.

Appendix

Pubmed/Medline Search strategy: (((((((“shoulder”[MeSH Terms] OR “shoulder”[Tiab]) AND (“prosthesis implantation”[MeSH Terms] OR (“prosthesis”[Tiab] AND “implantation”[Tiab]) OR “prosthesis implantation”[Tiab] OR “prosthesis”[Tiab] OR “prostheses and implants”[MeSH Terms] OR (“prostheses”[Tiab] AND “implants”[Tiab]) OR “prostheses and implants”[Tiab])) OR ((“shoulder”[MeSH Terms] OR “shoulder”[Tiab]) AND (“arthroplasty”[MeSH Terms] OR “arthroplasty”[Tiab]))) OR ((“shoulder”[MeSH Terms] OR “shoulder”[Tiab]) AND (“replantation”[MeSH Terms] OR “replantation”[Tiab] OR “replacement”[Tiab]))) OR ((“hip prosthesis”[MeSH Terms] OR (“hip”[Tiab] AND “prosthesis”[Tiab]) OR “hip prosthesis”[Tiab] OR “arthroplasty, replacement, hip”[MeSH Terms] OR (“arthroplasty”[Tiab] AND “replacement”[Tiab] AND “hip”[Tiab]) OR “hip replacement arthroplasty”[Tiab] OR (“hip”[Tiab] AND “prosthesis”[Tiab])) OR ((“hip”[MeSH Terms] OR “hip”[Tiab]) AND (“arthroplasty”[MeSH Terms] OR “arthroplasty”[Tiab])))) OR ((“arthroplasty, replacement, knee”[MeSH Terms] OR (“arthroplasty”[Tiab] AND “replacement”[Tiab] AND “knee”[Tiab]) OR “knee replacement arthroplasty”[Tiab] OR (“knee”[Tiab] AND “arthroplasty”[Tiab]) OR “knee arthroplasty”[Tiab]) OR (“knee prosthesis”[MeSH Terms] OR (“knee”[Tiab] AND “prosthesis”[Tiab]) OR “knee prosthesis”[Tiab] OR “arthroplasty, replacement, knee”[MeSH Terms] OR (“arthroplasty”[Tiab] AND “replacement”[Tiab] AND “knee”[Tiab]) OR “knee replacement arthroplasty”[Tiab] OR (“knee”[Tiab] AND “prosthesis”[Tiab])))) OR ((“ankle” [MeSH Terms] OR “ankle”[Tiab] OR “ankle joint”[MeSH Terms] OR (“ankle”[Tiab] AND “joint”[Tiab]) OR “ankle joint”[Tiab]) AND (“arthroplasty”[MeSH Terms] OR “arthroplasty”[Tiab])) OR (“ankle”[MeSH Terms] OR “ankle”[Tiab] OR “ankle joint”[MeSH Terms] OR (“ankle”[Tiab] AND “joint”[Tiab]) OR “ankle joint”[Tiab]) AND “prosthesis implantation”[MeSH Terms] OR (“prosthesis”[Tiab] AND “implantation”[Tiab]) OR “prosthesis implantation”[Tiab] OR “prosthesis”[Tiab] OR “prostheses and implants”[MeSH Terms] OR “‘prostheses”[Tiab]) AND ((ti2n[Tiab] OR TiNi[Tiab]) OR (“titanium nitride”[Tiab] AND coating[Tiab])) OR “titanium nitride”[Tiab].

Conflict of Interests

The authors declare that there is no conflict of interests regarding the publication of this paper.

Acknowledgment

The authors would like to thank W. Salemink for her valuable assistance with the search of the literature.

References

[1] L. E. Toth, *Transition Metal Carbides and Nitrides*, Academic Press, New York, NY, USA, 1971.

[2] A. M. Maurer, S. A. Brown, J. H. Payer, K. Merritt, and J. S. Kawalec, “Reduction of fretting corrosion of Ti-6Al-4V by various surface treatments,” *Journal of Orthopaedic Research*, vol. 11, no. 6, pp. 865–873, 1993.

[3] G. Sovak, A. Weiss, and I. Gotman, “Osseointegration of Ti6A14V alloy implants coated with titanium nitride by a new method,” *The Journal of Bone & Joint Surgery Series B*, vol. 82, no. 2, pp. 290–296, 2000.

[4] K. W. K. Yeung, R. W. Y. Poon, P. K. Chu et al., “Surface mechanical properties, corrosion resistance, and cytocompatibility of nitrogen plasma-implanted nickel-titanium alloys: a comparative study with commonly used medical grade materials,” *Journal of Biomedical Materials Research Part A*, vol. 82, no. 2, pp. 403–414, 2007.

[5] D. M. Gordin, T. Gloriant, V. Chane-Pane et al., “Surface characterization and biocompatibility of titanium alloys implanted with nitrogen by Hardion+ technology,” *Journal of Materials Science: Materials in Medicine*, vol. 23, no. 12, pp. 2953–2966, 2012.

[6] I. Dion, C. Baquey, B. Candelon, and J. R. Monties, “Hemocompatibility of titanium nitride,” *International Journal of Artificial Organs*, vol. 15, no. 10, pp. 617–621, 1992.

[7] D.-C. Sin, H.-L. Kei, and X. Miao, “Surface coatings for ventricular assist devices,” *Expert Review of Medical Devices*, vol. 6, no. 1, pp. 51–60, 2009.

[8] M. Schaldach, M. Hubmann, R. Hardt, and A. Weikl, “Titanium nitride cardiac pacemaker electrodes,” *Biomedizinische Technik*, vol. 34, pp. 185–190, 1989.

[9] S. F. Cogan, “Neural stimulation and recording electrodes,” *Annual Review of Biomedical Engineering*, vol. 10, pp. 275–309, 2008.

[10] P. R. Mezger and N. H. J. Creugers, “Titanium nitride coatings in clinical dentistry,” *Journal of Dentistry*, vol. 20, no. 6, pp. 342–344, 1992.

[11] A. Wisbey, P. J. Gregson, and M. Tuke, “Application of PVD TiN coating to Co-Cr-Mo based surgical implants,” *Biomaterials*, vol. 8, no. 6, pp. 477–480, 1987.

[12] S. Steinemenan, “Implants of titanium or a titanium alloy for the surgical treatment of bones,” US Patent 3643658 A, 1972.

[13] F. F. Buechel and M. J. Pappas, “Prosthesis with biologically inert wear resistant surface,” US Patent 5702448 A, 1995.

[14] A. V. Lombardi Jr., T. H. Mallory, B. K. Vaughn, and P. Drouillard, “Aseptic loosening in total hip arthroplasty secondary to osteolysis induced by wear debris from titanium-alloy modular femoral heads,” *Journal of Bone and Joint Surgery—American Volume*, vol. 71, no. 9, pp. 1337–1342, 1989.

[15] M. Annunziata, L. Guida, L. Perillo, R. Aversa, I. Passaro, and A. Oliva, "Biological response of human bone marrow stromal cells to sandblasted titanium nitride-coated implant surfaces," *Journal of Materials Science: Materials in Medicine*, vol. 19, no. 12, pp. 3585–3591, 2008.

[16] M. Annunziata, A. Oliva, M. A. Basile et al., "The effects of titanium nitride-coating on the topographic and biological features of TPS implant surfaces," *Journal of Dentistry*, vol. 39, no. 11, pp. 720–728, 2011.

[17] M. Manso-Silvan, J. M. Martínez-Duart, S. Ogueta, P. García-Ruiz, and J. Pérez-Rigueiro, "Development of human mesenchymal stem cells on DC sputtered titanium nitride thin films," *Journal of Materials Science: Materials in Medicine*, vol. 13, no. 3, pp. 289–293, 2002.

[18] S. Durual, F. Pernet, P. Rieder, M. Mekki, M. Cattani-Lorente, and H. W. A. Wiskott, "Titanium nitride oxide coating on rough titanium stimulates the proliferation of human primary osteoblasts," *Clinical Oral Implants Research*, vol. 22, no. 5, pp. 552–559, 2011.

[19] E. Czarnowska, J. Morgiel, M. Ossowski, R. Major, A. Sowinska, and T. Wierzchon, "Microstructure and biocompatibility of titanium oxides produced on nitrided surface layer under glow discharge conditions," *Journal of Nanoscience and Nanotechnology*, vol. 11, no. 10, pp. 8917–8923, 2011.

[20] J. J. A. M. van Raay, P. M. Rozing, C. A. van Blitterswijk, R. M. van Haastert, and H. K. Koerten, "Biocompatibility of wear-resistant coatings in orthopaedic surgery in vitro testing with human fibroblast cell cultures," *Journal of Materials Science: Materials in Medicine*, vol. 6, no. 2, pp. 80–84, 1995.

[21] S. Yeniyol, N. Bölükbaşı, A. Bilir, A. F. Çakır, M. Yeniyol, and T. Ozdemir, "Relative contributions of surface roughness and crystalline structure to the biocompatibility of titanium nitride and titanium oxide coatings deposited by PVD and TPS coatings," *ISRN Biomaterials*, vol. 2013, Article ID 783873, 9 pages, 2013.

[22] S. Williams, J. L. Tipper, E. Ingham, M. H. Stone, and J. Fisher, "In vitro analysis of the wear, wear debris and biological activity of surface-engineered coatings for use in metal-on-metal total hip replacements," *Proceedings of the Institution of Mechanical Engineers, Part H: Journal of Engineering in Medicine*, vol. 217, no. 3, pp. 155–163, 2003.

[23] B. Groessner-Schreiber, A. Neubert, W.-D. Müller, M. Hopp, M. Griepentrog, and K.-P. Lange, "Fibroblast growth on surface-modified dental implants: an in vitro study," *Journal of Biomedical Materials Research, Part A*, vol. 64, no. 4, pp. 591–599, 2003.

[24] A. P. Serro, C. Completo, R. Colaço et al., "A comparative study of titanium nitrides, TiN, TiNbN and TiCN, as coatings for biomedical applications," *Surface and Coatings Technology*, vol. 203, no. 24, pp. 3701–3707, 2009.

[25] L. A. Cyster, K. G. Parker, T. L. Parker, and D. M. Grant, "The effect of surface chemistry and nanotopography of titanium nitride (TiN) films on 3T3-L1 fibroblasts," *Journal of Biomedical Materials Research. Part A*, vol. 67, no. 1, pp. 138–147, 2003.

[26] D. R. Cho, A. S. Shanbhag, C.-Y. Hong, G. R. Baran, and S. R. Goldring, "The role of adsorbed endotoxin in particle-induced stimulation of cytokine release," *Journal of Orthopaedic Research*, vol. 20, no. 4, pp. 704–713, 2002.

[27] R. P. van Hove, P. A. Nolte, C. M. Semeins, and J. Klein-Nulend, "Differences in proliferation, differentiation, and cytokine production by bone cells seeded on titanium-nitride and cobalt-chromium-molybdenum surfaces," *Journal of Biomaterials Applications*, vol. 28, no. 2, pp. 278–287, 2013.

[28] P. Rieder, S. Scherrer, A. Filieri, H. W. A. Wiskott, and S. Durual, "TiNOx coatings increase human primary osteoblasts proliferation independently of the substrate: a short report," *Bio-Medical Materials and Engineering*, vol. 22, no. 5, pp. 277–281, 2012.

[29] W. C. Clem, V. V. Konovalov, S. Chowdhury, Y. K. Vohra, S. A. Catledge, and S. L. Bellis, "Mesenchymal stem cell adhesion and spreading on microwave plasma-nitrided titanium alloy," *Journal of Biomedical Materials Research Part A*, vol. 76, no. 2, pp. 279–287, 2006.

[30] S. A. Catledge, Y. K. Vohra, S. L. Bellis, and A. A. Sawyer, "Mesenchymal stem cell adhesion and spreading on nanostructured biomaterials," *Journal of Nanoscience and Nanotechnology*, vol. 4, no. 8, pp. 986–989, 2004.

[31] K. Hayashi, N. Matsuguchi, K. Uenoyama, T. Kanemaru, and Y. Sugioka, "Evaluation of metal implants coated with several types of ceramics as biomaterials," *Journal of Biomedical Materials Research*, vol. 23, no. 11, pp. 1247–1259, 1989.

[32] C. Larsson Wexell, P. Thomsen, B.-O. Aronsson et al., "Bone response to surface-modified titanium implants: studies on the early tissue response to implants with different surface characteristics," *International Journal of Biomaterials*, vol. 2013, Article ID 412482, 10 pages, 2013.

[33] A. Galvin, C. Brockett, S. Williams et al., "Comparison of wear of ultra-high molecular weight polyethylene acetabular cups against surface-engineered femoral heads," *Proceedings of the Institution of Mechanical Engineers, Part H: Journal of Engineering in Medicine*, vol. 222, no. 7, pp. 1073–1080, 2008.

[34] R. Venugopalan, J. J. Weimer, M. A. George, and L. C. Lucas, "The effect of nitrogen diffusion hardening on the surface chemistry and scratch resistance of Ti-6Al-4V alloy," *Biomaterials*, vol. 21, no. 16, pp. 1669–1677, 2000.

[35] B. F. Coll and P. Jacquot, "Surface modification of medical implants and surgical devices using TiN layers," *Surface and Coatings Technology*, vol. 36, no. 3-4, pp. 867–878, 1988.

[36] J. R. Goldberg and J. L. Gilbert, "In vitro corrosion testing of modular hip tapers," *Journal of Biomedical Materials Research—Part B Applied Biomaterials*, vol. 64, no. 2, pp. 78–93, 2003.

[37] J. A. Hendry and R. M. Pilliar, "The fretting corrosion resistance of PVD surface-modified orthopedic implant alloys," *Journal of Biomedical Materials Research*, vol. 58, no. 2, pp. 156–166, 2001.

[38] H. Kim, C. Y. Kim, D. W. Kim et al., "Wear performance of self-mating contact pairs of TiN and TiAlN coatings on orthopedic grade Ti-6Al-4V," *Biomedical Materials*, vol. 5, no. 4, Article ID 044108, 2010.

[39] D. Starosvetsky, A. Shenhar, and I. Gotman, "Corrosion behavior of PIRAC nitrided Ti-6Al-4V surgical alloy," *Journal of Materials Science: Materials in Medicine*, vol. 12, no. 2, pp. 145–150, 2001.

[40] D. Rodríguez, J. M. Manero, F. J. Gil, and J. A. Planell, "Low cycle fatigue behavior of Ti6AI4V thermochemically nitrided for its use in hip prostheses," *Journal of Materials Science: Materials in Medicine*, vol. 12, no. 10–12, pp. 935–937, 2001.

[41] E. Y. Gutmanas and I. Gotman, "PIRAC Ti nitride coated Ti-6AI-4V head against UHMWPE acetabular cup-hip wear simulator study," *Journal of Materials Science: Materials in Medicine*, vol. 15, no. 4, pp. 327–330, 2004.

[42] M. J. Pappas, G. Makris, and F. F. Buechel, "Titanium nitride ceramic film against polyethylene. A 48 million cycle wear test," *Clinical Orthopaedics and Related Research*, no. 317, pp. 64–70, 1995.

[43] C. D. Peterson, B. M. Hillberry, and D. A. Heck, "Component wear of total knee prostheses using Ti-6Al-4V, titanium nitride coated Ti-6Al-4V, and cobalt-chromium-molybdenum femoral components," *Journal of Biomedical Materials Research*, vol. 22, no. 10, pp. 887–903, 1988.

[44] J. Komotori, B. J. Lee, H. Dong, and P. A. Dearnley, "Corrosion response of surface engineered titanium alloys damaged by prior abrasion," *Wear*, vol. 250-251, no. 2, pp. 1239–1249, 2001.

[45] M. C. Galetz, E. W. Fleischmann, C. H. Konrad, A. Schuetz, and U. Glatzel, "Abrasion resistance of oxidized zirconium in comparison with CoCrMo and titanium nitride coatings for artificial knee joints," *Journal of Biomedical Materials Research, Part B, Applied Biomaterials*, vol. 93, no. 1, pp. 244–251, 2010.

[46] M. C. Galetz, S. H. Seiferth, B. Theile, and U. Glatzel, "Potential for adhesive wear in friction couples of UHMWPE running against oxidized zirconium, titanium nitride coatings, and cobalt-chromium alloys," *Journal of Biomedical Materials Research Part B: Applied Biomaterials*, vol. 93, no. 2, pp. 468–475, 2010.

[47] S. B. Lee, J. Y. Choi, W. W. Park et al., "A study of TiN-coated metal-on-polymer bearing materials for hip prosthesis," *Metals and Materials International*, vol. 16, no. 4, pp. 679–686, 2010.

[48] V. C. Jones, D. D. Auger, M. H. Stone, and J. Fisher, "New materials for mobile bearing knee prosthesis—titanium nitride counterface coatings for reduction of polyethylene wear," in *LCS Mobile Bearing Knee Arthroplasty*, pp. 349–351, Springer, Berlin, Germany, 2002.

[49] M. P. Gispert, A. P. Serro, R. Colaço, E. Pires, and B. Saramago, "The effect of roughness on the tribological behavior of the prosthetic pair UHMWPE/TiN-coated stainless steel," *Journal of Biomedical Materials Research, Part B, Applied Biomaterials*, vol. 84, no. 1, pp. 98–107, 2008.

[50] J. Fisher, X. Q. Hu, T. D. Stewart et al., "Wear of surface engineered metal-on-metal hip prostheses," *Journal of Materials Science: Materials in Medicine*, vol. 15, no. 3, pp. 225–235, 2004.

[51] J. Fisher, X. Q. Hu, J. L. Tipper et al., "An *in vitro* study of the reduction in wear of metal-on-metal hip prostheses using surface-engineered femoral heads," *Proceedings of the Institution of Mechanical Engineers, Part H: Journal of Engineering in Medicine*, vol. 216, no. 4, pp. 219–230, 2002.

[52] S. N. Massoud, J. B. Hunter, B. J. Holdsworth, W. A. Wallace, and R. Juliusson, "Early femoral loosening in one design of cemented hip replacement," *The Journal of Bone and Joint Surgery—British Volume*, vol. 79, no. 4, pp. 603–608, 1997.

[53] M. K. Harman, S. A. Banks, and W. Andrew Hodge, "Wear analysis of a retrieved hip implant with titanium nitride coating," *Journal of Arthroplasty*, vol. 12, no. 8, pp. 938–945, 1997.

[54] M. T. Raimondi and R. Pietrabissa, "The in-vivo wear performance of prosthetic femoral heads with titanium nitride coating," *Biomaterials*, vol. 21, no. 9, pp. 907–913, 2000.

[55] F. F. Buechel Sr. and M. J. Pappas, "A metal/ultrahigh-molecular-weight polyethylene cementless surface replacement," *Seminars in Arthroplasty*, vol. 22, no. 2, pp. 66–74, 2011.

[56] A. Malviya, S. Lobaz, and J. Holland, "Mechanism of failure eleven years following a Buechel Pappas hip resurfacing," *Acta Orthopaedica Belgica*, vol. 73, no. 6, pp. 791–794, 2007.

[57] E. Morscher, H. Bereiter, and C. Lampert, "Cementless press-fit cup. Principles, experimental data, and three-year follow-up study," *Clinical Orthopaedics and Related Research*, no. 249, pp. 12–20, 1989.

[58] A. Mohammed, A. Metcalfe, and D. Woodnutt, "Medium-term outcome of titanium nitride, mobile bearing total knee replacement," *Acta Orthopaedica Belgica*, vol. 80, no. 2, pp. 269–275, 2014.

[59] Y. E. Könst, J. Posthuma De Boer, and R. Saouti, "Fracture of a ceramic coated implant total knee prosthesis," *Nederlands Tijdschrift voor Orthopaedie*, vol. 17, pp. 122–124, 2010.

[60] S. Park, H. Kim, and Y. In, "Fracture of titanium nitride-coated femoral component after total knee arthroplasty," *The Knee*, vol. 21, no. 4, pp. 871–874, 2014.

[61] R. P. van Hove, R. M. Brohet, B. J. van Royen, and P. A. Nolte, "No clinical benefit of titanium nitride coating in cementless mobile-bearing total knee arthroplasty," *Knee Surgery, Sports Traumatology, Arthroscopy*, vol. 23, no. 6, pp. 1833–1840, 2015.

[62] F. F. Buechel Sr., F. F. Buechel Jr., T. E. Helbig, J. D'Alessio, and M. J. Pappas, "Two- to 12-year evaluation of cementless Buechel-Pappas total hip arthroplasty," *The Journal of Arthroplasty*, vol. 19, no. 8, pp. 1017–1027, 2004.

[63] F. F. Buechel Sr., F. F. Buechel Jr., and M. J. Pappas, "Ten-year evaluation of cementless Buechel-Pappas meniscal bearing total ankle replacement," *Foot and Ankle International*, vol. 24, no. 6, pp. 462–472, 2003.

[64] F. F. Buechel and M. J. Pappas, "Survivorship and clinical evaluation of cementless, meniscal-bearing total ankle replacements," *Seminars in Arthroplasty*, vol. 3, no. 1, pp. 43–50, 1992.

[65] R. Lappalainen and S. S. Santavirta, "Potential of coatings in total hip replacement," *Clinical Orthopaedics and Related Research*, no. 430, pp. 72–79, 2005.

Hindawi Publishing Corporation
BioMed Research International
Volume 2015, Article ID 650282, 10 pages
http://dx.doi.org/10.1155/2015/650282

Research Article

The Effect of Risk Factors on the Levels of Chemical Elements in the Tibial Plateau of Patients with Osteoarthritis following Knee Surgery

Natalia Lanocha-Arendarczyk,[1] Danuta Izabela Kosik-Bogacka,[1] Adam Prokopowicz,[2] Elzbieta Kalisinska,[1] Sebastian Sokolowski,[3] Maciej Karaczun,[3] Pawel Zietek,[3] Joanna Podlasińska,[4] Bogumila Pilarczyk,[5] Agnieszka Tomza-Marciniak,[5] Irena Baranowska-Bosiacka,[6] Izabela Gutowska,[7] Krzysztof Safranow,[6] and Dariusz Chlubek[6]

[1]*Department of Biology and Medical Parasitology, Pomeranian Medical University, Powstancow Wielkopolskich 72, 70-111 Szczecin, Poland*
[2]*Department of Chemical Hazards and Genetic Toxicology, Institute of Occupational Medicine and Environmental Health, Koscielna 13, 71-200 Sosnowiec, Poland*
[3]*Chair and Clinic of Orthopaedics and Traumatology, Pomeranian Medical University, Unii Lubelskiej 1, 71-252 Szczecin, Poland*
[4]*Department of Ecology, Environmental Management and Protection, Slowackiego 17, 71-434 Szczecin, Poland*
[5]*Department of Animal Reproduction Biotechnology and Environmental Hygiene, West Pomeranian University of Technology, Doktora Judyma 6, 71-466 Szczecin, Poland*
[6]*Department of Biochemistry and Medical Chemistry, Pomeranian Medical University, Powstancow Wielkopolskich 72, 70-111 Szczecin, Poland*
[7]*Department of Biochemistry and Human Nutrition, Pomeranian Medical University, Broniewskiego 24, 71-460 Szczecin, Poland*

Correspondence should be addressed to Natalia Lanocha-Arendarczyk; nlanocha@pum.edu.pl

Received 20 March 2015; Revised 13 May 2015; Accepted 18 May 2015

Academic Editor: Kengo Yamamoto

Copyright © 2015 Natalia Lanocha-Arendarczyk et al. This is an open access article distributed under the Creative Commons Attribution License, which permits unrestricted use, distribution, and reproduction in any medium, provided the original work is properly cited.

The aim of this study was to evaluate the aforementioned chemical elements in tibial plateau samples obtained during knee arthroplasty. The gender-specific analysis of chemical element levels in the bone samples revealed that there were statistically significant differences in the concentration of Pb and Se/Pb ratio. The contents of elements in the tibial plateau in the patients with osteoarthritis (OA) can be arranged in the following descending order: F^- > K > Zn > Fe > Sr > Pb > Mn > Se > Cd > THg. We observed statistical significant effects of environmental factors including smoking, seafood diet, and geographical distribution on the levels of the elements in tibial bone. Significant positive correlation coefficients were found for the relationships K-Cd, Zn-Sr, Zn-F^-, THg-Pb, Pb-Cd, Se-Se/Pb, Se-Se/Cd, Se/Pb-Se/Cd, Pb-Cd/Ca, Cd-Cd/Ca, and F^--F^-/Ca·1000. Significant negative correlations were found for the relationships THg-Se/Pb, Pb-Se/Pb, Cd-Se/Pb, K-Se/Cd, Pb-Se/Cd, Cd-Se/Cd, THg-Se/THg, Pb-Se/THg, Se-Pb/Cd, Zn-Cd/Ca, and Se/Cd-Cd/Ca. The results reported here may provide a basis for establishing reference values for the tibial plateau in patients with OA who had undergone knee replacement surgery. The concentrations of elements in the bone with OA were determined by age, presence of implants, smoking, fish and seafood diet, and sport activity.

1. Introduction

Osteoarthritis (OA), the most common form of arthritis, is a serious disease affecting the joints due to an imbalance between the processes of degeneration and regeneration of cartilage structures [1, 2]. Age-related and incurable OA is manifested by gradual degenerative arthritis, leading to premature motor disability.

The pathogenesis of osteoarthritic changes in the joints is complex, with metalloproteinases playing the central role in the degeneration of cartilage, although genetic and environmental factors such as age, gender, body mass, and sport activity are also mentioned [3]. The presence of OA in the knee is highly age-related but gender-specific differences are also evident. In persons younger than 50 years of age, the prevalence of this disease is higher in men [2]. OA is predicted to reach 30% of the population above 60 years of age by the year 2030 [4]. The symptoms of OA are stronger in women over 50 and in the postmenopausal period. Clinical symptoms include joint pain, tenderness, restriction of movement, loss of articular cartilage, sclerosis, and increased density of subchondral bone [5].

Many metals that are present in organisms accumulate in the bones and may be released due to various pathological conditions [6]. There is little research focusing on the element composition of bone or on correlations between metals in joint cartilage and bone tissues in patients with osteoarticular degeneration, including OA [7–10]. These few analyses usually examine the cancellous bone portions of patients following hip arthroplasty or the ribs of healthy people [8, 11]. The choice of the cancellous bone is related to its high sensitivity to hormones and other biological factors, and the onset of OA can cause cartilage loss and subchondral sclerosis [12]. However, the tibial plateau, which consists mainly of cortical bone, can also be an original source of material for biomonitoring research, especially due to its features that provide structural integrity-strength, density, and compactness.

Cadmium (Cd), lead (Pb), and mercury (THg) often cause acute and chronic environmental contamination and inflict damage primarily to the kidney, liver, brain, and bone. In one of the most drastic cases, in the 1950s in Japan, Cd poisoning resulted in the Itai-itai disease, a mixed pattern of bone diseases and damage to the kidney [10]. Over a lifetime, 90% of Pb will accumulate in the bones. Little is known about the effects of total THg on the human skeleton and concentrations in bone samples of the knee joint and/or hip joint. Moreover, interactions between the aforementioned metals can also affect their toxicity.

Prolonged exposure to large amounts of fluoride (F) in inhaled air or in the diet results in a deposition of fluoride ions (F^-) in bone tissue, mainly in cancellous bone. Fluoride reduces Ca absorption, leading to impaired mineralization of newly formed osteoid [13]. In contrast, iron (Fe), zinc (Zn), selenium (Se), and manganese (Mn) are considered by WHO to be essential elements for the correct functioning of living organisms but may be toxic at high levels of exposure [14]. The deficiencies of some of these elements can increase the accumulation and toxicity of various toxic metals. Fe and Zn deficiencies, for instance, increase the susceptibility to Cd and Pb toxicity [15]. Although strontium (Sr) stimulates bone formation and inhibits osteoclastic activity, it has not been proven to be essential. In hydroxyapatite crystal, Sr is antagonist to Ca [12, 16, 17]. For some years it has also been suggested that potassium (K) exerts a beneficial effect on the skeleton through anions provided by potassium salts and the anion-independent effect of K on Ca excretion and bone metabolism [18].

The aim of this present study was to evaluate the aforementioned 10 chemical elements in tibial plateau samples obtained during knee arthroplasty from patients from northern and western Poland. Furthermore, the aim was to examine synergistic and/or antagonistic relationships between chemical elements in the bone samples and environmental exposure factors, as well as examining the effects of environmental factors including smoking, diet, occupational exposure, sport activity, and supplementation, on the levels of the elements in tibial bone diagnosed with OA.

2. Materials and Methods

For this study 33 tibial plateau samples were examined. The specimens were obtained from women ($n = 22$) aged from 54 to 83 years (mean age 67.0) and men ($n = 11$) aged from 48 to 79 years (mean age 64.5) following knee joint arthroplasty. These patients had been hospitalized at orthopedic clinics in the West Pomeranian (WV) in Szczecin (WVS) and Koszalin (WVK) and Lubuskie (LV) voivodships in 2013-2014. The tibial plateau samples had been acquired intraoperatively from patients who had undergone knee joint arthroplasty due either to osteoarthritis (OA, $n = 28$) or knee injury (KI, $n = 5$). Patients with knee injuries were subject to knee replacement surgery due to mechanical trauma (accidents); the group included males ($n = 3$; mean age: 53.0) and females ($n = 2$; mean age: 59.5). The analysis excluded patients who had been treated with fluoride-containing preparations. All the patients were interviewed using a questionnaire to collect data on demographics, health status, occupational exposure to potentially toxic elements, smoking, diet, sport activity and supplementation. Among the patients, 18 persons had been cigarette smokers for at least 20 years, while 15 persons were non-smokers. The use of the bone tissue in the research was approved by the Bioethics Committee of Pomeranian Medical University in Szczecin (KB-0012/78/13).

Prior to analysis, the tissue samples had been stored at a temperature below −20°C. The sampled bones were cleaned of adhering soft tissue and marrow, and degreased with acetone (Chempur, Poland) for 3 h. Bone samples were dried to a constant weight at 55°C (for the determination of THg) and 105°C (for the determination of Se, F^-, Fe, Mn, Zn, Sr, Cd, Pb, Ni, K) for 3 weeks in a drying oven with forced air circulation (Binder GmbH, Germany) so that water content could be determined (gravimetric method), and then crushed in an agate mortar. Selenium concentrations in the bone samples were determined by spectrofluorimetric method (RF 5001 PC Shimadzu spectrophotofluorometer) according to Pilarczyk et al. [19]. Determination of THg concentrations was performed by atomic absorption spectroscopy (AAS) using an AMA 254 mercury analyzer. More details on the analytical procedures are available in our previous research [10]. Fluoride concentrations were determined by potentiometric method using an Orion ion-selective F electrode, as described by Palczewska-Komsa et al. [20]. To determine the levels of the other elements, a separated sample (0.3 g)

of dried bone tissue was placed in a PFA dish. 1.5 mL of concentrated nitric acid 69.0–70.0% (Avantor Performance Materials, J.T. Baker Analyzed Instra Reagent, USA) was added to the samples which were then digested in on a hot plate at 120°C for 16 hours. After cooling, 1.5 mL of 30% hydrogen peroxide (Baker Analyzed) was added, and the digestion continued for another 24 hours. The resulting sample was diluted with deionized water (milliQ) to 15 mL and analyzed for Pb, Cd, Sr, K, Zn, Mn, and Fe concentrations. The reference material and blank samples were prepared by the same digestion procedure. Lead, Cd, and Mn levels were determined by atomic absorption spectrometry with electrothermal atomization in a graphite furnace (GFAAS) using a PerkinElmer 4100ZL spectrometer (Perkin-Elmer Bodenseewerk, Überlingen, Germany) equipped with an autosampler and Zeeman background correction. Temperature and time programs for the graphite furnace were optimized for each element. Zn and Fe were determined by flame atomic absorption spectrometry (FAAS) in an air-acetylene flame using a UNICAM 939 Solaar atomic absorption spectrometer equipped with a deuterium background correction. Fe was determined using standard solutions prepared from the matrix of the sample. K and Sr were determined by flame atomic emission spectrometry (FAES) using a UNICAM 939 Solaar spectrometer and an air-acetylene flame to measure K or a nitrous oxide-acetylene flame to determine Sr. In both assays, ionization buffers were used: a 0.2% solution of sodium (NaCl) and a 0.2% solution of potassium (KCl), respectively. To validate the analytical techniques, reference samples NIST-SRM 1486 (Bone meal) and Fish Tissue IAEA-407 were used. The analytical values were within the range of certified values. Recoveries consistently remained in the range 88–97%. The concentrations of elements were expressed as mg/kg on dry mass basis (dm).

Statistical analysis was carried using the Statystyka PL program. The distribution normality was examined using a Shapiro-Wilk test. Due to the nonparametric distribution of results, intergroup comparisons were performed using the Mann-Whitney U test. The correlations between the analyzed variables were calculated with Spearman's rank correlation coefficient (r_s). The significance level was $p < 0.05$.

3. Results

The gender-specific analysis of chemical element levels in the bone samples revealed that there were statistically significant differences in the concentration of Pb and in the Se/Pb ratio (Tables 1 and 2). Lead concentrations were 1.74 times higher in the men than in the women. Likewise, Se/Pb ratio was higher in the men than in the women (Table 2). There were no statistically significant differences in the group of potential essential elements between the genders.

A comparison of chemical element levels between the two groups of patients with OA and KI showed statistically significant differences only in the F^- concentration in the inorganic portion of bone: F^-/Ca·1000 ($U = 29$; $p < 0.01$) and in age ($U = 11.0$, $p < 0.001$). Differences close to statistical significance ($p = 0.06$) were observed in F^- level and Se/THg ratio, as well as in relation to the number of dental amalgams in the OA group. In the tibial plateau, the concentrations of Sr, F^-, and Cd were higher in the OA patients than in the KI, while Zn and Mn levels were, respectively, lower, but these differences were not statistically significant.

A comparison of element levels in the bone between patients from northwestern Poland (WVS and WSK) and western Poland (LV) showed statistically significant differences only in Se levels, between LV and WVS ($U = 6.0$; $p < 0.01$), and between WVS and WVK ($U = 3.0$; $p < 0.01$). The highest Se concentrations were observed in the tibial plateau samples of the patients from WVS (0.047 mg/kg dm) and then from LV (0.037 mg/kg dm) and the lowest were found in those from WVK (0.024 mg/kg dm).

Between the patients occupationally exposed (OE) or unexposed (UE) to potentially toxic elements (Pb, THg, and Cd) no statistically significant differences were observed in bone tissue sample levels. However, the concentrations of Pb, THg in the OE patients who had undergone knee surgery were, respectively, more than 1.4 and 1.7 times higher than in the UE patients, at 2.40 versus 1.74, and 0.0067 versus 0.0040 mg/kg dm, respectively.

Analysis of element levels in the bone samples in relation to smoking (elements contained in cigarettes were taken into account) showed statistically significant differences in the concentrations of Pb and Cd in the smokers, with significantly higher ratios of Se/Pb, Se/Cd, and Se/THg, in the nonsmoking patients (Table 3). The widest differences were observed in Pb levels between the groups of smokers and nonsmokers.

The patients with dental amalgam fillings (DA) who had been exposed mainly to THg, Cd, and Zn contained in amalgams showed no statistically significant differences in element levels in bone tissue compared to the patients without amalgam fillings (NDA), despite higher THg concentrations in the patients with DA (over 1.5 times higher) than the NDA patients (0.0061 versus 0.0039 mg/kg dm). Furthermore, in terms of age and the number of dental amalgams, there were significant differences between the DA and NDA groups ($U = 35.0$, $p < 0.01$ and $U = 62.5$, $p < 0.01$, resp.).

The comparison of element levels in the tibial plateau between those who consumed fish and seafood (FD) and those who did not (NFD) showed statistically confirmed differences in Se, THg concentrations, and Se/THg ratio (U test: M-W = 71.5, $p < 0.04$; 60.0, $p < 0.01$; 73.0, $p < 0.04$, resp.). The lowest concentrations of Se and THg were found in the NFD group (0.036 and 0.004 mg/kg dm), compared to the FD group (0.042 and 0.006 mg/kg dm). In the tibial plateau samples from the FD group patients there was a lower Se/THg ratio compared to the NFD group participants (10.84 and 21.57, resp.).

A comparison of the mean levels of chemical elements showed no statistically significant differences between the participants who preferred dairy products to those who did not consume milk and cheese.

Moreover, there were significant differences in the concentrations of Se between the patients who used dietary supplements (WS) and those who did not (NS) ($U = 57.5$, $p < 0.02$). We also observed a difference in the

Table 1: Effect of gender on mean values of chemical contents in human tibial plateau from patients after knee surgery (mg/kg dm).

	K	Zn	Mn	Fe	Sr	Se	THg	Pb	Cd	F^-
					Female (n = 22)					
AM ± SD	446.80 ± 138.97	98.79 ± 14.15	0.30 ± 0.21	55.98 ± 39.44	45.30 ± 18.59	0.04 ± 0.01	0.005 ± 0.007	1.50 ± 0.69	0.04 ± 0.03	634.54 ± 379.85
Med.	405.22	96.15	0.23	35.17	44.63	0.04	0.0018	1.53	0.03	513.16
Range	295.69–881.57	76.73–129.09	0.08–0.81	12.73–142.97	25.15–116.82	0.02–0.06	0.0007–0.03	0.35–2.91	0.01–0.13	238.40–1815.18
Q_L–Q_U	344.48–505.98	89.21–103.70	0.15–0.37	28.46–69.95	34.08–48. 89	0.03–0.05	0.001–0.006	0.96–1.94	0.02–0.05	330.08–893.84
					Male (n = 11)					
AM ± SD	514.20 ± 157.67	99.12 ± 8.33	0.34 ± 0.30	62.14 ± 38.97	41.6 ± 9.90	0.04 ± 0.02	0.0043 ± 0.003	2.06 ± 1.60	0.06 ± 0.06	569.55 ± 300.49
Med.	455.25	100.55	0.27	49.62	38.65	0.03	0.004	2.06	20.04	449.31
Range	355.04–831.41	89.36–110.82	0.11–0.99	22.51–142.14	34.10–69.73	0.02–0.09	0.001–0.01	1.59–7.28	0.01–0.18	229.30–1153.61
Q_L–Q_U	418.73–557.02	89.63–107.9	0.13–0.35	47.41–81.02	34.99–42.88	0.03–0.04	0.002–0.006	1.94–2.60	0.03–0.06	330.96–716.14
					Total n = 33					
AM ± SD	469.90 ± 146.80	98.90 ± 12.37	0.31 ± 0.24	58.03 ± 38.78	44.10 ± 16.10	0.04 ± 0.03	0.005 ± 0.005	1.87 ± 1.18	0.05 ± 0.04	612.87 ± 351.95
Med.	449.20	97.62	0.23	45.75	41.01	0.04	0.003	1.72	0.04	511.46
Range	295.70–881.60	76.73–129.09	0.08–0.99	12.73–142.97	25.15–116.82	0.02–0.09	0.001–0.03	0.35–7.28	0.01–0.18	229.9–1815.18
Q_L–Q_U	370.70–513.34	89.63–103.70	0.15–0.36	28.98–69.95	34.99–46.70	0.03–0.04	0.001–0.006	1.34–2.14	0.02–0.05	330.96–874.01
					Female versus Male					
U	NS	NS	NS	NS	NS	NS	NS	48	NS	NS
p								0.01		

AM: arithmetic mean; SD: standard deviation; Q_L: lower quartile; Q_U: upper quartile; U: Mann-Whitney U test; p: level of significance; NS: nonsignificant difference.

Table 2: The concentration ratios chemical elements in human tibial plateau from patients after knee surgery (mg/kg dm).

	Se/Pb	Se/Cd	Se/THg	$F^-/Ca \cdot 1000$
		Female ($n = 22$)		
AM ± SD	0.03 ± 0.02	1.53 ± 1.12	19.13 ± 12.84	41.28 ± 21.81
Med.	0.03	1.15	14.56	40.16
Range	0.009–0.10	0.35–4.93	0.35–4.93	13.19–91.27
Q_L–Q_U	0.02–0.03	0.77–2.17	8.56–32.99	22.90–49.70
		Male ($n = 11$)		
AM ± SD	0.02 ± 0.02	1.30 ± 1.32	14.74 ± 13.84	39.52 ± 18.74
Med.	0.02	0.94	8.63	34.40
Range	0.01–0.04	0.18–4.5	3.12–47.41	16.40–73.82
Q_L–Q_U	0.01–0.02	0.42–1.32	4.70–18.51	19.90–54.97
		Total $n = 33$		
AM ± SD	0.03 ± 0.02	1.45 ± 1.17	17.66 ± 13.13	40.69 ± 20.56
Med.	0.02	1.05	13.40	37.71
Range	0.02–0.10	0.18–4.93	0.94–47.41	13.20–91.27
Q_L–Q_U	0.02–0.03	0.76–2.13	8.04–31.41	22.90–53.60
		Female versus Male		
U	35	NS	NS	NS
p	0.001			

AM: arithmetic mean; SD: standard deviation; Q_L: lower quartile; Q_U: upper quartile; U: Mann-Whitney U test; p: level of significance; NS: nonsignificant difference; $F^-/Ca \cdot 1000$: F^- concentration in the inorganic portion of bone.

Table 3: The concentrations of chemical elements and Se/elements ratios (mg/kg dm) in smokers and nonsmokers among examined patients (mg/kg dm).

Parameter	Mn	Pb	Cd	THg	Se/Pb	Se/Cd	Se/THg
			Smokers ($n = 18$)				
AM ± SD	0.31 ± 0.25	2.32 ± 1.38	0.06 ± 0.05	0.01 ± 0.01	0.02 ± 0.02	1.12 ± 1.11	14.18 ± 18.90
Med	0.22	2.09	0.04	0.004	0.02	0.80	8.36
Range	0.08–0.99	0.45–7.28	0.01–0.18	0.001–0.030	0.06–0.08	0.18–4.93	0.94–33.73
Q_L–Q_U	0.13–0.36	1.72–2.50	0.03–0.08	0.001–0.006	0.01–0.02	0.44–1.20	6.36–26.61
			Nonsmokers ($n = 15$)				
AM ± SD	0.32 ± 0.22	1.34 ± 0.57	0.03 ± 0.03	0.003 ± 0.002	0.04 ± 0.02	1.85 ± 1.16	21.85 ± 13.74
Med	0.28	1.45	0.03	0.002	0.03	1.40	18.52
Range	0.11–0.85	0.35–2.33	0.01–0.13	0.001–0.009	0.02–0.10	0.35–4.49	3.12–47.40
Q_L–Q_U	0.15–0.40	0.90–1.67	0.02–0.04	0.001–0.005	0.02–0.05	0.93–2.90	10.17–35.90
			Smokers versus Nonsmokers				
U	NS	49.0	74	NS	54	72	79
p		0.001	0.03		0.01	0.02	0.04

AM: arithmetic mean; SD: standard deviation; Q_L: lower quartile; Q_U: upper quartile; U: Mann-Whitney U test; p: level of significance; NS: nonsignificant difference.

concentration of Mn, which was close to statistical significance ($U = 67.0$, $p = 0.06$). Se and Mn concentrations for WS (0.047 and 0.38 mg/kg dm) were 1.4 and 1.3 times higher than for NS (0.034 and 0.29 mg/kg dm, resp.). Differences in chemical element contents in the bone samples between the patients with and without implants only proved to be statistically significant with regard to Fe level ($U = 30.0$, $p < 0.01$), at 106.13 and 45.09 mg/kg dm, respectively.

The greatest positive correlations were found between the concentrations of Pb and/or Cd/Ca, and the number of cigarettes smoked (Table 4). Correlation analysis showed an inverse correlation between Se/Pb ratio in the cigarette smokers, Se/THg ratio, and a fish and seafood diet. Negative

Table 4: Spearman correlation coefficients between chemical elements content, the concentration ratios, and environmental exposure factors.

	Fe	THg	Pb	Cd	Se/Pb	Se/THg	Cd/Ca	Se	$F^-/Ca \cdot 1000$
Age	0.39^{xx}	NS	NS	NS	NS	NS	NS	NS	0.30^{x}
Implants	0.48^{xxx}	NS	NS	NS	NS	NS	NS	NS	NS
Number of cigarettes smoked/day	NS	0.37^{xx}	0.71^{xxxx}	0.51^{xxx}	-0.48^{xxx}	NS	0.53^{xxx}	NS	NS
Fish and sea food diet	NS	0.42	NS	NS	NS	-0.36^{xxxx}	NS	0.32^{x}	NS
Sport activity	NS	NS	NS	NS	NS	NS	NS	-0.33^{x}	NS
Dental amalgams fillings	NS	NS	NS	NS	NS	NS	NS	NS	NS

Significant level: $^{x}p = 0.06$; $^{xx}p < 0.05$; $^{xxx}p < 0.01$; $^{xxxx}p < 0.001$; NS: nonsignificant difference; $F^-/Ca \cdot 1000$: F^- concentration in the inorganic portion of bone.

correlation close to significance between Se and sport activity was observed in the patients with OA.

Significant positive correlation coefficients were found for the relationships K-Cd, Zn-Sr, Zn-F^-, THg-Pb, Pb-Cd, Se-Se/Pb, Se-Se/Cd, Se/Pb-Se/Cd, Pb-Cd/Ca, Cd-Cd/Ca, and F^--F^-/Ca·1000. Significant negative correlations were found for the relationship THg-Se/Pb, Pb-Se/Pb, Cd-Se/Pb, K-Se/Cd, Pb-Se/Cd, Cd-Se/Cd, THg-Se/THg, Pb-Se/THg, Se-Pb/Cd, Zn-Cd/Ca, and Se/Cd-Cd/Ca.

4. Discussion

Some publications indicate that the levels of potentially toxic elements in bone depend on the gender of participants. In this study, the Pb concentration and Se/Pb ratio were higher in the men than in the women (Table 1). Similarly, in a previous analysis we observed that Pb concentration in the cartilage with cortical bone was about 28% higher in men than in women [10]. Also S. Zaichick and V. Zaichick [21] and Kubaszewski et al. [22] report higher Pb concentrations of males compared to females in the ribs and femoral head, respectively.

In the case of certain medical conditions including OA, osteoporosis, bone cancers, Ewing's sarcoma, and osteomyelitis, there are reports of both typical as well as reduced or elevated concentrations of various trace elements [8, 23–25]. In this study, element levels in the tibial plateau in the patients with OA can be arranged in the following descending order: F^- > K > Zn > Fe > Sr > Pb > Mn > Se > Cd > THg. A slightly different order in OA patients is presented by Lanocha et al. Fe > Zn > Sr > Se > Mn > Pb; Se and Pb concentrations in bone without osteoarticular degeneration are over 4 times higher than in bone with osteoporosis. In this research, the concentrations of Zn, Pb, Cd, and THg in cancellous bone of the patients with osteoporosis were 1.3, 3.7, 1.9, 1.5, and 2 times higher than in our previous research [24].

Osteoporosis and OA are both common conditions with a high age-related prevalence, and a large variety of intrinsic and extrinsic factors are involved in both diseases. Thomsen et al. [26] found that patients with OA have significantly higher Zn levels in serum and lower Zn levels in urine than osteoporotic patients, whereas Zn level in bone does not differ, which is consistent with the levels of Zn in the bone of the patients with OA and KI evaluated in this study. Zn concentrations in the bone samples were the same in both groups of patients with OA and KI, probably because Zn is firmly bound to bone and is not easily released in the case of a negative Zn balance. In our study the concentrations of Zn and Pb in the tibial plateau were higher than in the femur head in patients with OA [22].

Long-term exposure to Cd may result in skeletal disorders, that is, osteoporosis or osteomalacia with an increased number of bone fractures [8]. Wiechuła et al. [27] report that Pb and Cd concentrations in the femoral head of patients with coxarthrosis is equal to about 3 mg/kg and 0.07 mg/kg, respectively, and is higher than in the tibial plateau of patients with OA evaluated in this study. However, the Cd concentration in cortical bone from the femur head with coxarthrosis [28] is similar to the concentration of Cd in the tibial plateau of patients with OA. Much higher Cd levels are found in patients with degenerative changes of the hip joint from the Upper Silesian Region [8].

In this study, we observed a weak correlation between F^-/Ca·1000 and the age of the patients. Bohatyrewicz [13] proved that F^-/Ca·1000 is correlated with age and shows higher values in patients who had trochanteric fracture in older age. This could be due to the artificial fluoridation of drinking water, which ceased in Poland in the 1990s. The permissible F^- concentration in water in Poland is 1.5 mg·L^{-1}, while in tap water from the area of northwestern Poland, F^- concentration does not exceed 0.3 mg·L^{-1} [29]. Currently, in accordance with applicable law, measurements of air fluoride concentrations are not carried out in Poland or in other countries of the European Union.

The concentrations of elements are varied and depend on the geographical location. Se concentrations in human tissues obtained from adults in Japan, USA, and Canada are much higher than those in Poland, as they depend on the geographical location which determines Se content in the diet [30]. A large part of Europe, including some regions of Poland, is considered to be deficient in Se [19]. In our research, we observed a significant difference in the Se levels of Se patients coming from different parts of northern and western Poland. Low levels of Se (<0.05 mg/kg dm) contained in bone samples are probably an effect of its deficiency in the diet and depend on the region of the country. In Poland, the levels of Se in plasma depend on the geographical location; in the central, northern and northwestern parts they are estimated at 78.0, 72.3, and 54.8 μg/L, respectively [31].

In this study, the concentrations of Pb and THg in the OE patients following knee surgery were over 1.4 and 1.7 times higher than in the UE participants. In 2005, the emissions of Pb, Cd, and THg in Poland reached 526 t, 46 t, and 20.1 t, with the highest Pb, Cd, and THg emissions reported in the following voivodships: Lower Silesian and Silesian (167 t; 8 t, and 3.5 t) while the lowest in Lubuskie (3.7 t, 0.9 t, and 0.2 t) [15]. The largest concentrations of Cd were observed in patients from Upper Silesia and Cracow. They were over 20 and 1.3 times higher than in the occupationally exposed participants examined in this study [6, 8]. Kwapuliński et al. [32] state that cortical bone from the femur head of patients from the Upper-Silesian Industrial District contained the highest concentrations of THg ever reported in Poland—20 times higher than the THg levels found in the OE patients examined in this study.

Compared to data on Western Pomerania from our 2012 study, Pb and Cd levels in the cartilage and compact bone of the femoral head were lower by nearly 5 and 2 times than the levels observed in the OE patients [10]. Even higher Cd concentrations in bone were found in people living in highly industrialized Taiwan [33]. In patients living in various Asian countries (including South Korea and Taiwan) who had not been occupationally exposed to Pb and THg, there were much higher levels of Pb and THg than in the participants of our study [34].

Cigarette smoking is a major exposure route for Cd and Pb in the general population. Little is known about the effect of smoking on the pathogenesis and progression of symptomatic osteoarthritis of the knee, one of the leading causes of disability in elderly people. Amin et al. [35] indicate that men with symptomatic knee osteoarthritis who smoke have an increased risk of articular cartilage loss and more severe knee pain than men who do not smoke. In our study we found that Pb and Cd concentrations were higher in the group of smokers than in nonsmokers. In scientific literature, Pb and Cd concentrations in bone samples obtained from smokers vary and could be placed in the following decreasing order: 10 > 8 > 4.26 > 2.32 > 2.11 > 1.38 > 0.93 > 0.586 and 0.89 > 0.65 > 0.57 > 0.4 > 0.07 > 0.06 > 0.05 > 0.028 mg/kg dm, respectively (see [8, 14, 24, 36–39], this study). While a number of publications indicate a positive correlation between smoking and the incidence of vertebral, forearm, and thigh fractures, we detected a correlation between the concentration of Pb and/or Cd/Ca and the number of cigarettes smoked. Furthermore, a comparison of the concentration ratios in bone samples obtained from the smokers and nonsmokers allowed an assessment of Cd and Pb stress. Brodziak-Dopierała et al. [37] report increased Pb/Fe and Pb/Mn ratios in the bones of male smokers compared with nonsmokers. In this study, we found significantly higher Se/Pb, Se/Cd, Se/THg, and Cd/Ca ratios in the nonsmokers. Most likely, this is a result of Se interacting with the highly toxic elements and displacing them from the metallothionein complex, which leads to a reduction in the toxicity of i.a. Cd, Pb, and THg. Moreover, a correlation analyzed in this study showed an inverse correlation between Se/Pb ratio and the number of cigarettes smoked.

According to the American Dental Association, dental amalgam fillings do not cause any harmful effects; hypersensitivity to THg may occur in approximately 1% of the population. However, people with amalgam fillings do have significantly elevated THg levels in blood, about 3 to 5 times more THg in urine and 2 to 12 times more THg in their body tissues than individuals without dental amalgams. Hajduga and Jędrzejczyk [40] indicate that silver amalgam fillings cause an increase in the levels of THg and Pb in tooth tissues. Available scientific literature finds no relevant comparative data on dental amalgam fillings and THg concentration in bone. In this study, the THg levels in the patients with DA were over 1.5 times higher than in the patients from the NDA group.

Food is considered to be one of the main routes of entry for THg and Se into the human body. Marine fish at the top of the aquatic food chain contain, for instance, elevated levels of both toxic and essential elements, including THg and Se [41]. In Poland, the average Hg contamination of fish and seafood is 0.035 and 0.022 mg/kg, respectively. The consumption of THg in fish and seafood by an adult weighing 60 kg is estimated at 3.2% and 5.6% of PTWI (Provisional Tolerable Weekly Intake). The daily intake of Se in Poland is 0.06 mg, whereas the world average ranges from 0.03 to 0.5 mg—with seafood being one of the major sources of Se [15]. Lanocha et al. [24] show that THg concentrations in cartilage with adjacent compact bone were the lowest in the groups of patients who did not or only rarely ate fish and seafood and were almost twice as high in those consuming fish and seafood several times a month. In this study, there were statistically confirmed differences in Se, THg levels and Se/THg ratio in the tibial plateau between individuals consuming fish and seafood and those who did not prefer such a diet. The lowest concentrations of Se and THg were reported in the NFD group, being higher in FD patients. The tibial bone samples of patients from the FD group were characterized by a smaller Se/THg ratio compared to NFD, although dietary Se is postulated to protect against THg. In our research we observed a negative relationship between Se/THg ratio and fish and seafood diet.

Dietary supplements contain mostly vitamins and minerals and also amino acids, fatty acids, fiber, and various vegetable products, among others. Patients with OA and joint injuries most often supplement themselves with glucosamine, chondroitin, and methylsulfonylmethane, although available research does not unequivocally confirm that the use of such supplements has a positive effect [42]. In this study we observed significant differences in the concentration of Se in the patients receiving dietary supplementation, although it should be pointed out that it may be toxic at higher concentrations, as the difference between the therapeutic and toxic levels is narrow.

Osteolysis surrounding an implant is a complex biochemical process closely linked to the mechanical functioning of the implant. The presence of material implanted in the body and its corrosion leading to metallosis may also become a source of microelements including Fe and cause adverse reactions in the body. In this study, Fe levels in the patients with surgical implants were over two times higher than in

Table 5: Spearman correlation coefficients between chemical elements contents and the concentration ratios in tibial plateau from patients who had undergone knee joint arthroplasty.

	K	Zn	Sr	F^-	Se	THg	Pb	Cd	Se/Pb	Se/Cd	Se/THg	Cd/Pb	Cd/Ca	$F^-/Ca \cdot 1000$
K	—													
Zn	NS	—												
Sr	NS	0.43^{xxx}	—											
F^-	NS	0.36^{xx}	NS	—										
Se	NS	NS	NS	NS	—									
THg	NS	NS	NS	NS	NS	—								
Pb	NS	NS	NS	NS	NS	0.53^{xx}	—							
Cd	0.42^{xx}	NS	NS	NS	NS	NS	0.47^{xxx}	—						
Se/Pb	NS	NS	NS	NS	0.47^{xxx}	-0.31^{xx}	-0.74^{xxx}	-0.38^{xx}	—					
Se/Cd	-0.41^{xx}	NS	NS	NS	0.34^{xxx}	NS	-0.32^{xx}	-0.90^{xxx}	0.46^{xxx}	—				
Se/THg	NS	NS	NS	NS	NS	-0.37^{xx}	-0.48^{xx}	NS	NS	NS	—			
Pb/Cd	NS	NS	NS	NS	-0.38^{xx}	NS	NS	NS	NS	NS	NS	—		
Cd/Ca	NS	-0.32^{xx}	NS	NS	NS	NS	0.45^{xxx}	0.97^{xxxx}	NS	-0.88^{xxxx}	NS	NS	—	
$F^-/Ca \cdot 1000$	NS	NS	NS	0.96^{xxxx}	NS	NS	NS	NS	NS	NS	NS	NS	NS	—

Significant level: $^{xx}p < 0.05$; $^{xxx}p < 0.01$; $^{xxxx}p < 0.001$; NS: nonsignificant difference; $F^-/Ca \cdot 1000$: F^- concentration in the inorganic portion of bone.

the patients without implants. Scientific literature does not provide any appropriate comparative data, although Sidun and Dabrowski [43] have proven the transition of metal ions from the surface of the implant to the bone.

The Osteoarthritis Research Society International recommends only moderate levels of exercise for people with OA to prevent joint overload caused by higher levels of physical activity [44]. In this research we detected a statistically significant negative correlation between Se concentration and sport activity in the patients with OA.

Imbalances in the metabolism of trace metals may lead to metal interactions with potential pathophysiological significance. Knowledge of these correlations is essential for the understanding of kinetic interactions of trace metals in the body [45]. The results of such interactions are highly variable and range from antagonistic to synergistic depending on the metal, its external concentration and exposure, exposure period, and specific organs [14, 17]. We observed positive correlations between THg-Pb and THg-Pb/Cd (Table 5). Additionally, research by Brodziak-Dopierala et al. [14] performed on trabecular bone samples taken from human femoral heads reveals interactions between Pb and Cd with a high correlation coefficient. Bogunia et al. [38] show the correlation coefficient between K-Cd in bone samples. Kwapuliński et al. [32] report that THg is correlated with Pb in cancellous and cortical bone, and we observed a similar relationship in our research. Furthermore, we found antagonistic relationship between element levels and concentration ratios: K-Se/Cd.

Selenium protects against the toxicity of several metals including THg, Pb, and Cd, and in this study we observed negative interactions for the relationship Se-Pb/Cd, Se-Pb/Cd, THg-Se/Pb, THg-Se/THg, Pb-Se/Pb, Pb-Se/Cd, Pb-Se/THg, Cd-Se/Pb, and Cd-Se/Cd, which may neutralize heavy metal toxicity by the formation of poorly soluble selenides excluding those metals from biochemical processes [15]. In addition, selenoproteins are antioxidant enzymes that participate in maintaining cell redox balance, which is important in the regulation of inflammation and bone cell proliferation/differentiation.

5. Conclusions

The results reported here may provide a basis for establishing reference values for the tibial plateau in patients with OA who had undergone knee replacement surgery. Our results may lead to a better understanding of the pathogenesis of bone with OA and an improvement in diagnostic efficiency, particularly in patients with symptomatic knee osteoarthritis who smoke, as smoking is a potentially modifiable risk factor.

Conflict of Interests

The authors declare that there is no conflict of interests regarding the publication of this paper.

Acknowledgment

Pomeranian Medical University in Szczecin (PUM) provided financial support (FSN-431-16/13).

References

[1] M. Blagojevic, C. Jinks, A. Jeffery, and K. P. Jordan, "Risk factors for onset of osteoarthritis of the knee in older adults: a systematic review and meta-analysis," *Osteoarthritis and Cartilage*, vol. 18, no. 1, pp. 24–33, 2010.

[2] M. Chojnacki, A. Kwapisz, M. Synder, and J. Szemraj, "Osteoarthritis: etiology, risk factors, molecular mechanisms,"

Advances in Hygiene and Experimental Medicine, vol. 68, pp. 640–652, 2014.

[3] M. Englund and L. S. Lohmander, "Risk factors for symptomatic knee osteoarthritis fifteen to twenty-two years after meniscectomy," *Arthritis & Rheumatism*, vol. 50, no. 9, pp. 2811–2819, 2004.

[4] P. Croft and E. Hay, "Osteoarthritis in primary care," *British Medical Journal*, vol. 333, no. 7574, pp. 867–868, 2006.

[5] L. Hendren and P. Beeson, "A review of the differences between normal and osteoarthritis articular cartilage in human knee and ankle joints," *Foot*, vol. 19, no. 3, pp. 171–176, 2009.

[6] A. Jurkiewicz, D. Wiechuła, R. Nowak, T. Gaździk, and K. Loska, "Metal content in femoral head spongious bone of people living in regions of different degrees of environmental pollution in Southern and Middle Poland," *Ecotoxicology and Environmental Safety*, vol. 59, no. 1, pp. 95–101, 2004.

[7] B. Brodziak-Dopierała, J. Kwapuliński, K. Sobczyk, and D. Wiechuła, "The content of manganese and iron in hip joint tissue," *Journal of Trace Elements in Medicine and Biology*, vol. 27, no. 3, pp. 208–212, 2013.

[8] B. Brodziak-Dopierała, J. Kwapuliński, K. Sobczyk, and D. Wiechuła, "Analysis of the content of cadmium and zinc in parts of the human hip joint," *Biological Trace Element Research*, vol. 163, no. 1-2, pp. 73–80, 2015.

[9] J. Kwapuliński, J. Mirosławski, D. Wiechuła, A. Jurkiewicz, and A. Tokarowski, "The femur capitulum as a biomarker of contamination due to indicating lead content in the air by participation of the other metals," *Science of the Total Environment*, vol. 175, no. 1, pp. 57–64, 1995.

[10] N. Lanocha, E. Kalisinska, D. I. Kosik-Bogacka, H. Budis, S. Sokolowski, and A. Bohatyrewicz, "Concentrations of trace elements in bones of the hip joint from patients after hip replacement surgery," *Journal of Trace Elements in Medicine and Biology*, vol. 26, no. 1, pp. 20–25, 2012.

[11] S. Zaichick and V. Zaichick, "The effect of age and gender on 38 chemical element contents in human femoral neck investigated by instrumental neutron activation analysis," *Biological Trace Element Research*, vol. 137, no. 1, pp. 1–12, 2010.

[12] Z. Noor, S. B. Sumitro, M. Hidayat, A. H. Rahim, A. Sabarudin, and T. Umemura, "Atomic mineral characteristics of Indonesian osteoporosis by high-resolution inductively coupled plasma mass spectrometry," *The Scientific World Journal*, vol. 2012, Article ID 372972, 6 pages, 2012.

[13] A. Bohatyrewicz, "Effects of fluoride on bone metabolism and mechanical competence: clinical observations and experimental studies in rats. Habilitation thesis," *Annales Academiae Medicae Stetinensis*, vol. 73, pp. 1–85, 2002.

[14] B. Brodziak-Dopierala, J. Kwapulinski, D. Kusz, Z. Gajda, and K. Sobczyk, "Interactions between concentrations of chemical elements in human femoral heads," *Archives of Environmental Contamination and Toxicology*, vol. 57, no. 1, pp. 203–210, 2009.

[15] A. Kabata-Pendias and B. Szteke, *Trace Elements in Geo- and Biosphere*, Institute of Soil Science and Plant Cultivation, Puławy, Poland, 2012.

[16] H. Budis, E. Kalisinska, N. Lanocha et al., "The concentration of manganese, iron, and strontium in hip joint bone obtained from patients undergoing hip replacement surgery," *Journal of Trace Elements in Medicine and Biology*, vol. 28, no. 1, pp. 39–44, 2014.

[17] M. Martiniakova, R. Omelka, A. Jancova, G. Formicki, R. Stawarz, and M. Bauerova, "Accumulation of risk elements in kidney, liver, testis, uterus and bone of free-living wild rodents from a polluted area in Slovakia," *Journal of Environmental Science and Health. Part A Toxic/Hazardous Substances and Environmental Engineering*, vol. 47, no. 9, pp. 1202–1206, 2012.

[18] K. Zhu, A. Devine, and R. L. Prince, "The effects of high potassium consumption on bone mineral density in a prospective cohort study of elderly postmenopausal women," *Osteoporosis International*, vol. 20, no. 2, pp. 335–340, 2009.

[19] B. Pilarczyk, A. Tomza-Marciniak, A. Mituniewicz-Małek et al., "Selenium content in selected products of animal origin and estimation of the degree of cover daily Se requirement in Poland," *International Journal of Food Science and Technology*, vol. 45, no. 1, pp. 186–191, 2010.

[20] M. Palczewska-Komsa, E. Kalisińska, D. I. Kosik-Bogacka et al., "Fluoride in the bones of foxes (*Vulpes vulpes* Linneaus, 1758) and raccoon dogs (*Nyctereutes procyonoides* Gray, 1834) from North-Western Poland," *Biological Trace Element Research*, vol. 160, no. 1, pp. 24–31, 2014.

[21] S. Zaichick and V. Zaichick, "The effect of age and gender on 38 chemical element contents in human iliac crest investigated by instrumental neutron activation analysis," *Journal of Trace Elements in Medicine and Biology*, vol. 24, no. 1, pp. 1–6, 2010.

[22] Ł. Kubaszewski, A. Zioła-Frankowska, M. Frankowski et al., "Comparison of trace element concentration in bone and intervertebral disc tissue by atomic absorption spectrometry techniques," *Journal of Orthopaedic Surgery and Research*, vol. 9, no. 1, article 99, 2014.

[23] T. R. Helliwell, S. A. Kelly, H. P. J. Walsh et al., "Elemental analysis of femoral bone from patients with fractured neck of femur or osteoarthrosis," *Bone*, vol. 18, no. 2, pp. 151–157, 1996.

[24] N. Lanocha, E. Kalisinska, D. I. Kosik-Bogacka et al., "The effect of environmental factors on concentration of trace elements in hip joint bones of patients after hip replacement surgery," *Annals of Agricultural and Environmental Medicine*, vol. 20, no. 3, pp. 487–493, 2013.

[25] V. Zaichick and S. Zaichick, "The Ca, Cl, Mg, Na, and P mass fractions in human bone affected by Ewing's sarcoma," *Biological Trace Element Research*, vol. 159, no. 1–3, pp. 32–38, 2014.

[26] J. S. Thomsen, P. T. Nielsen, P. H. Christensen et al., "Differences in zinc status, bone turnover and femoral head bone density and biomechanical properties between patients with osteoarthritis and osteoporosis," *The Journal of Musculoskeletal Neuronal Interactions*, vol. 8, no. 1, article 22, 2008.

[27] D. Wiechuła, A. Jurkiewicz, and K. Loska, "An assessment of natural concentrations of selected metals in the bone tissues of the femur head," *Science of the Total Environment*, vol. 406, no. 1-2, pp. 161–167, 2008.

[28] A. Jurkiewicz, D. Wiechuła, S. Mrozek, R. Nowak, and M. Służałek, "The cadmium contents in the femoral head in inhabitants of Upper Silesia," *Ortopedia Traumatologia Rehabilitacja*, vol. 3, no. 3, pp. 350–353, 2001.

[29] A. Lubkowska, "Assessment of the safety of drinking water in the West-Pomeranian voivodship, Poland," *Fresenius Environmental Bulletin*, vol. 18, no. 7, pp. 1086–1089, 2009.

[30] B. A. Zachara, H. Pawluk, E. Bloch-Boguslawska et al., "Tissue level, distribution, and total body selenium content in healthy and diseased humans in Poland," *Archives of Environmental Health*, vol. 56, no. 5, pp. 461–466, 2001.

[31] E. Hać, J. Krechniak, and M. Szyszko, "Selenium levels in human plasma and hair in northern Poland," *Biological Trace Element Research*, vol. 85, no. 3, pp. 277–285, 2002.

[32] J. Kwapuliński, Ł. Paprotny, A. Paukszto et al., "Influence of the type of tree habitat on the character of co-occurrence of Fe, Mn, Zn, Cu, Pb, Ni, Cr and Co in the soil of the Tatra Mountain National Park," *Annals of Agricultural and Environmental Medicine*, vol. 20, no. 3, pp. 494–499, 2013.

[33] H.-W. Kuo, S.-M. Kuo, C.-H. Chou, and T.-C. Lee, "Determination of 14 elements in Taiwanese bones," *Science of the Total Environment*, vol. 255, no. 1–3, pp. 45–54, 2000.

[34] Y. C. Yoo, S. K. Lee, J. Y. Yang et al., "Interrelationship between the concentration of toxic and essential elements in Korean tissues," *Journal of Health Science*, vol. 48, no. 2, pp. 195–200, 2002.

[35] S. Amin, J. Niu, A. Guermazi et al., "Cigarette smoking and the risk for cartilage loss and knee pain in men with knee osteoarthritis," *Annals of the Rheumatic Diseases*, vol. 66, no. 1, pp. 18–22, 2007.

[36] B. Brodziak-Dopierała, J. Kwapuliński, J. Rzepka, E. Nogaj, M. Bogunia, and B. Ahnert, "Influence of smoking tobacco on the occurrence metals in some parts and profiles of femur head," *Przegląd Lekarski*, vol. 64, no. 10, pp. 720–722, 2007.

[37] B. Brodziak-Dopierała, J. Kwapuliński, E. Kosterska, and J. Toborek, "Influence of passive smoking on content of aluminium in pharyngeal tonsils from children living in Southern Poland," *Przegląd Lekarski*, vol. 62, no. 10, pp. 1075–1078, 2005 (Polish).

[38] M. Bogunia, B. Brodziak-Dopierała, J. Kwapuliński, B. Ahnert, J. Kowol, and E. Nogaj, "The occurance lead and cadmium in hip joint in aspect of exposure on tobacco smoke," *Przegląd Lekarski*, vol. 65, no. 10, pp. 529–532, 2008 (Polish).

[39] F. García, A. Ortega, J. L. Domingo, and J. Corbella, "Accumulation of metals in autopsy tissues of subjects living in Tarragona County, Spain," *Journal of Environmental Science and Health, Part A: Toxic/Hazardous Substances and Environmental Engineering*, vol. 36, no. 9, pp. 1767–1786, 2001.

[40] M. Hajduga and D. Jędrzejczyk, "The amalgam as an additional risk to the patient," *Twój Przegląd Stomatologiczny*, vol. 5, pp. 31–34, 2002 (Polish).

[41] H. M. Chan, A. M. Scheuhammer, A. Ferran, C. Loupelle, J. Holloway, and S. Weech, "Impacts of mercury on freshwater fish-eating wildlife and humans," *Human and Ecological Risk Assessment*, vol. 9, no. 4, pp. 867–883, 2003.

[42] H. Bojarowicz and P. Dźwigulska, "Dietary supplements. Part II. Selected components of dietary supplements and their application," *Hygeia Public Health*, vol. 47, no. 4, pp. 433–441, 2012.

[43] J. Sidun and J. A. Dabrowski, "Biomechanical aspects of damage to facial skeleton fixation miniplates," *Motrol*, vol. 11, no. 11, pp. 176–181, 2009.

[44] J. A. Buckwalter and J. A. Martin, "Sports and osteoarthritis," *Current Opinion in Rheumatology*, vol. 16, no. 5, pp. 634–639, 2004.

[45] R. Rahil-Khazen, B. J. Bolann, A. Myking, and R. J. Ulvik, "Multi-element analysis of trace element levels in human autopsy tissues by using inductively coupled atomic emission spectrometry technique (ICP-AES)," *Journal of Trace Elements in Medicine and Biology*, vol. 16, no. 1, pp. 15–25, 2002.

Hindawi Publishing Corporation
BioMed Research International
Volume 2014, Article ID 548968, 11 pages
http://dx.doi.org/10.1155/2014/548968

Research Article

Study of the Polycarbonate-Urethane/Metal Contact in Different Positions during Gait Cycle

Sergio Gabarre,[1] Antonio Herrera,[2,3] Jesús Mateo,[2,3,4] Elena Ibarz,[1] Antonio Lobo-Escolar,[2,3,4] and Luis Gracia[1]

[1] *Department of Mechanical Engineering, Engineering and Architecture School, University of Zaragoza, María de Luna 3, 50018 Zaragoza, Spain*
[2] *Department of Surgery, Medicine School, University of Zaragoza, Domingo Miral s/n, 50009 Zaragoza, Spain*
[3] *Aragón Health Sciences Institute, Avenida San Juan Bosco 13, 50009 Zaragoza, Spain*
[4] *Department of Orthopaedic Surgery and Traumatology, Miguel Servet University Hospital, Avenida Isabel la Católica 3, 50009 Zaragoza, Spain*

Correspondence should be addressed to Luis Gracia; lugravi@unizar.es

Received 27 June 2014; Accepted 25 July 2014; Published 27 August 2014

Academic Editor: Kengo Yamamoto

Copyright © 2014 Sergio Gabarre et al. This is an open access article distributed under the Creative Commons Attribution License, which permits unrestricted use, distribution, and reproduction in any medium, provided the original work is properly cited.

Nowadays, a growing number of young and more active patients receive hip replacement. More strenuous activities in such patients involve higher friction and wear rates, with friction on the bearing surface being crucial to ensure arthroplasty survival in the long term. Over the last years, the polycarbonate-urethane has offered a feasible alternative to conventional bearings. A finite element model of a healthy hip joint was developed and adjusted to three gait phases (heel strike, mid-stance, and toe-off), serving as a benchmark for the assessment of the results of joint replacement model. Three equivalent models were made with the polycarbonate-urethane Tribofit system implanted, one for each of the three gait phases, after reproducing a virtual surgery over the respective healthy models. Standard body-weight loads were considered: 230% body-weight toe-off, 275% body-weight mid-stance, and 350% body-weight heel strike. Contact pressures were obtained for the different models. When comparing the results corresponding to the healthy model to polycarbonate-urethane joint, contact areas are similar and so contact pressures are within a narrower value range. In conclusion, polycarbonate-urethane characteristics are similar to those of the joint cartilage. So, it is a favorable alternative to traditional bearing surfaces in total hip arthroplasty, especially in young patients.

1. Introduction

The modern age of total hip arthroplasty (THA) began with Charnley in the 60s of past century [1]. This technique has entailed one of the greatest advances in orthopaedic surgery. Since long term survival of implants is a surgeon's primary goal, over the past half-century there have been important developments in implant designing, implant to bone fixation techniques, and bearing surfaces [2].

Nowadays, a growing number of young and more active patients receive hip replacement [3]. Increased and more strenuous activities in such patients involve higher friction moments and higher wear rates [4, 5]. As activity increases friction on the bearing surface increases accordingly, leading to a temperature rise which is a risk factor for implant stability in the long term [6]. As a consequence, increased friction can contribute to an aseptic loosening of implants in the mid and long term [7, 8]. Thus, friction reduction becomes crucial for the long term survival of hip arthroplasty [6].

The use of bearing surfaces with low wear rates is essential to prevent wear debris, which could trigger immunological reactions leading to aseptic loosening. At present, the most common bearing surfaces are as follows.

1.1. Metal on Metal Bearing (M-o-M). Apart from some historical precedents, McKee and Watson-Farrar designed in the 60s the first hip prosthesis with a M-o-M bearing surface [9]. Since then, several alternatives have emerged until hip

resurfacing appeared in the 90s [10]. Although M-o-M bearings have a low friction coefficient ($\mu = 0.004$), low wear rate (3.5 mm/year), and smaller wear debris particles than metal on polyethylene (UHMWPE) bearing couple [11], the risk of adverse biologic reactions caused by metallic debris and pseudotumors [12–15] has brought into question M-o-M bearings. Nevertheless, classic M-o-M hip implants, with mild contents of cobalt and chromium, have achieved superb long term outcomes [16–19]. We agree with Migaud et al. [20] that M-o-M bearing couplings are still useful provided that surgical indication, implant design, and surgical technique are suitable.

1.2. PE on Metal Bearing (PE-M). Polyethylene-metal bearing was introduced by Charnley more than fifty years ago. Its friction coefficient is within a range of 0.05–0.15. Conventional polyethylene has a high wear rate. The biological response to wear debris particles can lead to aseptic loosening of the femoral or, more often, the acetabular component. About 20% to 40% of all revision hip arthroplasties are due to aseptic loosening of implants [21]. Highly cross-linked polyethylene has lowered the amount of wear by 50–62% according to various studies [22–27]. But its use is discouraged in young patients with a high activity and long life expectancy [6–8].

1.3. Ceramic-on-Ceramic (C-o-C). Ceramic bearing surfaces were first introduced by Boutin in the 70s of past century [28] and have experienced a significant evolution. The introduction of the hot isostatic pressing (HIP), during the 90s, increased alumina's durability and the emergence of alumina matrix composite, at the beginning of the 21th century, improved mechanical wear resistance [29]. This fourth generation of composite ceramics of alumina matrix (BIOLOX Delta, CeramTec GmbH, Germany) is composed of 82% of alumina and 17% zirconia. Improved oxidation resistance, hardness and wear were achieved adding a 0.5% of chromium oxide [30]. C-o-C bearing has a friction coefficient of 0.09 and exhibits minimal wear (3.9 μm/year is estimated [31]). Some authors state that ceramic debris particles are within the same size range as those from polyethylene (mean size of 0.7 microns), which are able to generate a biologic response [32]. Conversely, a comparative work in the literature reported smaller size for wear particles of C-o-C (10–30 nm) than polyethylene particles (0.1–1.0 micron) [33]. Its major limitations are the dramatic cracking failure consequences and squeaking. Ceramic bearing surfaces are considered to be an excellent choice in THA in young patients [27, 30, 34, 35].

1.4. Polyethylene-Ceramic Bearing. The combination of polyethylene acetabular liners with zirconia femoral heads [36] began to be used in the 1980s. It has been proven that, after walking for an hour, a significant rise in temperature is produced inside the joint [37], which could contribute to polyethylene wear [38, 39]. In accordance with some authors this bearing coupling does not offer advantages over the polyethylene on metal option [40]. Nevertheless, there is some controversy about this aspect as recent works reported in the literature outlined that the lowest wear rate of PE is achieved when combined with ceramic Biolox heads [41–43].

1.5. Polycarbonate-Urethane-Metal Bearing (PCU-M). Friction minimizing between bearing surfaces remains crucial to ensure THA survival in the long term [6]. At the outset, clinical use of polyurethane was hampered by its manufacturing processes [44]. Over the last years, the polycarbonate-urethane Bionate 80A production has offered a feasible alternative to conventional bearings. Its biostability and high resistance to hydrolysis, oxidation, and calcification have been demonstrated in vitro. [45]. Three-year follow-up, in vivo studies have proved the absence of appreciable signs of biodegradation [46]. Comparative wear studies between PCU on metal and highly cross-linked polyethylene (including gamma irradiation) on metal over several million loading cycles showed that polyurethane has a lower wear rate, better corrosion resistance, and wear debris particles less prone to cause osteolysis [47–51]. All these polyurethane features make it a favorable alternative as THA bearing surface.

There is growing interest in this new coupling which has been subject of study in recent years. To our knowledge, no finite elements simulation study on this kind of material has been conducted so far. Therefore, our study can be assumed as an innovative research which supports and is added to all the aforementioned related works.

The aim of this work is to analyze the contact pressures generated during gait cycle in the polycarbonate-urethane/metal bearing, comparing the results with the corresponding to a healthy joint. Several finite element (FE) models were implemented in order to simulate different situations, both in the healthy joint and after total hip replacement. Three stages of the gait cycle were studied: heel strike, mid-stance and the late stance peak toe off.

2. Materials and Methods

A first FE model of a healthy hip joint was developed. The geometry of the model was obtained from a femur, pelvis, and sacrum of a 65-year-old male donor. A computed tomography (CT) scan (512 × 512 acquisition matrix, FOV = 240 mm, slice thickness = 0.5 mm in plane resolution) was obtained using a TOSHIBA Aquilion 64 scanner (Toshiba Medical Systems, Zoetermeer, The Netherlands). Stacks of images from each bone are processed using Mimics Software (Materialise, Leuven) [52]. Polylines referred to cortical and trabecular bone are exported to I-deas 11 NX Series software (Siemens, Plano, Texas) [53].

Afterwards, each of the bone components of the hip joint was examined by means of a 3D Roland PICZA (Irvine, California) scanner in order to get a better precision of the outer geometry. This device has a 0.2 mm voxel resolution and two sweep modes, rotational and plane-based type. The scanner provides a cloud of points representing the initial geometry and, by means of its own software, initial cleaning operations are performed: deleting abnormal surfaces and pulling the 3D image out of the scan noise. The next step is to convert the latter geometry to a polygonal mesh with

the Roland Pixform software (Irvine, California) [54]. In contrast to the first one, this software allows us a deeper geometry processing: global and local operations can be made by registering different scans of the same bone in order to get a wrapping group of surfaces where total number and order of their points of control can be modified.

The final geometry is imported to I-deas 11 NX Series software [53], where it is combined with the inner geometry previously obtained via CT scans. Based on the external and internal geometries, transition from cortical to cancellous bone is determined.

After defining the geometry of the different materials, the mesh can be generated. A sensitivity analysis was performed to determine the minimal size mesh required for an accurate simulation of contact. For this purpose, a mesh refinement was performed in order to achieve a convergence towards a minimum of the potential energy, both for the whole model and for each of its components, with a tolerance of 1% between consecutive meshes.

Due to the difficulties in obtaining accurate soft tissue images in CT scans, a methodology was developed to generate, into the model, those soft tissues needed to keep the contact between bearing surfaces. Geometry of the acetabular socket and the femoral head was used as a baseline to build up the geometry of both cartilages, which also come into contact with the labrum. According to several anatomical 3D atlas, three different zones of thickness were sketched onto the bone geometry, ranging from 0.5 mm to 2.0 mm. Auxiliary splines were used to shape several sections, from which both cartilage volumes were created. A similar technique was used to generate the labrum around the acetabular rim. A structured mesh of hexahedral elements was generated in both cartilages. This type of elements is more suitable for solving contact problems than tetrahedral ones [55].

After being meshed, the set of soft tissues and bones are joined in a unique model: the complete model of the hip joint. The final model is shown in Figures 1 and 2. The statistics of the FE model are presented in Tables 1 and 2.

Three FE models were made, one for each of the three most representative phases of gait cycle: heel strike, mid-stance and toe off. These three gait situations are simulated matching the behaviour of healthy model with the Tribofit system model [56]. The healthy joint model serves as a benchmark in the assessment of the results of joint replacement model. In the arthroplasty model, the Tribofit system buffer with shell was used. The system consists of a metallic shell which is inserted directly on the acetabulum and a PCU buffer insert placed on the inside of the shell (buffer-with-shell configuration). The femoral component consists of a spherical metallic head (Cobalt-Nickel-Chromium-Molybdenum alloy), a femoral stem (Ti6-Al4-V alloy), and a stem sleeve which is fixed on the neck of the stem to match the cone of the femoral head.

All the prosthetic components, with the exception of the femoral stem, can be modelled from analytical geometries. The geometry of the stem is more complex; therefore, the same procedure followed for the bones is applied to the stem. After obtaining the geometry of the implant, a surgery was done at the Department of Orthopaedic and Trauma Surgery of the Miguel Servet University Hospital. A senior surgeon implanted the femoral stem and the Tribofit buffer and shell in the cadaveric bones used in our study.

Table 1: Mesh statistics of the healthy model: bone.

Healthy model	Cortical bone	Cancellous bone	Element type
Femur	164818	63689	4-node linear tetrahedron
Pelvis	176729	39456	4-node linear tetrahedron
Half sacrum	92055	34505	4-node linear tetrahedron

Table 2: Mesh statistics of the healthy model: soft tissues.

Healthy model	Number of elements	Element type
Acetabular cartilage	12420	8-node linear brick
Femoral cartilage	12384	8-node linear brick
Labrum	6203	4-node linear tetrahedron
Capsule	36288	8-node linear brick
Fovea	7345	4-node linear tetrahedron
Transverse ligament	2328	4-node linear tetrahedron

Afterwards, a new 3D scan of the entire ensemble was made, and the surgical procedure was reproduced with the I-DEAS software. In this way, we ensure that implant's alignment and bone cuts are similar to those achieved in surgical conditions. The final FE model is shown in Figure 3. To guarantee the accuracy of the FE results, a sensitivity analysis was performed with a mesh refinement in order to achieve a convergence towards a minimum of the potential energy, with a 1% tolerance between consecutive meshes, for both the healthy and implanted models. The statistics of the FE model are presented in Tables 3 and 4. Material properties are included in Table 5 [57, 58].

Three gait phases were simulated: heel strike, midstance, and toe-off, developing three different FE models. The pelvic and the sacral bones were kept in same position in the three models, whereas femur was positioned 10° in anteversion (heel strike) and 0° (mid-stance) and 15° in retroversion (toe-off), respectively (according to bony landmarks described in [59]). Although the whole pelvis model was developed, only a hemipelvis model has been calculated and postprocessed for each group of models: the right side of the pelvis is defined as the healthy model and the left side is modeled as the operated one. Sacrum's sagittal plane is defined as the boundary limit. In both cases load is vertically applied at the top of the sacrum, and femur is fully constrained at its condyles, as shown in Figure 4. Body-weight (BW) loads where considered according to orthoload's database [59]: 230% BW toe-off, 275% BW mid-stance and 350% BW heel strike.

In addition, another key point to be studied is the comparative biomechanical function in different situations. This requires standardising the conditions of loads analysis and path contact distances. Computation and postprocessing were done using Abaqus version 6.12 program (Dassault Systèmes, Providence, Rhode Island) [55].

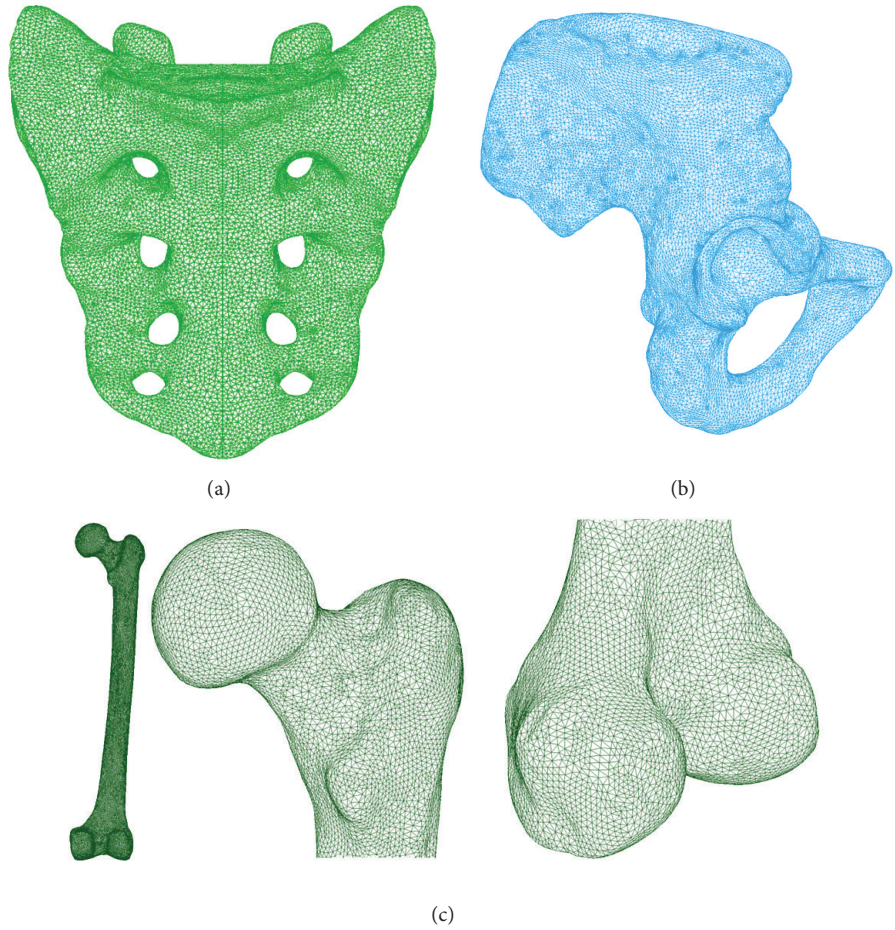

Figure 1: Final FE model of bones: (a) sacrum; (b) pelvis; (c) femur.

Table 3: Mesh statistics of model with Tribofit: bone.

Model with Tribofit	Cortical bone	Cancellous bone	Element type
Femur	93708	300036	4-node linear tetrahedron
Pelvis	337081	401196	4-node linear tetrahedron

Table 4: Mesh statistics of model with Tribofit: prosthesis.

Model with Tribofit	Number of elements	Element type
Shell	11808	6-node linear triangular prism, 8-node linear brick
Buffer	12672	6-node linear triangular prism, 8-node linear brick
Stem	31162	4-node linear tetrahedron
Mini stem	22773	4-node linear tetrahedron
Spherical head	7344	6-node linear triangular prism, 8-node linear brick
Stem sleeve	4608	6-node linear triangular prism, 8-node linear brick

Table 5: Material properties.

Elastic isotropic	Young modulus [MPa]	Poisson ratio
Cortical bone [58]	20000	0.3
Trabecular bone [58]	959	0.12
Cancellous bone [58]	1	0.3
Implant*	214000	0.3
Stem*	110316	0.3
Hyperelastic Mooney-Rivlin	C_{10} [MPa]	C_{01} [MPa]
Buffer*	2.912	−1.025
Hyperelastic Neo-Hookean	G [MPa]	K [Mpa]
Cartilage [57]	13.6	1.359

*Values supplied by the manufacturer [56].

3. Results

Results of the healthy model are presented for the three analyzed phases of gait, showing contact pressures between the femoral and the acetabular cartilages. Similarly, contact pressures between the buffer and the metallic femoral head

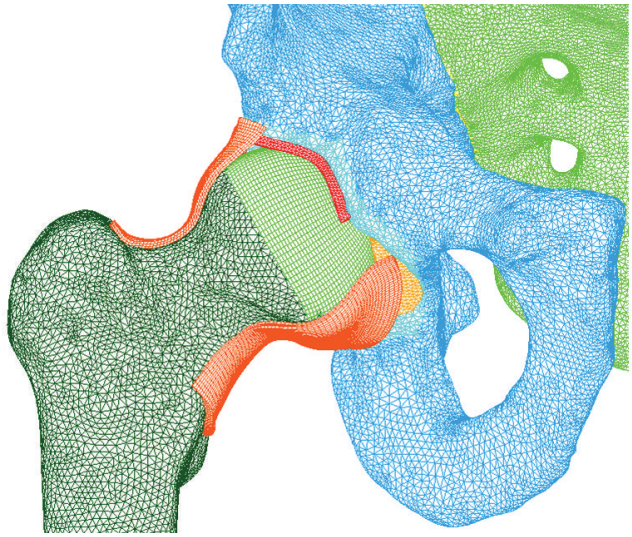

Figure 2: Final model of the complete healthy hip (joint's capsule is cut for a better visibility).

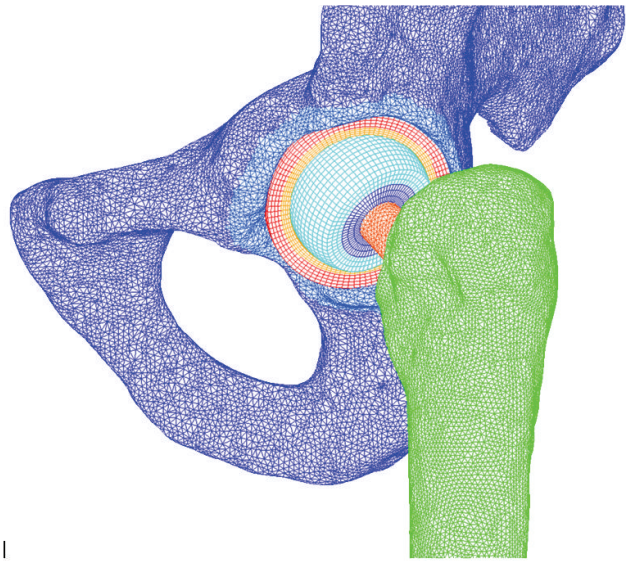

Figure 3: FE complete model with hip implant.

are shown in the prosthetic Tribofit model. Healthy model acts as benchmark for comparison of the prosthetic model results. Since contact tracks are tridimensional and, at times, quite irregular, two representative and nearly perpendicular paths traversing the maximum are chosen. Both paths provide information in the most relevant directions.

Results corresponding to the midstance phase are shown in Figure 5. So, Figure 5(a) illustrates the contact pressure map in the acetabular cartilage for the healthy joint, including the paths used for procesing the values shown in Figure 5, whereas Figure 5(b) corresponds to the contact pressure map for the polycarbonate-urethane cup in the replaced hip joint, including again the processed paths.

As can be seen in Figure 5, contact surface is smaller in the polycarbonate-urethane cup than in the acetabular cartilage and, consequently, the maximum contact pressure peak is higher in the former (Figure 6). The peak ratio between the two models is 2.57.

In the same way, heel strike results are presented in Figure 7. Figure 7(a), shows a bicentric contact pattern more marked than in the mid-stance phase, which is congruent with the femur positioning relative to the acetabulum. When compared to PCU joint, contact areas are similar and so, contact pressures are within a narrower value range (Figure 8). The peak ratio between the two models is 1.6.

Finally, it can be observed as the contact area migrates forward in the toe-off phase. Although the contact pattern of the healthy model is bicentric, it is less pronounced than in the midstance phase (see Figure 9). Contact areas in the healthy and operated models are similar; thereby, contact pressure ratio is nearly 1 (see Figure 10).

In view of this result, it can be concluded that PCU is a new bearing surface with stiffness close to that of healthy cartilage. That is why contact areas and pressures are in the same range of the healthy hip, mimicking the healthy cartilage accurately.

4. Discussion

In this paper, a pioneer investigation based on finite element simulations of hip arthroplasty with the new PCU soft bearing surface is presented.

Two finite element models of the entire hip joint were developed. The first one reproduces in a very reliable way the bone structure of the human hip joint, including cartilages and soft tissues, in order to assess the joint contact pressures during different phases of gait cycle. The second model was developed after replacing the hip joint with a metallic acetabular shell with a PCU buffer insert and a femoral stem with a metallic head, using a regular surgical technique. All the components were implanted at the donor's bones which had been used to develop the healthy model, so that the models were comparable. Simulations for the three gait phases were conducted in both models. Joint contact pressures were calculated in both models and were compared against each other.

The healthy model exhibits a wide contact pattern. Contact pressures reached 6 MPa for midstance, 10 MPa for heel strike, and 5 MPa for toe-off phase. These values are in range of other previous studies which stands the peak range in 8–12 MPa [57, 60].

The operated model with PCU buffer showed a narrower, but more uniform, contact pattern than the healthy model as a result of better geometry accuracy. Peak contact pressures reached 16.6 MPa in the midstance phase, 18 MPa in the heel strike, and 4.6 MPa in the toe-off phase. In the toe-off phase the whole "contact dome" is developed, producing a peak contact pressure even slightly lower than that of the healthy model. All the aforementioned values are very close to those obtained in healthy hip model simulations. However, the latter are much lower than values obtained with other bearing surfaces: ceramic-on-ceramic 40–250 MPa [61], metal-on-metal 200 MPa [62], metal-on-ceramic 40–112 MPa [63], and polyethylene-on-metal 22 MPa [63]. Contact pressure values

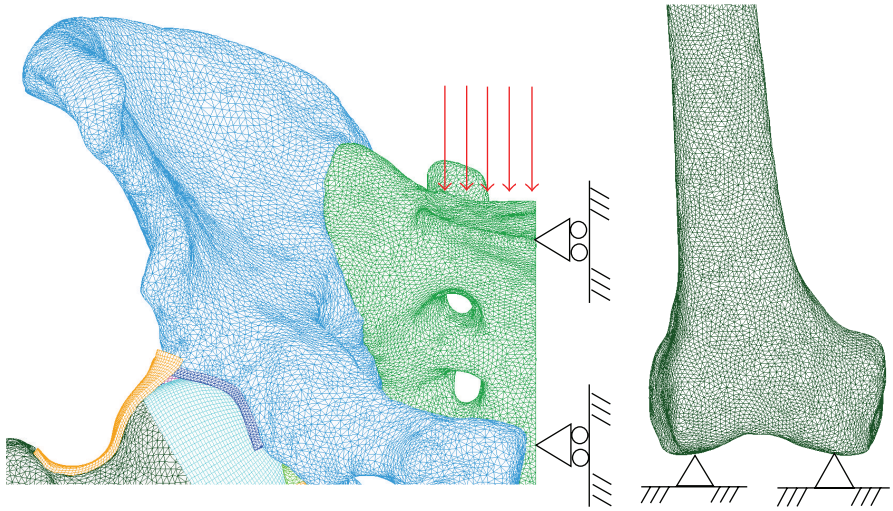

(a) (b)

Figure 4: Boundary conditions: (a) load and restraints on sacrum; (b) restraints at femoral condyles.

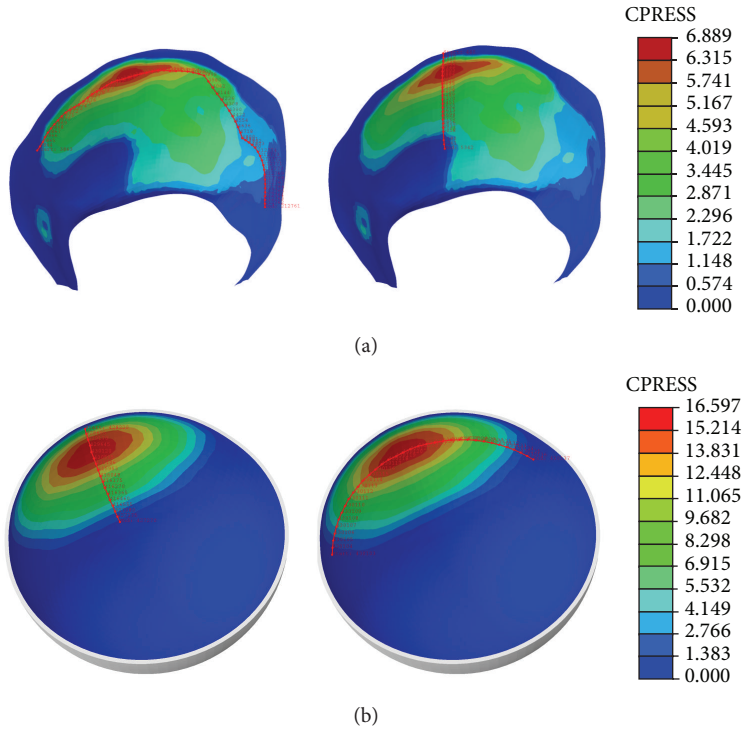

Figure 5: Contact track in midstance: (a) healthy model; (b) model with PCU.

are important because they modify the tribologic behavior of the implant and the wear rate over the time. Clearly, contact pressure values in the PCU model closely approximate to those of healthy model. Moreover, hydrophilic PCU feature promotes lubrication between bearing surfaces reducing wear. This fluid lubrication film is similar to that in the healthy joint and is thicker than in other bearing surfaces, providing an excellent lubrication [64]. Low contact pressure values combined with an improved lubrication result in a low wear debris rate [65].

Biocompatibility, biostability, and high oxidation, hydrolysis, and calcification resistance of PCU have been proved [45], and in vivo studies have confirmed its high biodegradation resistance [46]. All these features, together with a lower wear debris rate as compared with highly cross-linked polyethylene, good corrosion resistance, and osteolysis

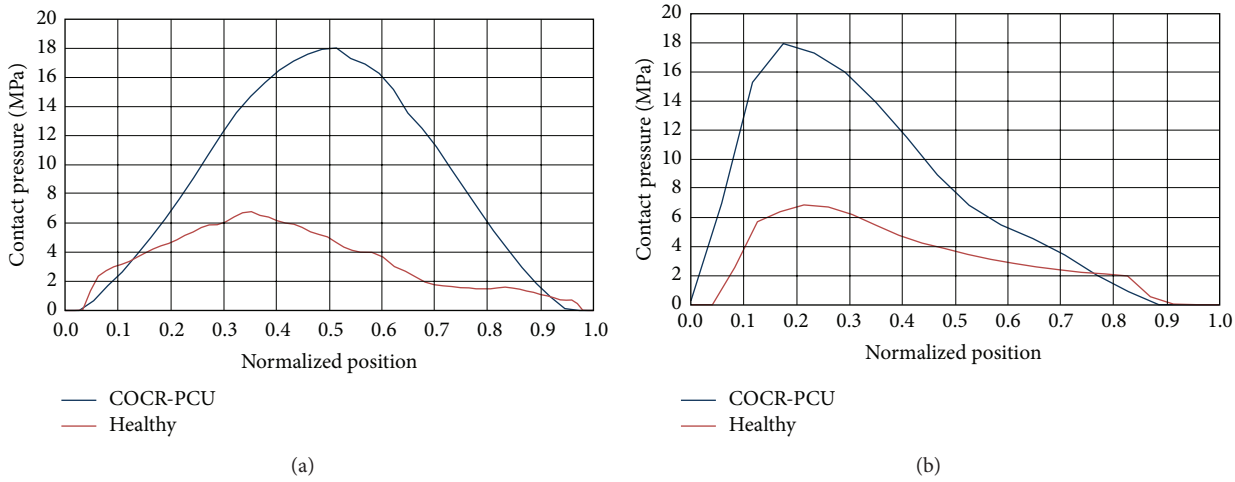

Figure 6: Comparative charts in mid-stance: (a) longitudinal path; (b) transversal path.

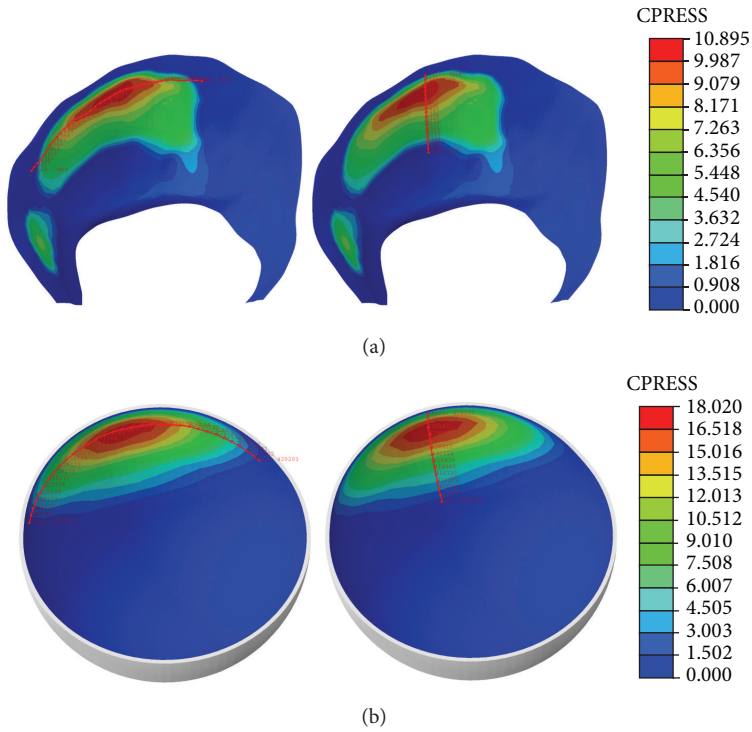

Figure 7: Contact track in heel strike: (a) healthy model; (b) model with PCU.

absence [47–51], make PCU a very suitable material for joint implants fabrication. Some previous studies have analyzed retrieved PUC buffers, measuring a minimum volumetric wear rate (1.4–14 mm^3/year), and a low number of wear debris particles without tissular reaction [66, 67], supporting previous in vivo studies [46]. Available clinical studies are based on small samples with a limited follow-up [68]. Long term follow-up studies are needed to ascertain that PCU can be an alternative to traditional bearing surfaces.

Two options have been suggested for using the PCU buffer. The first one uses PCU as a bearing surface interposed between the metal shell and the spherical metal head. Mechanically, this is the most suitable way of use in our opinion, because metallic wear debris and its harmful impact are prevented [69], improving the long term outcome of the implant without the issues of metal on metal bearing surface.

Another possibility is to fit the PCU buffer directly onto the osseous joint surface of the acetabulum. In this case, PCU

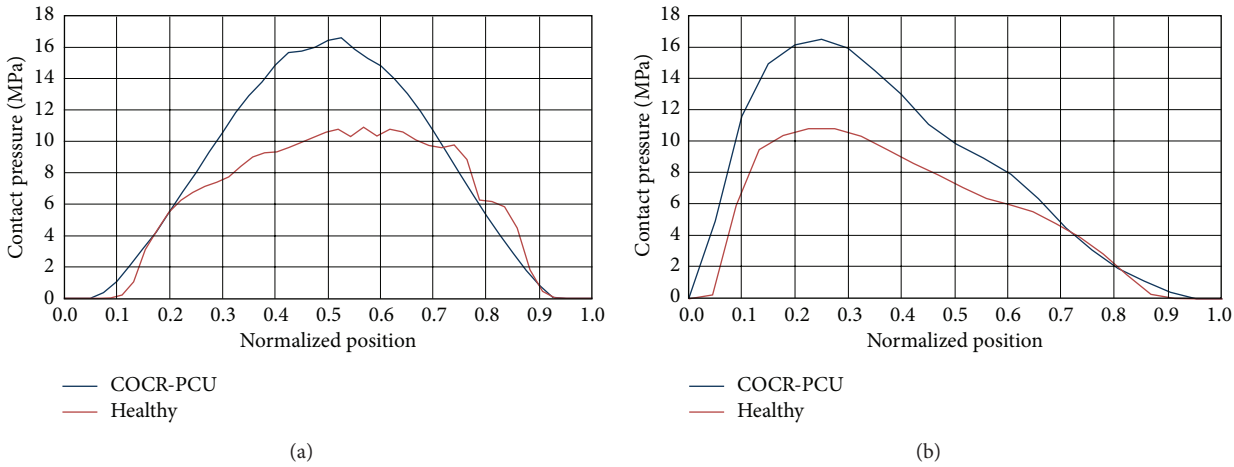

Figure 8: Comparative charts in heel strike: (a) longitudinal path; (b) transversal path.

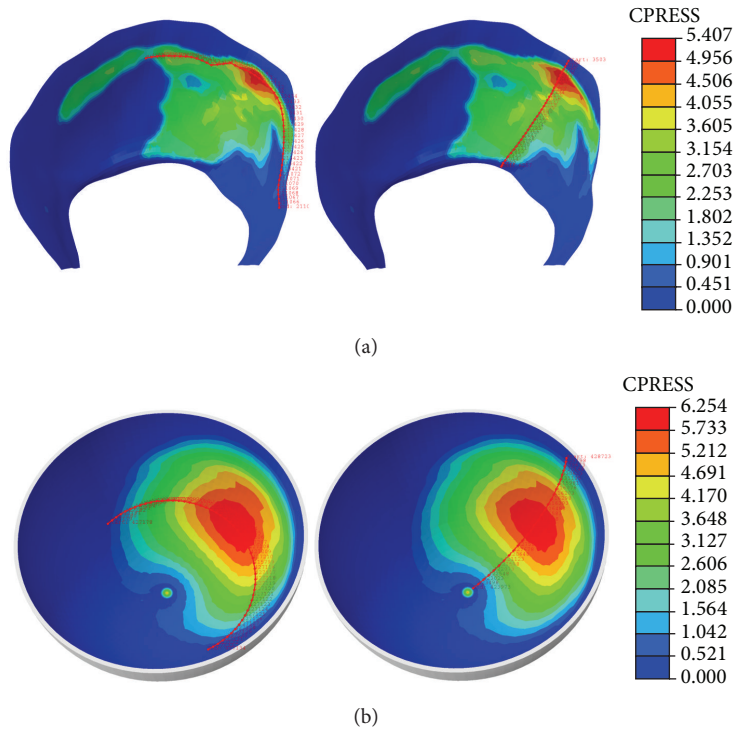

Figure 9: Contact track in toe-off: (a) healthy model; (b) model with PCU.

might be used as a total hip replacement in osteoarthritis, or as a hip replacement in femoral neck fractures. Though our experience in femoral neck fractures has been satisfactory in the short term, a recent paper presents bad results in fracture cases [70]. In elderly patients with osteoporotic bone, implant selection must be balanced with an individualized patient assessment. It can be difficult to get an adequate press fit of the buffer when bone quality is too poor. In such cases, this way of use of the "buffer-on-bone" is contraindicated

A limitation of the study is the lack of comparison with experimental testing, due to the absence of specific references in the specialized literature about PCU contact stresses. However, as is usual for a correct validation of FE models, a sensitivity analysis was performed to determine the minimal size mesh required for an accurate simulation of contact. The final mesh was achieved after a mesh refinement performed considering convergence towards a minimum of the potential energy, with a tolerance of 1% between consecutive meshes.

5. Conclusion

As conclusion from the obtained results, PCU biomechanical characteristics are similar to those of the joint cartilage

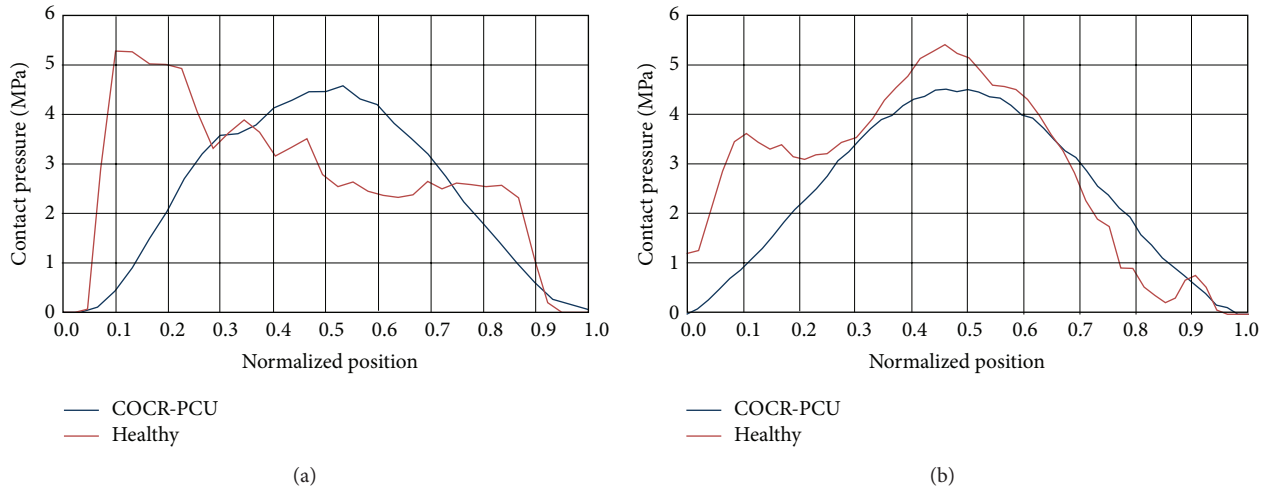

Figure 10: Comparative charts in toe-off: (a) longitudinal path; (b) transversal path.

so it is a favorable alternative to traditional bearing surfaces in total hip arthroplasty, with lower and closer to physiological contact pressures values, especially in young patients. Although clinical experience is still limited PCU could prevent the complications caused by wear debris, such as osteolytic lesions and aseptic loosening, improving the long term survival of hip implants.

Abbreviations

BW:	Body weight
THA:	Total hip arthroplasty
FE:	Finite elements
PCU:	Polycarbonate-urethane
UHMWPE:	Ultra high molecular weight polyethylene
CT:	Computed tomography
3D:	Three-dimensional.

Conflict of Interests

The authors declare that there is no conflict of interests regarding the publication of this paper.

Authors' Contribution

Antonio Herrera and Luis Gracia conceived the design of the study and coordinated the work between surgeons and engineers. Sergio Gabarre and Elena Ibarz conceived and developed the finite element model and carried out all the simulations and results processing. Jesús Mateo and Antonio Lobo-Escolar performed the surgery and supervised the right prosthesis positioning. All authors participated in the drawing up of the paper and read and approved the final paper.

References

[1] J. Charnley, "Arthroplasty of the hip: a new operation," *The Lancet*, vol. 277, no. 7187, pp. 1129–1132, 1961.

[2] W. H. Harris, "The first 50 years of total hip arthroplasty: lessons learned," *Clinical Orthopaedics and Related Research*, vol. 467, no. 1, pp. 28–31, 2009.

[3] J. R. Lieberman, "Two alternative bearings for total hip arthroplasty: more data are needed," *Journal of the American Academy of Orthopaedic Surgeons*, vol. 17, no. 2, pp. 61–62, 2009.

[4] K. Huch, K. A. C. Müller, T. Stürmer, H. Brenner, W. Puhl, and K.-. Günther, "Sports activities 5 years after total knee or hip arthroplasty: the Ulm osteoarthritis study," *Annals of the Rheumatic Diseases*, vol. 64, no. 12, pp. 1715–1720, 2005.

[5] U. Chatterji, M. J. Ashworth, P. L. Lewis, and P. J. Dobson, "Effect of total hip arthroplasty on recreational and sporting activity," *ANZ Journal of Surgery*, vol. 74, no. 6, pp. 446–449, 2004.

[6] P. Damm, J. Dymke, R. Ackermann et al., "Friction in total hip joint prosthesis measured in vivo during walking," *PLoS ONE*, vol. 8, no. 11, Article ID e78373, 2013.

[7] G. B. Flugsrud, L. Nordsletten, B. Espehaug, L. I. Havelin, and H. E. Meyer, "The effect of middle-age body weight and physical activity on the risk of early revision hip arthroplasty: a cohort study of 1,535 individuals," *Acta Orthopaedica*, vol. 78, no. 1, pp. 99–107, 2007.

[8] H. P. Malchau H, P. Söderman, and A. Odén, "A Prognosis of Total Hip Replacement. The Swedish national hip arthroplasty registry," 2000.

[9] G. K. McKee and J. Watson-Farrar, "Replacement of arthritic hips by the McKee-Farrar prosthesis," *Journal of Bone and Joint Surgery B*, vol. 48, no. 2, pp. 245–259, 1966.

[10] D. McMinn, R. Treacy, K. Lin, and P. Pynsent, "Metal on metal surface replacement of the hip. Experience of the McMinn prothesis," *Clinical Orthopaedics and Related Research*, supplement 1, no. 329, pp. S89–S98, 1996.

[11] I. Catelas and M. A. Wimmer, "New insights into wear and biological effects of metal-on-metal bearings," *The Journal of Bone and Joint Surgery American*, vol. 93, supplement 2, pp. 76–83, 2011.

[12] H. Pandit, S. Glyn-Jones, P. McLardy-Smith et al., "Pseudotumours associated with metal-on-metal hip resurfacings," *Journal of Bone and Joint Surgery B*, vol. 90, no. 7, pp. 847–851, 2008.

[13] R. A. E. Clayton, I. Beggs, D. M. Salter, M. H. Grant, J. T. Patton, and D. E. Porter, "Inflammatory pseudotumor associated with femoral nerve palsy following metal-on-metal resurfacing of the hip: a case report," *Journal of Bone and Joint Surgery A*, vol. 90, no. 9, pp. 1988–1993, 2008.

[14] D. J. Langton, S. S. Jameson, T. J. Joyce, N. J. Hallab, S. Natu, and A. V. F. Nargol, "Early failure of metal-on-metal bearings in hip resurfacing and large-diameter total hip replacement: a consequence of excess wear," *Journal of Bone and Joint Surgery B*, vol. 92, no. 1, pp. 38–46, 2010.

[15] Y.-. Kwon, S. Glyn-Jones, D. J. Simpson et al., "Analysis of wear of retrieved metal-on-metal hip resurfacing implants revised due to pseudotumours," *Journal of Bone and Joint Surgery B*, vol. 92, no. 3, pp. 356–361, 2010.

[16] B. G. Weber, "Experience with the metasul total hip bearing system," *Clinical Orthopaedics and Related Research*, no. 329 supplement, pp. S69–S77, 1996.

[17] M. Wagner and H. Wagner, "Preliminary results of uncemented metal on metal stemmed and resurfacing hip replacement arthroplasty," *Clinical Orthopaedics and Related Research*, no. 329, supplement, pp. S78–S88, 1996.

[18] H.-P. Sieber, C. B. Rieker, and P. Köttig, "Analysis of 118 second-generation metal-on-metal retrieved hip implants," *The Journal of Bone and Joint Surgery—British volume*, vol. 81, no. 1, pp. 46–50, 1999.

[19] S.-Y. Kim, H. Kyung, J. Ihn, M. Cho, K. Koo, and C. Kim, "Cementless metasul metal-on-metal total hip arthroplasty in patients less than fifty years old," *Journal of Bone and Joint Surgery A*, vol. 86, no. 11, pp. 2475–2481, 2004.

[20] H. Migaud, S. Putman, A. Combes et al., "Metal-on-metal bearing: is this the end of the line? We do not think so," *HSS Journal*, vol. 8, no. 3, pp. 262–269, 2012.

[21] L. I. Havelin, A. M. Fenstad, R. Salomonsson et al., "The nordic arthroplasty register association: a unique collaboration between 3 national hip arthroplasty registries with 280,201 THRs," *Acta Orthopaedica*, vol. 80, no. 4, pp. 393–401, 2009.

[22] G. Digas, J. Kärrholm, J. Thanner, H. Malchau, and P. Herberts, "Highly cross-linked polyethylene in cemented THA: randomized study of 61 hips," *Clinical Orthopaedics and Related Research*, no. 417, pp. 126–138, 2003.

[23] G. Digas, J. Kärrholm, J. Thanner, H. Malchau, and P. Herberts, " The Otto Aufranc Award. Highly cross-linked polyethylene in total hip arthroplasty: randomized evaluation of penetration rate in cemented and uncemented sockets using radiostereometric analysis," *Clinical Orthopaedics and Related Research*, no. 429, pp. 6–16, 2004.

[24] R. W. McCalden, S. J. MacDonald, C. H. Rorabeck, R. B. Bourne, D. G. Chess, and K. D. Charron, "Wear rate of highly cross-linked polyethylene in total hip arthroplasty: a randomized controlled trial," *Journal of Bone and Joint Surgery A*, vol. 91, no. 4, pp. 773–782, 2009.

[25] G. E. R. Thomas, D. J. Simpson, S. Mehmood et al., "The seven-year wear of highly cross-linked polyethylene in total hip arthroplasty: a double-blind, randomized controlled trial using radiostereometric analysis," *Journal of Bone and Joint Surgery A*, vol. 93, no. 8, pp. 716–722, 2011.

[26] E. García-Rey, E. García-Cimbrelo, and A. Cruz-Pardos, "New polyethylenes in total hip replacement: a ten- to 12-year follow-up study," *Journal of Bone and Joint Surgery B*, vol. 95, no. 3, pp. 326–332, 2013.

[27] A. Herrera, J. Mateo, A. Lobo-Escolar, J. J. Panisello, E. Ibarz, and L. Gracia, "Long-term outcomes of a new model of anatomical hydroxyapatite-coated hip prosthesis," *The Journal of Arthroplasty*, vol. 28, no. 7, pp. 1160–1166, 2013.

[28] P. Boutin, "Total arthroplasty of the hip by fritted aluminum prosthesis. Experimental study and 1st clinical applications," *Revue de Chirurgie Orthopedique et Reparatrice de l'Appareil Moteur*, vol. 58, no. 3, pp. 229–246, 1972.

[29] M. Kuntz, "Validation of a new high performance alumina matrix composite for use in total joint replacement," *Seminars in Arthroplasty*, vol. 17, no. 3-4, pp. 141–145, 2006.

[30] J. A. D'Antonio and K. Sutton, "Ceramic materials as bearing surfaces for total hip arthroplasty," *The Journal of the American Academy of Orthopaedic Surgeons*, vol. 17, no. 2, pp. 63–68, 2009.

[31] M. Bohler, Y. Mochida, T. W. Bauer, H. Plenk Jr., and M. Salzer, "Wear debris from two different alumina-on-alumina total hip arthroplasties," *The Journal of Bone and Joint Surgery*, vol. 82, no. 6, pp. 901–909, 2000.

[32] T. R. Yoon, S. M. Rowe, S. T. Jung, K. J. Seon, and W. J. Maloney, "Osteolysis in association with a total hip arthroplasty with ceramic bearing surfaces," *Journal of Bone and Joint Surgery A*, vol. 80, no. 10, pp. 1459–1468, 1998.

[33] A. Hatton, J. E. Nevelos, A. A. Nevelos, R. E. Banks, J. Fisher, and E. Ingham, "Alumina-alumina artificial hip joints. Part I: a histological analysis and characterisation of wear debris by laser capture microdissection of tissues retrieved at revision," *Biomaterials*, vol. 23, no. 16, pp. 3429–3440, 2002.

[34] R. Nizard, D. Pourreyron, A. Raould, D. Hannouche, and L. Sedel, "Alumina-on-alumina hip arthroplasty in patients younger than 30 years old," *Clinical Orthopaedics and Related Research*, vol. 466, no. 2, pp. 317–323, 2008.

[35] P. Hernigou, S. Zilber, P. Filippini, and A. Poignard, "Ceramic-ceramic bearing decreases osteolysis: a 20-year study versus ceramic-polyethylene on the contralateral hip," *Clinical Orthopaedics and Related Research*, vol. 467, no. 9, pp. 2274–2280, 2009.

[36] C. Piconi, W. Burger, H. G. Richter et al., "Y-TZP ceramics for artificial joint replacements," *Biomaterials*, vol. 19, no. 16, pp. 1489–1494, 1998.

[37] G. Bergmann, F. Graichen, A. Rohlmann, N. Verdonschot, and G. H. van Lenthe, "Frictional heating of total hip implants, part 1: measurements in patients," *Journal of Biomechanics*, vol. 34, no. 4, pp. 421–428, 2001.

[38] P. Hernigou and T. Bahrami, "Zirconia and alumina ceramics in comparison with stainless-steel heads. Polyethylene wear after a minimum ten-year follow-up," *The Journal of Bone and Joint Surgery B*, vol. 85, no. 4, pp. 504–509, 2003.

[39] T. von Schewelov, L. Sanzén, I. Önsten, Å. Carlsson, and J. Besjakov, "Total hip replacement with a zirconium oxide ceramic femoral head: a randomised roentgen stereophotogrammetric study," *The Journal of Bone and Joint Surgery*, vol. 87, no. 12, pp. 1631–1635, 2005.

[40] J. Langlois, S. El Hage, F. Madi, J. Courpied, M. Kerboull, and M. Hamadouche, "Charnley-Kerboull total hip arthroplasty combining zirconia on polyethylene. A minimum eight-year follow-up prospective study," *International Orthopaedics*, vol. 37, no. 3, pp. 355–360, 2013.

[41] Y. L. Jung and S. Y. Kim, "Alumina-on-polyethylene bearing surfaces in total hip arthroplasty," *The Open Orthopaedics Journal*, vol. 4, pp. 56–60, 2010.

[42] S. Wang, S. Zhang, and Y. Zhao, "A comparison of polyethylene wear between cobalt-chrome ball heads and alumina ball heads after total hip arthroplasty: a 10-year follow-up," *Journal of Orthopaedic Surgery and Research*, vol. 8, no. 1, article 20, 2013.

[43] D. J. Cash and V. Khanduja, "The case for ceramic-on-polyethylene as the preferred bearing for a young adult hip replacement," *Hip International*, 2014.

[44] C. O. Townley, "Hemi and total articular replacement arthroplasty of the hip with the fixed femoral cup," *Orthopedic Clinics of North America*, vol. 13, no. 4, pp. 869–894, 1982.

[45] I. Khan, N. Smith, E. Jones, D. S. Finch, and R. E. Cameron, "Analysis and evaluation of a biomedical polycarbonate urethane tested in an in vitro study and an ovine arthroplasty model, part I: materials selection and evaluation," *Biomaterials*, vol. 26, no. 6, pp. 621–631, 2005.

[46] I. Khan, N. Smith, E. Jones, D. S. Finch, and R. E. Cameron, "Analysis and evaluation of a biomedical polycarbonate urethane tested in an in vitro study and an ovine arthroplasty model. Part II: in vivo investigation," *Biomaterials*, vol. 26, no. 6, pp. 633–643, 2005.

[47] A. Szelest-Lewandowska, B. Masiulanis, M. Szymonowicz, S. Pielka, and D. Paluch, "Modified polycarbonate urethane: synthesis, properties and biological investigation *in vitro*," *Journal of Biomedical Materials Research A*, vol. 82, no. 2, pp. 509–520, 2007.

[48] R. A. Smith, A. Maghsoodpour, and N. J. Hallab, "*In vivo* response to cross-linked polyethylene and polycarbonate-urethane particles," *Journal of Biomedical Materials Research A*, vol. 93, no. 1, pp. 227–234, 2010.

[49] S. M. Kurtz, R. Siskey, and M. Reitman, "Accelerated aging, natural aging, and small punch testing of gamma-air sterilized polycarbonate urethane acetabular components," *Journal of Biomedical Materials Research B: Applied Biomaterials*, vol. 93, no. 2, pp. 442–447, 2010.

[50] J. J. Elsner, Y. Mezape, K. Hakshur et al., "Wear rate evaluation of a novel polycarbonate-urethane cushion form bearing for artificial hip joints," *Acta Biomaterialia*, vol. 6, no. 12, pp. 4698–4707, 2010.

[51] K. St. John and M. Gupta, "Evaluation of the wear performance of a polycarbonate-urethane acetabular component in a hip joint simulator and comparison with UHMWPE and cross-linked UHMWPE," *Journal of Biomaterials Applications*, vol. 27, no. 1, pp. 55–65, 2012.

[52] Belgium, M.M.L.

[53] Siemens 2013, http://www.plm.automation.siemens.com/.

[54] "Imagine Roland 2013," http://es.rolanddga.com/products/software/pixformpro/.

[55] "Dassault Systèmes 2013," http://www.3ds.com/.

[56] A. Implants, "Active implants Tribofit System," 2013.

[57] M. D. Harris, A. E. Anderson, C. R. Henak, B. J. Ellis, C. L. Peters, and J. A. Weiss, "Finite element prediction of cartilage contact stresses in normal human hips," *Journal of Orthopaedic Research*, vol. 30, no. 7, pp. 1133–1139, 2012.

[58] A. Herrera, J. J. Panisello, E. Ibarz, J. Cegoñino, J. A. Puértolas, and L. Gracia, "Long-term study of bone remodelling after femoral stem: a comparison between dexa and finite element simulation," *Journal of Biomechanics*, vol. 40, no. 16, pp. 3615–3625, 2007.

[59] "Orthoload data base. Loading of Orthopaedic Implants," http://www.orthoload.com.

[60] A. E. Anderson, B. J. Ellis, S. A. Maas, and J. A. Weiss, "Effects of idealized joint geometry on finite element predictions of cartilage contact stresses in the hip," *Journal of Biomechanics*, vol. 43, no. 7, pp. 1351–1357, 2010.

[61] M. Mak, Z. Jin, J. Fisher, and T. D. Stewart, "nfluence of acetabular cup rim design on the contact stress during edge loading in ceramic-on-ceramic hip prostheses," *Journal of Arthroplasty*, vol. 26, no. 1, pp. 131–136, 2011.

[62] L. Wang, X. Liu, D. Li, F. Liu, and Z. Jin, "Contact mechanics studies of an ellipsoidal contact bearing surface of metal-on-metal hip prostheses under micro-lateralization," *Medical Engineering and Physics*, vol. 36, no. 4, pp. 419–424, 2014.

[63] Q. Meng, F. Liu, J. Fisher, and Z. Jin, "Contact mechanics and lubrication analyses of ceramic-on-metal total hip replacements," *Tribology International*, vol. 63, pp. 51–60, 2012.

[64] S. C. Scholes, A. Unsworth, J. M. Blamey, I. C. Burgess, E. Jones, and N. Smith, "Design aspects of compliant, soft layer bearings for an experimental hip prosthesis," *Proceedings of the Institution of Mechanical Engineers H: Journal of Engineering in Medicine*, vol. 219, no. 2, pp. 79–87, 2005.

[65] A. Moroni, M. Hoque, G. Micera et al., "Cushion form bearings in total hip arthroplasty: nature's approach to the synovial joint problem," in *Tribology in Total Hip Arthroplasty*, K. Knahr, Ed., pp. 195–206, Springer, Berlin, Germany, 2011.

[66] W. E. Siebert, S. Mai, and S. Kurtz, "Retrieval analysis of a polycarbonate-urethane acetabular cup: a case report," *Journal of Long-Term Effects of Medical Implants*, vol. 18, no. 1, pp. 69–74, 2008.

[67] B. Wippermann, S. Kurtz, N. J. Hallab, and R. Treharne, "Explantation and analysis of the first retrieved human acetabular cup made of polycarbonate urethane: a case report," *Journal of Long-Term Effects of Medical Implants*, vol. 18, no. 1, pp. 75–83, 2008.

[68] W. E. Siebert, S. Mai, A. Moroni, E. Chiarello, and S. Giannini, "A two-year prospective and retrospective multi-center study of the TriboFit Hip System," *Journal of Long-Term Effects of Medical Implants*, vol. 19, no. 2, pp. 149–155, 2009.

[69] A. Moroni, E. Nocco, M. Hoque et al., "Cushion bearings versus large diameter head metal-on-metal bearings in total hip arthroplasty: a short-term metal ion study," *Archives of Orthopaedic and Trauma Surgery*, vol. 132, no. 1, pp. 123–129, 2012.

[70] M. Cadossi, E. Chiarello, L. Savarino et al., "A comparison of hemiarthroplasty with a novel polycarbonate-urethane acetabular component for displaced intracapsular fractures of the femoral neck: a randomised controlled trial in elderly patients," *Bone and Joint Journal*, vol. 95, no. 5, pp. 609–615, 2013.

Hindawi Publishing Corporation
BioMed Research International
Volume 2014, Article ID 808369, 13 pages
http://dx.doi.org/10.1155/2014/808369

Research Article

Highly Cross-Linked Polyethylene in Total Hip and Knee Replacement: Spatial Distribution of Molecular Orientation and Shape Recovery Behavior

Yasuhito Takahashi,[1,2] Toshinori Masaoka,[2] Giuseppe Pezzotti,[3] Takaaki Shishido,[2] Toshiyuki Tateiwa,[2] Kosuke Kubo,[2] and Kengo Yamamoto[2]

[1] *Department of Bone and Joint Biomaterial Research, Tokyo Medical University, 6-7-1 Nishishinjuku, Shinjuku-ku, Tokyo 160-0023, Japan*
[2] *Department of Orthopaedic Surgery, Tokyo Medical University, 6-7-1 Nishishinjuku, Shinjuku-ku, Tokyo 160-0023, Japan*
[3] *Ceramic Physics Laboratory, Kyoto Institute of Technology, Sakyo-ku, Matsugasaki, Kyoto 606-8585, Japan*

Correspondence should be addressed to Yasuhito Takahashi; yasuhito@tokyo-med.ac.jp

Received 27 May 2014; Accepted 11 July 2014; Published 27 August 2014

Academic Editor: Hiroshi Ito

Copyright © 2014 Yasuhito Takahashi et al. This is an open access article distributed under the Creative Commons Attribution License, which permits unrestricted use, distribution, and reproduction in any medium, provided the original work is properly cited.

The present study investigated effects of processing procedures on morphology of highly cross-linked and re-melted UHMWPE (XLPE) in total hip and knee arthroplasty (THA, TKA). The shape recovery behavior was also monitored via uniaxial compression test at room temperature after non-destructive characterizations of the in-depth microstructure by confocal/polarized Raman spectroscopy. The goal of this study was to relate the manufacturing-induced morphology to the *in vivo* micromechanical performance, and ultimately to explore an optimal structure in each alternative joint bearing. It was clearly confirmed that the investigated XLPE hip and knee implants, which were produced from different orthopaedic grade resins (GUR 1050 and GUR 1020), consisted of two structural regions in the as-received states: the near-surface transitional anisotropic layer (≈100 μm thickness) and the bulk isotropic structural region. These XLPEs exhibited a different crystalline anisotropy and molecular texture within the near-surface layers. In addition, the knee insert showed a slightly higher efficiency of shape recovery against the applied strain over the hip liner owing to a markedly higher percentage of the bulk amorphous phase with intermolecular cross-linking. The quantitative data presented in this study might contribute to construct manufacturing strategies for further rationalized structures as alternative bearings in THA and TKA.

1. Introduction

Increased incidence of periprosthetic osteolysis with increasing polyethylene wear has historically been the leading complication of total hip arthroplasty (THA), resulting in the growing necessity of revision surgery due to aseptic loosening of implant devices [1–3]. In the late 1990s, cross-linked and thermally treated ultrahigh molecular weight polyethylene (UHMWPE), the so-called first-generation highly cross-linked polyethylene (XLPE), was hence developed for THA with expectation of the improved wear resistance over conventional UHMWPE [4–6]. The implementation of XLPE acetabular liners certainly contributed to a dramatic reduction in the volumetric wear [4–8] as well as in the oxidative degradation [9]. Nevertheless, the concomitant decrease in toughness, ultimate tensile strength, and fatigue crack propagation resistance was also recognized [9–13]. The above trade-off problem, associated with intermolecular cross-linking of C–C chemical bonds between adjacent chains, led to a subject of considerable discussion as to its application to tibial inserts used in total knee arthroplasty (TKA) [14].

The kinematics of knee joint represents more anisotropic/constrained motions within small surface area of contact, leading to higher compressive and shear stresses as compared

to that of hip joint. Under the applied loading of 3000 N (the entire joint load on the component), the maximum compressive stresses at the surface of UHMWPE components were computed by finite element analysis (FEA) as ≈15 MPa and ≈40 MPa for hip (using 28 mm head) and knee joint, respectively [15]. On the other hand, the maximum shear stresses were found at the very surface for the hip but at the depth of 1-2 mm below the surface for the knee, whose values were evaluated as ≈5 MPa and ≈10 MPa, respectively [15, 16]. Moreover, it should be noted that the most common cause of revision TKA has been mechanical loosening (40%) rather than wear/osteolysis (9%) [17]. This epidemiological data may support the results of the above theoretical considerations for the biomechanical and kinematic differences between hip and knee joints. In this context, the required microstructure for each joint application should carefully be considered and optimized at the molecular scale.

Although several manufacturing attempts in industry have been made so far to rationalize preferred choices of resin types (GUR 1050 or GUR 1020), consolidation methods (sheet compression, ram extrusion, or direct compression molding), and radiation doses (50~300 kGy), consensus for alternative bearings has not been achieved yet among polymer scientists [18, 19]. A key underlying concept of balancing among the wear resistance and mechanical properties could be given by the optimization of molecular anisotropy, entanglement characteristics, and the balanced percentages between crystalline and noncrystalline phases, that is, amorphous and third intermediate phase. More specifically, the importance should be placed on minimizing the occurrence of strain-softening (strain-weakening) phenomenon [19–21] and irrecoverable plastic deformation during each characteristic *in vivo* motion of hip and knee joints. From this viewpoint, it would be of tremendous benefits to explore the effects of the manufacturing-induced local strain and plastic deformation on the initial molecular anisotropies in the final products for maximizing the potential wear performances.

The present investigation focuses on quantifying the molecular anisotropy and phase percentages such as crystalline, amorphous, and third intermediate phase along the depths of commercially available XLPE hip and knee joint prostheses by means of high spatial resolution Raman microscopy. In addition, the deformation and shape recovery behaviors from external uniaxial compressive forces were also monitored. The quantitative data obtained in this study might contribute to construct further improved manufacturing strategies for highly rationalized structures as alternative joint bearings for hip and knee arthroplasty applications and also to minimize the time-consuming manufacturing trials.

2. Materials and Methods

2.1. Study Design. The first-generation XLPE hip and knee implants were evaluated through the following quantitative analyses: (i) phase percentages, that is, amorphous, crystalline, and third intermediate phase; (ii) preferred orientation of molecular chains; (iii) degree of crystalline anisotropy; and (iv) deformation and shape recovery behaviors from applied uniaxial compression. We have also built a structural model based on the results of the above morphological characterizations in order to discuss the potential *in vivo* performance and functionality of each type of prosthesis.

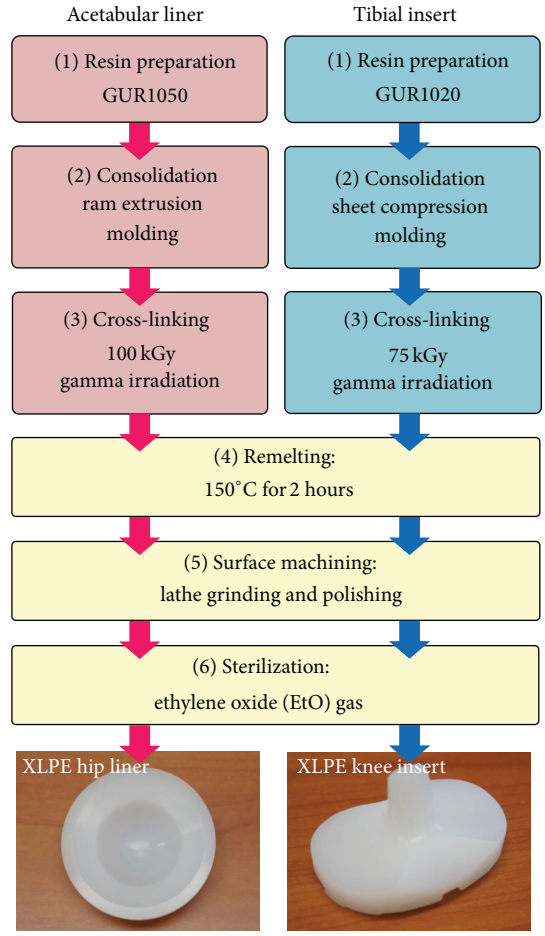

Figure 1: Processing methods for XLPE acetabular liner and tibial insert for total hip and knee arthroplasty.

2.2. XLPE Hip and Knee Prostheses. The never implanted, first-generation remelted XLPE acetabular liner and tibial insert ($n = 3$ for each prosthesis) were analyzed in this study. The investigated hip and knee bearings are both referred to as the same trade name, XLPE, which were manufactured by Smith & Nephew Orthopedics, Inc. (Memphis, Tennessee, USA). XLPE has been clinically introduced since 2001 for THA and 2008 for TKA in USA. The thickness of these test components was 10 mm for the hip and 11 mm for the knee in posterior stabilized (PS) designs. A comparison of the processing procedures for each XLPE component was given in Figure 1. The manufacturing of XLPE hip liners starts from GUR 1050 resin (Ticona Inc., Florence, KY, USA) with a molecular weight of approximately 6.0 million g/mol. Ram-extruded GUR 1050 rods were cross-linked by gamma-ray irradiation with a total dose of 100 kGy and then remelted at 150°C for 2 hours to eliminate all the free radicals. On the other hand, XLPE knee inserts start from GUR 1020 resin (Ticona Inc., Florence, KY, USA) with a molecular weight of approximately 3.5 million g/mol. Compression-molded GUR

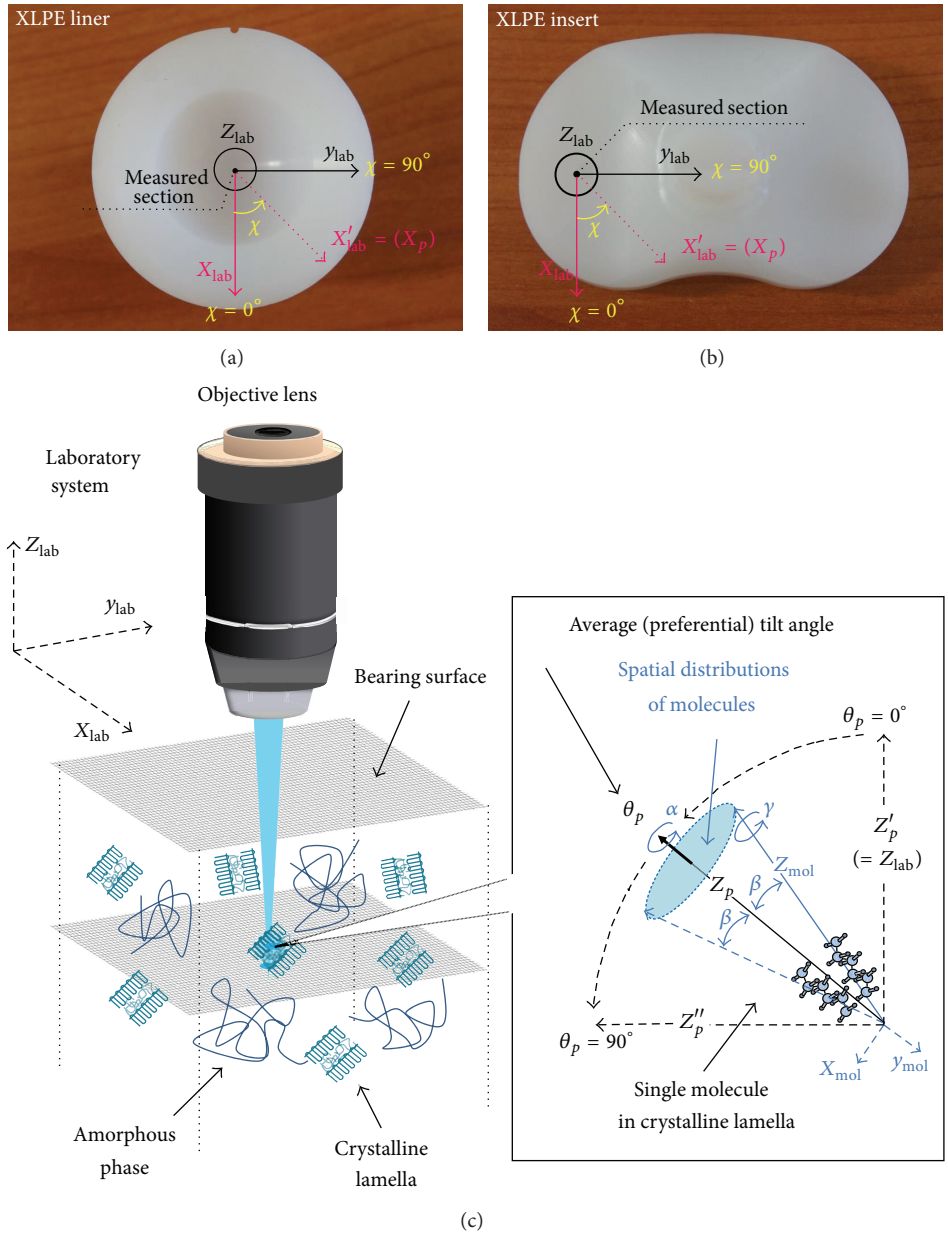

FIGURE 2: (a) Schematic of the selected measurement sections and definition of inplane rotation angle, χ, for XLPE hip and knee components. (b) Schematic of our choice of Cartesian reference systems and of the Euler angles governing their rotations in space, as explained in the text (Section 2.3.2).

1020 sheets were cross-linked by gamma-ray irradiation with a total dose of 75 kGy and then remelted under the same condition (150°C for 2 hours). After being machined into the final shapes of the acetabular liners or the tibial inserts, the materials were barrier packaged and exposed to ethylene oxide (EtO) gas for the sterilization purposes.

2.3. Raman Spectroscopy

2.3.1. Phase Volume Fractions Analyses. For the phase fractional assessments of melt-like amorphous (α_a), orthorhombic crystal (α_c), and third intermediate region (α_t), nondestructive Raman spectroscopic analyses were conducted. The measured sections for each test sample, where intensive plastic deformation and wear would be expected to occur during the *in vivo* services [22], were indicated in Figures 2(a)-2(b). All the spectroscopic measurements in this study were made by means of Raman microprobe spectrometer (MS3504i, SOL Instruments Ltd., Minsk, Republic of Belarus) in back-scattering geometry. The excitation source was 514.5 nm Ar-ion laser (GLG3103, Showa Optronics Co., Ltd., Tokyo, Japan) yielding a power of approximately 20 mW on the sample surfaces. The confocal configuration of the probe adopted throughout the present experiments corresponded to a ×100 objective; numerical aperture, focal length, and pinhole diameter were fixed as 0.6, 7.6 mm, and 100 μm, respectively. Individual spectra were typically collected in

15 seconds. The recorded spectra were averaged over three successive measurements. The focal plane was eventually shifted toward the sample subsurface direction in order to nondestructively screen the depth regions of the samples. At each depth of samples, an inplane sampling of 2.5 μm lateral steps was applied within the area of $50 \times 50\ \mu m^2$ (for a total of 1323 spectra per each map). A total of 2205 different locations (= 441 points/map × 5 maps) were selected within the sections, and the average value was assumed to be representative of the phase fractions at each selected depth. The computations of these fractions were made according to the following equations [23–25]:

$$\alpha_a = \frac{I_{1080}}{0.79\left(I_{1296} + I_{1310}\right)},$$
$$\alpha_c = \frac{I_{1418}}{0.46\left(I_{1296} + I_{1310}\right)}, \quad (1)$$

where I is the integral intensity of the Raman band whose wavenumber is identified by the subscript. Note also that the sum $(\alpha_a + \alpha_c)$ might locally be <1, because of the possible presence of an anisotropic intermediate state (usually referred to as the "third phase" [26]). The volume fraction of α_t can be thus provided by

$$\alpha_t = 1 - \left(\alpha_c + \alpha_a\right). \quad (2)$$

2.3.2. Molecular Orientation of Carbon Chains and Anisotropy Analyses. For the assessments of three-dimensional molecular orientation of the carbon chains (the C–C alkyl chains) and the degree of crystalline anisotropy, polarized measurements combined with confocal Raman spectroscopy were conducted in the same sections where the phase percentages were examined. During the measurements, a parallel polarization filter and a half-wave plate were placed between samples and spectrometer and set to pass scattered Raman radiation horizontally to a CCD camera. To express the spatial position and distribution of the molecular orientation, three different Cartesian coordinate systems were defined as a system $(x_{\text{lab}}y_{\text{lab}}z_{\text{lab}})$ describing the laboratory frame, a system $(x_py_pz_p)$ to describe the average preferential molecular orientation (as detected by the Raman probe of finite dimensions), and a system $(x_{\text{mol}}y_{\text{mol}}z_{\text{mol}})$ to describe the orientation of individual molecular chains with respect to the mean axes of preferential orientation. Euler angles for the above three Cartesian frames can be defined as a set of angle (θ, φ, χ) describing the rotation of $(x_{\text{mol}}y_{\text{mol}}z_{\text{mol}})$ with respect to $(x_{\text{lab}}y_{\text{lab}}z_{\text{lab}})$, a set of angle $(\theta_p, \varphi_p, \chi_p)$ describing the rotation of $(x_py_pz_p)$ with respect to $(x_{\text{lab}}y_{\text{lab}}z_{\text{lab}})$, and a set of angle (α, β, γ) describing the rotation of $(x_{\text{mol}}y_{\text{mol}}z_{\text{mol}})$ with respect to $(x_py_pz_p)$. Note that the $(\theta_p, \varphi_p, \chi_p)$ determines the preferential molecular orientation in the XLPE components and (α, β, γ) determines the spatial distribution angles from preferential orientation $(\theta_p, \varphi_p, \chi_p)$. However, taking into consideration the cylindrical symmetries of the long linear polyethylene chains, the numbers of the orientation angles relevant to Raman scattering may be reduced. In such a symmetric case, we can neglect the dependences of any torsional orientation such as $\varphi, \varphi_p, \alpha$, and γ. In this study, we set the angle θ_p, that is, the out-of-plane tilt angle, as the preferred molecular orientation. Specifically, $\theta_p = 0^\circ$ indicates the alignment of C–C chains perpendicular to the articulating surfaces, while $\theta_p = 90^\circ$ indicates the alignment of C–C chains parallel to the surfaces. In addition, we assumed the existence of a uniaxial symmetry with respect to the preferential orientation of the molecular chains, which is only dependent on one polar angle, β (Figure 2(c)); that is, angles α and γ do not enter the expression of molecular distribution. Thus, the probability of finding polyethylene molecules with orientations between β and $(\beta + d\beta)$ can be analytically formulated as follows [26]:

$$\int_{\gamma=0}^{\gamma=2\pi}\int_{\alpha=0}^{\alpha=2\pi}\int_{\beta=0}^{\beta=2\pi} f(\beta)\sin\beta d\beta d\alpha d\gamma = 1\left(f(\beta) \geq 0\right), \quad (3)$$

where $f(\beta)$ is called orientational probability distribution or orientation distribution function (ODF).

As the experimental procedures, XLPE samples were placed on a χ-axis (inplane angle on the bearing surface) rotation jig and polarized Raman spectra in parallel configuration were collected at 19 different azimuthal angles within the interval $0 \leq \chi \leq 180^\circ$, with sequential rotational steps of 10° (Figures 2(a)-2(b)). Particular care was taken in order to align the axis of the microscope with the axis of the rotation jig. It is known that the polarized Raman band located at $1130\ cm^{-1}$ related to the C–C stretching vibration (A_g + B_{1g} mode) is the most affected by polyethylene orientation [27, 28] and its angular dependence was used also in this study as a sensor to examine preferential orientation and its degree of order. Considering that the observed scattering intensity represents the contribution from all the individual polyethylene molecules existing within the volume of laser probe, the overall polarized Raman intensity ($I^{\parallel}_{1130}$) for XLPE products is provided by the following general equation [28, 29]:

$$I^{\parallel}_{1130} = \frac{\int_{\gamma=0}^{\gamma=2\pi}\int_{\alpha=0}^{\alpha=2\pi}\int_{\beta=0}^{\beta=2\pi} I^{\parallel}_{A_g+B_{1g}}(\theta,\chi)\, f(\beta)\sin\beta d\beta d\alpha d\gamma}{\int_{\gamma=0}^{\gamma=2\pi}\int_{\alpha=0}^{\alpha=2\pi}\int_{\beta=0}^{\beta=2\pi} f(\beta)\sin\beta d\beta d\alpha d\gamma}, \quad (4)$$

where $I^{\parallel}_{A_g+B_{1g}}$ is the dependence of Raman intensity of a single polyethylene molecular chain in parallel polarization configuration according to its angular dependence on Euler angles, θ and χ (note that θ and χ are functions of θ_p and χ_p) [28, 29], and the ODF, $f(\beta)$, representative of the molecules oriented in a cone around the orientation axis (cf. Figure 2(c)), will take the following form:

$$f(\beta) = A\exp\left\{-\left[\lambda_2 P_2(\cos\beta) + \lambda_4 P_4(\cos\beta)\right]\right\}, \quad (5)$$

where A is a constant and the parameters λ_i $(i = 2, 4)$ are the so-called Lagrange multipliers; that is, $P_2(\cos\beta) = (3\cos^2\beta - 1)/2$, $P_4(\cos\beta) = (35\cos^4\beta - 30\cos^2\beta + 3)/8$, used in the definition of the principle of maximum information entropy [30, 31]. A mathematical procedure was performed

by using (4)-(5) to find the best-fitting curves to data sets of polarized Raman intensity collected at different inplane orientation (χ). Setting a computational routine, θ_p and $f(\beta)$ can be determined, and the degree of molecular orientation can be calculated using the following equation [28, 29, 31, 32]:

$$\int_{\gamma=0}^{\gamma=2\pi}\int_{\alpha=0}^{\alpha=2\pi}\int_{\beta=0}^{\beta=\pi} P_2(\cos\beta)\, f(\beta)\sin\beta d\beta d\alpha d\gamma = \langle P_2(cos\beta)\rangle, \quad (6)$$

where $\langle P_2(\cos\beta)\rangle$ is referred to as Herman's orientation parameter and represents the degree of molecular orientation. A value 0 for it indicates that the molecular orientation is fully random (isotropic), while a value 1 represents a perfect orientation along a preferential orientation axis. For a partial molecular orientation, the value should be $0 < \langle P_2(\cos\beta)\rangle < 1.0$.

2.4. Compression Deformation Test. In the present investigation, a compressive deformation was applied at room temperature (24 ± 2°C) in the samples purposely prepared by cutting the unused XLPE acetabular liner and tibial insert into rectangular prisms 3 × 3 × 6 mm in dimension. These rectangular samples ($n = 3$ for each liner) were obtained from each surface of these samples where the morphological assessments were performed by means of Raman spectroscopy. Deformation tests (cross-head speed of 0.1 mm/min) were performed using uniaxial compression equipment. The rectangular specimens were obtained from the sections corresponding to the Raman investigations. Particular care was taken in order to smooth down only the four corners of the slightly concave surfaces of the samples. This latter procedure enabled us to flatten the originally concave surfaces to match the compressive surface of the jig while preserving the original microstructure of the samples, thus reproducing as closely as possible the conditions encountered during *in vivo* loading. One-dimensional stress relaxation tests were also performed. The residual strain in each as-received material was assumed as $\varepsilon = 0$ and an increasing compressive load was applied by a 3% strain (180 μm) step. At each step, the materials were subjected to a compressive strain of a predetermined magnitude, which was kept constant for at least 24 hours in order to allow the full development of internal deformation allowed by the microstructure. The load was then released and the samples allowed recovering of the inelastic strain for at least 24 hours, a time interval sufficient to obtain a nearly full recovery, especially at low and moderate levels of deformation, as in the case of the present investigation [33, 34]. At each step, the engineering strain was measured along the sample long axis by means of a micrometer caliper both before and after recovery, henceforth referred to as ε_i and ε_f, respectively.

3. Results

3.1. Phase Volume Fractions. Figures 3(a)–3(c) show the depth profiles of the amorphous, crystalline, and third intermediate phase percentages (α_a, α_c, and α_t, resp.) as detected in XLPE hip liner and knee insert. Confocal Raman analyses confirmed that the phase fractions in both products rapidly change along the subsurface depths within the first 35 μm from the articulating surface, but subsequently show the nearly constant and homogeneous trends. The differences between minimum and maximum values along the α_c and α_t profiles (Figures 3(b) and 3(c)) were larger in the knee insert; that is, $\Delta\alpha_c$ and $\Delta\alpha_t$ were 14.0% and 19.3% for the knee and 10.9% and 17.4% for the hip liner, respectively. Although GUR 1020, used as the starting resin for manufacturing the knee insert, initially possesses a higher α_c value before gamma irradiation and remelting as compared to GUR 1050 resin used for the hip liner [35], a similar percentage of the bulk crystallinity ($\alpha_c = 45.04 \pm 1.15\%$ and $45.13 \pm 1.37\%$ in the hip and knee, resp.) was observed in their final products. On the other hand, their bulk profiles exhibited about 9% difference in the α_a and α_t. XLPE knee showed a markedly higher amorphous phase percentage, that is, a lower third intermediate phase content, in its bulk region, as compared to the hip.

3.2. Molecular Orientation of Carbon Chains. The normalized Raman intensities ($I^{\parallel}_{1130}$) of XLPE hip and knee implants depending on the inplane sample rotation angle (χ) were plotted in Figures 4(a) and 4(b), respectively. According to the least-square method, the best-fitting curves determined using (4)-(5) with minimum deviations from the data points were also plotted in the figures. The good agreement between theoretical curves and experimental plots was confirmed, indicating the high degree of accuracy and reproducibility of the results. The variation of the polarized Raman intensity depending on the rotation angle is pronounced when the sample possesses a high degree of anisotropy. In addition, the π or $\pi/2$ angular periodicities of $I^{\parallel}_{1130}$ plots are indicative of a preferred molecular orientation (θ_p) nearly parallel or perpendicular to the articulating surfaces, respectively, while the constant intensity (no angular periodicity) trend implies the isotropic molecular structure (no preferred orientation).

The depth profiles of the θ_p angle obtained from the data sets of Figures 4(a)-4(b) were given in Figure 4(c). As explained in Section 2.3.2, $\theta_p = 0^\circ$ represents the C–C chain alignment perpendicular to the sample surface, while $\theta_p = 90^\circ$ indicates the chain alignment parallel to the surface. The C–C chains at the superficial layers of the hip and knee components preferentially lie in a direction parallel to each surface and subsequently tend to reach a direction nearly perpendicular to the surface with proceeding along the subsurface depths. Isotropic structure appears at the depths within 75 to 100 μm. There was a significant difference in the θ_p profiles within the first 50 μm depth between the two prostheses. The θ_p angles of the hip liner more rapidly decrease from the surface down to subsurface than the knee insert. In other words, the knee insert possesses a thicker layer of parallel molecular orientation in its near-surface region.

In addition to the tilt angle of θ_p, the preferred inplane orientation angle, χ_p, also can be obtained simultaneously in the same fitting procedures. However, this angle apparently cannot be identified in the hip acetabular liner due to its

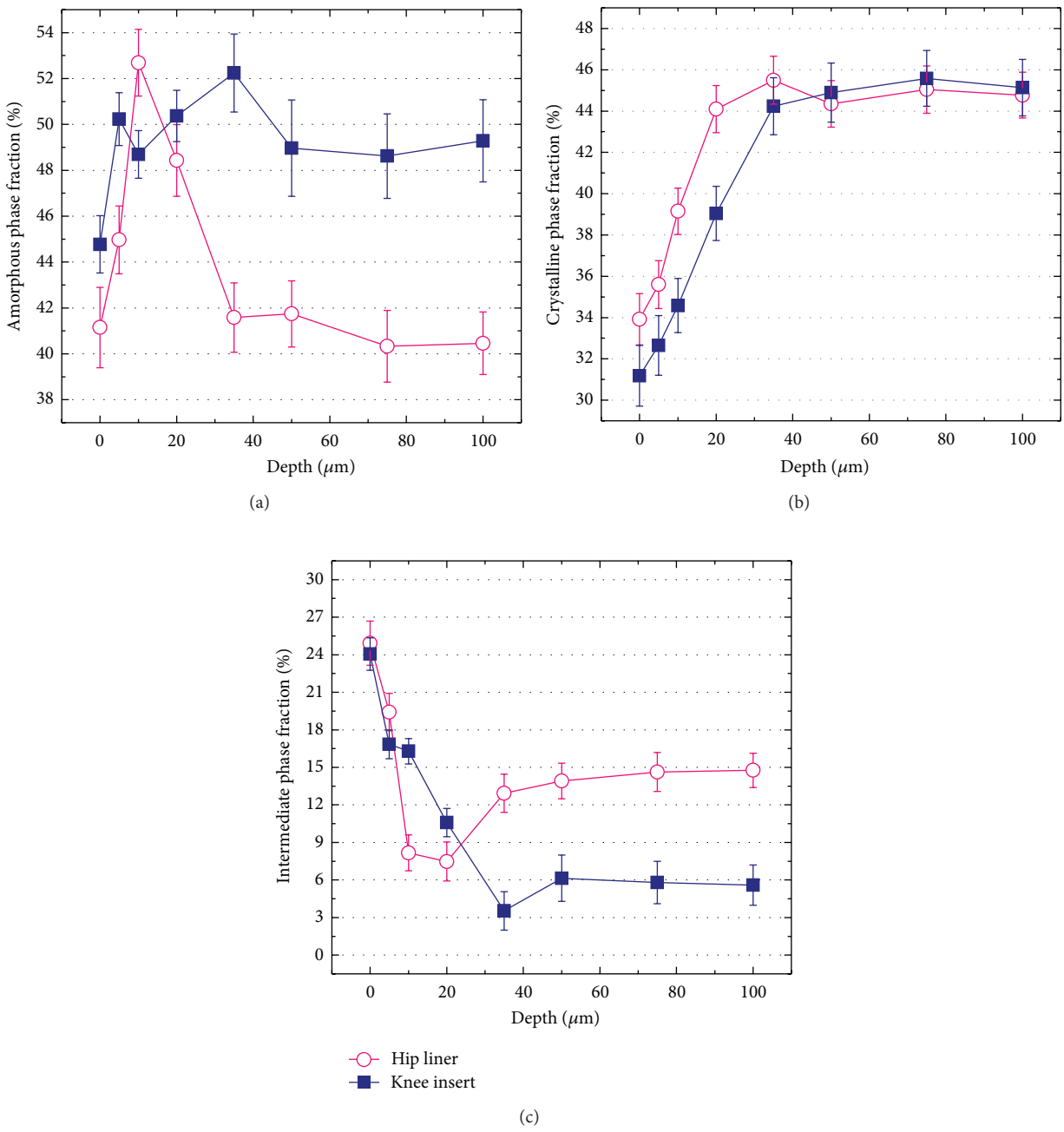

FIGURE 3: Depth profiles of phase volume fractions collected in the as-received XLPE hip and knee components ((a) amorphous fraction, α_a, (b) crystallinity, α_c, and (c) intermediate fraction, α_i, resp.).

rotationally symmetric shape (cf. Figure 2(a)). Thus, the depth profile of χ_p was given only for the knee insert in Figure 4(c). The C–C chains were preferentially oriented at an angle of $\chi_p = 80^\circ \pm 2^\circ$, which represents the molecules oriented at 10° away from the medial-lateral axis of the knee components in a clockwise direction. It was also confirmed that the surface and subsurface angles were slightly twisted ($\Delta\chi_p \leq 20^\circ$) within the depth of about 75 μm and the C–C chains gradually rotated toward the anterior-posterior axis with proceeding along the depth.

3.3. Orientational Probability Distribution and Degree of Anisotropy. Figures 5(a)-5(b) show the orientation distribution functions (ODFs, $f(\beta)$) as determined at each depth of the hip and knee samples. The angle β represents orientation of individual molecular chains with respect to the mean preferential orientation (θ_p). Note that the molecular axis of $\beta = 0$ corresponds to the axis of θ_p. Therefore, a material with a higher anisotropy shows a narrower (shaper) shaped curve of ODF, while a lower anisotropic material represents a broader (flatter) ODF.

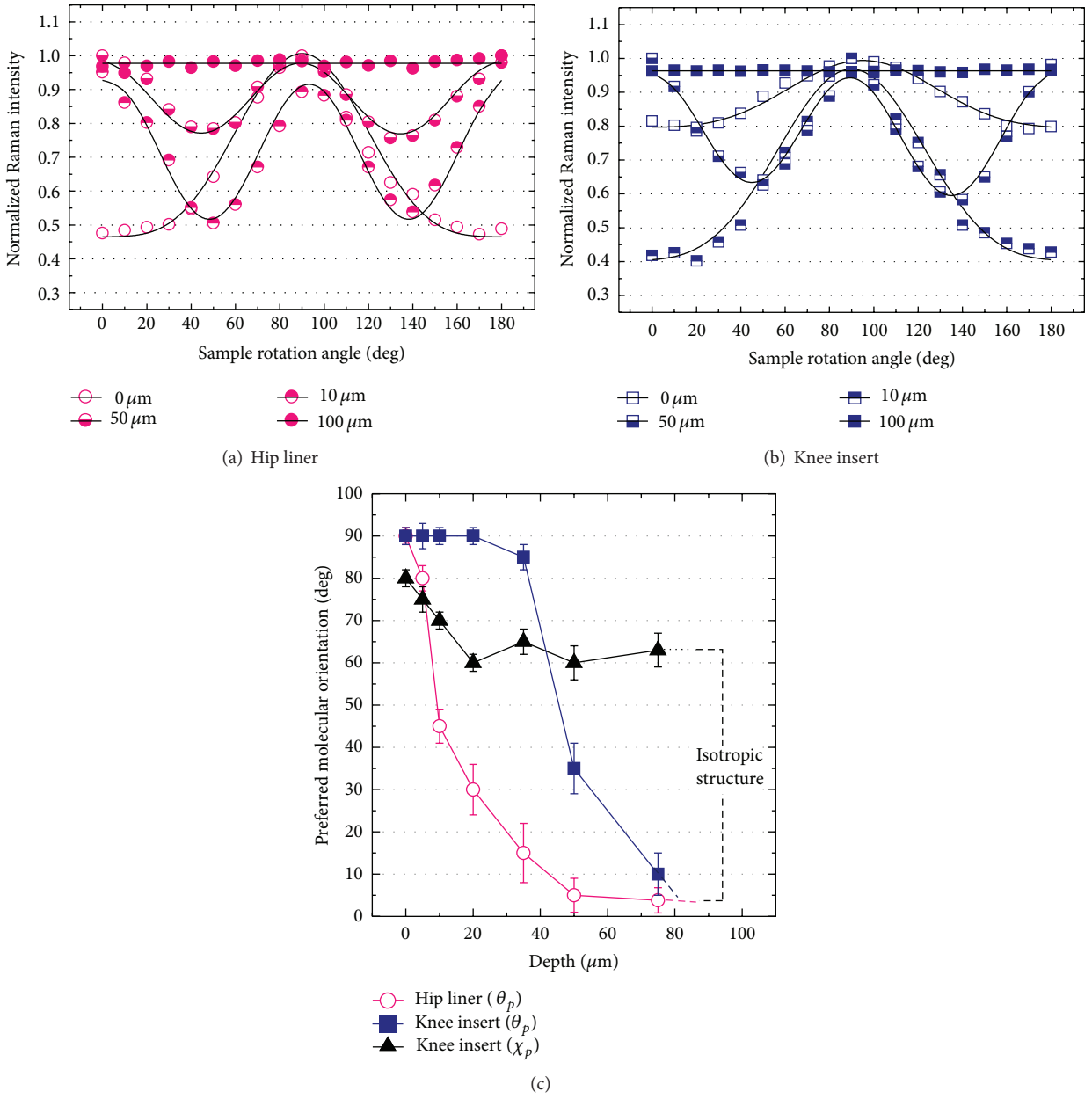

FIGURE 4: Experimental plots of the angular dependence of polarized Raman scattering intensities recorded upon inplane rotation χ at different depth of the as-received XLPE hip (a) and knee (b) components. Full lines represent the results of best fitting to the experimental data according to (4) in Section 2.3.2. Depth profiles of preferential orientation of the carbon chains (the C–C alkyl chains) collected in the as-received XLPE hip and knee components (c).

In the superficial layers of both components, quite different ODFs were obtained. In the hip liner, significantly narrow distributions of C–C chain orientation were found within the first 5 μm below the surface, while ODFs for the knee start from a much broader distribution at the surface and then rapidly increase up to the subsurface depth of 10 μm. Beyond the depth, both components showed a similar trend of ODFs, which were gradually getting broader with the increase in the subsurface depths.

The degree of anisotropy $\langle P_2(\cos\beta)\rangle$ was plotted in Figure 5(c) as a function of depth in the studied implants. As already defined in the previous section, $\langle P_2(\cos\beta)\rangle$ takes a range of values from a minimum of 0 (isotropic) to a maximum of 1.0 (perfect orientation). Figure 5(c) showed that the hip liner possessed a highly anisotropic surface, and the $\langle P_2(\cos\beta)\rangle$ value was obtained as 0.68±0.05. However, the knee surface showed a much lower value ($\langle P_2(\cos\beta)\rangle$ = 0.34± 0.03). The maximum values of $\langle P_2(\cos\beta)\rangle$ were observed at the depths of 0 and 10 μm for the hip and knee, respectively, and these subsequently decreased down to 0 at the depth of 100 μm. In the subsurface regions from 10 to 100 μm, the knee insert had a slightly higher anisotropic structure.

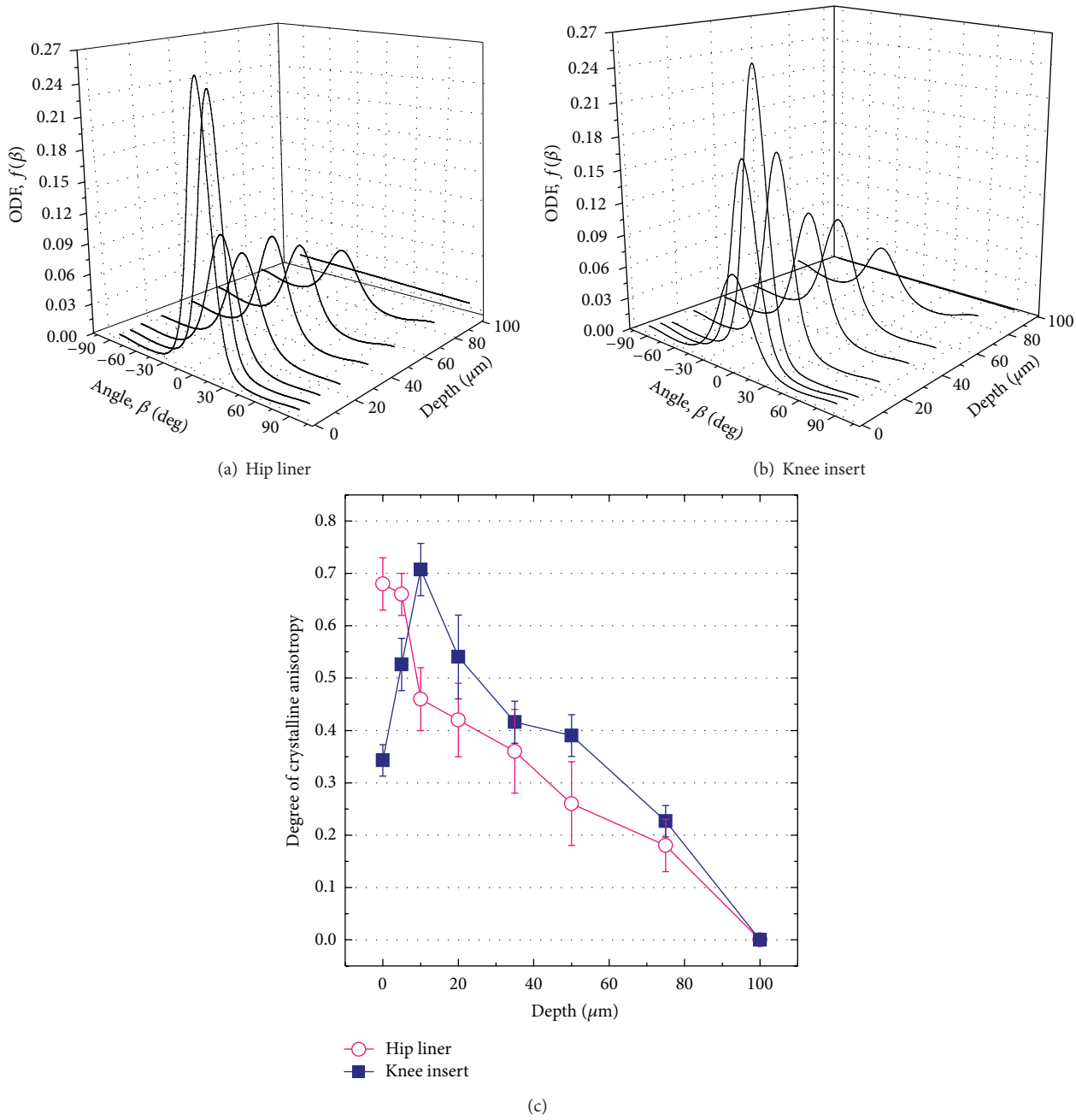

FIGURE 5: Orientation distribution functions (ODFs, $f(\beta)$) calculated at the different depth of the as-received XLPE hip (a) and knee (b) components. Depth profiles of degree of crystalline anisotropy, $\langle P_2(\cos\beta)\rangle$ collected in the as-received XLPE hip and knee components (c).

3.4. Compression Deformation Test. Figure 6 shows the plots of residual plastic strain (ε_f) as a function of externally applied strain (ε_i) for the hip and knee bearings. The full lines represent the fitting curves to the experimental data. The strain behaviors of these components before and after shape recovery were found to phenomenologically obey the quadratic functions as follows:

$$\varepsilon_f = 0.0054{\varepsilon_i}^2 + 0.2440\varepsilon_i, \quad \left(R^2 = 0.999\right),$$
$$\varepsilon_f = 0.0067{\varepsilon_i}^2 + 0.1983\varepsilon_i, \quad \left(R^2 = 0.998\right), \tag{7}$$

for XLPE hip and knee prostheses, respectively. This experimental data suggests that the microstructure of the knee insert has a slightly higher capacity of shape recovery than the hip insert despite the lower amount of radiation, that is, a lower residual plastic strain (ε_f) accumulation in the knee insert.

4. Discussion

Confocal/polarized Raman spectroscopy allows quantitative and rigorous assessments of the three-phase percentages and

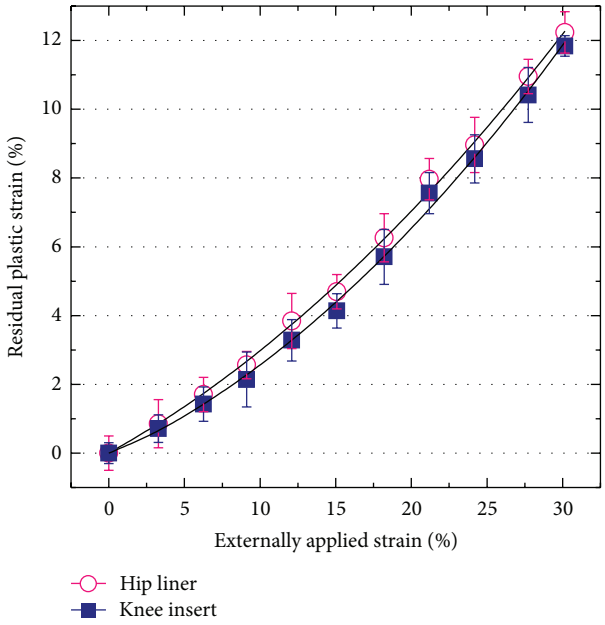

Figure 6: Experimental plots of the compressive deformation and shape-recovery behavior of the as-received XLPE hip and knee components.

crystallographic texture of XLPE hip and knee implants. It was clearly confirmed that all the microstructural parameters investigated in this study showed a transitional behavior from the surface down to the subsurface regions (cf. Figures 3–5). The phase percentages rapidly change within the first 35 μm below their surfaces and the lowest crystallinity (α_c) was always detected in the very surfaces. Correspondingly, molecular chain orientation parallel to the articulating surface with high anisotropy was also observed within those regions. The above structural characteristics can be considered the main effects of decrystallization induced by surface finishing performed at the end process of manufacturing, that is, lathe grinding and polishing. According to our past study using Raman spectroscopy, the original bulk α_c of GUR 1050 resin was reported as ≈50% in its nonirradiated and nonheated state [36]. Considering the α_c values detected in the bulk region of XLPE hip liner ($\alpha_c = 45.04 \pm 1.15\%$), a ≈5 vol.% loss of crystalline phase can be identified as a result of its fabrication processes. The gamma irradiation by itself might possibly destroy the crystalline regions at certain high doses but the 100 kGy irradiation does not substantially influence crystallinity change [37, 38]. Thus, it mostly appears to be due to the postirradiation remelting. Although remelting is highly beneficial from the perspective of oxidation resistance [38], the present results indicate that it comes at the price of the reduced crystallinity which is induced by heating above the melting temperature. On the other hand, it was reported that the as-received resin of GUR 1020 initially possessed about 6% a higher α_c over the GUR 1050 [35], but XLPE knee insert eventually showed a comparable α_c level to the analyzed hip liner, indicating a total of ≈11 vol.% loss of crystalline phase during its remelting. Spiegelberg et al. [39] reported that since GUR 1020 has a higher polydispersion index, its efficiency of cross-linking was rather lower than GUR 1050 under the same dose level. Thus, the irradiated GUR 1050 has lower degree of freedom in molecular motion due to more topologically constrained (cross-linked) structure networks. In other words, the irradiated GUR 1020 resin with lower molecular weight as well as lower cross-link density can possess higher mobility and activity of molecular chains, possibly resulting in the increased susceptibility to thermal treatment and consequently in greater decrystallization during remelting.

As illustrated in Figures 3–5, the investigated implants showed marked differences in the near-surface morphologies by contrast to the similarities on the bulk microstructure. A slightly lower crystallinity was detected in the knee surface as compared to the hip surface. In addition, it was clearly confirmed that the surface anisotropy was low in the knee but high in the hip. The above structural features might imply the technological differences in each machining procedure adopted for producing the geometrically different shape components of the hip and knee joint prostheses. Microstructural models for summarizing the preferred chain orientation and anisotropic features were given in Figures 7(a)–7(c) for each product. As shown in Figures 7(a)-7(b), the ≈100 μm thick anisotropic layer with transitional morphologies was located on the isotropic region which accounts for a large part (≈99%) of the overall thickness of each component. The anisotropic surfaces with the decreased crystallinity are a clear structural evidence for initial existence of plasticity layer formed in their manufacturing stages. It can be considered that the above two phases of the anisotropic surface and isotropic bulk structures are mainly responsible for wear and creep resistance, respectively. The mechanical properties of polyethylene are governed by (i) molecular weight (ii) balance among amorphous, crystalline, and third intermediate phase percentages; (iii) preferred molecular orientation; (iv) degree of crystalline anisotropy; (v) degree of cross-linking; and (vi) presence or absence of additives. The tested two prostheses had no preferential orientation in their bulks and contain no additives such as calcium stearate and antioxidant agent. Although, as explained above, the knee insert can possess a less cross-link density, it showed a slightly higher capacity of shape recovery, that is, a less accumulation of residual strain, against the applied uniaxial compressive load (cf. Figure 6). It was reported that a higher molecular weight GUR 1050 had greater elastic properties and higher resistance to permanent deformation over GUR 1020 in the as-received states [40]. In principle, the driving force of polyethylene shape recovery is the elastic force associated with the relaxation of amorphous phase having a physical entanglement, that is, cross-linking. This phase is known to be highly recoverable in a rubber-like manner after removal of the applied compressive load [34, 41]. As far as the above-mentioned structural features are concerned, a markedly higher percentage of amorphous bulk in the knee insert (cf. Figure 3(a)) can be deemed to contribute to a slightly higher efficiency of recovery against the same magnitudes of the applied strain despite its possibly less cross-linking within the amorphous regions. Nevertheless, since this phase is the most easily to be distorted within

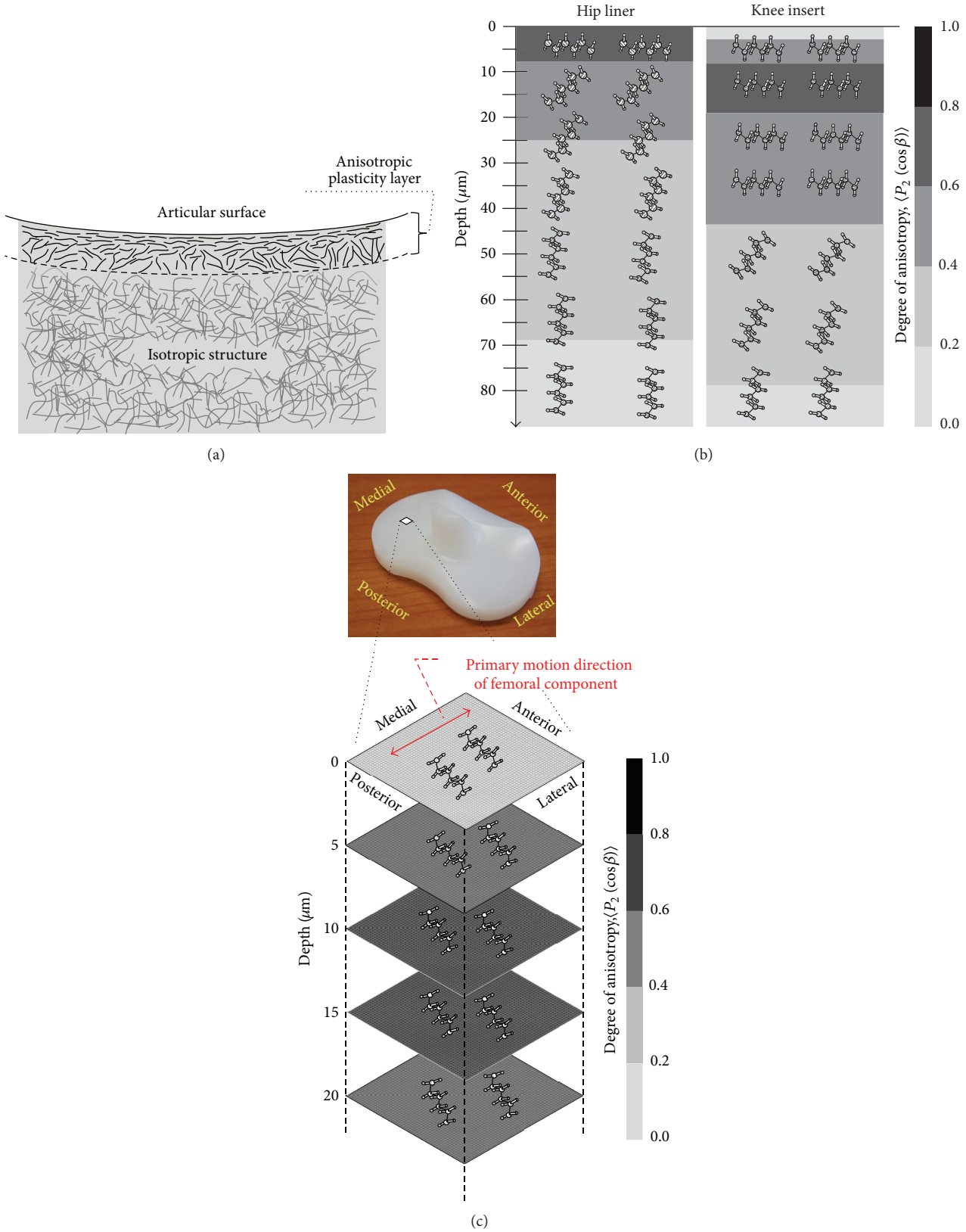

Figure 7: Schematic of the as-received XLPE microstructure consisting of anisotropic plasticity layer and isotropic random structure (a), the enlarged cross-section view of the near-surface anisotropic layers indicating the preferential tilt angles of molecular chains and the degree of crystalline anisotropy in the as-received XLPE hip and knee components (b), and the enlarged longitudinal sectional view of the near-surface anisotropic layers indicating the preferential inplane angles of molecular chains and the degree of crystalline anisotropy in the as-received XLPE knee component (c).

the structures during an application of ongoing compression, the amorphous-phase-rich knee insert might be less resistant to a time-dependent (creep) deformation under the same magnitudes of external stresses than the hip liner. Our previous result of strain recovery test conducted at the same condition for different types of thermally treated XLPEs [42] showed a linear dependence between ε_i and ε_f. The currently observed quadratic dependence of ε_i-ε_f plots can partly be interpreted as a consequence of higher percentages of the noncrystalline regions.

For the wear resistance viewpoints, scientific links between frictional characteristics and anisotropic structure had long been studied in conventional (nonhighly cross-linked) UHMWPE under lubricated and unlubricated dry sliding conditions [19, 20, 43]. It is well recognized that, under multidirectional stress fields generated by joint articulation, a highly anisotropic polymer surface leads to a decreased resistance to adhesive wear due to frequent occurrence of strain-softening and weakening even in absence of third-body particles [19, 20, 43]. This micromechanical phenomenon was originally based on the finding of Ramamurti et al. [21] and Wang et al. [19] in which there was a crossing of multidirectional shear forces at intersection of wear paths on femoral head surface. Thus, these observations provided with the perspective that a polyethylene hip liner with highly anisotropic surface can be susceptible to shear forces and wear damage due to an occurrence of sliding motion in a direction traverse to preferred orientation of molecular chains. However, unlike in the case of conventional UHMWPE, the introduction of cross-linking can mitigate adverse impacts of surface anisotropy on wear resistance due to the increased inter- and intralamellar covalent bonds. The validity of such positive effects of cross-linking has already been ascertained by hip joint simulator study under nonabrasive/abrasive conditions demonstrating a significant reduction in volumetric wear for XLPE liner compared to non-cross-linked liner [44] despite having high anisotropy on its surface (cf. Figure 5(c)). Although the predominant factor deciding the wear resistance of XLPE hip liner would be the cross-link density, a surface treatment to reduce its initial anisotropy (e.g., a change in machining conditions) may have a potential clinical benefit in further improving the wear resistance.

On the other hand, Wang et al. [19] pointed out that the strain-softening would not be severe even under combined knee motions of flexion/extension and internal/external rotation because of small difference (<20%) of maximum shear stress component for a knee joint between traverse and longitudinal direction. It is hence considered that strain-softening is more directly relevant to a hip-joint kinematics rather than a knee joint. However, according to the inplane orientation model shown in Figure 7(c), strain-softening is actually still a possibility for the knee due to the existence of the oriented chains orthogonal to the primary-motion direction of femoral component, that is, anterior to posterior direction. The previous joint-simulator study found a much higher sensitivity to abrasion wear in XLPE knee insert than in XLPE hip liner [44]. This fact could be partly associated with the detrimental effects of the surface oriented chains orthogonal to the primary motion on the knee wear. Therefore, a careful consideration should be given to the negative effects of surface molecular orientation on wear behavior even though the polyethylene prosthetic surface has a highly cross-linked microstructure. In the above contexts, our present morphological observations can highlight the importance for XLPE prostheses to optimize by different technological regimes (e.g., reconsideration of machining conditions or techniques) the spatial arrangement of initial molecular orientation relative to the primary directions of motion at each joint for further maximizing their wear performances.

5. Conclusion

The quantitative and nondestructive analyses of confocal/polarized Raman spectroscopy were applied to describe and compare the depth profiles of the three-phase percentages and crystalline anisotropy between XLPE hip and knee replacement implants of the first-generation highly cross-linked ultrahigh molecular weight polyethylene. The impacts of the surface and subsurface morphologies on plastic deformation and wear were explicitly discussed from the viewpoints of the molecular mobility and strain-softening resistance. The main outcomes of our investigation can be summarized as follows.

(i) After the procedure of remelting, a higher loss of crystallinity percentage was observed in the irradiated GUR 1020 resin used for the knee insert, as compared to the irradiated GUR 1050 for the hip liner.

(ii) It was confirmed that the studied hip and knee components consisted of two structural regions induced by the manufacturing procedures: the near-surface transitional anisotropic layer (≈100 μm thickness) and the bulk isotropic structural region.

(iii) The knee insert showed a slightly higher capacity of the shape recovery against the applied uniaxial compressive load over the hip liner owing to a markedly higher percentage of the bulk amorphous phase with cross-linking.

(iv) Our present observations implied the possibility to further maximize their wear performances by the surface rearrangements of crystalline texture as the outcome of different technological regimes for surface machining and polishing during the production processes.

Conflict of Interests

All authors declare that there is no conflict of interests regarding the publication of this paper.

References

[1] S. M. Kurtz, F. J. Medel, D. W. MacDonald, J. Parvizi, M. J. Kraay, and C. M. Rimnac, "Reasons for revision of first-generation

highly cross-linked polyethylenes," *Journal of Arthroplasty*, vol. 25, no. 6, pp. 67–74, 2010.

[2] S. D. Ulrich, T. M. Seyler, D. Bennett et al., "Total hip arthroplasties: what are the reasons for revision?" *International Orthopaedics*, vol. 32, no. 5, pp. 597–604, 2008.

[3] J. C. Clohisy, G. Calvert, F. Tull, D. McDonald, and W. J. Maloney, "Reasons for revision hip surgery: a retrospective review," *Clinical Orthopaedics and Related Research*, vol. 429, pp. 188–192, 2004.

[4] O. K. Muratoglu, K. Wannomae, S. Christensen, H. E. Rubash, and W. H. Harris, "Ex vivo wear of conventional and cross-linked polyethylene acetabular liners," *Clinical Orthopaedics and Related Research*, no. 438, pp. 158–164, 2005.

[5] O. K. Muratoglu, C. R. Bragdon, D. O. O'Connor et al., "Unified wear model for highly crosslinked ultra-high molecular weight polyethylenes (UHMWPE)," *Biomaterials*, vol. 20, no. 16, pp. 1463–1470, 1999.

[6] H. McKellop, F. W. Shen, B. Lu, P. Campbell, and R. Salovey, "Development of an extremely wear-resistant ultra high molecular weight polyethylene for total hip replacements," *Journal of Orthopaedic Research*, vol. 17, no. 2, pp. 157–167, 1999.

[7] E. García-Rey, E. García-Cimbrelo, A. Cruz-Pardos, and J. Ortega-Chamarro, "New polyethylenes in total hip replacement: a prospective, comparative clinical study of two types of liner," *Journal of Bone and Joint Surgery B*, vol. 90, no. 2, pp. 149–153, 2008.

[8] C. A. Engh Jr., A. S. Stepniewski, S. D. Ginn, S. E. Beykirch, C. J. Sychterz-Terefenko, and R. H. Hopper Jr., "A randomized prospective evaluation of outcomes after total hip arthroplasty using cross-linked marathon and non-cross-linked Enduron polyethylene liners," *Journal of Arthroplasty*, vol. 21, no. 6, pp. 17–25, 2006.

[9] J. P. Collier, B. H. Currier, F. E. Kennedy et al., "Comparison of cross-linked polyethylene materials for orthopaedic applications," *Clinical Orthopaedics and Related Research*, no. 414, pp. 289–304, 2003.

[10] S. A. Atwood, D. W. Van Citters, E. W. Patten, J. Furmanski, M. D. Ries, and L. A. Pruitt, "Tradeoffs amongst fatigue, wear, and oxidation resistance of cross-linked ultra-high molecular weight polyethylene," *Journal of the Mechanical Behavior of Biomedical Materials*, vol. 4, no. 7, pp. 1033–1045, 2011.

[11] E. Oral, A. S. Malhi, and O. K. Muratoglu, "Mechanisms of decrease in fatigue crack propagation resistance in irradiated and melted UHMWPE," *Biomaterials*, vol. 27, no. 6, pp. 917–925, 2006.

[12] L. A. Pruitt, "Deformation, yielding, fracture and fatigue behavior of conventional and highly cross-linked ultra high molecular weight polyethylene," *Biomaterials*, vol. 26, no. 8, pp. 905–915, 2005.

[13] L. Bradford, D. Baker, M. D. Ries, and L. A. Pruitt, "Fatigue crack propagation resistance of highly crosslinked polyethylene," *Clinical Orthopaedics and Related Research*, no. 429, pp. 68–72, 2004.

[14] M. D. Ries, "Highly cross-linked polyethylene: the debate is over—in opposition," *Journal of Arthroplasty*, vol. 20, no. 1, pp. 59–62, 2005.

[15] D. L. Bartel, V. L. Bicknell, and T. M. Wright, "The effect of conformity, thickness, and material on stresses in ultra-high molecular weight components for total joint replacement," *Journal of Bone and Joint Surgery A*, vol. 68, no. 7, pp. 1041–1051, 1986.

[16] D. L. Bartel, J. J. Rawlinson, A. H. Burstein, C. S. Ranawat, and W. F. Flynn Jr., "Stresses in polyethylene components of contemporary total knee replacements," *Clinical Orthopaedics and Related Research*, no. 317, pp. 76–82, 1995.

[17] Y. Kasahara, T. Majima, S. Kimura, O. Nishiike, and J. Uchida, "What are the causes of revision total knee arthroplasty in Japan?" *Clinical Orthopaedics and Related Research*, vol. 471, no. 5, pp. 1533–1538, 2013.

[18] S. M. Kurtz, O. K. Muratoglu, M. Evans, and A. A. Edidin, "Advances in the processing, sterilization, and crosslinking of ultra-high molecular weight polyethylene for total joint arthroplasty," *Biomaterials*, vol. 20, no. 18, pp. 1659–1688, 1999.

[19] A. Wang, A. Essner, V. K. Polineni, C. Stark, and J. H. Dumbleton, "Lubrication and wear of ultra-high molecular weight polyethylene in total joint replacements," *Tribology International*, vol. 31, no. 1–3, pp. 17–33, 1998.

[20] A. Wang, D. C. Sun, S. S. Yau et al., "Orientation softening in the deformation and wear of ultra-high molecular weight polyethylene," *Wear*, vol. 203-204, pp. 230–241, 1997.

[21] B. S. Ramamurti, C. R. Bragdon, D. O. O'Connor et al., "Loci of movement of selected points on the femoral head during normal gait: three-dimensional computer simulation," *Journal of Arthroplasty*, vol. 11, no. 7, pp. 845–852, 1996.

[22] S. Okita, M. Hasegawa, Y. Takahashi, L. Puppulin, A. Sudo, and G. Pezzotti, "Failure analysis of sandwich-type ceramic-on-ceramic hip joints: a spectroscopic investigation into the role of the polyethylene shell component," *Journal of the Mechanical Behavior of Biomedical Materials*, vol. 31, pp. 55–67, 2004.

[23] G. R. Strobl and W. Hagedorn, "Raman spectroscopic method for determining the crystallinity of polyethylene," *Journal of Polymer Science: Polymer Physics Edition*, vol. 16, no. 7, pp. 1181–1193, 1978.

[24] F. Rull, A. C. Prieto, J. M. Casado, F. Sobron, and H. G. M. Edwards, "Estimation of crystallinity in polyethylene by Raman spectroscopy," *Journal of Raman Spectroscopy*, vol. 24, no. 8, pp. 545–550, 1993.

[25] M. Glotin and L. Mandelkern, "A Raman spectroscopic study of the morphological structure of the polyethylenes," *Colloid & Polymer Science*, vol. 260, no. 2, pp. 182–192, 1982.

[26] R. Mutter, W. Stille, and G. Strobl, "Transition regions and surface melting in partially crystalline polyethylene: a Raman spectroscopic study," *Journal of Polymer Science B: Polymer Physics*, vol. 31, no. 1, pp. 99–105, 1993.

[27] J. Maxfield, R. S. Stein, and M. C. Chen, "Polarized Raman studies of crystalline and amorphous orientation in polyethylene," *Journal of Polymer Science: Polymer Physics Edition*, vol. 16, no. 1, pp. 37–48, 1978.

[28] Y. Takahashi, L. Puppulin, W. Zhu, and G. Pezzotti, "Raman tensor analysis of ultra-high molecular weight polyethylene and its application to study retrieved hip joint components," *Acta Biomaterialia*, vol. 6, no. 9, pp. 3583–3594, 2010.

[29] L. Puppulin, Y. Takahashi, W. Zhu, N. Sugano, and G. Pezzotti, "Polarized Raman analysis of the molecular rearrangement and residual strain on the surface of retrieved polyethylene tibial plates," *Acta Biomaterialia*, vol. 7, no. 3, pp. 1150–1159, 2011.

[30] E. T. Jaynes, "Information theory and statistical mechanics," *Physical Review*, vol. 106, pp. 620–630, 1957.

[31] R. Pérez, S. Banda, and Z. Ounaies, "Determination of the orientation distribution function in aligned single wall nanotube polymer nanocomposites by polarized Raman spectroscopy," *Journal of Applied Physics*, vol. 103, no. 7, Article ID 074302, 2008.

[32] M. van Gurp, "The use of rotation matrices in the mathematical description of molecular orientations in polymers," *Colloid & Polymer Science*, vol. 273, no. 7, pp. 607–625, 1995.

[33] R. W. Meyer and L. A. Pruitt, "The effect of cyclic true strain on the morphology, structure, and relaxation behavior of ultra high molecular weight polyethylene," *Polymer*, vol. 42, no. 12, pp. 5293–5306, 2001.

[34] Z. Bartczak, R. E. Cohen, and A. S. Argon, "Evolution of the crystalline texture of high-density polyethylene during uniaxial compression," *Macromolecules*, vol. 25, no. 18, pp. 4692–4704, 1992.

[35] D. Barron and C. Birkinshaw, "Ultra-high molecular weight polyethylene—evidence for a three-phase morphology," *Polymer*, vol. 49, no. 13-14, pp. 3111–3115, 2008.

[36] Y. Takahashi, K. Yamamoto, T. Shishido et al., "Strain-induced microstructural rearrangement in ultra-high molecular weight polyethylene for hip joints: a comparison between conventional and vitamin E-infused highly-crosslinked liners," *Journal of the Mechanical Behavior of Biomedical Materials*, vol. 31, pp. 31–44, 2014.

[37] W. P. Slichter and E. R. Mandell, "Molecular structure and motion in irradiated polyethylene," *Journal of Physical Chemistry*, vol. 62, no. 3, pp. 334–340, 1958.

[38] O. K. Muratoglu, "Highly crosslinked and melted UHMWPE," in *UHMWPE Biomaterials Handbook, Second Edition: Ultra-High Molecular Weight Polyethylene in Total Joint Replacement and Medical Devices*, S. M. Kurtz, Ed., pp. 197–204, Academic Press, Burlington, Ma, USA, 2009.

[39] S. H. Spiegelberg, S. M. Kurtz, and A. Edidin, "Effects of molecular weight distribution on the network properties of radiation- and chemically crosslinked ultra-high molecular weight polyethylene," in *Proceedings of the 25th Annual Meeting of Society for Biomaterials*, p. 215, 2003.

[40] J. Cybo, J. Maszybrocka, A. Barylski, and J. Kansy, "Resistance of UHMWPE to plastic deformation and wear and the possibility of its enhancement through modification by radiation," *Journal of Applied Polymer Science*, vol. 125, no. 6, pp. 4188–4196, 2012.

[41] Z. Bartczak, A. S. Argon, and R. E. Cohen, "Deformation mechanisms and plastic resistance in single-crystal-textured high-density polyethylene," *Macromolecules*, vol. 25, no. 19, pp. 5036–5053, 1992.

[42] Y. Takahashi, N. Sugano, L. Puppulin, W. Zhu, and G. Pezzotti, "Raman spectroscopic study of remelting and annealing-induced effects on microstructure and compressive deformation behavior of highly crosslinked UHMWPE for total hip arthroplasty," *Journal of Biomedical Materials Research B: Applied Biomaterials*, 2014.

[43] C. R. Bragdon, D. O. O'Connor, J. D. Lowenstein, M. Jasty, and W. D. Syniuta, "The importance of multidirectional motion on the wear of polyethylene," *Proceedings of the Institution of Mechanical Engineers H: Journal of Engineering in Medicine*, vol. 210, no. 3, pp. 157–165, 1996.

[44] V. D. Good, K. Widding, M. Scott, and S. Jani, "The sensitivity of crosslinked UHMWPE to abrasive wear: hips versus knees, ASTM STP 1445," in *Crosslinked and Thermally Treated Ultra-High Molecular Weight Polyethylene for Joint Replacements*, S. M. Kurtz, R. Gsell, and J. Martell, Eds., pp. 104–116, ASTM international, West Conshohocken, Pa, USA, 2003.